

University of California - Davis

UCD-95-28
ILL-(TH)-95-28
December 1995

WEAKLY-COUPLED HIGGS BOSONS

J.F. Gunion

*Davis Institute for High Energy Physics
University of California, Davis, CA 95616*

A. Stange

*Brookhaven National Laboratory
Upton, Long Island, NY 11973*

S. Willenbrock

*Department of Physics, University of Illinois
1110 W. Green St., Urbana, IL 61801*

Abstract

We review the search for the standard Higgs boson, the Higgs bosons of the supersymmetric standard model, and Higgs bosons from a variety of other models at present and future colliders.

1 Introduction

1.1 Standard Higgs model

The evidence is overwhelming that the electroweak interaction is described by an $SU(2)_L \times U(1)_Y$ gauge theory, spontaneously broken to electromagnetism, $U(1)_{EM}$. The symmetry breaking provides the masses of the W and Z bosons, as well as the masses of the fermions and the Cabibbo-Kobayashi-Maskawa (CKM) mixing between the quarks (including CP violation). Electroweak symmetry breaking is therefore associated with most of the aspects of the electroweak interaction which remain beyond our grasp. Uncovering the electroweak-symmetry-breaking mechanism is essential for progress in our quest to describe nature at a deeper level.

Little is known about the mechanism which breaks the electroweak symmetry. The fact that the relation $m_W = m_Z \cos \theta_W$ is nearly satisfied suggests that the symmetry-breaking sector possesses a global $SU(2)$ symmetry, often called a “custodial” symmetry [1, 2, 3]. Precision electroweak experiments [4, 5] and

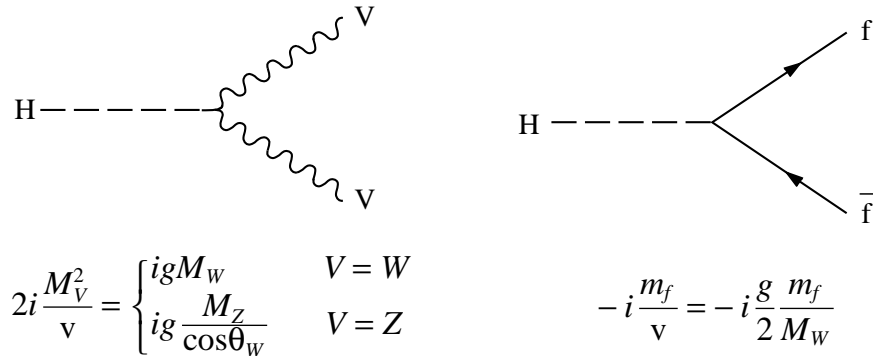


Figure 1: Couplings of the standard Higgs boson to weak vector bosons and fermions. The coupling to weak vector bosons is multiplied by the metric tensor $g^{\mu\nu}$.

flavor-changing-neutral-current processes [6] indirectly constrain the electroweak-symmetry-breaking sector.

The simplest model which is consistent with all constraints is the standard Higgs model, in which the symmetry is broken by a fundamental scalar field which acquires a non-zero vacuum-expectation value [7]. The scalar field, ϕ , is an $SU(2)_L$ doublet with hypercharge $+1/2$, and a potential

$$V(\phi) = -\mu^2 |\phi|^2 + \lambda |\phi|^4. \quad (1)$$

The minimum of the potential is at $|\phi|^2 = \mu^2/2\lambda \equiv v^2/2$, where $v = (\sqrt{2}G_F)^{-1/2}$. The sole prediction of this model is the existence of a neutral scalar particle, the Higgs boson, ϕ^0 , of unknown mass ($m_{\phi^0}^2 = 2\lambda v^2$), but with fixed couplings to other particles. The couplings of the Higgs boson to the weak vector bosons and the fermions are shown in Fig. 1.

Despite the simplicity of the standard Higgs model, it does not appear to be a candidate for a fundamental theory. The introduction of a fundamental scalar field is *ad hoc*; the other fields in the theory are spin-one gauge fields and spin-half fermion fields. Furthermore, the model does not explain why the scalar field acquires a vacuum-expectation value, nor why it produces the curious pattern of fermion masses and the CKM matrix. Thus the standard Higgs model accommodates, but does not explain, those features of the electroweak theory for which it is responsible.

One response to these criticisms is to regard the standard Higgs model as an effective field theory, valid up to some energy scale above the Higgs mass. In fact, an ordinary scalar field theory *cannot* be valid up to arbitrarily high energies; it must eventually be subsumed by a more fundamental theory. This is due to the fact that the running scalar-field self coupling, λ , increases with increasing energy,

which is related to the “triviality” of scalar field theory. To a good approximation, the relation between the Higgs mass and the cutoff Λ above which the theory becomes incomplete is [8]

$$m_{\phi^0}^2 < \frac{4\pi^2 v^2}{3 \ln(\Lambda/m_{\phi^0})} . \quad (2)$$

If Λ is taken to infinity, m_{ϕ^0} approaches zero, as does the Higgs-field self-interaction, $\lambda = m_{\phi^0}^2/2v^2$; the theory is “trivial”. However, we know for certain that new physics enters at the Planck scale, $(8\pi G_N)^{-1/2} \sim 10^{18}$ GeV; if we demand that the scalar field theory is valid up to this energy, the upper bound on the Higgs mass is about 200 GeV [8]. At the other extreme, if Λ is only a few times m_{ϕ^0} , the maximum value of the Higgs mass is about 700 GeV [9, 10].

A different argument leads to a *lower* bound on the Higgs mass for a given value of the top-quark mass [8, 11]. The top quark induces a $|\phi|^4$ interaction at one loop, which is added to the tree-level scalar potential, Eq. 1. This induced interaction enters with the opposite sign from the tree-level $\lambda|\phi|^4$ interaction, and can destabilize the potential at large values of $|\phi|$ if it becomes dominant. The value of $|\phi|$ at which this occurs is interpreted as a scale Λ at which the theory must be replaced by a more fundamental theory. CDF has observed the top quark at a mass $m_t = 176 \pm 8 \pm 10$ GeV [12], and D0 has observed the top quark at a mass $m_t = 199 \pm 20 \pm 22$ GeV [13]. These observations are consistent with indirect bounds from precision electroweak experiments [14]. We assume a (pole) mass of $m_t = 175$ GeV throughout this report. After including re-summed next-to-leading log corrections and imposing the somewhat less stringent demand that the vacuum must be metastable, it is found [15] that for $\Lambda \sim 10^{18}$ GeV the lower bound on the Higgs mass is about 130 GeV; this bound is reduced to roughly 100 GeV for $m_t = 160$ GeV. For $\Lambda = 1$ TeV, the lower bound is about 70 GeV, close to the existing experimental lower bound.

Taken together, the above two arguments imply (roughly) $100 \text{ GeV} \leq m_{\phi^0} \leq 200 \text{ GeV}$, if the theory is valid up to the Planck scale. However, another argument suggests that the scale, Λ , at which the standard Higgs model must be replaced by a more fundamental theory cannot be much larger than the weak scale itself. This is because the vacuum-expectation value of the Higgs field, v , depends sensitively on the scale Λ [1]. The relation between the bare vacuum-expectation value, v_0 , and the renormalized vacuum-expectation value, $v = (\sqrt{2}G_F)^{-1/2} = 246$ GeV, at one loop is

$$v^2 = v_0^2 + \mathcal{O}(\Lambda^2) . \quad (3)$$

If Λ is much larger than v , then v_0 must be adjusted precisely to yield the desired value of v . Such a fine tuning is unnatural. We are led to conclude that the standard Higgs model is an acceptable effective field theory as long as it is subsumed by a more fundamental theory at an energy not much greater than $v = 246$ GeV. The vacuum-stability lower bound is then essentially eliminated, and the triviality

bound is $m_{\phi^0} \lesssim 700 \text{ GeV}$.

It is possible that this fine-tuning problem is solved by a mechanism which we have not yet imagined. This point of view is supported by our failure to find any realistic mechanism to yield a small value of the cosmological constant, as required by observation. This is an even more severe fine-tuning problem than the vacuum-expectation value of the Higgs field.

1.2 Remarks on general Higgs sector extensions

The standard model (SM) Higgs sector is particularly simple, but many possible extensions have been considered [16]. The most attractive possibility is to allow for additional Higgs doublet fields; for such an extension $\rho = 1$ remains automatic at tree level. A popular test case is the general two-Higgs-doublet model (2HDM) [17]. If CP is conserved, then the two-doublet model yields five physical Higgs CP-eigenstates: two CP-even neutral Higgs bosons, h^0 and H^0 ; a CP-odd Higgs, A^0 ; and a charged Higgs boson pair, H^\pm . If the Higgs potential violates CP, then in general all the neutral states mix, and there are simply three neutral mass eigenstates of mixed CP character. One drawback of the 2HDM extension (also shared by all other extensions) should be noted: it is not *a priori* guaranteed that $U(1)_{EM}$ remains unbroken — parameters in the Higgs potential can be chosen such that $m_{H^\pm}^2 < 0$. But requiring $m_{H^\pm}^2 > 0$ is also perfectly natural, and does not require fine tuning of the parameters. However, the fine-tuning and naturalness problems associated with one-loop quadratically divergent contributions to Higgs boson squared masses remain.

An important parameter of a 2HDM is $\tan\beta = v_2/v_1$, where v_2 (v_1) is the vacuum expectation value of the neutral member of the Higgs doublet that couples to up-type (down-type) quarks. (We restrict our discussion to the type-II 2HDM models in which up and down quarks couple to different Higgs doublets; see [16] for a discussion of alternative coupling patterns.) Assuming that CP is conserved, a second phenomenologically crucial angle emerges — α , the mixing angle arising from the diagonalization of the 2×2 mass matrix for the CP-even Higgs sector. In a general two-doublet model the masses of the Higgs bosons are all additional independent parameters, completely independent of one another. Constraints on the 2HDM Higgs masses arise from the requirement that the Higgs sector contribution to $\Delta\rho$ be small (which implies limited mass splitting between any two Higgs bosons that couple significantly to either the Z or W [16]) and from the $b \rightarrow s\gamma$ branching ratio (which places a significant lower bound on m_{H^\pm} [18]).

The most direct indication of a two-Higgs-doublet sector for the standard model would be the observation of more than a single neutral Higgs boson or detection of the charged Higgs bosons. However, even if only a single neutral Higgs boson of the 2HDM is observed, in general it will have properties that are very distinct from the ϕ^0 . In the 2HDM, the couplings of any one of the three neutral Higgs

bosons to the various channels can be very different from the couplings of the ϕ^0 . Significant deviations from predictions for the ϕ^0 production and decay rates could easily occur. If such deviations are seen, then a general 2HDM becomes a rather attractive first possibility for the appropriate Higgs sector extension. If the single neutral Higgs boson is found to have couplings to $b\bar{b}$, $\tau^+\tau^-$ and WW^* that are within 10-20% of the values expected for the ϕ^0 , this will strongly suggest that the only two-doublet extensions that should be considered are ones in which the other Higgs bosons of the two-doublet model have decoupled, leaving behind one neutral Higgs boson that will then automatically have couplings that are close to SM values [19]. The minimal supersymmetric two-doublet extension, to be discussed shortly, is the most attractive theory of this type.

Higher representations of $SU(2)_L$ can also be considered in the context of the standard model electroweak gauge group, the next most complicated being a Higgs triplet. If $Y = 0$, the triplet field can be real; if $Y \neq 0$, it is complex. As is well-known [16] $\rho = 1$ is not automatic in such a case. Various possibilities for obtaining $\rho = 1$ at tree level in the presence of a Higgs triplet can be entertained. One possibility is that the neutral member of the Higgs triplet has very small or zero vacuum-expectation value [20]. In this case, the triplet simply decouples from electroweak-symmetry-breaking physics. If the triplet vacuum-expectation value is significant there are still a number of ways to obtain $\rho = 1$. For example, it could be that there is fourth generation with a large $t' - b'$ mass splitting. In this case the $t' - b'$ doublet yields a large positive contribution to $\Delta\rho$ which could be cancelled by the negative $\Delta\rho$ that would arise from a $T = 1$, $|Y| = 2$ complex triplet representation. Obviously, this would require fine tuning the triplet vacuum expectation value. A second possibility is to combine one doublet Higgs field with one real ($T = 1, Y = 0$) and one complex ($T = 1, |Y| = 2$) field [21, 22, 23, 16]. If the neutral members of the two triplet representations have the same vacuum expectation value, then $\rho = 1$ is maintained at tree level. In either case, $\rho = 1$ is not maintained at 1-loop. Indeed, unlike the case of doublet models, ρ is infinitely renormalized in triplet models (due to the fact that the interactions of the B gauge field with the Higgs bosons violate custodial $SU(2)$) [22, 23]. Thus, fine-tuning would be required to maintain $\rho = 1$ after renormalization.

Another issue of concern for triplet models is grand unification of the gauge couplings. This will be discussed in more detail in the next section. Here we simply make two observations. First, in the non-supersymmetric context gauge coupling unification (without intermediate scale physics) occurs for a single doublet and a single $|Y| = 2$ triplet. However, a $Y = 0$ triplet cannot also be present, implying that the $|Y| = 2$ triplet must have a very small vacuum-expectation value to achieve $\rho \sim 1$ at tree-level. Second, in the supersymmetric context the presence of either type of triplet completely destroys gauge coupling unification.

If the gauge group is expanded beyond $SU(2)_L \times U(1)$, many new possibilities for Higgs triplets arise. Left-right symmetric $SU(2)_L \times SU(2)_R \times U(1)_{B-L}$ models are

an attractive possibility [24]. The Higgs sector of the left-right symmetric models has received much attention [25, 16]. Typically, the Higgs sector contains two Higgs doublet fields (in a bi-doublet) and two separate sets of Higgs triplet fields, one connecting to the usual W_L sector and the other responsible for giving mass to the right-handed W_R . Despite the presence of Higgs triplets, gauge coupling unification is possible in this context for an appropriate choice of the Higgs sector and intermediate mass scale matter fields [26]. However, the naturalness problem for ρ is not solved. The phenomenology of the left-right Higgs sector is quite intricate, and will not be detailed here.

An especially interesting feature of Higgs triplet models is the fact that a triplet field can have lepton-number violating couplings. In left-right symmetric models, such couplings can lead in a natural way to the see-saw mechanism for generating neutrino masses; certain aspects of the phenomenology of the left-right Higgs sector become closely tied to neutrino physics.

Because of the difficulties with ρ and the need for intermediate scale physics in order to have grand unification, models in which Higgs triplets play a substantial role in electroweak symmetry breaking are generally not in favor with theorists. However, this should not deter the experimental community from searching for the many new signatures that would arise. A simple and spectacular signal for a triplet model is direct detection of the doubly charged Higgs boson(s) contained in complex Higgs triplet representation(s). At an e^+e^- collider, $e^+e^- \rightarrow H^{++}H^{--}$ production via virtual Z or photon exchange only requires adequate machine energy, $\sqrt{s} \gtrsim 2m_{H^{++}}$. $H^{++}H^{--}$ pair production is also possible at a hadron collider, and yields substantial rates at the LHC for $m_{H^{++}} \lesssim 500$ GeV. Assuming a significant vacuum expectation value in the triplet sector, a hadron collider of adequate energy can produce the H^{--} and H^{++} at an observable rate via W^-W^- and W^+W^+ fusion [23], and at an e^-e^- collider H^{--} production via W^-W^- fusion is an exciting prospect [27]. In addition, there is the possibility of direct s -channel production, $e^-e^- \rightarrow H^{--}$ [28] — this process is a direct probe of the very interesting lepton-number-violating couplings to the Higgs triplet field and would be observable for an $e^-e^- \rightarrow H^{--}$ coupling strength squared that is some nine order of magnitude smaller than current limits. (See Ref. [29] for a recent survey of limits.) Billions of H^{--} 's would be produced each year if the coupling strength were close to current limits. Since limits on the $\mu^-\mu^- \rightarrow H^{--}$ coupling are even weaker, a $\mu^-\mu^-$ collider might yield even larger numbers of H^{--} 's.

1.3 Minimal supersymmetric standard model

The partial success of SU(5) grand unification [30] encourages one to consider a scenario in which there is no new physics between the weak scale and the grand-unified (GUT) scale, $M_U \sim 10^{16}$ GeV. This is based on the observation that each generation of fermions fits into the $\bar{5} + 10$ representation of SU(5), and that the

$SU(3)_c$, $SU(2)_L$, and $U(1)_Y$ couplings nearly converge (when normalized according to $SU(5)$) when extrapolated up to M_U . The fact that the grand-unified scale and the Planck scale are relatively close provides further encouragement.

One is thus led to search for new physics at the weak scale which improves upon the partial success of the $SU(5)$ model, and which allows the weak scale to be much less than the grand-unified scale. Supersymmetry (SUSY) is the unique weakly-coupled theory which eliminates the quadratic renormalization of the Higgs-field vacuum-expectation value, Eq. 3, to all orders in perturbation theory, and thus allows $v = 246$ GeV to occur naturally, if the scale of supersymmetry breaking is comparable to the weak scale [31]. Further, in the minimal supersymmetric model, the supersymmetric partners of the gauge bosons and Higgs fields affect the relative evolution of the gauge couplings [32] in a favorable way. (The supersymmetric partners of the fermions do not influence the relative evolution at one loop.) There are *exactly* two Higgs doublet fields in the minimal supersymmetric model. At least two Higgs doublet fields are necessary to provide masses for both down-type and up-type quarks; in addition, only for an even number of Higgs doublets do the gauge anomalies cancel amongst the Higgs superpartners. The relative evolution of the gauge couplings in the presence of multiple doublets and their supersymmetric partners [33] is such that for the minimal two-Higgs-doublet sector the net effect is precisely that desired; if all particles and their superpartners have masses in the TeV range, the gauge couplings merge rather precisely at a scale of about 10^{16} GeV [34]. This is a non-trivial result, and is not easy to reproduce in models of dynamical electroweak symmetry breaking [35].

Although the addition of still more pairs of Higgs doublets and associated superpartners preserves the anomaly cancellation, gauge coupling unification is destroyed. As noted earlier, Higgs bosons (and superpartners) in triplet (and higher) representations also destroy the gauge unification. Only Higgs singlet representations can be appended to the minimal two doublets while preserving coupling constant unification. Thus, the minimal supersymmetric model with exactly two Higgs doublets is an especially attractive theory.

The imposition of supersymmetry and the addition of a second Higgs doublet have far-reaching consequences for the electroweak-symmetry-breaking mechanism. The potential for the Higgs doublets, ϕ_1 and ϕ_2 , including soft supersymmetry-breaking terms, is

$$V(\phi_1, \phi_2) = m_1^2 |\phi_1|^2 + m_2^2 |\phi_2|^2 - m_{12}^2 (\epsilon_{ij} \phi_1^i \phi_2^j + h.c.) + \frac{1}{8} (g^2 + g'^2) (|\phi_1|^2 - |\phi_2|^2)^2 + \frac{1}{2} g^2 |\phi_1^* \phi_2|^2 \quad (4)$$

where g and g' are the $SU(2)_L$ and $U(1)_Y$ couplings. The most important feature of this potential is that, unlike in the standard model, the magnitudes of the quartic potential terms are not arbitrary; they are constrained by the supersymmetry to be of magnitude g^2, g'^2 . This has the consequence that triviality and vacuum

stability are not issues; the mass of any physical Higgs boson that is SM-like, in that it has significant WW and ZZ couplings, is strictly limited, as are the radiative corrections to the quartic potential terms. Electroweak symmetry breaking occurs if the origin in Higgs-field space is a saddle point, which requires $S \equiv m_1^2 m_2^2 - m_{12}^4 < 0$. In the limit of exact supersymmetry, one has $m_1 = m_2 = \mu$ (where μ is the coefficient of the term $-\mu \epsilon_{ij} \hat{H}_1^i \hat{H}_2^j$ in the superpotential; \hat{H}_1 and \hat{H}_2 are the Higgs superfields) and $m_{12} = 0$, so electroweak symmetry breaking does not occur. Thus the Higgs-field vacuum-expectation values, v_1, v_2 , are naturally of the same size as the supersymmetry-breaking scale. Supersymmetry also makes the presence of fundamental scalar fields natural, although the Higgs fields are not the superpartners of any of the known fermions.

In supergravity grand-unified models, electroweak symmetry breaking arises “radiatively”, that is by evolving the parameters of the Higgs sector (including the soft SUSY-breaking parameters) from the GUT scale down to the weak scale via the renormalization group equations [36]. Due to the large mass of the top quark, the parameter m_2^2 is driven more rapidly towards zero (often to negative values) than are m_1^2 and m_{12}^2 , so that S is driven negative at the weak scale, triggering electroweak symmetry breaking. Thus, in these models, electroweak symmetry breaking is explained by the large top-quark mass (more precisely, by the large top-quark Yukawa coupling). Supergravity models can also explain why the scale of supersymmetry breaking (*i.e.*, the scale of the soft-supersymmetry-breaking terms) is comparable to the weak scale, rather than the GUT scale; this is a natural result if supersymmetry breaking occurs via a “hidden” sector.

As in the general 2HDM, the presence of two Higgs-doublet fields implies that the spectrum of Higgs particles is much richer in the minimal supersymmetric model than in the standard model. However, the two-doublet MSSM is a highly constrained version of the general 2HDM. First, the two-doublet MSSM Higgs couplings are automatically type-II, with one Higgs doublet (H_1) coupling only to down-type quarks and leptons, and the other (H_2) coupling only to up-type quarks. Secondly, in the MSSM, CP conservation in the Higgs sector is automatic (for a review and references, see [16]), and we find the previously-mentioned five physical Higgs particles: two CP -even neutral scalars, h^0 and H^0 ; a CP -odd neutral scalar (often called a pseudoscalar), A^0 ; and a pair of charged Higgs bosons, H^\pm . Further, due to the special form of the potential, Eq. 4, dictated by softly-broken supersymmetry, the Higgs sector is described (at tree level) by just two free parameters, only one more than the standard Higgs model. It is conventional to choose the mass of the pseudoscalar Higgs boson, m_{A^0} , and the ratio of the Higgs-field vacuum-expectation values, $\tan \beta \equiv v_2/v_1$, as the free parameters. Other parameters of the model affect the Higgs sector after including loop corrections [37]; the most important of these are the top-quark and the stop-squark masses, with parameters that influence stop-squark mixing also playing a significant role.

The dominant radiative corrections arise from an incomplete cancellation of the

virtual top-quark and stop-squark loops. The two stop-squark masses ($m_{\tilde{t}_1}$ and $m_{\tilde{t}_2}$) are obtained by diagonalizing a 2×2 stop-squark squared-mass matrix; the off-diagonal elements of this matrix involve the parameters μ and A_t , where μ is the coefficient of the term $-\mu\epsilon_{ij}\hat{H}_1^i\hat{H}_2^j$ in the superpotential (\hat{H}_1 and \hat{H}_2 are the Higgs superfields), and A_t is the coefficient appearing in the soft-supersymmetry-breaking potential term $A_th_t\epsilon_{ij}H_2^j\tilde{Q}^i\tilde{U}$ where, in the case of the stop squarks, $\tilde{Q} = \begin{pmatrix} \tilde{t}_L \\ \tilde{b}_L \end{pmatrix}$ and $\tilde{U} = \tilde{t}_R^*$. Here, h_t is the top-quark Yukawa coupling, $h_t = gm_t/(\sqrt{2}m_W)$.

We first give a summary of the corrections to the Higgs sector at one-loop, and then discuss the most important two-loop effects and renormalization group improvement of the one-loop terms. The leading effects (*i.e.* those proportional to m_t^4 , neglecting terms¹ of order $m_W^2m_t^2$ and $m_b^4\tan^2\beta$) at one-loop on the Higgs sector can be expressed [39] in terms of

$$\begin{aligned}\delta m_{11}^2 &\equiv \frac{3g^2}{16\pi^2 m_W^2} m_t^4 \mu^2 X_t^2 g(m_{\tilde{t}_1}^2, m_{\tilde{t}_2}^2) \\ \delta m_{12}^2 &\equiv \frac{3g^2}{16\pi^2 m_W^2} m_t^4 \mu X_t \left\{ h(m_{\tilde{t}_1}^2, m_{\tilde{t}_2}^2) + A_t X_t g(m_{\tilde{t}_1}^2, m_{\tilde{t}_2}^2) \right\} \\ \delta m_{22}^2 &\equiv \frac{3g^2}{16\pi^2 m_W^2} m_t^4 \left\{ 2 \ln \left(\frac{m_{\tilde{t}_1} m_{\tilde{t}_2}}{m_t^2} \right) + A_t X_t \left[2h(m_{\tilde{t}_1}^2, m_{\tilde{t}_2}^2) + A_t X_t g(m_{\tilde{t}_1}^2, m_{\tilde{t}_2}^2) \right] \right\},\end{aligned}\quad (5)$$

where $X_t \equiv A_t - \mu \cot \beta$. The functions $h(a, b)$ and $g(a, b)$ are defined by

$$h(a, b) \equiv \frac{1}{a-b} \ln \left(\frac{a}{b} \right), \quad g(a, b) \equiv \frac{1}{(a-b)^2} \left[2 - \frac{a+b}{a-b} \ln \left(\frac{a}{b} \right) \right]. \quad (6)$$

Note that in the $X_t = 0$ limit, where squark mixing is negligible, only δm_{22}^2 is non-zero, with its magnitude being determined by $\ln(m_{\tilde{t}_1} m_{\tilde{t}_2}/m_t^2)$, which vanishes in the supersymmetric limit of $m_{\tilde{t}_1} = m_{\tilde{t}_2} = m_t$.

For $m_{A^0} \sim \mathcal{O}(m_Z)$, the squared-masses of the CP-even neutral scalar Higgs bosons are obtained by diagonalizing the matrix:

$$\mathcal{M}^2 \equiv \begin{pmatrix} m_{A^0}^2 \sin^2 \beta + m_Z^2 \cos^2 \beta + \frac{\delta m_{11}^2}{\sin^2 \beta} & -(m_{A^0}^2 + m_Z^2) \sin \beta \cos \beta - \frac{\delta m_{12}^2}{\sin^2 \beta} \\ -(m_{A^0}^2 + m_Z^2) \sin \beta \cos \beta - \frac{\delta m_{12}^2}{\sin^2 \beta} & m_{A^0}^2 \cos^2 \beta + m_Z^2 \sin^2 \beta + \frac{\delta m_{22}^2}{\sin^2 \beta} \end{pmatrix} \quad (7)$$

yielding

$$m_{h^0, H^0}^2 = \frac{1}{2} [m_{A^0}^2 + m_Z^2 + (\delta m_{11}^2 + \delta m_{22}^2)/\sin^2 \beta]$$

¹The subdominant terms of $\mathcal{O}(m_W^2 m_t^2)$, not shown explicitly in the following equations, can be found in Ref. [38].

$$\pm \frac{1}{2} \left\{ [(m_{A^0}^2 - m_Z^2) \cos 2\beta + (\delta m_{22}^2 - \delta m_{11}^2) / \sin^2 \beta]^2 + [(m_{A^0}^2 + m_Z^2) \sin 2\beta + \delta m_{12}^2 / \sin^2 \beta]^2 \right\}^{1/2} \quad (8)$$

where $m_{h^0} < m_{H^0}$ by definition. Note that the neutral Higgs bosons satisfy the mass sum rule

$$m_{h^0}^2 + m_{H^0}^2 = m_{A^0}^2 + m_Z^2 + (\delta m_{11}^2 + \delta m_{22}^2) / \sin^2 \beta. \quad (9)$$

For $m_{A^0} \gg m_Z$, one of the two Higgs doublets decouples, leaving behind one light physical Higgs state with couplings identical to those of the SM Higgs boson. In this limit, m_{h^0} is obtained simply as the large- m_{A^0} limit of Eq. 8,

$$\begin{aligned} m_{h^0}^2 &\simeq m_Z^2 \cos^2 2\beta + [\delta m_{22}^2 + \delta m_{11}^2 \cot^2 \beta - 2\delta m_{12}^2 \cot \beta] \\ &= m_Z^2 \cos^2 2\beta + \frac{3g^2 m_t^4}{8\pi^2 m_W^2} \ln \left(\frac{m_{\tilde{t}_1} m_{\tilde{t}_2}}{m_t^2} \right) \\ &\quad + \frac{3g^2 m_t^4 X_t^2}{16\pi^2 m_W^2} [2h(m_{\tilde{t}_1}^2, m_{\tilde{t}_2}^2) + X_t^2 g(m_{\tilde{t}_1}^2, m_{\tilde{t}_2}^2)]. \end{aligned} \quad (10)$$

Eq. 10 sets an upper bound on m_{h^0} which is critical to ensuing discussions. Without the inclusion of the one-loop correction, the bound would be $m_{h^0} < m_Z$, and the lightest scalar Higgs boson would have been unable to escape detection at LEP2. After including the one-loop correction, m_{h^0} can be substantially larger than m_Z . For $m_{A^0} \gg m_Z$, the mass of the heavier H^0 cannot be obtained as the large m_{A^0} limit of Eq. 8 since radiative corrections must be computed at the large scale $\mathcal{O}(m_{A^0})$. Instead, one obtains the result

$$m_{H^0}^2 \simeq m_{A^0}^2 + m_Z^2 \sin^2 2\beta + \frac{3g^2 m_t^4 X_t Y_t \cot^2 \beta}{16\pi^2 m_W^2} [2h(m_{\tilde{t}_1}^2, m_{\tilde{t}_2}^2) + X_t Y_t g(m_{\tilde{t}_1}^2, m_{\tilde{t}_2}^2)], \quad (11)$$

where $Y_t = A_t + \mu \tan \beta$. The corrections proportional to m_t^4 are absent for $X_t = 0$, in which case the leading corrections are $\mathcal{O}(m_W^2 m_t^2)$.

The lower bound on m_{H^0} for any given $\tan \beta$ occurs for $m_{A^0} = 0$. An approximate form for the lower bound on m_{H^0} , obtained by evaluating Eq. 8 at $m_{A^0} = 0$ and neglecting terms proportional to $[\delta m_{ij}^2]^2$ relative to $m_Z^2 \delta m_{ij}^2$, is

$$m_{H^0}^2 \geq m_Z^2 + [\delta m_{22}^2 + \delta m_{11}^2 \cot^2 \beta]. \quad (12)$$

One-loop corrections proportional to m_t^4 to the charged Higgs boson mass arise only if there is mixing. One finds

$$m_{H^\pm}^2 \simeq m_{A^0}^2 + m_W^2 + \frac{\delta m_\pm^2}{\sin^2 \beta}, \quad (13)$$

with

$$\delta m_{\pm}^2 = \frac{3g^2}{32\pi^2 m_W^2} m_t^4 \mu^2 f(m_{t_1}^2, m_{t_2}^2), \quad (14)$$

where

$$f(a, b) \equiv \frac{-1}{a-b} \left[1 - \frac{b}{a-b} \ln \left(\frac{a}{b} \right) \right]. \quad (15)$$

There are also contributions to δm_{\pm}^2 that are of order $m_t^2 m_b^2 \tan^2 \beta$ and $m_b^4 \tan^4 \beta$, which could be as important as the m_t^4 terms if $\tan \beta \sim m_t/m_b$. For small μ , Eq. 13 implies that the charged Higgs boson has a lower bound of

$$m_{H^\pm}^2 > m_W^2. \quad (16)$$

The scalar Higgs boson mass eigenstates discussed above are mixtures of the neutral components of the real parts of the Higgs-doublet fields. In the case of the MSSM, the mixing angle, α , rather than being a free parameter as in the general two-Higgs-doublet model, is determined by m_{A^0} , $\tan \beta$ and (at one loop) the δm_{ij}^2 :

$$\begin{aligned} \sin 2\alpha &= \frac{2\mathcal{M}_{12}^2}{\sqrt{(\mathcal{M}_{11}^2 - \mathcal{M}_{22}^2)^2 + 4\mathcal{M}_{12}^4}} \\ \cos 2\alpha &= \frac{\mathcal{M}_{11}^2 - \mathcal{M}_{22}^2}{\sqrt{(\mathcal{M}_{11}^2 - \mathcal{M}_{22}^2)^2 + 4\mathcal{M}_{12}^4}} \end{aligned} \quad (17)$$

leading to, for example,

$$\tan 2\alpha = \frac{(m_{A^0}^2 + m_Z^2) \sin 2\beta + 2\delta m_{12}^2 / \sin^2 \beta}{(m_{A^0}^2 - m_Z^2) \cos 2\beta + (\delta m_{22}^2 - \delta m_{11}^2) / \sin^2 \beta}. \quad (18)$$

In our convention $0 < \beta < \pi/2$. The result for $\sin 2\alpha$ in Eq. 17 then implies that $-\pi/2 < \alpha < 0$ ($+\pi/2 > \alpha > 0$) for $\mathcal{M}_{12}^2 < 0$ (> 0). Referring to Eq. 7, we see that positive α is only possible if β is near 0 or $\pi/2$ and $\delta m_{12}^2 < 0$. The ensuing discussion assumes that $\alpha < 0$, as holds if δm_{12}^2 is small compared to $(m_{A^0}^2 + m_Z^2) \cos \beta \sin \beta$ and/or positive. Results for the alternative case are easily worked out.

There is an important transition that occurs at $\mathcal{M}_{11}^2 - \mathcal{M}_{22}^2 = 0$, *i.e.* $m_{A^0} = \sqrt{m_Z^2 - (\delta m_{22}^2 - \delta m_{11}^2) / (\cos 2\beta \sin^2 \beta)}$. For m_{A^0} values below this, $\cos 2\alpha$ is positive, implying that $-\pi/4 < \alpha < 0$. For larger m_{A^0} , $-\pi/2 < \alpha < -\pi/4$. In particular, for $\tan \beta \rightarrow \infty$ (*i.e.* $\beta \rightarrow \pi/2$) and neglecting δm_{12}^2 in \mathcal{M}_{12}^2 , if $m_{A^0} > \sqrt{m_Z^2 + (\delta m_{22}^2 - \delta m_{11}^2)}$ then $\alpha \simeq r(\beta - \pi/2) \rightarrow 0$, whereas for $m_{A^0} < \sqrt{m_Z^2 + (\delta m_{22}^2 - \delta m_{11}^2)}$ $\alpha \simeq -\pi/2 + r(\pi/2 - \beta) \rightarrow -\pi/2$ when $\beta \rightarrow \pi/2$, where

$$r \equiv \frac{m_{A^0}^2 + m_Z^2}{|m_{A^0}^2 - (m_Z^2 + \delta m_{22}^2 - \delta m_{11}^2)|}. \quad (19)$$

Note that $r = 1$ for $m_{A^0}^2 \rightarrow \infty$; $r = 1$ is also obtained at $m_{A^0}^2 = 0$ if the one-loop radiative corrections are small compared to m_Z^2 . These different behaviors of α will have important implications for the couplings of the h^0 and H^0 in the large $\tan\beta$ limit, as will be discussed in more detail shortly.

Two-loop corrections to the Higgs sector are also significant and can reduce the one-loop addition to the upper bound on m_{h^0} [38, 40]. Results for the leading $[\mathcal{O}(g^2\alpha_s m_t^4)$ and $\mathcal{O}(g^4 m_t^6)]$ two-loop corrections have been computed in the large $\tan\beta$ limit [38]. The most important two-loop effects can be incorporated by replacing m_t in the formulae above by the running top quark mass evaluated at m_t :

$$m_t(m_t) = m_t \left[1 - \frac{4}{3\pi}\alpha_s + \frac{1}{2\pi}\alpha_t \right] \approx 0.966m_t, \quad (20)$$

where $\alpha_t = h_t^2/(4\pi)$ and we maintain the notation m_t for the pole mass. For $m_t = 175$ GeV, $m_t(m_t)$ is roughly 169 GeV. Due to the leading m_t^4 behavior of the one-loop corrections, the replacement of m_t by $m_t(m_t)$ in the one-loop equations is numerically important, leading, as noted above, to a significant reduction in the upper bound on m_{h^0} .

If the scale of supersymmetry breaking is much larger than m_Z , then large logarithmic terms arise in the perturbative expansion (as seen, for example, in Eq. 10). These large logarithms can be re-summed to all orders in perturbation theory using renormalization group equations (RGE's). The formula for the full one-loop radiatively corrected Higgs mass is very complicated [41]. Moreover, the computation of the RGE-improved one-loop corrections requires numerical integration of a coupled set of RGE's [42]. (The dominant two-loop next-to-leading logarithmic results are also known [43]). Although this program has been carried out in the literature, the procedure is unwieldy and not easily amenable to large-scale Monte-Carlo analyses. Fortunately, very accurate and simple analytic formulae can be developed that incorporate the dominant effects of the RGE improvements. In particular, many of these effects can be included simply by a correct choice of the scale at which to evaluate the running top-quark mass in various pieces of the one-loop formulae. The method can be easily implemented, and incorporates both the leading one-loop and two-loop effects and the RGE improvement. Although the results are conceptually simple, complications arise when supersymmetric thresholds are fully taken into account. The details can be found in Ref. [38], along with other references to the original literature. Complementary work can be found in Ref. [40].

For the results presented in this review, we employ a numerical program based on the work of Ref. [38], combined with numerical routines developed for the work of Refs. [44, 45]. When referring to these results, we shall use the phrase ‘two-loop/RGE-improved’ to indicate that the corrections to the Higgs boson masses and the mixing angle α have included leading-logarithmic re-summation as well as the one-loop and two-loop corrections.

At the two-loop/RGE-improved level, *i.e.* after including one- and two-loop

radiative corrections and leading-log re-summation via the RGE's, the lower bound on m_{h^0} is significantly above m_Z ; for $m_t = 150, 175, 200$ GeV, if squark mixing is absent and $m_{\tilde{t}_1} = m_{\tilde{t}_2} \equiv m_{\tilde{t}} = 1$ TeV, the bound (reached for $\tan\beta \gg 1$ and large m_{A^0}) is of order $m_{h^0} < 102, 113, 127$ GeV, respectively. [These upper bounds can be compared to the values $m_{h^0} < 108, 122, 140$ (106, 118, 134) GeV obtained from the one-loop formulae using the pole (running $m_t(m_t)$) top-quark mass in Eq. 8.] The lower bounds on m_{H^0} (attained for high $\tan\beta$ and $m_{A^0} \rightarrow 0$) are essentially the same as the upper bounds on m_{h^0} — roughly 102, 113, 127 GeV for the above top masses.

The large m_{A^0} upper bound on m_{h^0} is less for smaller values of $\tan\beta$ and/or smaller $m_{\tilde{t}}$. For example, if $\tan\beta$ is near 1 then the mass of the h^0 typically arises primarily from loop corrections to the tree-level mass, with the result that $m_{h^0} \lesssim 100$ GeV is quite probable. More specifically, for $\tan\beta = 1.5$, $m_{\tilde{t}} = 1$ TeV and large m_{A^0} one finds (at the ‘two-loop/RGE-improved’ level) $m_{h^0} = 60, 78, 98$ GeV for $m_t = 150, 175, 200$ GeV, respectively.

As further illustration, Fig. 2 gives the mass contours in $(m_{A^0}, \tan\beta)$ parameter space for the h^0 and H^0 in the case of $m_t = 175$ GeV and for degenerate stop-squark masses of $m_{\tilde{t}} = 1$ TeV (upper plots) and 500 GeV (lower plots), after including two-loop/RGE-improved corrections. Note that for the lower stop mass the radiative corrections are substantially reduced. For $m_{\tilde{t}} \sim 300$ GeV, the upper limit of m_{h^0} is ~ 100 GeV. Fig. 2 not only illustrates the upper bound on m_{h^0} at large m_{A^0} and $\tan\beta$, but also demonstrates the rapid decline of m_{h^0} from its upper bound and approach of m_{H^0} to its lower bound in the (as we shall see, unlikely) case that $m_{A^0} < \sqrt{m_Z^2 + (\delta m_{22}^2 - \delta m_{11}^2)}$. Below, we shall see that when $m_{A^0} > \sqrt{m_Z^2 + (\delta m_{22}^2 - \delta m_{11}^2)}$ the h^0 has roughly SM-like couplings while the H^0 decouples from WW, ZZ , whereas for lower m_{A^0} the H^0 has roughly SM-like couplings (squared), and the h^0 decouples from WW, ZZ .

As we have already seen, the above results are altered in the presence of significant squark mixing because of large values for the supersymmetry parameters A_t and μ , defined earlier. If A_t and/or μ are large, then the upper bound on m_{h^0} increases due to an increase in the two-loop/RGE-improved corrections, which grow with larger mixing in the stop squark sector. (At very large $\tan\beta$, mixing in the sbottom squark sector can also play a role. We assume that $A_b = A_t$ and denote the common value by A .) In what follows, in addition to the ‘no-mixing’ scenario for which we have given specific numerical results above, we also consider the ‘typical-mixing’ scenario with $A = -\mu = M_{SUSY}$ and ‘maximal-mixing’ scenario with $A = \sqrt{6}M_{SUSY}$, $\mu = 0$. M_{SUSY} is to be identified with the value of $m_{\tilde{t}}$ in the no-mixing scenario. In the maximal-mixing case, the upper bound on m_{h^0} for $M_{SUSY} = 1$ TeV at large $\tan\beta$ and large m_{A^0} is ~ 125 GeV (~ 150 GeV) for $m_t = 175$ GeV (200 GeV).

Placing the MSSM in the context of unified supergravity or string boundary

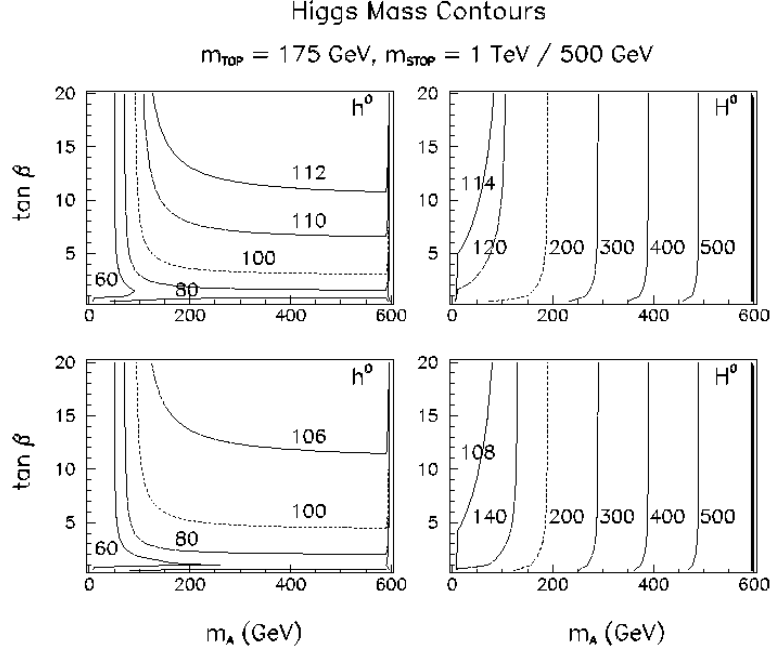


Figure 2: Contours for the h^0 and H^0 masses in $(m_{A^0}, \tan \beta)$ parameter space. Results are given for $m_t = 175 \text{ GeV}$, with $m_{\tilde{t}} = 1 \text{ TeV}$ (upper plots) and $m_{\tilde{t}} = 500 \text{ GeV}$ (lower plots). The masses are computed including two-loop/RGE-improved radiative corrections, neglecting squark mixing.

conditions leads to substantial prejudice as to what the relevant parameters are [46, 47]. Such models are attractive, not only in that gauge coupling unification at a high scale M_X is successful, but also in that proper electroweak symmetry breaking at scales below a TeV is more or less automatic. Minimal constraints on the models from the requirements of correct Z mass, uncharged LSP, perturbative Yukawa couplings and no SUSY particles (such as charginos or sneutrinos) below $m_Z/2$ are already sufficient to imply significant constraints on the m_Z -scale Higgs sector parameters. Typically, there are few or no M_X -scale parameter choices that yield values of m_{A^0} below about $2m_Z$. Additional theoretical prejudices can yield very strong additional constraints. For example, unification of the Yukawa couplings of the b and τ at M_X is only possible if $\tan\beta$ is very near 1 or else very large ($\gtrsim 30$) [48]. As another example, dilatonic or no-scale supergravity style M_X -scale boundary conditions often lead to modest values for the squark masses (especially for the lightest stop squark) [49].

The neutral Higgs sector angles α (see Eq. 18) and β figure prominently in the couplings of the SUSY Higgs bosons to weak vector bosons and fermions. We list these couplings in Table 1; these factors multiply the corresponding standard-model coupling in Fig. 1. The neutral scalar Higgs bosons, h^0 and H^0 , couple to the weak bosons proportional to $\sin(\beta - \alpha)$ and $\cos(\beta - \alpha)$, respectively; they share the squared-coupling of the standard Higgs boson to the weak bosons. Similarly, WW , ZZ and ZA share the squared-coupling to a given scalar Higgs boson. Note that there are no tree-level $W^\mp Z H^\pm$, AWW , nor AZZ couplings.

Table 1: Couplings of the neutral Higgs bosons of the minimal supersymmetric model. These multiply the couplings of the standard Higgs boson given in Fig. 1.

	WW, ZZ	ZA^0	$t\bar{t}$	$b\bar{b}, \tau^+\tau^-$
h^0	$\sin(\beta - \alpha)$	$\cos(\beta - \alpha)$	$\cos\alpha/\sin\beta$	$-\sin\alpha/\cos\beta$
H^0	$\cos(\beta - \alpha)$	$\sin(\beta - \alpha)$	$\sin\alpha/\sin\beta$	$\cos\alpha/\cos\beta$
A^0	0	0	$\gamma_5 \cot\beta$	$\gamma_5 \tan\beta$

Table 2: Couplings of the h^0 and H^0 in the limit of $\alpha \rightarrow r(\beta - \pi/2)$, applicable for: i) $m_{A^0} \rightarrow \infty$, for which $r \rightarrow 1$; ii) $\tan\beta \rightarrow \infty$ (*i.e.* $\beta \rightarrow \pi/2$), $m_{A^0} > \sqrt{m_Z^2 + \delta m_{22}^2 - \delta m_{11}^2}$, and $\delta m_{12}^2 \sim 0$, with r as defined in Eq. 19.

	WW, ZZ	ZA^0	$t\bar{t}$	$b\bar{b}, \tau^+\tau^-$
h^0	1	0	1	r
H^0	0	1	$-r \cot\beta$	$\tan\beta$

Table 3: Couplings of the h^0 and H^0 in the limit of $\alpha \rightarrow -\pi/2 + r(\pi/2 - \beta)$, applicable for $\tan \beta \rightarrow \infty$ (*i.e.* $\beta \rightarrow \pi/2$), $m_{A^0} < \sqrt{m_Z^2 + \delta m_{22}^2 - \delta m_{11}^2}$, and $\delta m_{12}^2 \sim 0$, with r as defined in Eq. 19.

	WW, ZZ	ZA^0	$t\bar{t}$	$b\bar{b}, \tau^+\tau^-$
h^0	0	-1	$r \cot \beta$	$\tan \beta$
H^0	-1	0	-1	r

There are three limits which are of particular interest:

1. $m_{A^0} \rightarrow \infty$: In this limit, the mass of h^0 is driven to its upper bound, given at one-loop by Eq. 10. In addition, $\alpha \rightarrow \beta - \pi/2$. The limits of the couplings are given in Table 2, with $r = 1$. The couplings of h^0 become identical to those of the standard Higgs boson. The H^0 decouples from the weak bosons. The squares of the fermionic couplings of H^0 and A^0 become identical. The masses of the H^0 , A^0 , and H^\pm become degenerate and heavy, leaving behind h^0 , which acts like the minimal standard Higgs boson.
2. $\tan \beta \rightarrow \infty$, $m_{A^0}^2 > m_Z^2 + \delta m_{22}^2 - \delta m_{11}^2$: In this limit, if squark mixing is small so that δm_{12}^2 can be neglected, $\alpha \rightarrow r(\beta - \pi/2)$ as $\beta \rightarrow \pi/2$, where r is defined in Eq. 19 (see discussion associated with Eq. 18). The couplings, given in Table 2, are similar to those obtained in the large m_{A^0} limit, except for the fact that $r \neq 1$ in general (see Eq. 19). The WW, ZZ and $t\bar{t}$ couplings of the h^0 become equal to those of the standard Higgs boson, while the $h^0 \rightarrow b\bar{b}$ coupling acquires an extra factor of r . The (enhanced) $H^0 \rightarrow b\bar{b}$ coupling becomes equal to the $A^0 \rightarrow b\bar{b}$ coupling, while the (suppressed) $H^0 \rightarrow t\bar{t}$ coupling acquires an extra factor of $-r$ relative to the $A^0 \rightarrow t\bar{t}$ coupling. If $\delta m_{12}^2 \neq 0$, α no longer approaches 0 exactly, and the couplings are correspondingly modified.
3. $\tan \beta \rightarrow \infty$, $m_{A^0}^2 < m_Z^2 + \delta m_{22}^2 - \delta m_{11}^2$: If δm_{12}^2 can be neglected, then $\alpha \rightarrow -\pi/2 + r(\pi/2 - \beta)$ as $\beta \rightarrow \pi/2$, with r given by Eq. 19. The couplings then have the limits given in Table 3. The H^0 has couplings to WW, ZZ and $t\bar{t}$ that are the same as the SM Higgs up to an overall sign, but the $b\bar{b}$ coupling differs by a factor of r relative to the SM value. The h^0 has the same coupling as the A^0 to $b\bar{b}$, but its coupling to $t\bar{t}$ differs by a factor of r . If $\delta m_{12}^2 \neq 0$, α no longer approaches $-\pi/2$ exactly, and these results are correspondingly modified.

These limits, as well as the sometimes rather slow approach to the $m_{A^0} \rightarrow \infty$ limits are illustrated in Fig. 3. There we plot the ratios of the $H^0 WW$, $H^0 b\bar{b}$, $H^0 t\bar{t}$,

$h^0 b\bar{b}$ and $h^0 t\bar{t}$ squared couplings to the corresponding ϕ^0 squared couplings as a function of m_{A^0} for the case of $\tan\beta = 5$, taking $m_t = 175$ GeV and $m_{\tilde{t}} = 1$ TeV, and including two-loop/RGE-improved corrections assuming no squark mixing. Especially important features to note from this figure are:

1. the continuing enhancement of the $h^0 b\bar{b}$ squared coupling out to quite large m_{A^0} values;
2. the very rapid fall of the $H^0 WW$ squared coupling, $\propto \cos^2(\beta - \alpha)$, implying a correspondingly rapid approach of the $h^0 WW$ squared coupling to the SM value; and
3. the very rapid rise of the $H^0 b\bar{b}$ squared coupling as m_{A^0} passes above m_Z .

Each of these features will have crucial phenomenological implications in what follows. The lightest SUSY Higgs boson, h^0 , has particular significance for the search for supersymmetry because it is the only particle whose mass is bounded from above. If supersymmetry is relevant to weak-scale physics, it may first appear via the discovery of this particle.

1.4 Higgs decays

The standard Higgs boson couples to the weak bosons proportionally to their squared mass, and to fermions proportional to their mass, as shown in Fig. 1. Thus the Higgs boson tends to decay to the heaviest pair of particles which is kinematically allowed [50]. There are important exceptions to this rule, however. If the Higgs boson is heavier than twice the top-quark mass, it will still decay dominantly to weak-vector-boson pairs; for $m_t = 175$ GeV, the branching ratio to $t\bar{t}$ is at most 20% (for $m_{\phi^0} \sim 500$ GeV). If the Higgs-boson mass is not far below the WW threshold, it has a sizable branching ratio to one real, one virtual W boson (WW^*), as well as to one real, one virtual Z boson (ZZ^*) [51]. The dominant fermionic decay mode in this region is $b\bar{b}$, and the suppressed coupling of the Higgs boson to the bottom quark allows the one real, one virtual weak boson decays to be competitive (for $m_{\phi^0} \gtrsim 120$ GeV). The next largest fermionic branching ratio is to $\tau^+\tau^-$, which is suppressed relative to $b\bar{b}$ due to the heavier b -quark mass and the three b -quark colors. The branching ratio of the standard Higgs boson to various final states is shown in Fig. 4. Ref. [52] provides an up-to-date review of the QCD radiative corrections that must be incorporated in the branching ratio calculations. The specific results presented here for the SM Higgs and later for SUSY Higgs bosons are obtained with the following inputs: i) we take $\Lambda_{\overline{MS}} = 290$ MeV for $N_f = 4$ flavors, corresponding to $\alpha_s(m_Z) \simeq 0.115$ at two-loops; ii) we take running masses of $m_c(m_c) = 1.23$ GeV and $m_b(m_b) = 4.0$ GeV; iii) we use a renormalization scale of $\mu = m_h/2$, where m_h is the mass of the decaying Higgs boson; iv) partial width contributions arising from QCD correction diagrams

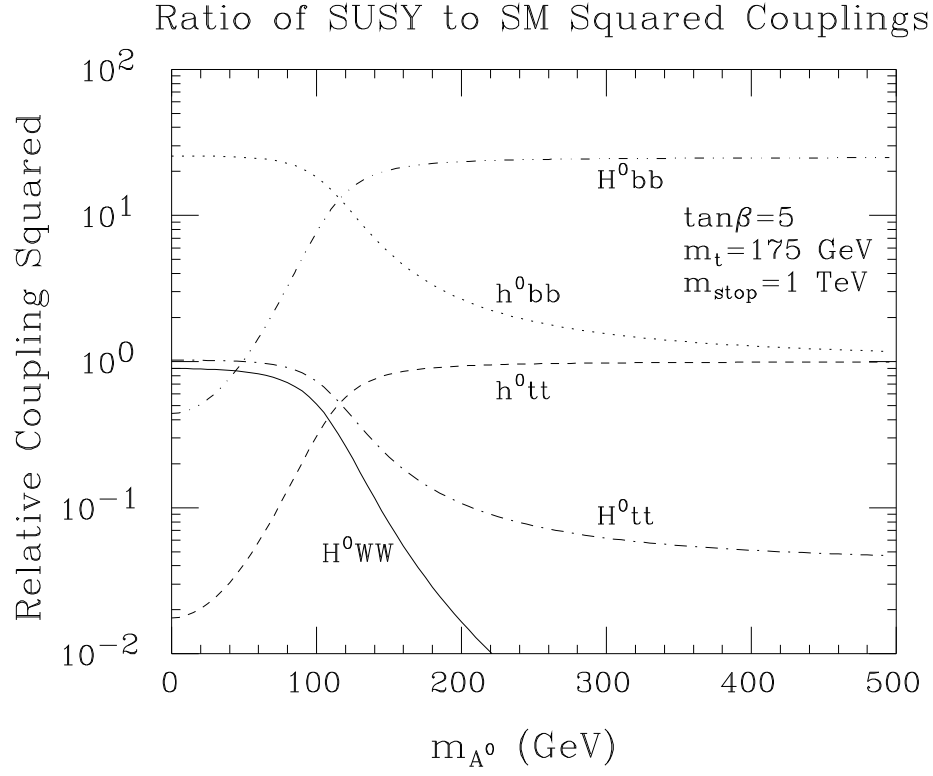


Figure 3: Ratios of SUSY Higgs squared couplings to the corresponding SM values as a function of m_{A^0} for the case of $\tan\beta = 5$, taking $m_t = 175 \text{ GeV}$ and $m_{\tilde{t}} = 1 \text{ TeV}$. Two-loop/RGE-improved radiative corrections to the CP-even Higgs sector mass matrix are included and squark mixing is neglected.

containing one gluon and a $q\bar{q}$ pair are added to the $q\bar{q}$ pair partial width, and not included in the two-gluon partial width; v) semi-virtual decays of the type $t\bar{t}^*$, and (for SUSY Higgs) Z^*A and $W^\mp H^\pm$, are not included; and, finally, vi) double virtual W^*W^* and Z^*Z^* decays are neglected, but, of course, semi-virtual WW^* and ZZ^* decays are incorporated.

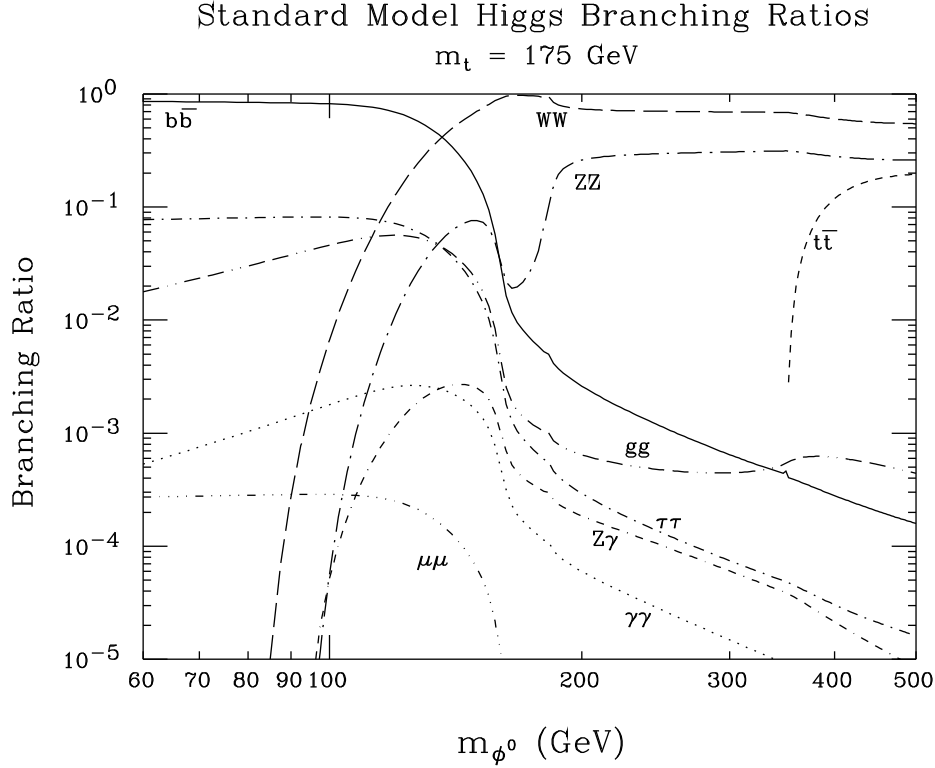


Figure 4: Branching ratios for the Standard Model Higgs boson. We have taken $m_t = 175 \text{ GeV}$.

Another phenomenologically-important decay mode is to $\gamma\gamma$, which occurs via a one-loop diagram [53]. The W boson gives the dominant contribution to the loop; the next most important is the top quark, which contributes with the opposite sign, but much less than the W loop. The branching ratio peaks at about 2×10^{-3} , for $m_{\phi^0} \approx 125 \text{ GeV}$. The branching ratio to $Z\gamma$, which also occurs at one loop, is comparable to $\gamma\gamma$, although it is not phenomenologically useful due to the small branching ratio of $Z \rightarrow \ell\ell$ ($\ell = e, \mu$) [54].

The branching ratios (and production cross sections) of the SUSY Higgs bosons can be very different from those of the standard Higgs boson. We restrict our discussion to the most important features. The following features are evident from Tables 1, 2 and 3, and are displayed in Fig. 3. The coupling of the neutral

scalar Higgs bosons to the weak bosons is at most as large as that of the standard Higgs boson. Thus, the branching ratio of the SUSY Higgs bosons to weak-vector-boson pairs can be suppressed with respect to the standard Higgs. For example, as $m_{A^0} \rightarrow \infty$, the heavy scalar Higgs decouples from weak-vector-boson pairs. On the other hand, the coupling of the SUSY Higgs bosons to $b\bar{b}, \tau^+\tau^-$ can be increased over that of the standard Higgs for $\tan\beta > 1$. In particular, the A^0 , and for $m_{A^0} > \sqrt{m_Z^2 - (\delta m_{22}^2 - \delta m_{11}^2)/(\cos 2\beta \sin^2 \beta)}$ the H^0 , both have enhanced $b\bar{b}, \tau^+\tau^-$ couplings, while these couplings for the h^0 become increasingly SM-like as m_{A^0} becomes large. For $m_{A^0} < \sqrt{m_Z^2 - (\delta m_{22}^2 - \delta m_{11}^2)/(\cos 2\beta \sin^2 \beta)}$ the $b\bar{b}, \tau^+\tau^-$ couplings of the h^0 are enhanced as $\tan\beta$ increases, and the squares of the H^0 couplings to WW, ZZ and $t\bar{t}$ become SM-like; the $H^0 \rightarrow b\bar{b}$ coupling is generally somewhat reduced relative to the SM-like value. (As noted earlier, see Eq. 18 and associated discussion, the transition as to whether it is the h^0 or H^0 that has enhanced couplings is determined by the denominator of $\tan 2\alpha$, which determines whether $\alpha \rightarrow 0$ or $\alpha \rightarrow -\pi/2$ when $\beta \rightarrow \pi/2$, *i.e.* $\tan\beta \rightarrow \infty$.) Enhanced $b\bar{b}, \tau^+\tau^-$ couplings further suppress the branching ratio of the SUSY Higgs bosons to weak vector bosons. In general, even at large m_{A^0} the SM-like h^0 will have slightly enhanced $b\bar{b}, \tau^+\tau^-$ and slightly suppressed WW couplings and branching ratios; this is illustrated in Fig. 3 and in a later section in Fig. 24. In addition, this combination implies a suppression of the decay width and branching ratio of the h^0 to the $\gamma\gamma$ channel.

MSSM Higgs bosons can also decay to channels that are not present in the case of the SM ϕ^0 . To determine those additional channels that are important requires a rather complete specification of the MSSM parameters. Aside from the SM decay modes there is the possibility of decays to channels involving the other Higgs bosons ($h^0 \rightarrow A^0 A^0$, $A^0 \rightarrow Z h^0$, $H^0 \rightarrow h^0 h^0$, $A^0 A^0$, $H^+ \rightarrow W^+ h^0, W^+ A^0$), and all the Higgs bosons can have large branching ratios for decay to pairs of supersymmetric particles (for example, $h^0 \rightarrow \tilde{\chi}_1^0 \tilde{\chi}_1^0$ and $H^0, A^0 \rightarrow \tilde{\chi}_1^0 \tilde{\chi}_1^0, \tilde{\chi}_2^0 \tilde{\chi}_1^0, \tilde{\chi}_1^+ \tilde{\chi}_1^-, \tilde{\ell} \tilde{\ell}$ — here the $\tilde{\chi}$'s are the charginos and neutralinos and $\tilde{\ell}$ denotes a slepton). The decay of A^0, H^0, H^+ to channels containing the h^0 are typically quite important below the $A^0, H^0 \rightarrow t\bar{t}$, $H^+ \rightarrow t\bar{b}$ thresholds, and in the case of the A^0 and H^0 can even be dominant over the normal $b\bar{b}$ channel unless $\tan\beta$ is large. For example, we illustrate the importance of the $h^0 h^0$ decay mode for the H^0 in Fig. 5, taking $\tan\beta = 2$, $m_t = 175$ GeV, $m_{\tilde{t}} = 1$ TeV and neglecting squark mixing. At the lowest m_{H^0} values, $A^0 A^0$ and, even, $Z A^0$ decays are also important. At low m_{H^0} , the ZZ^* partial width is also rather suppressed after including the two-loop/RGE-improved corrections, which lower the minimum m_{H^0} value. In combination with the large partial widths for the $h^0 h^0, A^0 A^0, Z A^0$ modes, this implies a rather small ZZ^* branching ratio at the lowest m_{H^0} values. Similarly, for small to moderate values of $\tan\beta$ the supersymmetric-pair channels will often dominate over all other modes if kinematically allowed. Of particular note is the $\tilde{\chi}_1^0 \tilde{\chi}_1^0$ decay mode, where $\tilde{\chi}_1^0$ is

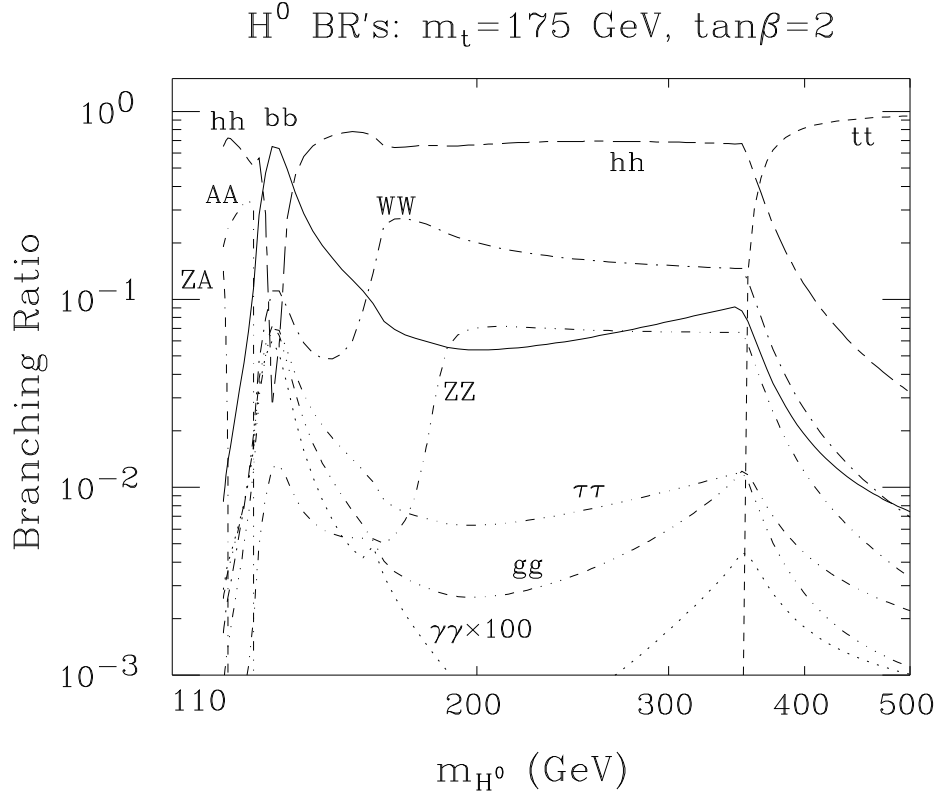


Figure 5: Selected branching ratios for the MSSM H^0 for $\tan\beta = 2$ and $m_t = 175$ GeV. Two-loop/RGE-improved radiative corrections to the CP-even Higgs sector mass matrix and Higgs self-couplings are included for $m_{\tilde{t}} = 1$ TeV and neglecting squark mixing. SUSY decays are assumed to be absent.

presumed to be the lightest supersymmetric particle and therefore invisible in an R -parity conserving model. For more graphs of branching ratios in some typical cases (before including two-loop/RGE-improved corrections), see Refs. [44, 45], especially the latter for the case of light $\tilde{\chi}$'s. In what follows, we will occasionally discuss the complications which these two additional classes of decay modes can create.

1.5 Higgs total widths

The magnitude of the width of a Higgs boson plays an important role in determining appropriate techniques for its discovery, and ultimately is a very important probe of the Higgs boson's interactions and decays. Higgs boson widths are extremely mass and model dependent.

In the case of the SM ϕ^0 , the Higgs boson width is very small for m_{ϕ^0} below about $2m_W$. Once $m_{\phi^0} \gtrsim 2m_W$ the Higgs width increases rapidly as the WW and then ZZ channels open up. The width as a function of mass is plotted in Fig. 6.

The widths of the neutral MSSM Higgs bosons are also plotted as a function of mass in Fig. 6 for two values of $\tan\beta$ — $\tan\beta = 2$ and $\tan\beta = 20$. We have taken $m_{\tilde{t}} = 1$ TeV and $m_t = 175$ GeV and included two-loop/RGE-improved corrections to masses and mixing angles; stop squark mixing has been neglected and SUSY decay channels are assumed to be absent. The width of the h^0 depends very strongly on its mass. For masses substantially below the upper limit (as arise for $m_{A^0} \lesssim m_Z$) and $\tan\beta$ values above 1, its width will be much larger than the width of a SM ϕ^0 of the same mass. As m_{h^0} approaches its upper limit, the h^0 becomes more and more SM-like and its width approaches that of the SM ϕ^0 . As far as its couplings to $f\bar{f}$ and WW, ZZ channels are concerned, the H^0 becomes roughly (see earlier coupling discussion) SM-like for m_{H^0} very near its lower limit (*i.e.* at small m_{A^0}). However, the $H^0 \rightarrow A^0 A^0, ZA^0, h^0 h^0$ decay channels are open and give large contributions to the total width of the H^0 when $\tan\beta = 2$ (see Fig. 5), implying $\Gamma_{tot}(H^0) \gg \Gamma_{tot}(\phi^0)$ for m_{H^0} near its lower bound. The $H^0 \rightarrow h^0 h^0$ channel is also responsible for the larger H^0 total width as compared to the A^0 total width in the 200 – 300 GeV mass range when $\tan\beta = 2$. At $\tan\beta = 20$, for h^0, A^0 when $m_{A^0} \lesssim m_Z$ and for H^0, A^0 when $m_{A^0} \gtrsim m_Z$ the $b\bar{b}$ decay channel is dominant due to its very large partial width. This partial width is large and more or less the same for the two members of a given pair due to the fact that their $b\bar{b}$ couplings are both related to the SM value by a factor of $\tan\beta$ when $\tan\beta \gg 1$ (see Tables 1, 2 and 3, and associated comments). Thus, one sees a smooth transition as m_{A^0} passes above $\sim m_Z$ where the h^0 and H^0 interchange roles.

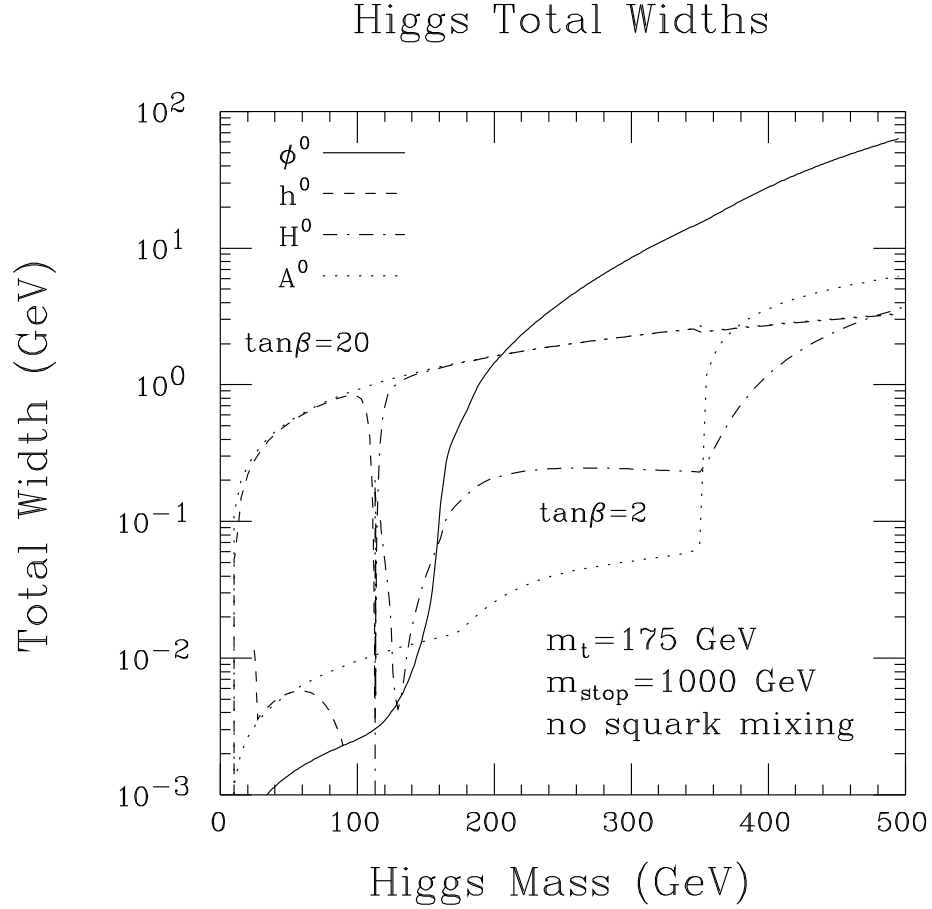


Figure 6: Total width versus mass of the SM and MSSM Higgs bosons for $m_t = 175$ GeV. In the case of the MSSM, we have plotted results for $\tan\beta = 2$ and 20, taking $m_{\tilde{t}} = 1$ TeV and including two-loop/RGE-improved radiative corrections, neglecting squark mixing; SUSY decay channels are assumed to be absent.

1.6 Biases from precision electroweak data

Sensitivity to the Higgs mass from precision electroweak data is only logarithmic. If the analysis is carried out without ascribing the excess in $R_{b\bar{b}}$ to new physics (supersymmetry or whatever), then a not insignificant preference for light Higgs boson masses emerges. The current situation has been summarized in Refs. [55, 56, 57]. A typical example is the recent work of Ref. [58] — see also Refs. [60, 61]. In Ref. [58] the $\Delta\chi^2 = 1$ contours yield a Higgs mass of 36^{+56}_{-22} GeV based on precision electroweak data alone, and a mass of 76^{+152}_{-50} GeV after including the CDF/D0 m_t measurement. In the latter case, the 2σ upper limit on the mass is 700 GeV, definitely in the perturbative Higgs sector domain. The Higgs mass values in the vicinity of the χ^2 minimum are remarkably consistent with the MSSM expectations for the h^0 . Indeed, Ref. [58] states that after including theoretical constraints (such as Higgs mass bounds from stability and experiment) the 1σ mass range is found to be slightly more preferred in the MSSM than in the minimal standard model.

However, if the $R_{b\bar{b}}$ excess arises from new physics, and the precision electroweak data is refit after reducing $R_{b\bar{b}}$ to its SM-like value, the above preference for low values of the Higgs mass essentially disappears [59].

1.7 Goals and organization

In this report we review the search for the standard Higgs boson, and the Higgs bosons of the minimal supersymmetric standard model, at present and future colliders. A short summary of this work appeared in Ref. [62]. The order of presentation is as follows:

- CERN LEP I - $\sqrt{s} = 91$ GeV e^+e^- collider.
- CERN LEP2 - $\sqrt{s} = 176 - 184$ GeV, with an upgrade to 192 GeV. We also consider upgrades to 205 and 240 GeV.
- CERN Large Hadron Collider (LHC) - $\sqrt{s} = 14$ TeV pp collider. We also comment on an intermediate-stage LHC with $\sqrt{s} = 10$ TeV.
- Fermilab Tevatron and Tev* - $\sqrt{s} = 2$ TeV $p\bar{p}$ collider. The Tev* (“Tev-star”) is a proposed luminosity upgrade of the Tevatron.
- Fermilab DiTevatron - A proposed $\sqrt{s} = 4$ TeV $p\bar{p}$ collider in the Tevatron tunnel.
- Next linear e^+e^- collider (NLC) - $\sqrt{s} = 500 - 1500$ GeV, including $\gamma\gamma$ and $e\gamma$ collider modes.
- A $\mu^+\mu^-$ collider - $\sqrt{s} = 500 - 4000$ GeV.

We attempt to summarize the results of the most current analyses of the search for Higgs bosons at present and future colliders. Throughout this report, we consider a particle to be discovered when the signal exceeds a five sigma fluctuation of the background ($S/\sqrt{B} > 5$). We also consider the measurement of the properties of the Higgs bosons.

2 LEP I

2.1 Standard Higgs boson

The standard Higgs boson is searched for in Z decays via the process $Z \rightarrow Z^* \phi^0$, with $Z^* \rightarrow f\bar{f}$ (Z^* denotes a virtual Z boson), where $f\bar{f} = \nu\bar{\nu}, e^+e^-, \mu^+\mu^-$ [63]. The lower bound on the Higgs mass is given in Table 4 for all four LEP experiments [64, 65]. Although a combined limit does not exist, one can be estimated as $m_{\phi^0} > 64.5$ GeV [65]. The most recent summary [66] does not find a significantly different result. Since the branching ratio falls rapidly with increasing Higgs mass, and because there exist Higgs candidate events at the highest masses, this bound will not improve significantly with increased statistics. Thus the ultimate reach of LEP I is likely to be close to the existing bound.

Table 4: Lower limits (95% C. L.) on the Higgs-boson mass from the four LEP experiments [65]. The limits include data taken in 1993, and are slightly higher than the published limits [64]. The combined limit is an estimate [65] (see also Ref. [66]).

	m_{ϕ^0} (GeV)
ALEPH	60.3
DELPHI	58.3
L3	58.0
OPAL	56.9
<hr/>	
Combined	64.5

The decay $Z \rightarrow \phi^0 \gamma$, which occurs at one loop, does not have a large enough branching ratio to be useful [54, 65].

2.2 SUSY Higgs bosons

There are two production mechanisms for SUSY Higgs bosons at LEP I. The analogue of the standard Higgs process is $Z \rightarrow Z^* h^0$. There is also the decay

$Z \rightarrow A^0 h^0$, if both h^0 and A^0 are light. The $Z \rightarrow A^0 h^0$ decay can yield a variety of final states: $\tau^+ \tau^- b \bar{b}$, $\tau^+ \tau^- \tau^+ \tau^-$, and $b \bar{b} b \bar{b}$. If $m_{h^0} > 2m_{A^0}$, the decay $h^0 \rightarrow A^0 A^0$ becomes the dominant decay mode of the h^0 , leading to $Z \rightarrow A^0 h^0 \rightarrow A^0 A^0 A^0$. This yields six-body final states with b 's and τ 's. The contribution of $Z \rightarrow A^0 h^0$ to the Z width can also be used as a probe of this decay mode.

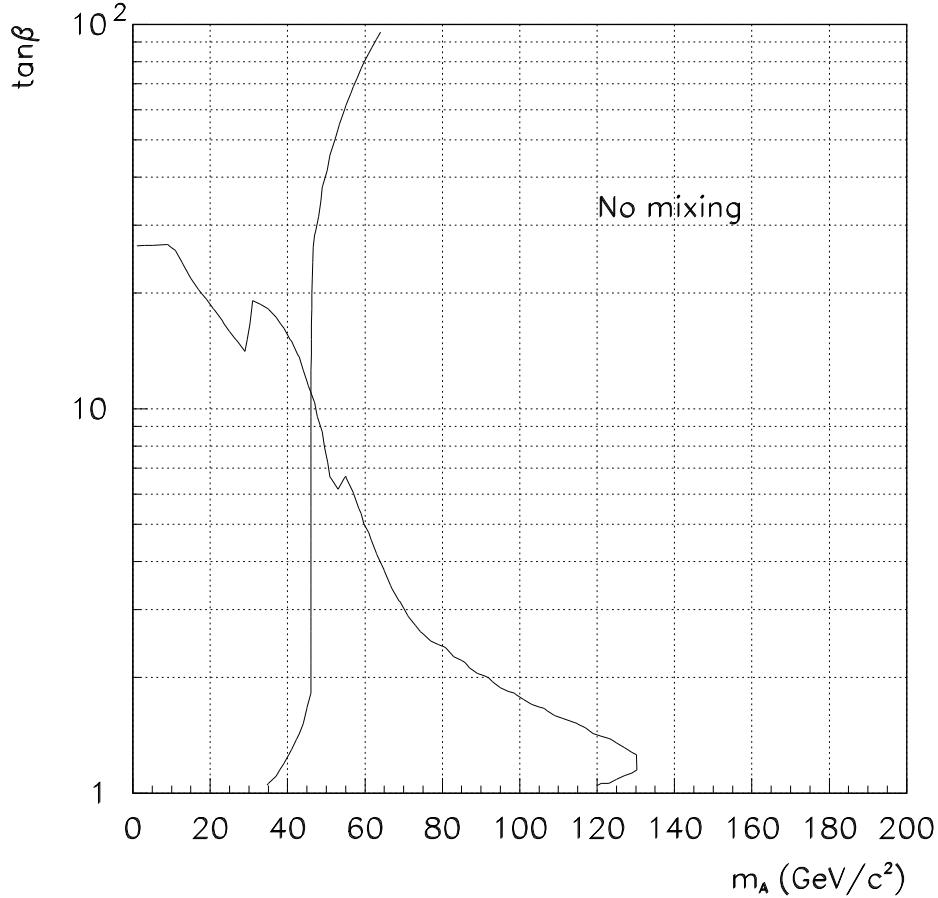


Figure 7: Excluded regions in the $(m_{A^0}, \tan \beta)$ plane of the minimal supersymmetric model from LEP I for the ‘no-mixing’ scenario with $A = \mu = 0$, $M_{SUSY} = 1 \text{ TeV}$ and $m_t = 175 \text{ GeV}$. The regions excluded by $Z \rightarrow Z^* h^0$ and by $Z \rightarrow A^0 h^0$ (based on the Z width and the $\tau^+ \tau^- b \bar{b}$, $\tau^+ \tau^- \tau^+ \tau^-$, and $b \bar{b} b \bar{b}$ final states) are indicated separately. The more or less vertical curve defines the region excluded by $Z \rightarrow A^0 h^0$. Figure from Ref. [71].

The regions of SUSY parameter space that are excluded at LEP I using $Z \rightarrow A^0 h^0$ and $Z \rightarrow Z^* h^0$ are illustrated in Figs. 7–9. The $Z \rightarrow A^0 h^0$ decay is crucial in eliminating large $\tan \beta$ values at low m_{A^0} , while $Z \rightarrow Z^* h^0$ extends the excluded region at lower $\tan \beta$ values to somewhat higher m_{A^0} values. Fig. 7 shows the

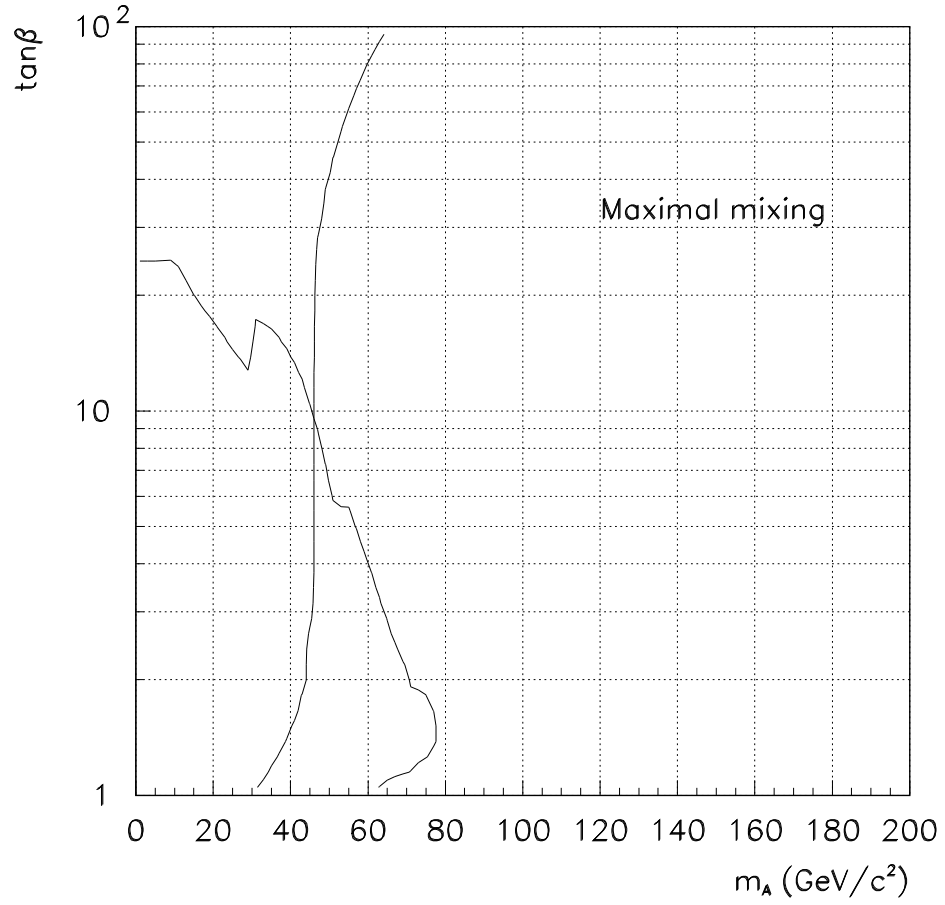


Figure 8: Excluded regions in the $(m_{A^0}, \tan\beta)$ plane of the minimal supersymmetric model from LEP I for the ‘maximal-mixing’ scenario with $A = \sqrt{6}M_{SUSY}$, $\mu = 0$, $M_{SUSY} = 1\text{ TeV}$ and $m_t = 175\text{ GeV}$. See caption for Fig. 7.

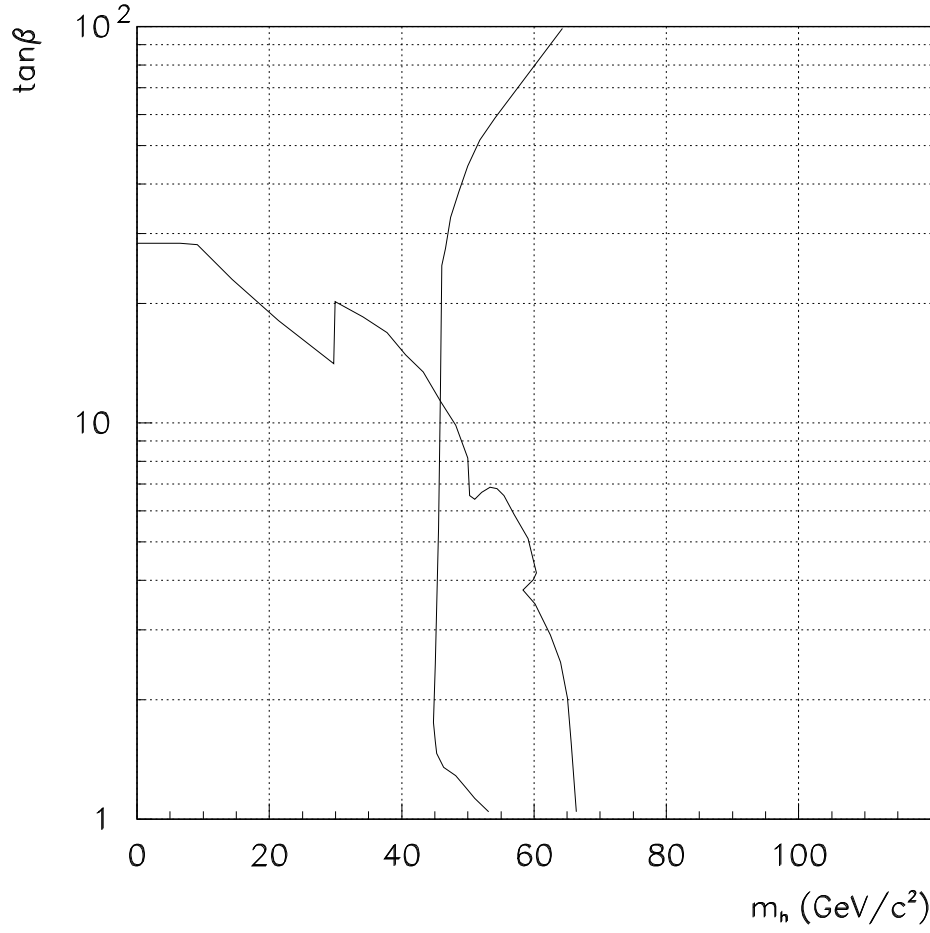


Figure 9: Excluded regions in the $(m_h, \tan\beta)$ plane of the minimal supersymmetric model from LEP I for $M_{SUSY} = 1 \text{ TeV}$ and $m_t = 175 \text{ GeV}$; boundaries for the different mixing scenarios cannot be distinguished in this parameter plane. See caption for Fig. 7.

excluded regions in the $(m_{A^0}, \tan \beta)$ plane from Ref. [71] in the ‘no-mixing’ scenario with $M_{SUSY} = 1$ TeV, $m_t = 175$ GeV and $A = \mu = 0$ (yielding $m_{\tilde{t}} \sim M_{SUSY}$). See also Refs. [67, 65, 69, 70, 72]. Excluded regions for the ‘maximal-mixing’ scenario with $M_{SUSY} = 1$ TeV, $m_t = 175$ GeV, $A = \sqrt{6}M_{SUSY}$, and $\mu = 0$ are given in Fig. 8. Fig. 9 gives excluded regions in the $(m_{h^0}, \tan \beta)$ plane. (The curves for the different mixing scenarios are very much the same in this plane.) From these figures, we see that both m_{A^0} and m_{h^0} must be larger than about 45 GeV.

The heavier scalar Higgs boson, H^0 , is too heavy to be produced via Z decays. The same is true of the charged Higgs boson.

3 LEP II

3.1 Standard Higgs boson

The production of the standard Higgs boson at LEP2 is via $e^+e^- \rightarrow Z\phi^0$ [73]. The reach in Higgs mass is determined by kinematics and luminosity. For relevant studies, see Ref. [74, 75, 68]. We shall quote the results of the latest study, Ref. [68]. LEP2 is scheduled to begin operation in 1996 with an energy above the W^+W^- threshold. As illustrated in Fig. 10, for the “standard” energy of $\sqrt{s} = 175$ GeV a $\gtrsim 5\sigma$ Higgs signal will be obtained for masses up to about 82 GeV if an average 150 pb^{-1} of integrated luminosity is accumulated by each of the four detectors. However, this energy no longer represents the initial LEP2 goal. The initial energy of LEP2 could reach as high as $\sqrt{s} = 184$ GeV, which would allow discovery of the standard Higgs boson up to a mass of about 87 GeV with 150 pb^{-1} of integrated luminosity per detector.

Larger Higgs masses are accessible with higher energy. The energy can potentially be increased to $\sqrt{s} = 192$ GeV with additional superconducting cavities, which would allow masses up to 95 GeV to be probed with 150 pb^{-1} of integrated luminosity per experiment, as illustrated in Fig. 10. The Higgs mass region $m_{\phi^0} \sim m_Z$ has a background from $e^+e^- \rightarrow ZZ$ which is comparable to $e^+e^- \rightarrow Z\phi^0$. This can be overcome by tagging b -quark jets using a silicon vertex detector (SVX) [75]; in the mass region of interest, $BR(\phi^0 \rightarrow b\bar{b}) \approx 85\%$, while $BR(Z \rightarrow b\bar{b}) \approx 15\%$.

An energy of 205 GeV could be achieved by nearly doubling the number of superconducting cavities necessary for $\sqrt{s} = 184$ GeV, and upgrading the cryogenic system. This energy would allow a search for the standard Higgs boson up to a mass of 103 GeV with 150 pb^{-1} of integrated luminosity per experiment, see Fig. 10.

The LEP magnets can keep electrons and positrons in orbit up to 125 GeV. However, the energy radiated via synchrotron radiation, already significant at $\sqrt{s} = 175$ GeV, grows as the fourth power of the beam energy. A machine energy as high as $\sqrt{s} = 240$ GeV is conceivable with yet more superconducting cavities and cryogenics upgrades. This would allow the exploration of the standard Higgs

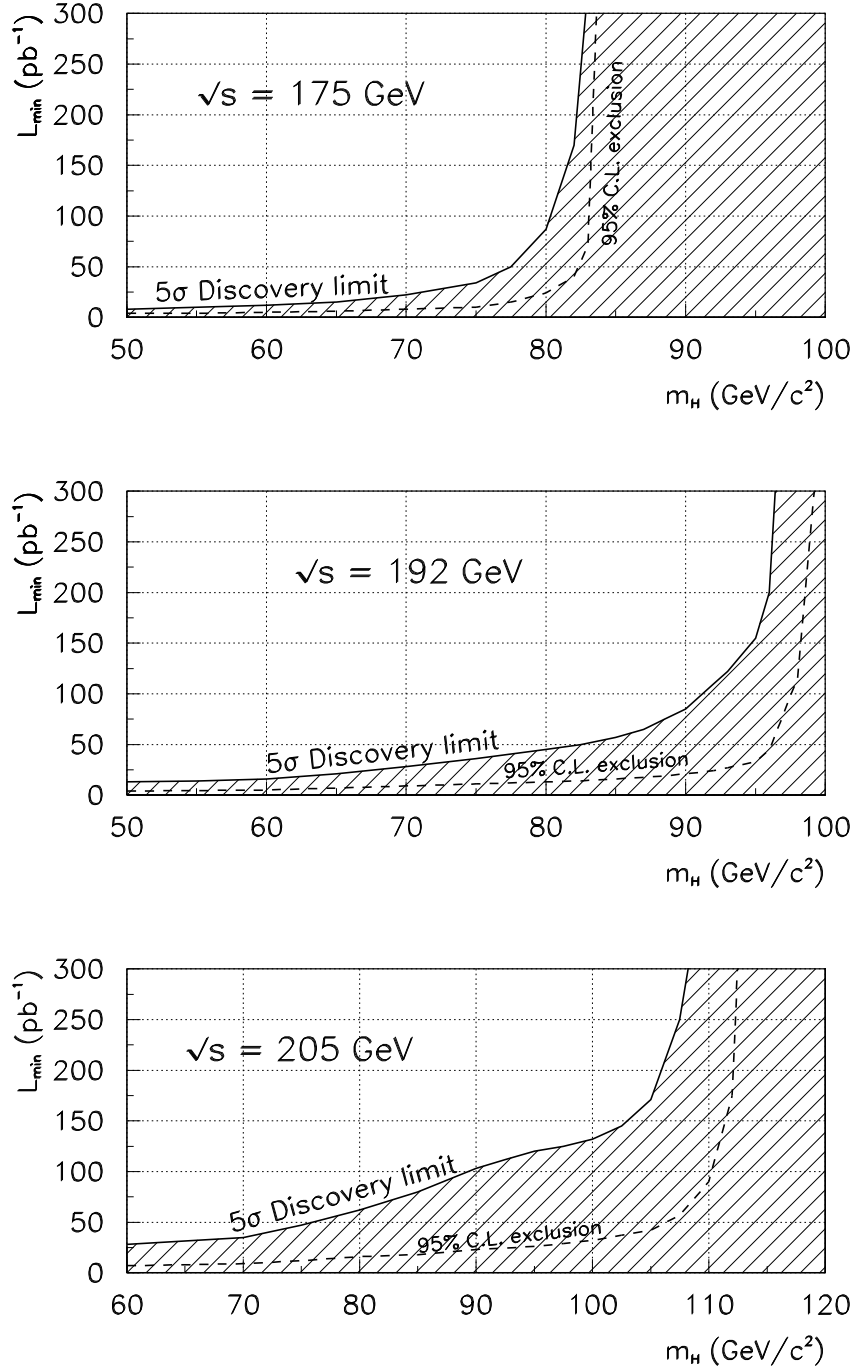


Figure 10: LEP2 discovery limits for the SM ϕ^0 (denoted by H in this figure) at $\sqrt{s} = 175, 192, 205 \text{ GeV}$. The luminosity L_{\min} is the minimum required per experiment, assuming that data from all four experiments is combined.

boson up to a mass of roughly 140 GeV with 75 pb^{-1} of integrated luminosity per detector.

3.2 SUSY Higgs bosons

At LEP2, the two main production processes of interest are $e^+e^- \rightarrow Zh^0$ and $e^+e^- \rightarrow A^0h^0$. Unless $m_{\tilde{t}}$ is small, the heavy scalar Higgs boson, H^0 , will be too heavy to be produced via $e^+e^- \rightarrow ZH^0$, and for the small values of m_{A^0} such that A^0H^0 production would be kinematically allowed, the associated coupling is small. The processes $e^+e^- \rightarrow b\bar{b}H^0, b\bar{b}A^0$ are kinematically allowed out to larger masses, but generally have very small rates because of the small $b\bar{b}H^0$ coupling; the Yukawa coupling would have to be larger than its perturbative limit for observable rates.

The regions of the $(m_{A^0}, \tan\beta)$ parameter space for which Zh^0 and h^0A^0 will be detectable are illustrated in Figs. 11, 12, 13 for $\sqrt{s} = 175, 192, 205 \text{ GeV}$. These figures assume $m_t = 175 \text{ GeV}$ and $M_{SUSY} = 1 \text{ TeV}$, and give contours for the earlier-defined ‘no-mixing’, ‘typical-mixing’, and ‘maximal-mixing’ scenarios. In the no-mixing case, $m_{\tilde{t}} \sim M_{SUSY}$. Discovery regions increase if M_{SUSY} lies below 1 TeV. For large m_{A^0} , the $e^+e^- \rightarrow A^0h^0$ process is kinematically forbidden, but m_{h^0} merely approaches its upper bound, given at one-loop by Eq. 10 (smaller after including two-loop/RGE-improved corrections). For $\tan\beta$ near 1 and small mixing this bound is small enough that the h^0 will be produced at an observable rate via $e^+e^- \rightarrow Zh^0$ at large m_{A^0} , even for the lowest $\sqrt{s} = 175 \text{ GeV}$ energy. At $\sqrt{s} = 205 \text{ GeV}$, the bound on m_{h^0} in the absence of mixing implies that Zh^0 will be observable for arbitrarily large values of $\tan\beta$ and m_{A^0} , indeed throughout all of parameter space except the $m_{A^0} \lesssim 100, \tan\beta \gtrsim 8$ corner where h^0A^0 production can instead be detected.

Since large m_{A^0} is preferred in many unified models, it is useful to further quantify the ultimate limit on h^0 detection at LEP2 in the case of large m_{A^0} . The question is for what portion of SUSY parameter space is LEP2, running at a certain energy, guaranteed to find the h^0 , as a function of the stop squark mass? (We shall assume negligible mixing, implying $M_{SUSY} = m_{\tilde{t}}$; substantial mixing can increase m_{h^0} , implying that higher machine energy would be required.) A crude approximation to the results of Ref. [68] is that roughly 125 Zh^0 events (summed over all experiments, and before including cuts and branching ratios) are needed in order to achieve a 5σ discovery signal. Assuming $m_t = 175 \text{ GeV}$ and $L = 600 \text{ pb}^{-1}$ (summed over all detectors), we present in Fig. 14 contours in $(E_{LEP}, m_{\tilde{t}})$ parameter space which define the boundary between the regions where 125 Zh^0 events will and will not be obtained at a given fixed $\tan\beta$ value when m_{A^0} is large (and hence m_{h^0} is close to its upper bound for a given $\tan\beta$). Evidently, the machine energy required to guarantee 125 events for all $\tan\beta$ values is quite sensitive to $m_{\tilde{t}}$. While $E_{LEP} \sim 205 \text{ GeV}$ is needed for high $\tan\beta$ and $m_{\tilde{t}} \sim 1 \text{ TeV}$ (see also Fig. 13), $E_{LEP} \lesssim 200 \text{ GeV}$ is adequate if $m_{\tilde{t}} \lesssim 500 \text{ GeV}$,

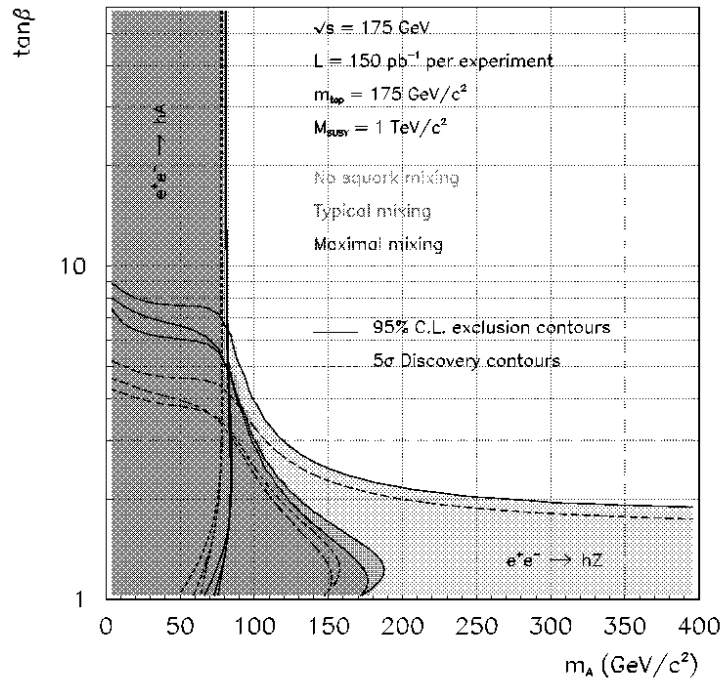


Figure 11: Regions in the minimal supersymmetric model parameter space for which Zh^0 and h^0A^0 will be observable at LEP2 with $\sqrt{s} = 175 \text{ GeV}$, assuming $m_t = 175 \text{ GeV}$ and $M_{\text{SUSY}} = 1 \text{ TeV}$. Results for various degrees of mixing in the stop-squark sector are shown. Figure from Ref. [68].

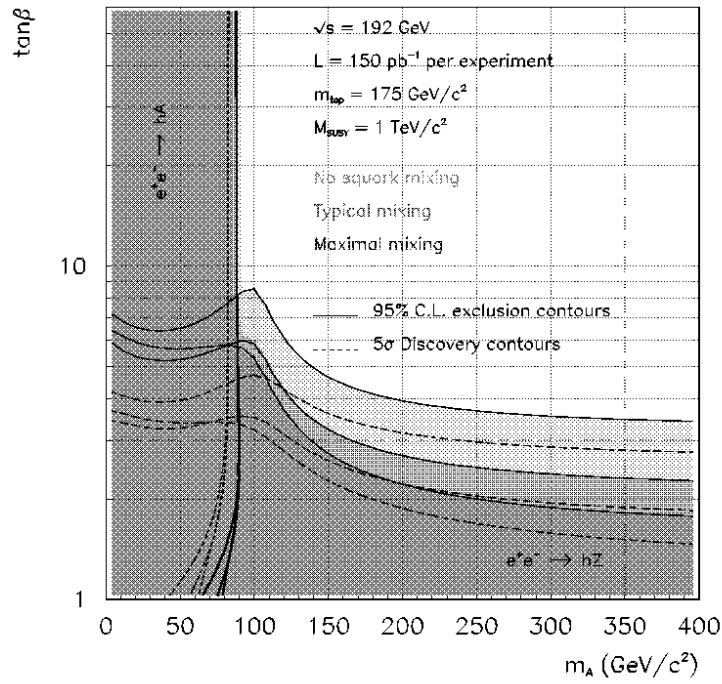


Figure 12: Regions in the minimal supersymmetric model parameter space for which Zh^0 and h^0A^0 will be observable at LEP2 with $\sqrt{s} = 192$ GeV, assuming $m_t = 175$ GeV and $M_{SUSY} = 1$ TeV. Results for various degrees of mixing in the stop-squark sector are shown. Figure from Ref. [68].

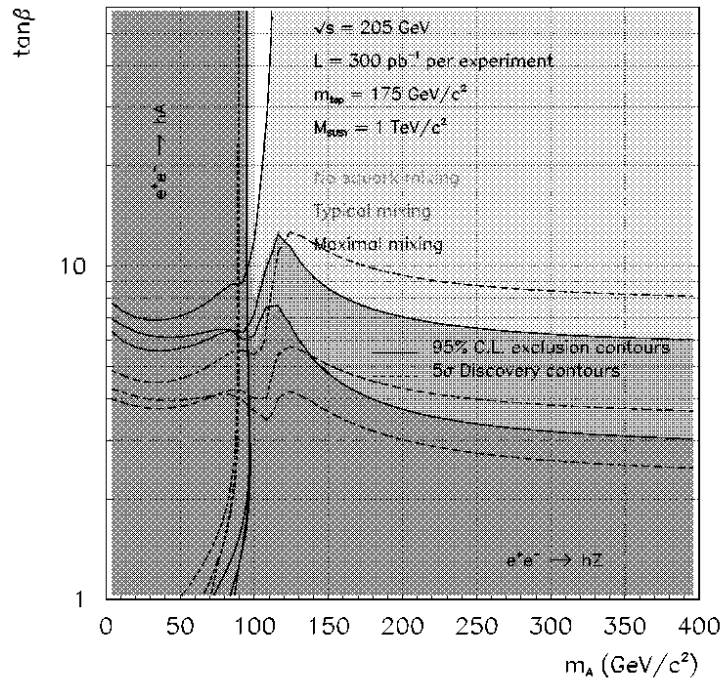


Figure 13: Regions in the minimal supersymmetric model parameter space for which Zh^0 and h^0A^0 will be observable at LEP2 with $\sqrt{s} = 205$ GeV, assuming $m_t = 175$ GeV and $M_{SUSY} = 1$ TeV. Results for various degrees of mixing in the stop-squark sector are shown. Figure from Ref. [68].

as in many unified scenarios. At low $\tan\beta$ (preferred in typical $b - \tau$ Yukawa-unified models) the machine energy needed to have a good chance of h^0 discovery is even more modest. However, for the canonical energy of $E_{LEP} = 192$ GeV, a summed luminosity of $L = 600$ pb $^{-1}$ guarantees h^0 discovery only for $\tan\beta \lesssim 3$ if $m_{A^0} = m_{\tilde{\tau}} = 1$ TeV, as is also apparent from Fig. 12.

Charged Higgs detection at LEP2 is a possibility if $Z \rightarrow H^+H^-$ is kinematically allowed. For machine energies $\sqrt{s} = 175, 190$ and 210 GeV and $L = 500$ pb $^{-1}$, more than 50 H^+H^- events will be present for $m_{H^\pm} < 77, 83$, and 88 GeV, respectively. (Mass reach rises slowly with increased energy at fixed luminosity due to the slow threshold turn-on of this P -wave final state.) The H^\pm decays to a mixture of cs and $\tau\nu$ in the mass region in question. Sensitivity is present for all final states, but significantly more than 50 events is generally required unless $\tan\beta$ is large enough that the $\tau\nu$ channel is completely dominant. At $\sqrt{s} = 200$ GeV, $L = 500$ pb $^{-1}$ allows detection of the H^\pm for masses up to ~ 67 GeV at moderate $\tan\beta$ and for masses as high as 80 GeV when $BR(H^+ \rightarrow \tau\nu) \sim 1$ (at large $\tan\beta$) [72]. In the MSSM, m_{H^\pm} is bounded from below by m_W for most parameter choices, implying that observation of H^+H^- pair production would almost certainly require LEP II energies above 200 GeV.

4 LHC

4.1 Standard Higgs boson

LEP2 will search for the standard Higgs boson up to a mass of at least 80 GeV (for $\sqrt{s} = 175$ GeV), and higher if higher energy is attained. We are therefore primarily interested in $m_{\phi^0} > 80$ GeV in our deliberations concerning future colliders.

The LHC is a 14 TeV pp collider which will reside in the LEP tunnel. It is expected to deliver 100 fb $^{-1}$ of integrated luminosity per year when operating at a luminosity of $\mathcal{L} = 10^{34}/\text{cm}^2/\text{s}$. With a bunch crossing time of 25 ns, this luminosity yields about 20 interactions per bunch crossing. For some Higgs searches, it may be advantageous to run at lower luminosity, to reduce the number of multiple interactions. It is anticipated that the machine will operate at an instantaneous luminosity of $\mathcal{L} = 10^{33}/\text{cm}^2/\text{s}$ during the first few years of running. Furthermore, the current plan for the construction of the LHC calls for the first stage to operate at this low luminosity and with $\sqrt{s} = 10$ TeV. We comment on the Higgs potential of this first-stage machine at the end of this section.

The total cross sections for various Higgs-boson production processes at the LHC are shown in Fig. 15 as a function of the Higgs mass. The dominant cross section is $gg \rightarrow \phi^0$ via a top-quark loop [76]; we assume $m_t = 175$ GeV here and throughout. The next largest cross section is from $WW, ZZ \rightarrow \phi^0$, where

125 Zh^0 Event Contours at LEP-II, $L_{\Sigma \text{ EXP}} = 600 \text{ pb}^{-1}$
 $m_t = 175 \text{ GeV}$, $m_A = 1 \text{ TeV}$

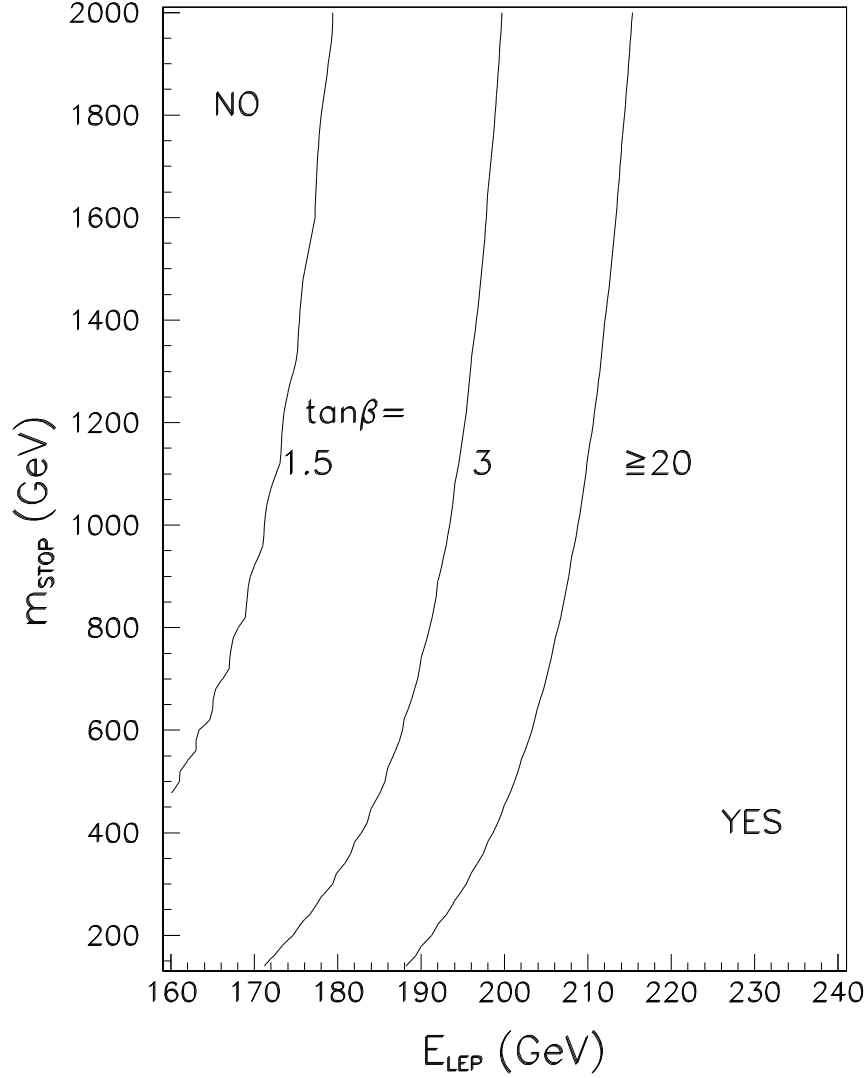


Figure 14: Fixed $\tan\beta$ contours in $(E_{\text{LEP}}, m_{\tilde{t}})$ parameter space for which 125 Zh^0 events are obtained. We have taken $L = 150 \text{ pb}^{-1}$ per experiment (*i.e.* 600 pb^{-1} summed over all experiments), $m_t = 175 \text{ GeV}$ and $m_{A^0} = 1 \text{ TeV}$, and included radiative corrections to the Higgs sector computed at the two-loop/RGE-improved level assuming no squark mixing.

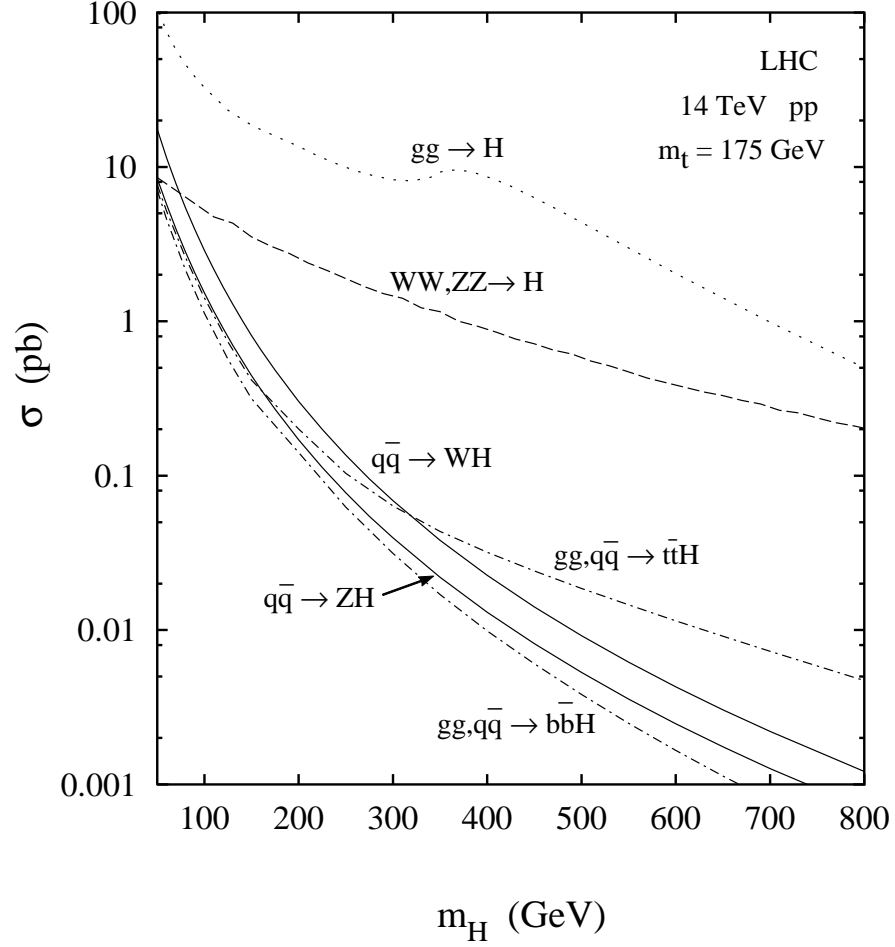


Figure 15: Cross sections for the production of the standard Higgs boson at the LHC ($\sqrt{s} = 14$ TeV) vs. the Higgs-boson mass. The cross sections include the QCD correction factors listed in Table 5. In this figure we use H to denote the SM Higgs boson.

the (virtual) W, Z bosons are radiated from the incoming quarks and antiquarks [77]. For relatively light Higgs bosons, two other processes are important. The production of the Higgs boson in association with a W or Z boson is the analogue of the LEP2 process $e^+e^- \rightarrow Z\phi^0$ [78]. The Higgs boson can also be produced in association with a heavy quark-antiquark pair, either $t\bar{t}$ [79] or $b\bar{b}$ [80].

Table 5: Approximate QCD correction factors (K factors) for various Higgs boson production cross sections at the LHC. The leading-order (LO) cross section was computed with LO parton distribution functions, while the next-to-leading order (NLO) cross section was computed with NLO parton distribution functions. The scale μ is the common renormalization and factorization scale. The K factors are from Ref. [81] ($gg \rightarrow \phi^0$), Ref. [82] ($VV \rightarrow \phi^0$), and Ref. [83] ($q\bar{q} \rightarrow V\phi^0$).

	μ	K factor
$gg \rightarrow \phi^0$	m_{ϕ^0}	1.6
$VV \rightarrow \phi^0$	M_V	1.1
$q\bar{q} \rightarrow V\phi^0$	$M_{V\phi^0}$	1.2

The cross sections in Fig. 15 were calculated at next-to-leading order (NLO) in QCD, except for $t\bar{t}\phi^0$ and $b\bar{b}\phi^0$, where such a calculation is lacking. The QCD correction may be approximated by an overall multiplicative factor, often called a “ K factor”. The K factor depends on both the factorization and renormalization scales; we set these scales equal, as is conventional. The most meaningful way to report the K factor is as the ratio of the NLO cross section convoluted with NLO parton distribution functions, to the LO cross section convoluted with LO parton distribution functions; this ratio is renormalization- and factorization-scheme independent. We list the K factors in Table 5, along with the common renormalization and factorization scale used. The parton distribution functions used are from the set CTEQ2 [84].

The Higgs mass range can be divided into three separate regions, with different search strategies. A heavy Higgs boson, $2m_Z < m_{\phi^0} < 700$ GeV, is searched for principally via the “gold-plated” mode, $gg \rightarrow \phi^0 \rightarrow ZZ \rightarrow \ell^+\ell^-\ell^+\ell^-$. The intermediate-mass region, $80 \text{ GeV} < m_{\phi^0} < 2m_Z$, divides into two segments. For $120 \text{ GeV} < m_{\phi^0} < 2m_Z$, the principal search mode is the same as the “gold-plated” mode, but with one Z boson off shell [85]. The mode $gg \rightarrow \phi^0 \rightarrow \gamma\gamma$ is also viable in this mass region. The “light” intermediate-mass region, $80 \text{ GeV} < m_{\phi^0} < 120 \text{ GeV}$, is the most challenging. The $\gamma\gamma$ decay mode, using $gg \rightarrow \phi^0$ as well as $W\phi^0$ and $t\bar{t}\phi^0$ production [86], has long been thought to be the best signal in this region. However, recent work indicates that the decay mode $\phi^0 \rightarrow b\bar{b}$, where the Higgs is produced via $W\phi^0$ [87, 88, 89, 90] and $t\bar{t}\phi^0$ [91], may also be viable in part of this same mass range. A combination of signals from various modes may be necessary

to discover a Higgs boson in the “light” intermediate-mass region.

We divide our discussion into the three Higgs mass regions. Wherever possible, we quote the results of the recent studies performed for the ATLAS [92] and CMS [93] Technical Proposals.

4.1.1 $80 \text{ GeV} < m_{\phi^0} < 120 \text{ GeV}$

The branching ratio of $\phi^0 \rightarrow \gamma\gamma$ exceeds 0.5×10^{-3} for $80 \text{ GeV} < m_{\phi^0} < 155 \text{ GeV}$ (see Fig. 4), and the cross section is sufficiently large in this region that thousands of $gg \rightarrow \phi^0 \rightarrow \gamma\gamma$ events are produced in 100 fb^{-1} . However, there is a large irreducible background from $q\bar{q}, gg \rightarrow \gamma\gamma$. The background from jj and γj , where the jet fakes a photon, can be reduced to a manageable level via hadronic activity, calorimetric isolation, shower shape, and γ/π^0 discrimination. The Higgs appears as a narrow bump in the $\gamma\gamma$ invariant-mass spectrum, so the statistical significance of the signal depends on the ability to measure photon energies and angles, which is detector dependent. For 100 fb^{-1} , ATLAS claims sensitivity to $110 \text{ GeV} < m_{\phi^0} < 140 \text{ GeV}$, while CMS claims coverage of $85 \text{ GeV} < m_{\phi^0} < 150 \text{ GeV}$. CMS benefits from an outstanding electromagnetic calorimeter made from PbWO_4 (lead tungstate). The low end of the mass range is the most challenging, due to the small branching ratio and the large backgrounds. ATLAS requires five years of running at peak luminosity (500 fb^{-1}) to reach down to a Higgs mass of 80 GeV . ATLAS claims a Higgs mass resolution of 1.4 GeV for $m_{\phi^0} = 100 \text{ GeV}$, and similar resolution for other Higgs masses. CMS claims a resolution of 0.87 GeV at high luminosity, and 0.54 GeV at low luminosity, for $m_{\phi^0} = 110 \text{ GeV}$. Thus the Higgs mass will be measured with very good precision if the Higgs is detected in its two-photon decay mode.

The associated-production processes $W\phi^0, t\bar{t}\phi^0$, followed by $\phi^0 \rightarrow \gamma\gamma$, are also useful [86]. The number of signal events is small, due to the relatively small cross sections and the small branching ratio. However, the background is greatly reduced by requiring an isolated charged lepton from either the W boson or the top quark. The irreducible backgrounds are $W\gamma\gamma$ and $t\bar{t}\gamma\gamma$, respectively. Unlike the process $gg \rightarrow \phi^0 \rightarrow \gamma\gamma$, the signal is comparable to the background, so the $\gamma\gamma$ invariant-mass resolution is not as important. The charged lepton also helps indicate the primary vertex, which aids in the reconstruction of the two-photon invariant mass. ATLAS finds about 15 signal events in 100 fb^{-1} in this mass region, yielding a signal with a significance of 4σ for $80 \lesssim m_{\phi^0} \lesssim 120 \text{ GeV}$. CMS finds a somewhat better signal with their “shashlik”-type electromagnetic calorimeter, which has an invariant-mass resolution of about 1 GeV . The statistical significance of the signal is at the $6 - 7\sigma$ level for $80 \lesssim m_{\phi^0} \lesssim 120 \text{ GeV}$. The PbWO_4 calorimeter improves the invariant-mass resolution by about a factor of two, and hence the significance of the signal by about a factor of $\sqrt{2}$. However, this conclusion has been questioned in Ref. [94].

CMS has studied the possibility of detecting the Higgs boson produced in association with two (or more) jets, followed by $\phi^0 \rightarrow \gamma\gamma$. The signal contains not only $gg \rightarrow \phi^0$ with jet radiation, but also weak-vector-boson fusion, $W\phi^0$ and $Z\phi^0$, and $t\bar{t}\phi^0$. Although the number of signal events and the significance of the signal is decreased with respect to the pure $\phi^0 \rightarrow \gamma\gamma$ search, the signal to background ratio is greatly improved, and is of order unity. With 100 fb^{-1} , CMS claims coverage of the region $70 \text{ GeV} < m_{\phi^0} < 150 \text{ GeV}$ via this mode, using the PbWO_4 calorimeter.

The CDF collaboration has established high-efficiency b -tagging via secondary vertices with a silicon vertex detector (SVX) in a hadron-collider environment. This allows the possibility to detect the “light” intermediate-mass Higgs boson in its dominant decay mode, $\phi^0 \rightarrow b\bar{b}$ [87, 88, 89, 90, 91]. Below we summarize the results of Ref. [88], which is the most complete analysis and is used by the ATLAS collaboration.

Early on, CDF achieved a b -tagging efficiency of 30%, with a 1% misidentification of light-quark and gluon jets as b jets, using a silicon-strip vertex detector [12]. The efficiency has recently been improved to about 45%, maintaining the same misidentification rate [95]. One can anticipate higher efficiency with pixel detectors, which are planned for ATLAS. The results from Refs. [92, 96] are shown in Fig. 16. At low luminosity, an efficiency of 60% with a fake rate of 1% can be achieved. At high luminosity 50% efficiency is possible with 2% mis-tag probability. The decrease in the high luminosity case arises if the innermost pixel layer, located 4 cm from the beam line, must be removed because of irradiation problems. The additional track density from multiple interactions at high luminosity is not a problem, since it is significantly smaller than the total track density inside the b jet [92]. Soft leptons may also be used to tag b jets which undergo semileptonic decay, with an efficiency of about 20% and a fake rate of 1%. We shall quote results based on $e_{b\text{-tag}} = 0.6$, $e_{\text{mis-tag}} = 0.01$ and $e_{b\text{-tag}} = 0.5$, $e_{\text{mis-tag}} = 0.02$ at low and high luminosity, respectively.

The simplest signal is $q\bar{q} \rightarrow W\phi^0$, with $W \rightarrow \ell\nu$ and $\phi^0 \rightarrow b\bar{b}$, where the charged lepton is used as a trigger. The best significance is attained if one tags both b jets. This process has a large number of backgrounds. The irreducible backgrounds are $Wb\bar{b}$ and, for $m_{\phi^0} \sim m_Z$, WZ with $Z \rightarrow b\bar{b}$. The latter background can be normalized via the leptonic decay modes of the weak vector bosons. The irreducible background $q\bar{q} \rightarrow t\bar{t} \rightarrow Wb\bar{b}$ is small at the LHC. The dominant reducible backgrounds are Wjj , where the jets fake b jets, and $t\bar{t} \rightarrow W^+W^-b\bar{b}$, where one W boson is missed. This last background, before rejecting the extra W boson, is much larger than the signal. An event which contains an extra isolated charged lepton, or an extra jet of $p_T > 15 \text{ GeV}$, is rejected; this brings the $t\bar{t}$ background down to a manageable level. Such a low p_T threshold is impossible to implement at peak luminosity due to the pile-up of minimum-bias events. A higher threshold allows too much of the $t\bar{t}$ background to survive. Thus the $W\phi^0$,

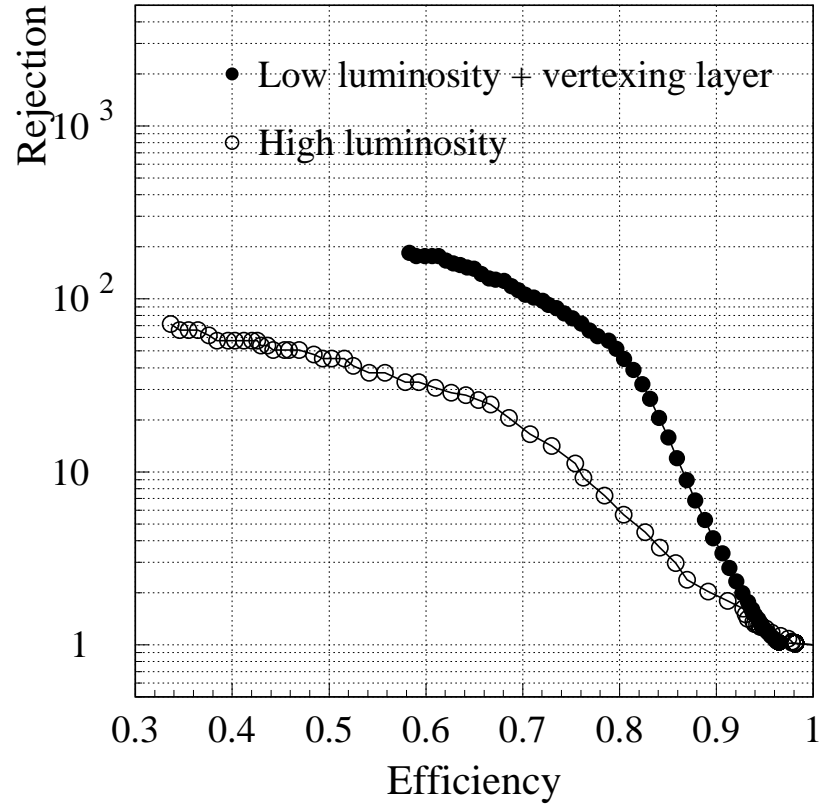


Figure 16: Rejection against prompt jets as a function of the efficiency for tagging b -jets in the ATLAS inner detector at low (closed circles) and high (open circles) luminosity.

with $\phi^0 \rightarrow b\bar{b}$ channel is likely to be useful only at a luminosity of $10^{33}/\text{cm}^2/\text{s}$ or below.

The second production process with which to observe the decay $\phi^0 \rightarrow b\bar{b}$ is $gg \rightarrow t\bar{t}\phi^0$ [91]. The cross section for this process is comparable to $q\bar{q} \rightarrow W\phi^0$. Including the top-quark decays, the final state is $W^+W^-b\bar{b}b\bar{b}$. Events are accepted if they contain a lepton from a W decay plus three b jets. The irreducible backgrounds are $t\bar{t}b\bar{b}$ and $t\bar{t}Z$, with $Z \rightarrow b\bar{b}$; the latter is small, so the mass region $m_{\phi^0} \sim m_Z$ is not particularly difficult. The reducible backgrounds are $t\bar{t}j$, $Wjjj$, and $Wb\bar{b}j$, where the jets fake a b jet. The signal process itself is also a background, as one does not know which pair of b jets to select to reconstruct the Higgs mass. This combinatoric background is minimized if one chooses the two lowest p_T jets as the Higgs candidate.

In the latest results, summarized in Fig. 3 of Ref. [96], it is found that at low luminosity (30 fb^{-1} per detector) combining ATLAS and CMS data will lead to an observable ($\geq 5\sigma$) signal for the $W\phi^0$ with $\phi^0 \rightarrow b\bar{b}$ process for $m_{\phi^0} \lesssim 105 \text{ GeV}$. By combining ATLAS and CMS data and the $W\phi^0$ ($\phi^0 \rightarrow b\bar{b}$) and inclusive $\phi^0 \rightarrow \gamma\gamma$ signals, $L = 60 \text{ fb}^{-1}$ (combined ATLAS+CMS luminosity) yields a 5σ signal for $m_{\phi^0} \leq 150 \text{ GeV}$. At $L = 100 \text{ fb}^{-1}$, $t\bar{t}\phi^0$ (with $\phi^0 \rightarrow b\bar{b}$), and $W\phi^0, t\bar{t}\phi^0$ (with $\phi^0 \rightarrow \gamma\gamma$), ATLAS alone can cover all of the difficult region $80 \text{ GeV} < m_{\phi^0} < 120 \text{ GeV}$ [92].

Aside from its discovery potential, the decay mode $\phi^0 \rightarrow b\bar{b}$ is important to establish the coupling of the Higgs to fermions. Furthermore, the $W\phi^0, t\bar{t}\phi^0$ with $\phi^0 \rightarrow b\bar{b}$ channels can be studied during the initial low-luminosity running of the LHC, and may provide the first sighting of the Higgs boson.

The process $t\bar{t}\phi^0$ with $\phi^0 \rightarrow b\bar{b}$ and semileptonic decay of both the top and anti-top quarks has been suggested to produce an observable signal in the two-jet invariant mass distribution without b tagging [98]. The main background is from $t\bar{t}jj$, which is much larger than the signal. This signal was also considered in Ref. [91], with a negative conclusion. It has not been studied by ATLAS and CMS.

4.1.2 $120 \text{ GeV} < m_{\phi^0} < 2m_Z$

The process $gg \rightarrow \phi^0 \rightarrow ZZ^* \rightarrow \ell^+\ell^-\ell^+\ell^-$ is the most reliable mode for detection of the “heavy” intermediate-mass Higgs boson. The branching ratio for this decay mode drops rapidly with decreasing Higgs mass, to 1% for $m_{\phi^0} = 120 \text{ GeV}$. The irreducible backgrounds, from $q\bar{q}, gg \rightarrow ZZ^*, Z\gamma^* \rightarrow \ell^+\ell^-\ell^+\ell^-$, are small. The dominant reducible backgrounds are from $t\bar{t} \rightarrow W^+W^-b\bar{b}$ and $Zb\bar{b}$, where the weak bosons and b quarks decay to charged leptons. Charged leptons also arise from cascade decays of the b quarks. These backgrounds can be reduced to a negligible level via lepton isolation and impact-parameter cuts. The lepton isolation cut requires a higher threshold at peak luminosity, and the signal efficiency is

thereby decreased. The significance of the signal is therefore only slightly improved for one year of running at peak luminosity versus three years at $10^{33}/\text{cm}^2/\text{s}$. CMS concentrates on the four-muon channel at peak luminosity. Both ATLAS and CMS find that the smallest Higgs mass that can be reached with 100 fb^{-1} is about 130 GeV. To reach as low as 120 GeV requires several years of running at peak luminosity. The signal significance generally increases with increasing Higgs mass, except for a dip near $m_{\phi^0} = 170 \text{ GeV}$, where the decay $\phi^0 \rightarrow W^+W^-$ suppresses the branching ratio of $\phi^0 \rightarrow ZZ^*$ (see Fig. 4). However, even a Higgs at this mass yields a detectable signal with 100 fb^{-1} . ATLAS finds that the Higgs mass resolution in this mode varies from 1.6 GeV to 2.2 GeV for $m_{\phi^0} = 120 - 180 \text{ GeV}$, so the Higgs mass measurement is very precise via this decay mode.

The branching ratio of $\phi^0 \rightarrow \gamma\gamma$ reaches its maximum at about 125 GeV. This process is discussed in the previous section. ATLAS claims discovery in this channel for a Higgs mass up to 140 GeV for 100 fb^{-1} , with a mass resolution of 1.7 GeV. CMS claims discovery up to 150 GeV for 100 fb^{-1} , and up to 150 GeV via the $jj\gamma\gamma$ mode. By combining ATLAS and CMS data, a $\gtrsim 7\sigma$ inclusive $\gamma\gamma$ signal is seen for $m_{\phi^0} \lesssim 150 \text{ GeV}$ and $L = 100 \text{ fb}^{-1}$ per detector [96].

Observation of both $\phi^0 \rightarrow \gamma\gamma$ and $\phi^0 \rightarrow ZZ^*$ would test the relative coupling of the Higgs to WW and ZZ , since the $\phi^0 \rightarrow \gamma\gamma$ amplitude is dominated by a W loop. These couplings are expected to be related as in the standard Higgs model, since this follows from custodial $\text{SU}(2)$. The $\phi^0 \rightarrow \gamma\gamma$ amplitude receives contributions from all electrically-charged heavy particles which obtain their mass via the Higgs mechanism, so a large deviation from the expected amplitude would suggest the presence of such heavy particles. Should any of these particles carry color, they would also contribute to the production amplitude $gg \rightarrow \phi^0$. If these heavy particles are fermions they reduce the $\phi^0 \rightarrow \gamma\gamma$ decay width and branching ratio, but enhance the $gg \rightarrow \phi^0$ coupling and cross section. The resulting $gg \rightarrow \phi^0 \rightarrow \gamma\gamma$ production rate can be either smaller or larger than in their absence; see, for example, Ref. [99].

The process $\phi^0 \rightarrow WW^* \rightarrow \ell^+\nu\ell^-\nu$ has been suggested as a signal for the “heavy” intermediate-mass Higgs [100]. The Higgs signal manifests itself as an excess of dilepton events. The signal-to-background ratio is near unity. However, the broad signal peak lies near the threshold for real WW production, and is difficult to extract. This process has not been studied by ATLAS or CMS.

4.1.3 $2m_Z < m_{\phi^0} < 700 \text{ GeV}$

The process $gg \rightarrow \phi^0 \rightarrow ZZ \rightarrow \ell^+\ell^-\ell^+\ell^-$ is the so-called “gold-plated” mode, due to its striking signal and small irreducible background (from $q\bar{q}, gg \rightarrow ZZ$). ATLAS claims detection of this mode up to a Higgs mass of 500 GeV even at low luminosity (10 fb^{-1}); CMS claims detection up to 400 GeV. Higher masses require higher luminosity; with 100 fb^{-1} , ATLAS claims a Higgs mass as high as 800 GeV

can be attained, while CMS is confident up to 600 GeV and a bit above. The irreducible background is non-negligible at these masses. For $m_{\phi^0} > 700$ GeV the search strategies become more sophisticated; see the report of the working group on “Strongly-Coupled Electroweak Symmetry Breaking” [101].

The width of the Higgs boson becomes greater than the $\ell^+\ell^-\ell^+\ell^-$ invariant-mass resolution for a sufficiently heavy Higgs boson, allowing a measurement of this quantity. A 300 GeV Higgs boson has a width of about 8 GeV, and the width grows rapidly with increasing Higgs mass (see Fig. 6). An approximate formula for a heavy Higgs boson is $\Gamma_{\phi^0}(\text{TeV}) = \frac{1}{2}[m_{\phi^0}(\text{TeV})]^3$. A direct measurement of the width would allow a determination of the $\phi^0 ZZ$ and $\phi^0 WW$ couplings (assuming they are related via custodial SU(2) symmetry), provided $\phi^0 \rightarrow t\bar{t}$ is kinematically forbidden or has a relatively small width (as in the standard model). Under these same assumptions $BR(\phi^0 \rightarrow ZZ)$ could also be determined. Since the $\ell^+\ell^-\ell^+\ell^-$ rate is proportional to $\Gamma(\phi^0 \rightarrow gg)BR(\phi^0 \rightarrow ZZ)$ one would then be able to compute $\Gamma(\phi^0 \rightarrow gg)$. This in turn would allow the determination of the $\phi^0 t\bar{t}$ coupling, which is responsible for the $\phi^0 gg$ coupling (via a top-quark loop).

There are a variety of other production modes in which to detect the Higgs decay to weak-vector-boson pairs. For example, for high m_{ϕ^0} values, $pp \rightarrow W^+W^-jjX$ via $W^+W^- \rightarrow \phi^0 \rightarrow W^+W^-$ fusion (the initial W^+ and W^- having been radiated from the two detected jets) has a cross section that is a significant fraction of that for $gg \rightarrow \phi^0 \rightarrow W^+W^-$. These production modes are usually regarded as being relevant to the Higgs search at masses beyond the reach of the gold-plated mode, roughly $m_{\phi^0} > 700$ GeV. Since this is the domain of the “strongly-coupled” Higgs, we defer a detailed discussion of these modes to the “Strongly-Coupled Electroweak Symmetry Breaking” subgroup [101]. However, these modes can also be used for lighter Higgs masses and potentially provide additional sensitivity to the couplings of the ϕ^0 to W^+W^- .

The channel $\phi^0 \rightarrow ZZ \rightarrow \ell^+\ell^-\nu\bar{\nu}$ has a six times higher rate than the gold-plated mode, but has a less distinctive signal. The Higgs appears as a resonance above the $ZZ \rightarrow \ell^+\ell^-\nu\bar{\nu}$ background in the $p_T(\ell^+\ell^-)$ spectrum. CMS claims a clear signal with only 10 fb^{-1} for $m_{\phi^0} = 500$ GeV. Since the Higgs width increases rapidly with increasing Higgs mass, the signal becomes very broad and difficult to recognize above the background at higher masses. Forward jet tagging suppresses the background while maintaining most of the signal from vector-boson fusion, and yields observable signals up to $m_{\phi^0} = 800$ GeV with 100 fb^{-1} .

For $m_{\phi^0} > 2m_t$, the decay mode $\phi^0 \rightarrow t\bar{t}$ becomes available. In the standard model, the branching ratio is at most 20% (for $m_{\phi^0} = 500$ GeV). The signal is swamped by the irreducible background from $gg \rightarrow t\bar{t}$ [102].

4.2 10 TeV LHC

The LHC was approved by the CERN Council in December 1994. One of the provisions is that the LHC will be staged, with the first stage being a machine of 10 TeV energy and peak luminosity $10^{33}/\text{cm}^2/\text{s}$. Detailed results for the Higgs discovery potential of such a machine are not yet available. Here we restrict our comments to very basic observations.

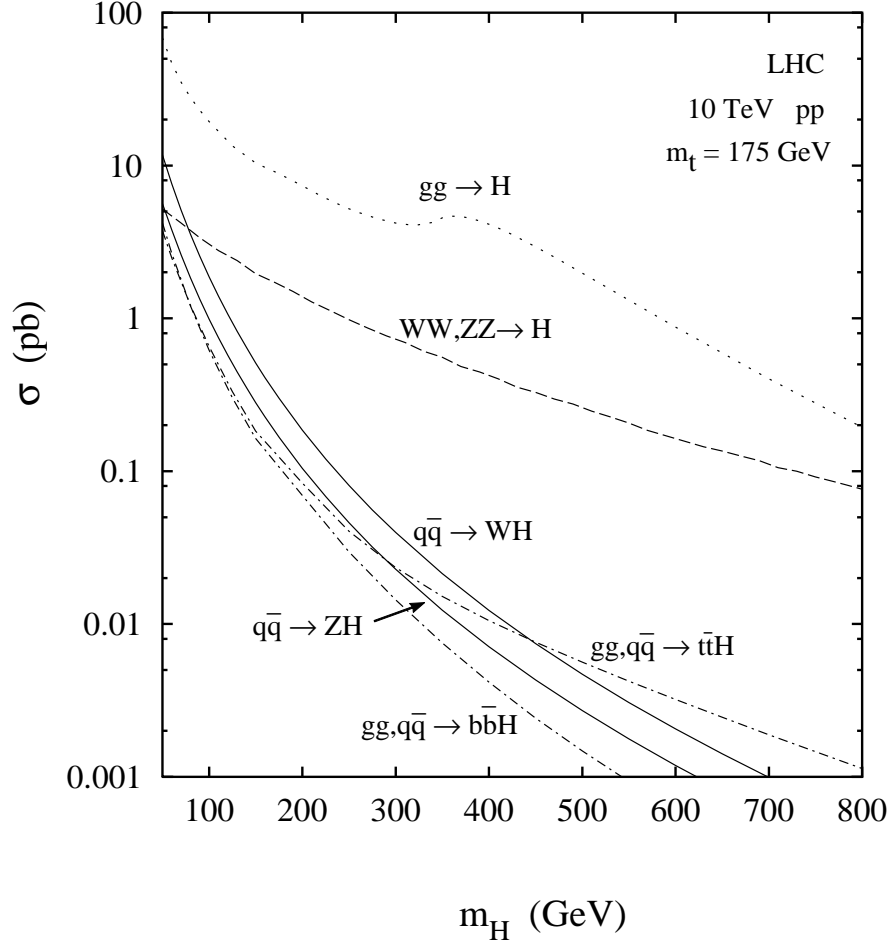


Figure 17: Cross sections for the production of the standard Higgs boson at the first-stage LHC ($\sqrt{s} = 10$ TeV) vs. the Higgs boson mass. The cross sections include the QCD correction factors listed in Table 5. In this figure we use H to denote the SM Higgs boson.

The various cross sections for production of the standard Higgs are shown in Fig. 17. The biggest differences from the full 14 TeV collider occur at the highest Higgs masses. The dominant cross section, $gg \rightarrow \phi^0$, is reduced by about

a factor of 2.5 for $m_{\phi^0} > 400$ GeV. The Higgs mass reach in the gold-plated mode, $\phi^0 \rightarrow ZZ \rightarrow \ell^+ \ell^- \ell^+ \ell^-$, with 30 fb^{-1} should therefore be comparable to the reach with 10 fb^{-1} at 14 TeV, about 500 GeV for ATLAS and 400 GeV for CMS. Although the $gg \rightarrow \phi^0$ cross section decreases by only about 40% in the intermediate mass region, this decrease must be combined with the lower luminosity anticipated. If we assume an integrated luminosity of $L = 30 \text{ fb}^{-1}$, then we estimate that, in the $\phi^0 \rightarrow \gamma\gamma$ mode, ATLAS would at best achieve a $\sim 3\sigma$ signal for $m_{\phi^0} \sim 120$ GeV, whereas with the high resolution PBWO₄ calorimeter CMS would achieve a 5σ signal (and not much more) for roughly $105 \lesssim m_{\phi^0} \lesssim 140$ GeV. In the $ZZ^* \rightarrow 4\ell$ mode, we estimate that for $L = 30 \text{ fb}^{-1}$ discovery of the ϕ^0 at the 5σ level would be possible for both ATLAS and CMS for $140 \text{ GeV} \lesssim m_{\phi^0} \lesssim 2m_Z$, except possibly in the vicinity of $m_{\phi^0} \sim 170$ GeV. Thus, Higgs discovery would just barely be possible throughout the upper portion of the intermediate mass region after three years of running.

4.3 SUSY Higgs bosons

Generally speaking, the SUSY Higgs bosons are more elusive than the standard Higgs boson at the LHC. There is very little of the parameter space in which all four SUSY Higgs bosons are observable; rather, one asks if at least one SUSY Higgs boson can be detected over the entire parameter space. This appears to be the case, using a combination of detection modes. The early theoretical studies of this issue [103, 104, 105, 106] and newer ideas (to be referenced below) have been confirmed and extended in detailed studies by the ATLAS and CMS detector groups [92, 93].

The first experimental detector collaboration studies of the search for SUSY Higgs bosons by ATLAS [92] and CMS [93] did not include the improved radiative corrections to the h^0 and H^0 masses. Thus, in the $(m_{A^0}, \tan\beta)$ parameter space plots given in these references, the contours for h^0 discovery must be reinterpreted; for small stop-squark mixing the h^0 contours apply for a top quark *pole* pass m_t of about 190 GeV. Certain aspects of the H^0 contours at lower m_{A^0} values are also sensitive to the two-loop/RGE-improved corrections. The discovery contours have also been evolving by virtue of improvements and alterations in the detector itself. A recent survey of the experimental studies is contained in Refs. [96, 97]. Updated figures for ATLAS+CMS at low ($L = 30 \text{ fb}^{-1}$) luminosity and high ($L = 300 \text{ fb}^{-1}$) luminosity from Refs. [96, 97] are included below as Figs. 18 and 19, respectively. Note that the ATLAS+CMS notation means that the signals from the two detectors are combined in determining the statistical significance of a given signal. Since not all modes of interest are included on these plots, we shall also occasionally refer to the original Technical Proposal figures on MSSM Higgs studies in Refs. [92, 93]. The CMS figure from Ref. [93] is reproduced below for the reader's convenience. We note that all results discussed in the following are those obtained without including

higher order QCD “ K ” factors in the signal and background cross sections. The K factors for both signal and background are presumably significant; if they are similar in size, then statistical significances would be enhanced by a factor of \sqrt{K} .

In the limit $m_{A^0} \rightarrow \infty$, the H^0 , A^0 , and H^\pm are all heavy, and decouple from the weak bosons. The lightest neutral scalar Higgs boson, h^0 , approaches its upper bound, and behaves like a standard Higgs boson. Since this bound (for pole mass $m_t = 175$ GeV) is about 113 GeV (assuming small stop-squark mixing and $m_{\tilde{t}} \leq 1$ TeV), the primary channels for h^0 detection will be those based on the $\gamma\gamma$ decay mode. The 5σ contours are shown in Figs. 18 and 19. At high luminosity h^0 discovery in its $\gamma\gamma$ decay mode is possible for $m_{A^0} \gtrsim 170$. For low luminosity the coverage of the $\gamma\gamma$ mode decreases substantially, reaching only down as far as $m_{A^0} \sim 270$ GeV at high $\tan\beta$ with no coverage for any m_{A^0} if $\tan\beta \lesssim 2$. For top quark masses $m_t \gtrsim 190$ GeV, the maximum m_{h^0} mass increases to about 122 GeV, and the h^0 will also be observable via $h^0 \rightarrow ZZ^* \rightarrow 4\ell$ over an overlapping part of the parameter space (see the $m_t = 175$ GeV one-loop contours in the CMS plot, Fig. 20).

For $\tan\beta \sim 1$, the lightest scalar Higgs is observable at LEP2 via $e^+e^- \rightarrow A^0 h^0, Zh^0$. Including two-loop/RGE-improved corrections ($m_{\tilde{t}} = 1$ TeV, no squark mixing) for $m_t = 175$ GeV the LEP-192 discovery region asymptotes at $\tan\beta \lesssim 3$, assuming $L = 150$ pb $^{-1}$ per detector, as shown in Figs. 18 and 19, as well as in the earlier Fig. 11.

For $60 \lesssim m_{A^0} \lesssim 2m_t$ the heavy scalar Higgs has high enough mass and for $\tan\beta \lesssim 3$ maintains enough of a coupling to weak vector bosons to allow its discovery via $H^0 \rightarrow ZZ^{(*)} \rightarrow 4\ell$ at high luminosity, as shown in Fig. 19. The height in $\tan\beta$ as a function of m_{A^0} of the $H^0 \rightarrow 4\ell$ discovery region varies significantly for $m_{A^0} \lesssim 2m_t$ due to large swings in the branching ratio for $H^0 \rightarrow h^0 h^0$ decays, rising as high as $\tan\beta \sim 8$ for $m_{A^0} \sim 190$ GeV (where $BR(H^0 \rightarrow h^0 h^0)$ actually has a zero). The importance of the $H^0 \rightarrow h^0 h^0$ decays makes the 4ℓ mode of marginal utility at low luminosity except for $m_{A^0} \sim 190$ GeV, see Fig. 18. At high luminosity, the $H^0 \rightarrow 4\ell$ contour is cut off for $m_{A^0} \approx m_{H^0} > 2m_t$ due to the dominance of the decay $H^0 \rightarrow t\bar{t}$. The $H^0 \rightarrow h^0 h^0$ and $H^0, A^0 \rightarrow t\bar{t}$ channels can also provide Higgs signals. The key ingredient in employing these channels is efficient and pure b -tagging. We will discuss these modes shortly.

For $m_{A^0} \approx 70$ GeV and $\tan\beta > 3$ (CMS) or 5 (ATLAS), the heavy scalar Higgs has a reasonable $\gamma\gamma$ branching ratio and is observable in its two-photon decay mode. This is indicated by the narrow vertical strip in Fig. 20 from Ref. [93] (see also the similar plot in Ref. [92]). (This region changes little if two-loop/RGE-improved corrections to m_{H^0} are included.)

These “standard” modes are not enough to cover the entire SUSY parameter space, so others must be considered. The uncovered region is for large $\tan\beta$ and moderate m_{A^0} . Since m_{h^0} is in the “light” intermediate mass region, the dominant decays for the light scalar are $h^0 \rightarrow b\bar{b}, \tau^+\tau^-$. The coupling of h^0 to weak vector

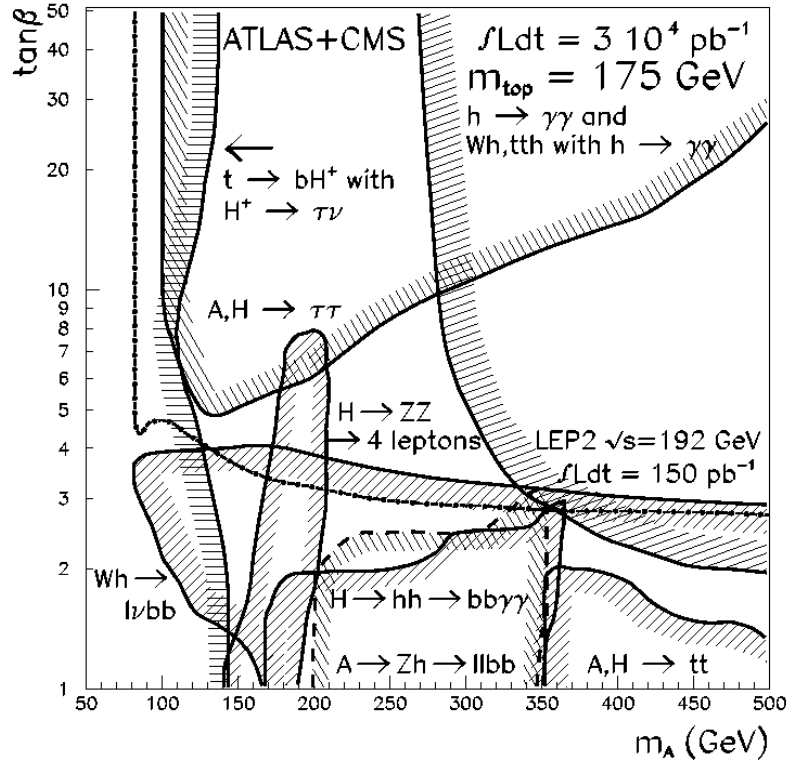


Figure 18: Discovery contours (5σ) in the parameter space of the minimal supersymmetric model for ATLAS+CMS at the LHC: $L = 30 \text{ fb}^{-1}$. Figure from Ref. [97]. Two-loop/RGE-improved radiative corrections to the MSSM Higgs sector are included assuming $m_{\tilde{t}} = 1 \text{ TeV}$ and no squark mixing.

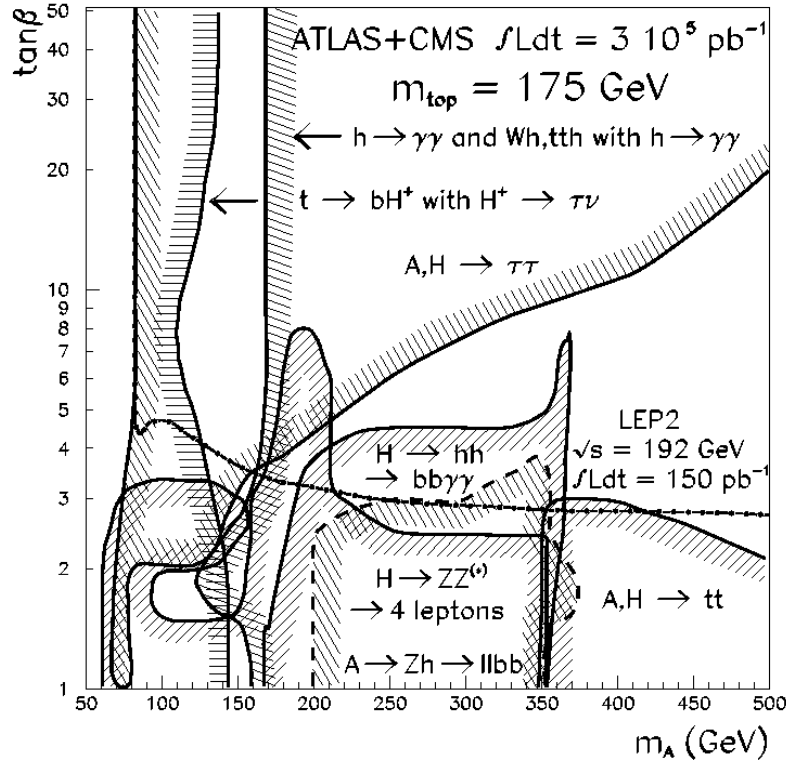
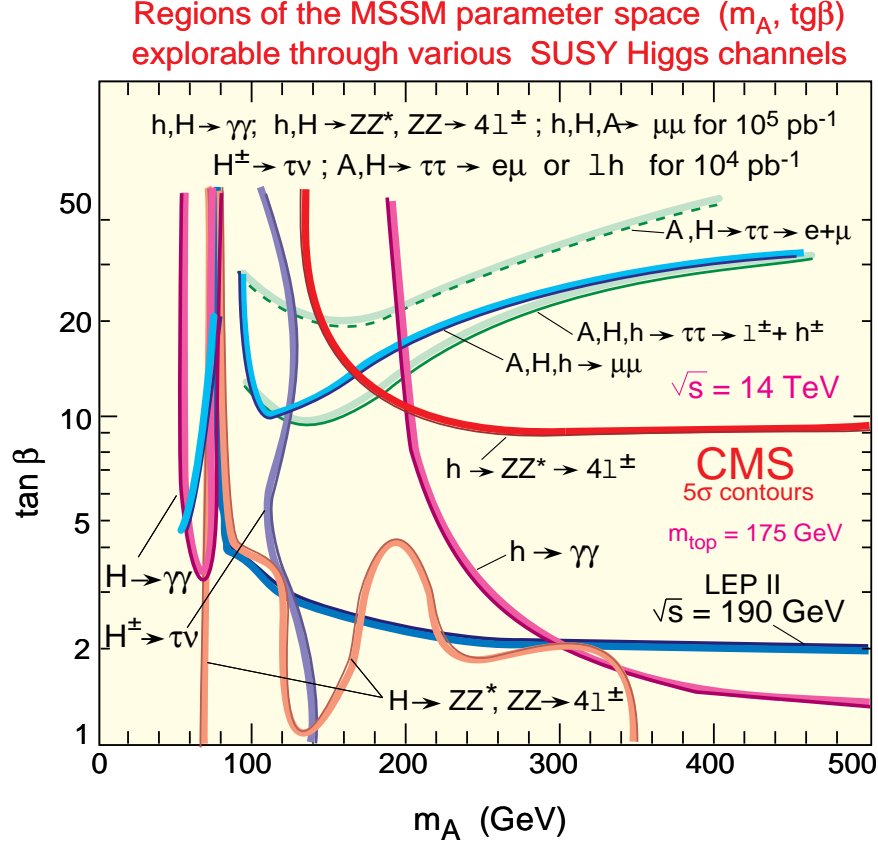


Figure 19: Discovery contours (5σ) in the parameter space of the minimal supersymmetric model for ATLAS+CMS at the LHC: $L = 300 \text{ fb}^{-1}$. Figure from Ref. [97]. Two-loop/RGE-improved radiative corrections to the MSSM Higgs sector are included assuming $m_{\tilde{t}} = 1 \text{ TeV}$ and no squark mixing.

Significance contours for SUSY Higgses



D.D 554c

Figure 20: Discovery contours (5σ) in the parameter space of the minimal supersymmetric model for the CMS detector at the LHC from the original Technical Proposal, Ref. [93]. The contours for $h^0, H^0 \rightarrow \gamma\gamma$, $h^0, H^0 \rightarrow ZZ^{(*)} \rightarrow 4\ell$, and $h^0, H^0, A^0 \rightarrow \mu\mu$ are shown for an integrated luminosity of 100 fb^{-1} . The contours for $H^0, A^0 \rightarrow \tau^+\tau^- \rightarrow e\mu, \ell h$ ($h = \text{hadron}$) and $t \rightarrow H^+b$ are shown for an integrated luminosity of 10 fb^{-1} . Also shown is the contour for the discovery region of LEP2. Nominally, this figure is for $m_t = 175 \text{ GeV}$. However, after accounting for two-loop/RGE-improved Higgs mass corrections, the h^0 and LEP2 discovery contours of this figure should be reinterpreted as those for a top quark pole mass of $m_t \sim 190 \text{ GeV}$.

bosons is close to full strength, but its coupling to $b\bar{b}$ and $\tau^+\tau^-$ is enhanced, so its branching ratio to vector boson pairs and two photons is suppressed. Thus h^0 must be sought in its decay to $b\bar{b}$ or $\tau^+\tau^-$ in this region. However, the $\tau^+\tau^-$ decay mode of the SUSY Higgs bosons has a large background from $Z \rightarrow \tau^+\tau^-$. Since $m_{h^0} < 113$ GeV for $m_t = 175$ GeV (taking $m_{\tilde{\tau}} = 1$ TeV and assuming no squark mixing) the lightest scalar Higgs is too close to the Z peak to be observed. Thus only H^0 and A^0 are candidates for observation via the $\tau^+\tau^-$ decay mode. For large $\tan\beta$, the cross section for the production of these particles in association with $b\bar{b}$ is greatly enhanced, and is the dominant production cross section [80].

The events are triggered by the leptonic decay of one τ , and the other τ is allowed to decay hadronically to maximize its branching ratio. Certain criteria, such as a single charged high- p_T track, are imposed to separate the hadronically decaying τ from an ordinary jet. This has an efficiency of about 25% for a jet rejection factor of about 400. Events are selected with large missing p_T due to the lost τ neutrinos. The missing p_T is projected along the τ directions, given roughly by the direction of their decay products since the τ 's are moving relativistically. This allows the reconstruction of the τ momenta and hence the $\tau^+\tau^-$ invariant mass [107]. The p_T^{miss} resolution thus directly affects the width of the reconstructed $\tau^+\tau^-$ invariant mass. Provided that the calorimetry coverage extends up to $|\eta| \lesssim 5$ (as expected for both CMS and ATLAS), the expected p_T^{miss} resolution is about 6 GeV for $A^0 \rightarrow \tau^+\tau^-$ events with $m_{A^0} \sim 200$ GeV and the reconstructed m_{A^0} resolution is 20 GeV at low luminosity. Since the p_T^{miss} resolution is deteriorated at full luminosity, this search may be best carried out during low-luminosity running. A comparison of Figs. 18 and 19 indicates, however, some overall improvement in the significance of the $\tau^+\tau^-$ signals by going to higher luminosity. A similar analysis is applied to events in which both τ 's decay leptonically, but the lower event rate leads to less statistical significance.

The region in the $(m_{A^0}, \tan\beta)$ plane which is covered by the $H^0, A^0 \rightarrow \tau^+\tau^-$ channel is shown in Figs. 18 and 19. For $L = 300 \text{ fb}^{-1}$ and $m_t = 175$ GeV the region over which the $A^0, H^0 \rightarrow \tau\tau$ discovery channel is viable extends all the way down to $\tan\beta = 1$ for $m_{A^0} \sim 70$ GeV, rising to $\tan\beta \sim 20$ by $m_{A^0} \sim 500$ GeV. (For $\tan\beta \lesssim 2$, the $gg \rightarrow A^0 \rightarrow \tau\tau$ reaction provides the crucial contribution to this signal.) This, in particular, means that discovery of the H^0, A^0 will be possible for $80 \text{ GeV} \lesssim m_{A^0} \lesssim 160 \text{ GeV}$ and $\tan\beta \gtrsim 4$ where the $h^0 \rightarrow \gamma\gamma$ modes are not viable and Zh^0 production cannot be observed at LEP2.

CMS has explored the decay modes $h^0, H^0, A^0 \rightarrow \mu^+\mu^-$ for large $\tan\beta$. Although the branching ratio is very small, about 3×10^{-4} , the large enhancement of the cross section for $b\bar{b}A^0$ and either $b\bar{b}H^0$ (high m_{A^0}) or $b\bar{b}h^0$ (low m_{A^0}) compensates. The main background is Drell-Yan production of $\mu^+\mu^-$. The resulting discovery contours with 100 fb^{-1} of integrated luminosity are shown in the CMS contour figure, Fig. 20. Very roughly, $\tan\beta \gtrsim 10$ is required for $m_{A^0} \sim 100$ GeV, rising to $\tan\beta \gtrsim 30$ by $m_{A^0} \sim 500$ GeV. The $\mu^+\mu^-$ contours are close to the $\tau^+\tau^-$

contour obtained with $L = 10 \text{ fb}^{-1}$, but the $\mu^+\mu^-$ channel yields a cleaner signal identification and better mass resolution. Nonetheless, by comparing the above-referenced $\mu^+\mu^-$ contours to Figs. 18 and 19, we see that even for $L = 30 \text{ fb}^{-1}$, the $\tau^+\tau^-$ mode will probe to lower $\tan\beta$ values at any given m_{A^0} . Both the $\tau^+\tau^-$ and $\mu^+\mu^-$ signals can be enhanced by tagging the b jets produced in association with the Higgs bosons. It will be interesting to see how the $\mu^+\mu^-$ and $\tau^+\tau^-$ modes compare once b -tagging is required.

The charged Higgs boson of the minimal supersymmetric model is best sought in top-quark decays, $t \rightarrow H^+b$. For $\tan\beta > 1$, the branching ratio of $H^+ \rightarrow \tau^+\nu_\tau$ exceeds 30%, and is nearly unity for $\tan\beta > 2$. CMS and ATLAS have studied the signal from $t\bar{t}$ events with one semileptonic top decay and one top decay to a charged Higgs, followed by $H^+ \rightarrow \tau^+\nu_\tau$. The main irreducible background is from top decay to a τ lepton through a W boson. This can be normalized by measuring the top semileptonic decay rate and using lepton universality. Reducible backgrounds are rejected by tagging one or both b jets in the signal. CMS and ATLAS find that, with 30 fb^{-1} of integrated luminosity, a charged Higgs of mass less than about 140 GeV can be detected for all values of $\tan\beta$, extending to $\lesssim 160 \text{ GeV}$ at low or high $\tan\beta$ values, in the case of a top-quark pole mass of 175 GeV. This is indicated by the approximately vertical contours that begin at $m_{A^0} = 140 \text{ GeV}$ at $\tan\beta = 1$ in Figs. 18 and 19.

The results of the Technical Proposals [92, 93] indicated that all of these processes combined were still not enough to guarantee detection of at least one MSSM Higgs boson throughout the entire SUSY parameter space. The hole that remained in the contour plots of Refs. [92, 93] (see Fig. 20) at moderate m_{A^0} and $\tan\beta \sim 3 - 10$ remains in Fig. 18, but disappears in Fig. 19 by virtue of the much more extensive coverage of the $h^0 \rightarrow \gamma\gamma$ and $H^0, A^0 \rightarrow \tau^+\tau^-$ modes at high luminosity. The observability of the $H^0, A^0 \rightarrow \tau^+\tau^-$ modes is such that $L = 600 \text{ fb}^{-1}$ (combining ATLAS+CMS) provides more than adequate coverage of the entire $(m_{A^0}, \tan\beta)$ parameter plane. At $L = 100 \text{ fb}^{-1}$ coverage is already complete.

We shall now turn to a discussion of additional detection modes that rely on b -tagging. Not only might these modes provide backup in this ‘hole’ region, they also expand the portions of parameter space over which more than one of the MSSM Higgs bosons can be discovered. Equally important, they allow a direct probe of the often dominant $b\bar{b}$ decay channel. In the early theoretical studies quoted, it was assumed (following Ref. [91]) that an efficiency of 25%-30% and purity of 99% for tagging b -jets with $p_T > 20 \text{ GeV}$ and central rapidity could be achieved. In obtaining their most recent results, ATLAS and CMS employ efficiency (purity) of 60% (99%) for $p_T \gtrsim 15 \text{ GeV}$ for low luminosity running and 50% (98%) for $p_T \gtrsim 30 \text{ GeV}$ for high luminosity running, obtained solely from vertex tagging, as outlined earlier; high- p_T lepton tags could further improve these efficiencies.

The most direct way to take advantage of b -tagging is to employ modes where the Higgs boson decays to $b\bar{b}$. We first discuss Higgs production in association

with a W boson [87] or $t\bar{t}$ [108]. Both have the potential to contribute in the hole region when the WW and $t\bar{t}$ couplings are of roughly standard model strength — the h^0 has approximately SM strength couplings once $m_{A^0} \gtrsim m_Z$, while the H^0 has roughly SM-like strength couplings when $m_{A^0} \lesssim m_Z$ and m_{H^0} approaches its lower bound (a more precise discussion appears in association with Tables 2 and 3). The W +Higgs and $t\bar{t}$ +Higgs processes were discussed above in the “light” intermediate-mass standard Higgs section. Recall that it is uncertain that the W +Higgs mode can be used at high luminosity [92], but it can definitely be employed at low luminosity, yielding a signal for $m_{\phi^0} \lesssim 105$ GeV if ATLAS and CMS data are combined assuming that the two detectors have similar capabilities in this channel. ATLAS finds that the $t\bar{t}\phi^0$ with $\phi^0 \rightarrow b\bar{b}$ process *can* be employed at high luminosity. New results are not yet available, but the Technical Proposal [92] claims coverage up to $m_{\phi^0} \sim 100$ GeV with 100 fb^{-1} of integrated luminosity. With 600 fb^{-1} of luminosity for ATLAS+CMS, this would be extended to at least $m_{\phi^0} \sim 120$ GeV.

Coming to the MSSM Higgs, we first note that for $\tan\beta > 1$ the $b\bar{b}$ coupling of the h^0 remains somewhat enhanced until m_{A^0} becomes very large (see Fig. 3), implying an enhanced value for $BR(h^0 \rightarrow b\bar{b})$ compared to the ϕ^0 . The $h^0 W^+ W^-$ and $t\bar{t}h^0$ couplings reach more-or-less full strength by $m_{A^0} \gtrsim 100$ GeV, implying an enhanced overall rate for Wh^0 and $t\bar{t}h^0$ with $h^0 \rightarrow b\bar{b}$ once $m_{A^0} \gtrsim 100$ GeV out to fairly large m_{A^0} . Thus, based on the results of the Technical Proposals, the discovery region for the Wh^0 and $t\bar{t}h^0$ modes should certainly extend to m_{h^0} values at least as large as the roughly 105 GeV ($L = 30 \text{ fb}^{-1}$) and 120 GeV ($L = 600 \text{ fb}^{-1}$) limits for the two modes, respectively, found for m_{ϕ^0} in the standard model case. Since m_{h^0} is below 113 GeV (unless $m_{\tilde{t}} > 1$ TeV and/or squark mixing is large), see Fig. 2, and since the ‘hole’ region is at moderate m_{A^0} , we see that the Wh^0 and $t\bar{t}h^0$ modes both are likely to allow h^0 detection in the ‘hole’ in the SUSY parameter space.

The experimental studies of the $t\bar{t}h^0$ (with $h^0 \rightarrow b\bar{b}$) mode have not been refined to the point that a corresponding contour has been included in Figs. 18 and 19. The theoretical results [108] claim substantial coverage in the hole region even for the somewhat pessimistic b -tagging assumptions employed in the study. (The radiative corrections were also done there at one loop, implying larger m_{h^0} values than found at the two-loop/RGE-improved level.) Thus, there is considerable cause for optimism. The impact of the Wh^0 (with $h^0 \rightarrow b\bar{b}$) mode has been examined in Refs. [96, 97]. The coverage provided by this mode for $L = 30 \text{ fb}^{-1}$ after combining the ATLAS signal with a presumably equal signal from CMS is illustrated in Fig. 18. There, the Wh^0 mode is shown to cover most of the $m_{A^0} \gtrsim 100$ GeV, $\tan\beta \lesssim 4$ region, where $m_{h^0} \lesssim 105$ GeV (Fig. 2). Unfortunately, it seems that the experimental analysis does not find enough enhancement for the h^0 rate relative to the ϕ^0 rate in this channel as to provide backup in the ‘hole’ region of the low-luminosity figure. It should be noted, however, that the boundary of $\tan\beta \lesssim 4$

is almost certainly a very soft one, depending delicately on the exact luminosity assumed, precise two-loop/RGE-improved radiative corrections employed, and so forth. For instance, as $m_{\tilde{t}}$ is lowered below 1 TeV, the upper bound on m_{h^0} decreases rapidly (see Fig. 2), and the region of viability for this mode would expand dramatically.

For large $\tan\beta$, the enhanced cross section for associated production of SUSY Higgs bosons with $b\bar{b}$, followed by Higgs decay to $b\bar{b}$, yields a four b -jet signal [109]. Tagging at least three b jets with $p_T > 15$ GeV is required to reduce backgrounds. It is necessary to establish an efficient trigger for these events in order to observe this signal; this is currently being studied by the ATLAS and CMS collaborations. The dominant backgrounds are $gg \rightarrow b\bar{b}b\bar{b}$, and $gg \rightarrow b\bar{b}g$ with a mis-tag of the gluon jet. Assuming the latest 60% efficiency and 99% purity for b -tagging at $L = 30 \text{ fb}^{-1}$, the $b\bar{b}h^0$ reaction yields a viable signal for $m_{A^0} \lesssim 125 \text{ GeV}$, $\tan\beta \gtrsim 4 - 5$; $b\bar{b}H^0$ production probes $m_{A^0} \gtrsim 125 \text{ GeV}$ for $\tan\beta \gtrsim 5$, rising to $\tan\beta \gtrsim 15$ for $m_{A^0} \gtrsim 500 \text{ GeV}$; $b\bar{b}A^0$ production will allow A^0 discovery throughout the region defined by $\tan\beta \gtrsim 4 - 5$ at low m_{A^0} rising smoothly to $\tan\beta \gtrsim 15$ at $m_{A^0} \gtrsim 500 \text{ GeV}$. These results, from Ref. [110] and displayed in Fig. 21, are a big improvement over those obtained for the SDC-like b -tagging capabilities assumed in Ref. [109]. They imply that the $4b$ final state could be competitive with the $\tau^+\tau^-$ final state modes for detecting the H^0 and A^0 if an efficient trigger can be developed for the former.

For $m_{H^\pm} > m_t + m_b$, one can consider searching for the decay of the charged Higgs to $t\bar{b}$. This signal is most promising when used in conjunction with the production process $gg \rightarrow t\bar{b}H^-$, and tagging several of the four b jets in the final state [111]. For moderate $\tan\beta$, the production cross section is suppressed such that the signal is not observable above the irreducible $t\bar{t}b\bar{b}$ background. The potential of this process is therefore limited to small and large values of $\tan\beta$. With 200 fb^{-1} , and assuming the now-pessimistic SDC-like b -tagging efficiency and purity, a signal may be observable for $\tan\beta < 1.7$ and $m_{H^\pm} < 400 \text{ GeV}$, and for $\tan\beta > 30$ and $m_{H^\pm} < 300 \text{ GeV}$. This limited region of utility can be expected to expand once the current ATLAS and CMS b -tagging scenarios are utilized.

CMS and ATLAS have considered the process $gg \rightarrow A^0 \rightarrow Zh^0 \rightarrow \ell^+\ell^-b\bar{b}$. For $\tan\beta < 2$, the branching ratio of $A^0 \rightarrow Zh^0$ is about 50%. They have demonstrated an observable signal with single and double b tagging. In Fig. 19 one finds a discovery region for $200 \lesssim m_{A^0} \lesssim 2m_t$ and $\tan\beta \lesssim 3$ for $L = 600 \text{ fb}^{-1}$ (*i.e.* $L = 300 \text{ fb}^{-1}$ for ATLAS and CMS separately), reduced to $\tan\beta \lesssim 2$ for $L = 60 \text{ fb}^{-1}$, Fig. 18.

Recent results from CMS and ATLAS for the mode $H^0, A^0 \rightarrow t\bar{t}$ also appear in Figs. 18 and 19. Even with good b -tagging, the decays $H^0, A^0 \rightarrow t\bar{t}$ are challenging to detect at the LHC due to the large background from $gg \rightarrow t\bar{t}$ (which can interfere destructively with the signal) [102]. Nonetheless, the preliminary studies indicate that, for the anticipated b -tagging capability, ATLAS and CMS can detect $A^0, H^0 \rightarrow t\bar{t}$ for $\tan\beta \lesssim 2 - 1.5$ with $L = 60 \text{ fb}^{-1}$ and for $\tan\beta \lesssim 3 - 2.5$ with

4b Final State 5 σ LHC Discovery Contours

$m_{\text{stop}}=1$ TeV, no squark mixing

$m_t=175$ GeV, $\varepsilon_{b\text{-tag}}=0.6$, $\varepsilon_{\text{mis-tag}}=0.01$

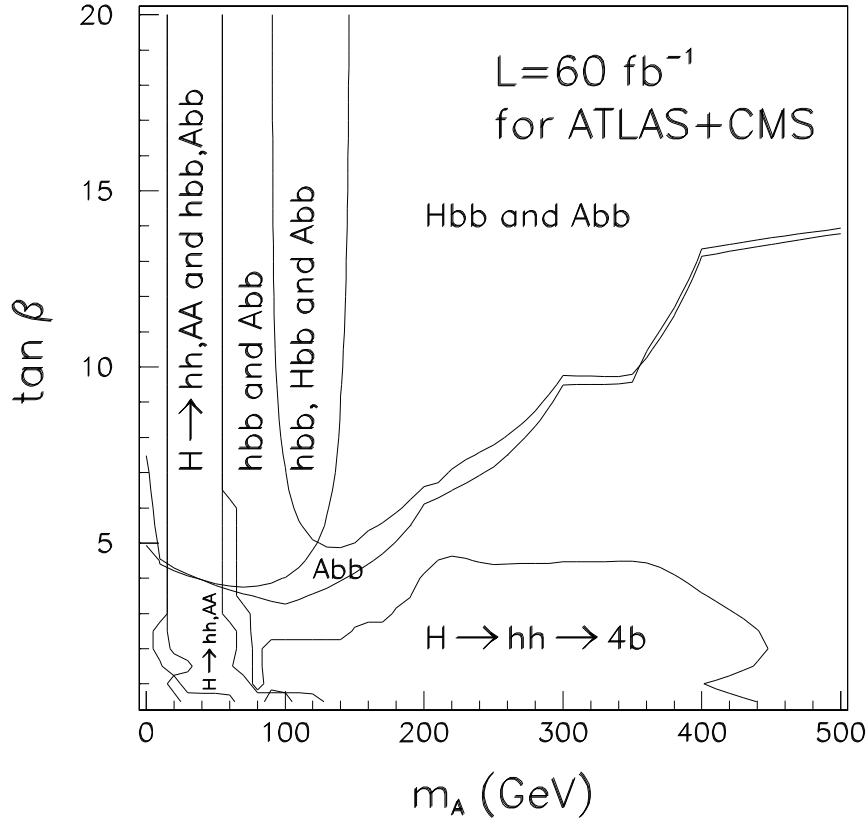


Figure 21: $4b$ final state 5σ discovery regions for $H^0 b\bar{b}$, $A^0 b\bar{b}$, $H^0 \rightarrow h^0 h^0$ and $H^0 \rightarrow A^0 A^0$ in $(m_{A^0}, \tan \beta)$ parameter space at the LHC for combined ATLAS+CMS luminosity of $L = 60 \text{ fb}^{-1}$, assuming that an efficient $4b$ trigger can be developed. Two-loop/RGE-improved radiative corrections to the MSSM Higgs sector are included assuming $m_t = 175 \text{ GeV}$, $m_{\tilde{t}} = 1 \text{ TeV}$ and no squark mixing.

$L = 600 \text{ fb}^{-1}$. Caution in accepting these preliminary results is perhaps warranted since they have been obtained by simply comparing signal and background cross section levels; excellent knowledge of the magnitude of the $t\bar{t}$ background will then be required since $S/B \sim 0.02 - 0.1$.

The $H^0 \rightarrow h^0 h^0$ mode can potentially be employed in the channels $h^0 h^0 \rightarrow b\bar{b}b\bar{b}$ and $h^0 h^0 \rightarrow b\bar{b}\gamma\gamma$. The former mode has been explored in Ref. [112]; using 4 b -tagging (with 50% efficiency and 98% purity for $p_T > 30 \text{ GeV}$ at $L = 600 \text{ fb}^{-1}$) and requiring that there be two $b\bar{b}$ pairs of mass $\sim m_{h^0}$ yields a viable signal for $170 \lesssim m_{A^0} \lesssim 500 \text{ GeV}$ and $\tan\beta \lesssim 5$. For $L = 60 \text{ fb}^{-1}$, b -tagging cuts can be softened and one can be sensitive to lower masses. Using 60% efficiency and 99% purity for $p_T \gtrsim 15 \text{ GeV}$, one finds that $H^0 \rightarrow h^0 h^0$ and/or $H^0 \rightarrow A^0 A^0$ can also be detected in the region $m_{A^0} \lesssim 60 \text{ GeV}$, $\tan\beta \gtrsim 1$. This is illustrated in Fig. 21. Note from this figure that the ATLAS+CMS $b\bar{b}h^0$, $b\bar{b}H^0$, $b\bar{b}A^0$, $H^0 \rightarrow h^0 h^0$ and $H^0 \rightarrow A^0 A^0$ $4b$ final state signals at combined $L = 60 \text{ fb}^{-1}$ yield a signal for one or more of the MSSM Higgs bosons over a very substantial portion of parameter space.

Because of uncertainty concerning the ability to trigger on the $4b$ final state, ATLAS and CMS have examined the $H^0 \rightarrow h^0 h^0 \rightarrow b\bar{b}\gamma\gamma$ final state. This is a very clean channel (with b tagging), but is rate limited. For $L = 600 \text{ fb}^{-1}$ (Fig. 19) a discovery region for ATLAS+CMS of $175 \text{ GeV} \lesssim m_{A^0} \lesssim 2m_t$, $\tan\beta \lesssim 4-5$ is found (using the 50% efficiency and 98% purity claimed by ATLAS at high luminosity); the region is substantially reduced for $L = 30 \text{ fb}^{-1}$ (Fig. 18). It is important to note that when both $H^0 \rightarrow h^0 h^0 \rightarrow 2b2\gamma$ and $4b$ can be observed, then it will be possible to determine the very important ratio $BR(h^0 \rightarrow b\bar{b})/BR(H^0 \rightarrow \gamma\gamma)$.

Putting together all these modes, we can summarize by saying that for moderate $m_{A^0} \lesssim 2m_t$ there is an excellent chance of detecting more than one of the MSSM Higgs bosons. However, for large $m_{A^0} \gtrsim 250 \text{ GeV}$ (as preferred in the GUT scenarios) only the h^0 is certain to be found. For $m_{A^0} \gtrsim 250 \text{ GeV}$, the h^0 modes that are guaranteed to be observable are the $h^0 \rightarrow \gamma\gamma$ production/decay modes ($gg \rightarrow h^0$, $t\bar{t}h^0$, and Wh^0 , all with $h^0 \rightarrow \gamma\gamma$). Even for m_{A^0} values as large as $400 - 500 \text{ GeV}$, it is also likely that the production/decay mode $t\bar{t}h^0$ with $h^0 \rightarrow b\bar{b}$ can be observed, especially if $m_{\tilde{t}}$ is sufficiently below 1 TeV that m_{h^0} is $\lesssim 100 \text{ GeV}$. For high enough $m_{\tilde{t}}$, $h^0 \rightarrow ZZ^*$ might also be detected. Whether or not it will be possible to see any other Higgs boson depends on $\tan\beta$. There are basically three possibilities when $m_{A^0} \gtrsim 250 \text{ GeV}$. i) $\tan\beta \lesssim 3-5$, in which case $A^0, H^0 \rightarrow t\bar{t}$ and $H^0 \rightarrow h^0 h^0 \rightarrow b\bar{b}\gamma\gamma, 4b$ will be observable; ii) $\tan\beta \gtrsim 6$ (increasing as m_{A^0} increases above 250 GeV), for which $A^0, H^0 \rightarrow \tau^+\tau^-$ (and at larger $\tan\beta$, $\mu^+\mu^-$) will be observable, supplemented by $b\bar{b}A^0, b\bar{b}H^0 \rightarrow 4b$ final states; and iii) $3-5 \lesssim \tan\beta \lesssim 6$ at $m_{A^0} \sim 250 \text{ GeV}$, increasing to $3-5 \lesssim \tan\beta \lesssim 13$ by $m_{A^0} \sim 500 \text{ GeV}$, which will be devoid of A^0, H^0 signals. Further improvements in b -tagging efficiency and purity would lead to a narrowing of this latter wedge of parameter space.

We must reiterate that the above results have assumed an absence of SUSY

decays of the Higgs bosons. For a light ino sector it is possible that $h^0 \rightarrow \tilde{\chi}_1^0 \tilde{\chi}_1^0$ will be the dominant decay. Detection of the h^0 in the standard modes becomes difficult or impossible. However, it has been demonstrated that detection in $t\bar{t}h^0$ [113] and Wh^0 [114, 115] production will be possible after employing cuts requiring large missing energy. Assuming universal gaugino masses at the GUT scale, our first warning that we must look in invisible modes would be the observation of $\tilde{\chi}_1^+ \tilde{\chi}_1^-$ production at LEP2. The A^0, H^0, H^\pm could all also have substantial SUSY decays, especially if m_{A^0} is large. Such decays will not be significant if $\tan\beta$ is large since the $b\bar{b}, \tau^+\tau^-, \mu^+\mu^-$ modes are enhanced, but would generally severely reduce signals in the standard channels when $\tan\beta$ is in the small to moderate range [16].

4.3.1 Distinguishing the MSSM h^0 from the SM ϕ^0 at the LHC

Suppose that m_{A^0} is moderately large and that $\tan\beta$ is in the middle range described above where only the h^0 can be detected. Then, only detailed measurements of the properties of the h^0 could reveal that it is part of the larger MSSM Higgs sector, and not just the minimal ϕ^0 . In this region of parameter space, the couplings of the h^0 are quite SM-like, and substantial precision in such measurements would be needed. For a SM-like h^0 , we are certain to be able to measure

- (a) $\sigma(gg \rightarrow h^0)BR(h^0 \rightarrow \gamma\gamma)$
- (b) $\sigma(Wh^0)BR(h^0 \rightarrow \gamma\gamma)$ and
- (c) $\sigma(t\bar{t}h^0)BR(h^0 \rightarrow \gamma\gamma)$.

From the latter two we can compute the ratio $\sigma(Wh^0)/\sigma(t\bar{t}h^0)$. If $m_{\tilde{t}}$ is very large, and/or squark mixing is large, so that m_{h^0} is above about 120 – 130 GeV, we shall also be able to measure

- (d) $\sigma(gg \rightarrow h^0)BR(h^0 \rightarrow ZZ^*)$.

Combining (a) with (d) we obtain the ratio $BR(h^0 \rightarrow \gamma\gamma)/BR(h^0 \rightarrow ZZ^*)$. If $m_{\tilde{t}} \lesssim 1$ TeV and squark mixing is not large, so that m_{h^0} is below about 120 GeV, then we instead observe

- (e) $\sigma(t\bar{t}h^0)BR(h^0 \rightarrow b\bar{b})$ and possibly
- (f) $\sigma(Wh^0)BR(h^0 \rightarrow b\bar{b})$.

Using (b)+(f) or, more likely, (c)+(e), we can compute $BR(h^0 \rightarrow \gamma\gamma)/BR(h^0 \rightarrow b\bar{b})$.

The three ratios mentioned above as well as the basic rate for (a) are all sensitive to small differences between the h^0 and a standard ϕ^0 of the same mass. To

quantify this sensitivity, we present [116] in Fig. 22 contours for the ratio of the MSSM predictions for these four quantities to those obtained for a ϕ^0 of exactly the same mass. For simplicity we have employed a uniform value of $m_{\tilde{t}} = 1$ TeV and neglected squark mixing in computing the MSSM Higgs sector radiative corrections. From the graphs, it would appear that the ratio $BR(\gamma\gamma)/BR(b\bar{b})$ provides the best probe, since deviations as large as 10% persist well beyond $m_{A^0} = 600$ GeV. However, as estimated in a later section (see Table 6), determination of this ratio with such precision from LHC data alone is not likely. The next most sensitive probe is the cross section times branching ratio $\sigma(gg \rightarrow h^0)BR(h^0 \rightarrow \gamma\gamma)$; deviations as large as 10% persist out to values of m_{A^0} as large as $m_{A^0} \sim 550$ GeV. In Table 6 we estimate that this product can be measured with roughly $\pm 4\%$ accuracy. However, it is important to keep in mind that we will not be able to distinguish a deviation due to the difference between the h^0 and ϕ^0 from a deviation due to some new physics contribution to the loops responsible for the Higgs- gg and/or Higgs- $\gamma\gamma$ coupling. Further, $BR(h \rightarrow \gamma\gamma)$ and $BR(h \rightarrow b\bar{b})$ ($h = h^0$ or ϕ^0) would both be affected by unexpected contributions to the total h decay width — for example, an enhanced $h \rightarrow gg$ partial width and/or invisible $h^0 \rightarrow \tilde{\chi}_1^0 \tilde{\chi}_1^0$ decays. In addition, there is a systematic uncertainty in our ability to determine $BR(h \rightarrow b\bar{b})$ due to uncertainty in the value of the running (\overline{MS}) mass $m_b(m_h)$;

$$\frac{\delta BR(b\bar{b})}{BR(b\bar{b})} \simeq BR(\text{non} - b) \frac{\delta \Gamma(b\bar{b})}{\Gamma(b\bar{b})} \sim BR(\text{non} - b) \frac{2\delta m_b}{m_b} \sim 2 - 3\%, \quad (21)$$

for a 5% uncertainty in m_b . Some current lattice calculations claim that $m_b(m_b)$ (in the \overline{MS} scheme) can be determined more accurately than this. Ref. [117] gives a result $m_b(m_b) = 4.0 \pm 0.1$ GeV, an error of 2.5%. Unfortunately, the more model-independent $h^0 WW/h^0 t\bar{t}$ coupling ratio encoded in the (b)/(c) cross section ratio will be very difficult to measure to the 2% or better accuracy required to probe out to large values of m_{A^0} ; in Table 6 we estimate an error of roughly $\pm 13\%$ for the numerator and denominator individually.

5 Tevatron and Tev*

The Tevatron is currently operating at $\sqrt{s} = 1.8$ TeV, at an instantaneous luminosity of $\mathcal{L} \approx 10^{31}/\text{cm}^2/\text{s}$. The Main Injector is expected to begin operation in 1999, increasing the luminosity to $\mathcal{L} \approx 2 \times 10^{32}/\text{cm}^2/\text{s}$, which provides about 2 fb^{-1} of integrated luminosity per year. The machine energy will be increased to $\sqrt{s} = 2$ TeV at that time.

One can consider increasing the luminosity even further. This idea is generically referred to as the Tev*, with an instantaneous luminosity around $5 \times 10^{32}/\text{cm}^2/\text{s}$. An instantaneous luminosity of $10^{33}/\text{cm}^2/\text{s}$ or higher can also be envisioned; this is referred to as Tev33. (We use Tev* to denote both Tev* and Tev33 in the following.)

LHC: MSSM/SM Light Higgs Ratio Contours

$m_{\text{TOP}} = 175 \text{ GeV}$, $m_{\text{STOP}} = 1 \text{ TeV}$

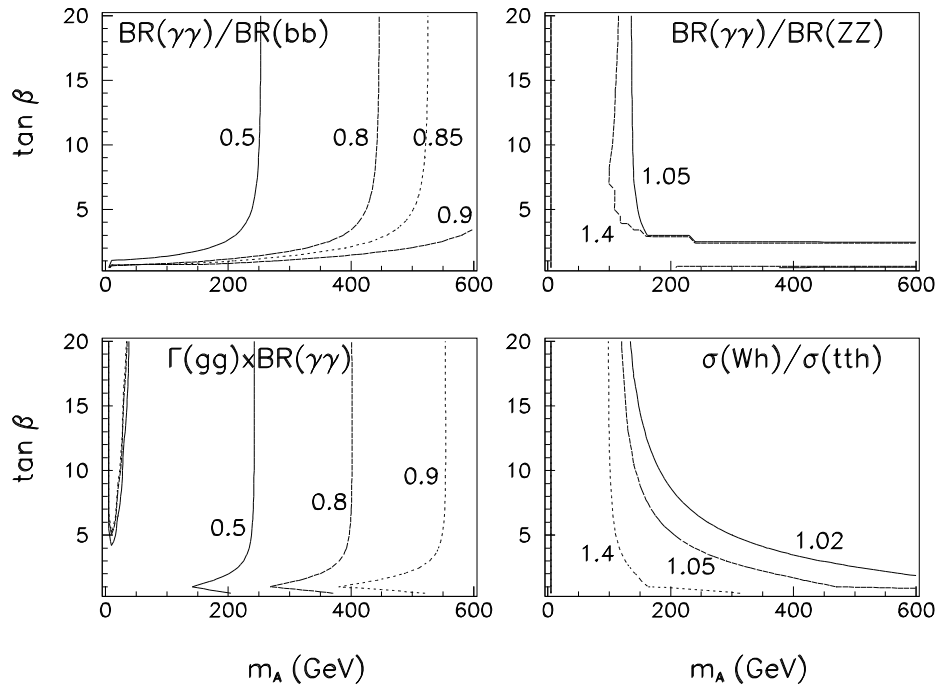


Figure 22: Contours for ratios of MSSM h^0 results to SM ϕ^0 results for $m_{h^0} = m_{\phi^0}$, in $(m_{A^0}, \tan \beta)$ parameter space. We take $m_t = 175 \text{ GeV}$, $m_{\tilde{t}} = 1 \text{ TeV}$, and neglect squark mixing in computing the two-loop/RGE-improved radiative corrections to the MSSM Higgs sector.

With the 132 ns bunch spacing of the Tevatron (with the Main Injector), this luminosity results in about 15 interactions per bunch crossing. The bunch spacing can be reduced in principle to 19 ns (comparable to the 25 ns timing of the LHC), yielding about 2 interactions per crossing. The luminosity upgrade and the reduced bunch spacing each require detector upgrades, or perhaps a new detector [118].

The most promising mode for the standard Higgs at the Tevatron and Tev^* is $W\phi^0$ production, followed by $\phi^0 \rightarrow b\bar{b}$ [119, 87, 89, 121]. This process was discussed in the section on the LHC. Since the production is via quark-antiquark annihilation, the cross section is only a factor of four less at the Tevatron than at the LHC (including acceptance). On the other hand, the top-quark backgrounds, which are the dominant backgrounds at the LHC, are much smaller at the Tevatron. The largest backgrounds at the Tevatron and Tev^* are the irreducible processes $Wb\bar{b}$ and WZ (for $m_{\phi^0} \approx m_Z$), and, for $m_{\phi^0} > 100 \text{ GeV}$, the top-quark backgrounds. Each of these backgrounds is comparable to the signal. The WZ background can be normalized via the leptonic decays of the weak vector bosons. However, should the Higgs mass happen to lie near the Z mass, this background may be particularly problematic, since the Higgs peak will simply add to the Z peak, and observation of the Higgs will rely on an excess of events in the peak region.

The most comprehensive study of the $W\phi^0$ with $\phi^0 \rightarrow b\bar{b}$ process at the Tevatron and the Tev^* is Ref. [122]. The search at the Tevatron ($2-4 \text{ fb}^{-1}$) will be limited to $m_{\phi^0} < m_Z$, a region that will already have been explored at LEP2. Should a Higgs be discovered at LEP2, it would be interesting to search for it at the Tevatron to test the relationship between the $\phi^0 ZZ$ and $\phi^0 W^+ W^-$ couplings (which are related by custodial $\text{SU}(2)$).

The most important issue in the analysis of $W\phi^0$ with $\phi^0 \rightarrow b\bar{b}$ at the Tevatron and the Tev^* is the $b\bar{b}$ invariant-mass resolution. Ref. [122] assumes this can be improved over the current resolution by inventing a jet-clustering algorithm that takes into account hard gluon radiation. With this improved resolution, a Higgs boson of mass $60 - 100 \text{ GeV}$ is detectable at the Tev^* with 10 fb^{-1} of integrated luminosity.

To attain Higgs masses much above the Z mass, higher luminosity is needed. Tev33 can potentially deliver 30 fb^{-1} in three years. Unless the bunch spacing is decreased, this will require dealing with about 15 interactions per bunch crossing. Fortunately, since the $t\bar{t}$ background is small, one does not have to veto jets with small p_T , which is difficult to do in this environment. Ref. [122] concludes that a Higgs mass of 120 GeV requires approximately 25 fb^{-1} of integrated luminosity.

Should Higgs masses above 100 GeV be observable via $W\phi^0$ with $\phi^0 \rightarrow b\bar{b}$, it would have particular significance for the lightest SUSY Higgs scalar, h^0 . For $\tan \beta > 1$, the coupling and, hence, partial width for $h^0 \rightarrow b\bar{b}$ are enhanced even for fairly large m_{A^0} values (see Fig. 3), thereby suppressing its branching ratio to two photons. The best chance to observe this particle may thus lie in its dominant decay mode to $b\bar{b}$.

The processes $W\phi^0, Z\phi^0$, with $\phi^0 \rightarrow \tau^+\tau^-$ and $W, Z \rightarrow jj$, may also provide an opportunity for detection of the intermediate-mass Higgs boson [89]. The $\tau^+\tau^-$ invariant mass can be reconstructed from the one-prong decays of the τ 's by projecting the missing p_T (from neutrinos) along the direction of motion of the charged track from the τ decay [107, 89]. The dominant background is Zjj with $Z \rightarrow \tau^+\tau^-$, which is much larger than the signal, so this mode is restricted to Higgs masses somewhat above the Z mass. A Higgs of mass 110 – 120 GeV may be accessible with 30 fb^{-1} of integrated luminosity. This requires high-efficiency τ identification, a goal worth pursuing. The signal peak lies on the tail of the rapidly falling Zjj background, which complicates its extraction. If $\phi^0 \rightarrow \tau^+\tau^-$ can be observed for $m_{\phi^0} > 110 \text{ GeV}$, it would have particular significance for the lightest Higgs scalar, h^0 , for the same reason as discussed above for the mode $h^0 \rightarrow b\bar{b}$.

The most comprehensive study of $W\phi^0, Z\phi^0$, with $\phi^0 \rightarrow \tau^+\tau^-$ and $W, Z \rightarrow jj$, is Ref. [123]. This study concludes that a Higgs signal (for $m_{\phi^0} = 120 \text{ GeV}$) is not observable even with 100 fb^{-1} of integrated luminosity. This is largely due to the fact that this study assumed a missing p_T resolution achievable in existing detectors, while Ref. [89] assumed improved resolution in upgraded detectors.

The gold-plated mode, $gg \rightarrow ZZ^* \rightarrow \ell^+\ell^-\ell^+\ell^-$, has been studied in Ref. [120]. Compared with the LHC, the signal cross section is greatly reduced with respect to the irreducible background $q\bar{q} \rightarrow ZZ$. Even with 100 fb^{-1} of integrated luminosity, there is no Higgs mass at which an observable signal can be established, due both to the background and the small number of signal events.

Finally, we note that, in the case of the SUSY Higgs sector with $m_{\tilde{t}} = 1 \text{ TeV}$ and no squark mixing, the $H^0 \rightarrow h^0h^0, A^0A^0 \rightarrow 4b$ final state mode is predicted to yield a 5σ signal for $m_{A^0} \lesssim 60 \text{ GeV}$ and $\tan\beta \gtrsim 1$ [112] if $e_{b\text{-tag}} = 0.75$ with $e_{\text{mis-tag}} = 0.0025$ could ultimately be achieved.

6 DiTevatron

The energy of the Tevatron can be increased by replacing the existing magnets with magnets of higher field strength. The existing magnets have a field strength of 4.4 Tesla; replacing them with 8.8 Tesla magnets (comparable to the 8.36 Tesla LHC magnets) doubles the energy to $\sqrt{s} = 4 \text{ TeV}$. This is referred to as the DiTevatron. A luminosity upgrade, similar to the Tev*, can be implemented as well, if desired. In the following we assume a luminosity upgrade, and consider the discovery potential with 30 fb^{-1} of integrated luminosity.

There is apparently little or no advantage for the process $W\phi^0$ with $\phi^0 \rightarrow b\bar{b}$ at the DiTevatron as compared with the Tev* [87, 120, 88, 89, 121]. Although the signal cross section roughly doubles, the top-quark backgrounds increase much more, and become non-negligible for all Higgs masses at the DiTevatron. The statistical significance of the signal is no better at the DiTevatron than at the Tev*

for the same integrated luminosity.

The most comprehensive study of $W\phi^0$ with $\phi^0 \rightarrow b\bar{b}$ at the DiTevatron is Ref. [88]. This study finds that Higgs masses above m_Z cannot be probed with 30 fb^{-1} . However, several refinements in the analysis, such as those in Ref. [122], would likely change this conclusion. Still, there is no reason to believe that the DiTevatron is superior to the Tev* (for the same integrated luminosity) for this channel.

The process $W\phi^0$ with $\phi^0 \rightarrow \tau^+\tau^-$ is less promising at the DiTevatron compared with the Tevatron due to the increase in the Zjj background relative to the signal [89]. The Higgs mass region $110 - 120 \text{ GeV}$, which may be accessible at the Tev*, falls below the level of observability at the DiTevatron, due to the large increase in the Zjj background. For the same reason, this process is hopeless at the LHC.

A variety of signals involving Higgs-boson decay to vector-boson pairs has been studied at the DiTevatron [120]. The most promising of these is the gold-plated mode, $gg \rightarrow ZZ^{(*)} \rightarrow \ell^+\ell^-\ell^+\ell^-$. In the intermediate-mass region, it is crucial to be able to efficiently identify leptons at low p_T in order to have enough events. A lepton p_T threshold of 10 GeV yields about 10 events in 30 fb^{-1} at $m_{\phi^0} = 150 \text{ GeV}$, with no irreducible background. For $m_{\phi^0} > 2m_Z$, the irreducible ZZ background is comparable to the signal. With 30 fb^{-1} , a Higgs of mass close to 200 GeV may be observable. The extraction of the signal at this mass is confounded by the fact that it is close to the threshold for the ZZ background.

The process $gg \rightarrow \phi^0 \rightarrow W^+W^- \rightarrow \ell\nu jj$ suffers from an enormous irreducible background, approximately 100 times as large as the signal. A statistically significant signal is obtained for $m_{\phi^0} \approx 170 \text{ GeV}$. However, the extraction of the signal is once again confounded by the fact that it is close to the threshold for the background.

The process $gg \rightarrow \phi^0 \rightarrow W^+W^- \rightarrow \ell^+\nu\ell^-\bar{\nu}$ has a very large background from W^+W^- production which is about an order of magnitude above the signal. The signal is broad and lies near the threshold for the background, so is difficult to extract.

The process $gg \rightarrow \phi^0 \rightarrow ZZ \rightarrow \ell^+\ell^-\nu\bar{\nu}$ yields a statistically significant signal for $m_{\phi^0} = 200 - 250 \text{ GeV}$. However, the background from processes such as Zj , where the jet transverse momentum is badly mismeasured or the jet is lost in the forward direction, has not been included in this analysis, and could render this process unobservable.

The processes involving Higgs decay to vector-boson pairs would be aided by increased integrated luminosity. For example, if 100 fb^{-1} can be collected, the gold-plated mode could cover the mass regions $m_{\phi^0} = 200 - 300 \text{ GeV}$ and $m_{\phi^0} \sim 150 \text{ GeV}$. The actual reach in these modes cannot be established until a more complete study, including efficiencies and detector simulation, has been performed.

7 Determining the properties of the SM Higgs from hadron collider data

In this section we summarize the extent to which the expected observations for a light ($m_{\phi^0} \lesssim 2m_W$) SM-like Higgs can be used for a detailed determination of its properties, including total width and partial widths for various channels. After combining all hadron collider information, let us presume that we measure accurately those cross sections listed earlier:

- (a) $\sigma(gg \rightarrow \phi^0)BR(\phi^0 \rightarrow \gamma\gamma)$,
- (b) $\sigma(W\phi^0)BR(\phi^0 \rightarrow \gamma\gamma)$,
- (c) $\sigma(t\bar{t}\phi^0)BR(\phi^0 \rightarrow \gamma\gamma)$, and either
- (d) $\sigma(gg \rightarrow \phi^0)BR(\phi^0 \rightarrow ZZ^*)$ (for $m_{\phi^0} \gtrsim 120$ GeV) or
- (e) $\sigma(t\bar{t}\phi^0)BR(\phi^0 \rightarrow b\bar{b})$ and
- (f) $\sigma(W\phi^0)BR(\phi^0 \rightarrow b\bar{b})$ (for, very optimistically, $m_{\phi^0} \lesssim 120$ GeV).

In order to achieve this list we assume that if Tev/Tev*/DiTevatron measurements are employed for (f), then extrapolation to LHC energy can be done accurately so that we can analyze the situation as though all data is available at a single energy. Further, we presume that the Tevatron $W\phi^0$ with $\phi^0 \rightarrow \tau^+\tau^-$ rates are converted to the equivalent $W\phi^0$ with $\phi^0 \rightarrow b\bar{b}$ rates assuming the standard relation between $\phi^0 b\bar{b}$ and $\phi^0 \tau^+\tau^-$ couplings.

From (b)+(c) we determine the $\phi^0 t\bar{t}$ to $\phi^0 WW$ coupling ratio. This allows us to check the SM prediction. From (a)+(c) we determine the $\phi^0 gg$ to $\phi^0 t\bar{t}$ coupling ratio. This can then be checked against the assumption of t -loop dominance. The presence of extra (heavy) colored particle loop contributions to the $gg\phi^0$ coupling would be easily apparent as a large discrepancy. For $m_{\phi^0} \lesssim 120$ GeV, from (b)+(f) and also (c)+(e) we can determine $BR(\phi^0 \rightarrow \gamma\gamma)/BR(\phi^0 \rightarrow b\bar{b})$. Deviations of this ratio from expectations would indicate extra heavy charged particle loop contributions to the $\phi^0 \gamma\gamma$ coupling, deviations of the total ϕ^0 width from expectations (including contributions from invisible channels), deviations in the $\phi^0 \rightarrow b\bar{b}$ coupling, and/or deviations in the $\phi^0 WW$ coupling that controls the dominate W -loop contribution. These effects would be difficult to disentangle without further information. For $m_{\phi^0} \gtrsim 120$ GeV (a)+(d) allows determination of $BR(\phi^0 \rightarrow \gamma\gamma)/BR(\phi^0 \rightarrow ZZ^*)$ which could deviate from expectations for the same reasons as summarized above. Of course, one could test the internal consistency of SM choices for all couplings. The simplest examples of such tests for $m_{\phi^0} \lesssim 120$ GeV would be to see if the predicted value for $BR(\phi^0 \rightarrow b\bar{b})$ combined with (e) and (f) yields the expected $\phi^0 t\bar{t}$ and $\phi^0 WW$ couplings. For

$m_{\phi^0} \gtrsim 120 \text{ GeV}$, the predicted $BR(\phi^0 \rightarrow ZZ^*) + (d)$ could be used to extract the $\phi^0 gg$ coupling which could in turn be tested against the top-quark loop prediction.

Obviously, it will be important for the experimental collaborations to assess the errors (both systematic and statistical) that will accompany the above analysis. We give some very rough estimates in a later section, see Table 6. Certainly, though, it is clear that a model-independent analysis of couplings and total width is not possible for $m_{\phi^0} \lesssim 2m_W$ using hadron collider data alone. We shall see, however, that by combining with data from a linear e^+e^- collider (which on its own can also not provide a complete model-independent determination of the total width and all couplings) an essentially complete analysis is within reach.

8 A Next Linear e^+e^- Collider

A Next Linear Collider (NLC) can be expected to play a very important role in unravelling the physics of a light Higgs sector, whether that of the standard model or that of an extended Higgs sector such as a multi-doublet model, including the constrained two-doublet structure of the minimal supersymmetric standard model. We shall focus on expectations for the SM and the MSSM, with additional remarks on a general two-Higgs-doublet model (2HDM) and the inclusion of extra Higgs singlet fields. Theories containing Higgs triplet fields, even if constructed to preserve $\rho \equiv m_W/(\cos \theta_W m_Z) = 1$ at tree-level, must be fine-tuned in order to maintain $\rho = 1$ at one-loop, since ρ is infinitely renormalized [23]. Thus, we only briefly remark on Higgs triplets here.

8.1 Machine and Detector Considerations

The probable design of the NLC has progressed enormously over the last few years. It has become conventional to assume that a $\sqrt{s} = 500 \text{ GeV}$ e^+e^- collider can be built with an instantaneous luminosity of the order $5 \times 10^{33} \text{ cm}^{-2} \text{ s}^{-1}$, corresponding to an annual integrated luminosity in the neighborhood of $L = 50 \text{ fb}^{-1}$. It is also normally assumed that expansion of the collider to $\sqrt{s} = 1 - 1.5 \text{ TeV}$ with annual $L \sim 200 \text{ fb}^{-1}$ would be feasible. We shall adopt these luminosity assumptions in the discussions to follow.

Other characteristics of the machine and detector also play critical roles in assessing our ability to study light Higgs bosons at the NLC. First, the collision energy will generally be very well defined; neither simple initial-state radiation nor, for current designs, beamstrahlung leads to much spread in the collision energy. For those relatively rare instances in which there is significant radiation, it has been shown [124] that it is almost always due to the emission of a photon by only one of the initial-state fermions, not both, leaving the missing energy in an event equal to the observed longitudinal boost. Thus, kinematic fitting using center-of-mass energy constraints can be used to take full advantage of the clean initial

state. Regarding the detector, the performance level of SLC/LEP-type detectors is more than adequate for even detailed studies of Higgs boson branching ratios and the like. The detector simulations that will be referenced in what follows typically include: limited forward calorimeter acceptance, with no detector elements below 10° from the beamline; hermetic calorimetry, which allows accurate energy-flow determination; efficient, large acceptance central tracking; efficient electron, muon, and photon identification; and powerful heavy quark flavor tagging via a microvertex detector.

8.2 Backgrounds at the NLC

The obvious advantage of e^+e^- colliders over hadron colliders is that the high- p_T background processes that might obscure a Higgs signal are relatively small in size and are accurately calculable. At energies between $\sqrt{s} = 500$ GeV and 1.5 TeV, the dominant backgrounds are due to hard electroweak and QCD processes, in particular $e^+e^- \rightarrow W^+W^-$, $e^+e^- \rightarrow q\bar{q}$, and $e^+e^- \rightarrow e\nu W$. Other backgrounds that have been included in the simulations include $e^+e^- \rightarrow Z\gamma$, $e^+e^- Z$, $\nu\bar{\nu}\gamma$, ZZ , $W^+W^-\gamma$, $\nu\bar{\nu}Z$, $e^+e^-W^+W^-$, W^+W^-Z , $e\nu WZ$, $\nu\bar{\nu}W^+W^-$, $t\bar{t}Z$, $\nu\bar{\nu}ZZ$, e^+e^-ZZ , ZZZ and $\nu\bar{\nu}t\bar{t}$, in rough order of descending cross section; see, for example, Ref. [125].

8.3 The SM Higgs boson at the NLC

The dominant production mechanisms for a SM Higgs boson are $e^+e^- \rightarrow \nu\bar{\nu}\phi^0$, via W^+W^- fusion, and $e^+e^- \rightarrow Z\phi^0$ via virtual Z^* . For Higgs bosons in the 80 to 200 GeV range, the cross sections for these two reactions are similar in size at $\sqrt{s} = 500$ GeV — for $m_{\phi^0} \sim 200$ GeV both yield $\sigma/\sigma_{pt} \sim 0.1$, where $\sigma_{pt} = 100 \text{ fb}/s(\text{TeV}^2) \sim 400 \text{ fb}$ [16]. Thus, at an integrated luminosity of 50 fb^{-1} , for $m_{\phi^0} \sim 200$ GeV we have roughly 2000 Higgs boson events of each type with which to work. As m_{ϕ^0} decreases, the W^+W^- fusion process rapidly becomes larger than the $Z\phi^0$ process, while for $m_{\phi^0} > 200$ GeV the $Z\phi^0$ cross section is larger than that from W^+W^- fusion. Generally speaking, the $Z\phi^0$ final state will be the preferred channel in which to search for a Higgs boson with a $\sqrt{s} = 500$ GeV machine since observation of the Z allows a direct determination of the Higgs boson four-momentum.

The branching ratios for a SM Higgs boson are illustrated in Fig. 4. At low mass, the important discovery channels are $b\bar{b}$ and $\tau^+\tau^-$. Various search techniques have been developed for virtually all of the possible event topologies resulting from the decay of the ϕ^0 when produced in the $Z\phi^0$ channel [126, 75, 127, 128], as well as for the primary modes of the W^+W^- -fusion reaction [129, 126]. For example, for m_{ϕ^0} values such that the ϕ^0 decays primarily to $b\bar{b}$ and $\tau\tau$ the following channels have been analyzed in the case of the $Z\phi^0$ production mode: $e^+e^- \rightarrow q\bar{q}\phi^0 \rightarrow 4j$; $e^+e^- \rightarrow Z\phi^0$, with $\phi^0 \rightarrow \tau\tau$ (with about 30% as many events as in the $4j$ topology);

$e^+e^- \rightarrow \ell^+\ell^-\phi^0$ ($\ell = e, \mu$) by examining the recoil mass corresponding to m_{ϕ^0} using the incoming beams and the lepton pair from the Z ; $e^+e^- \rightarrow Z\phi^0$, with $Z \rightarrow \nu\bar{\nu}$ (b tagging needed for $m_{\phi^0} \sim m_Z$). The results of these studies, using all the decay topologies listed above, and the analogous ones required for other reactions and/or other mass regions, are summarized below [127, 130]. It is assumed that a 5σ excess in events at a particular Higgs mass is required.

Using the $Z\phi^0$ production channel, a SM Higgs boson with $m_{\phi^0} \sim 130$ GeV (200 GeV) can be discovered in one week (one month) of running at typical design luminosities of $5 \times 10^{33} \text{cm}^{-2}\text{s}^{-1}$. For heavier masses, the discovery can be made in either of the the main decay channels $\phi^0 \rightarrow W^+W^-$ or ZZ . This is possible for any of the decay modes of the vector bosons, although the hadronic decays are favored due to their larger branching ratios. For m_{ϕ^0} up to 350 GeV, discovery is possible within one year for $L = 50 \text{fb}^{-1}$ at $\sqrt{s} = 500$ GeV [126]. For 50fb^{-1} of data, the $e^+e^- \rightarrow \nu\bar{\nu}W^+W^- \rightarrow \phi^0\nu\bar{\nu}$ fusion process is observable up to $m_{\phi^0} = 300$ GeV. For still heavier Higgs bosons, higher machine energies are required. The $e^+e^- \rightarrow \nu\bar{\nu}\phi^0$ (WW -fusion) process provides a clean discovery of any Higgs boson with $m_{\phi^0} \lesssim 0.7\sqrt{s}$ for typical planned luminosities. For example, the expandability of a linear collider to $\sqrt{s} = 1$ TeV with yearly luminosity of 200fb^{-1} would ensure that any Higgs boson with mass below about 700 GeV can eventually be discovered at an e^+e^- linear collider. Consequently, the entire mass range for which the Higgs boson is ‘weakly coupled’ will be accessible. The requirements for exploring a strongly-coupled Higgs sector are delineated in the companion report of the working group on “Strongly-Coupled Electroweak Symmetry Breaking” [101].

Of course, other production mechanisms for the Higgs boson are also of considerable interest. In particular, the $e^+e^- \rightarrow t\bar{t}\phi^0$ process is accessible for $m_{\phi^0} \lesssim 120$ GeV at $\sqrt{s} = 500$ GeV [131]. The $\gamma\gamma$ collider mode of operation, which will be discussed at more length later, will allow Higgs detection up to $m_{\phi^0} \sim 300 - 350$ GeV, *i.e.* it does not extend the reach of the machine for the standard Higgs [130].

8.3.1 Detailed study of Higgs total width, partial widths and couplings

Once the Higgs boson has been found, a rather precise determination of all of its properties will be the next order of business. In particular, it would be highly desirable to be able to determine (in a model-independent fashion) not only its exact mass, but also its total width and its couplings to all types of particles. We shall see that a reasonably complete study can be performed, especially if e^+e^- collision data is combined with hadron collider data and $\gamma\gamma$ collision data. The use of measurements beyond e^+e^- collisions is especially crucial when $m_{\phi^0} < 2m_W$ (where the total width is too small to be experimentally measurable from the resonance shape). We first outline the basic strategies, and then give estimates of the level of uncertainty that will be encountered due to experimental errors.

From the detection mode in which $Z\phi^0 \rightarrow \ell^+\ell^-X$, the Higgs mass peak is

observed as a peak in the recoil mass obtained from the initial energy and outgoing Z momentum; this peak automatically includes all possible Higgs decays. The value of the total cross section $\sigma(e^+e^- \rightarrow Z\phi^0)$ is obtained simply from the production rate and the known $Z \rightarrow \ell^+\ell^-$ branching ratio, thereby allowing an absolute normalization of the $\phi^0 ZZ$ coupling. Given this determination of $\sigma(Z\phi^0)$, measurements of $\sigma(Z\phi^0)BR(\phi^0 \rightarrow X)$ for any channel will yield the absolute value of $BR(\phi^0 \rightarrow X)$. The $\phi^0 WW$ coupling can be directly determined using the measured rates for WW fusion reactions $e^+e^- \rightarrow \nu\bar{\nu}\phi^0 \rightarrow \nu\bar{\nu}X$ for those final states for which $BR(\phi^0 \rightarrow X)$ has been determined using the $Z\phi^0$ measurements. The value obtained for the $\phi^0 WW$ coupling can be cross checked with that computed from the $\phi^0 ZZ$ coupling assuming custodial symmetry. Given the $\phi^0 WW$ coupling, the partial width for $\phi^0 \rightarrow WW^{(*)}$ can be computed. (Here, $W^{(*)}$ is a real or virtual W depending upon m_{ϕ^0} .)

In principle, the partial width for any channel X (and associated $\phi^0 \rightarrow X$ coupling) can be obtained from NLC data alone. After obtaining the partial width for $\phi^0 \rightarrow WW^{(*)}$ as outlined above, one would compute:

$$\Gamma_{\phi^0}^{\text{tot}} = \Gamma(\phi^0 \rightarrow WW^{(*)})/BR(\phi^0 \rightarrow WW^{(*)}), \quad (22)$$

and then

$$\Gamma(\phi^0 \rightarrow X) = \Gamma_{\phi^0}^{\text{tot}} BR(\phi^0 \rightarrow X). \quad (23)$$

In particular, this procedure would apply for $X = f\bar{f}$. Further, by comparing the $Z\phi^0 \rightarrow \ell^+\ell^-X$ inclusive (recoil-mass) channel to the explicit sum over observable channels, *e.g.* the $b\bar{b}$, $\tau^+\tau^-$, $c\bar{c} + gg$, $WW^{(*)}$ and $ZZ^{(*)}$ channels, one can, in principle, determine if there are additional modes (including invisible decays) contributing to the total width. Unfortunately, there are difficulties in practice in carrying out the above program.

For smaller m_{ϕ^0} , roughly $m_{\phi^0} \lesssim 120 - 140$ GeV, the $f\bar{f} = b\bar{b}, \tau^+\tau^-$ branching ratios will be determined with reasonable accuracy (*e.g.* $\pm 7\%, \pm 14\%$, respectively, for $m_{\phi^0} = 120$ GeV), but the $WW^{(*)}$ and $ZZ^{(*)}$ branching ratios will be very difficult to measure with reasonable errors (in the case of $WW^{(*)}$, $\pm 50\%, \pm 35\%, \pm 25\%$ for $m_{\phi^0} \sim 120, 130, 140$ GeV, respectively). (Typical errors will be reviewed in more detail later). Thus, neither the total ϕ^0 width nor the $f\bar{f}$ absolute partial widths (and couplings) could be determined accurately.

At larger m_{ϕ^0} (roughly beginning about $m_{\phi^0} \gtrsim 145$ GeV), the $WW^{(*)}$ branching ratio should be measured with good accuracy. This means that the ϕ^0 total width could be determined in this region as in Eq. 22 within reasonable errors. (Of course, for m_{ϕ^0} above about $2m_W$ the total width is larger than 0.2 GeV, large enough to also allow direct measurement by resonance shape.) However, for $m_{\phi^0} \sim 140$ GeV, errors on the $b\bar{b}$ and $\tau\tau$ branching ratios of the ϕ^0 increase to $\gtrsim 12\%$ and $\gtrsim 24\%$, respectively (worsening rapidly as m_{ϕ^0} increases further). For $m_{\phi^0} \gtrsim 150$ GeV the $X = f\bar{f}$ partial widths and couplings would then be rather poorly determined through Eq. 23.

The $\phi^0 t\bar{t}$ coupling might prove more accessible. In principle, the $t\bar{t}$ branching ratio measurement could prove feasible once $m_{\phi^0} \gtrsim 2m_t$, although for the ϕ^0 this branching ratio is never more than about 20%. At low masses, $m_{\phi^0} \lesssim 120$ GeV, we have already noted that it is probably possible to measure $\sigma(t\bar{t}\phi^0)BR(\phi^0 \rightarrow b\bar{b})$ [92]; this allows a determination of the $\phi^0 t\bar{t}$ coupling by employing the value of $BR(\phi^0 \rightarrow b\bar{b})$ measured in $Z\phi^0$ production. Note that were $\sigma(b\bar{b}\phi^0)BR(\phi^0 \rightarrow b\bar{b})$ not too small to be measurable, one could have used it and the measured $BR(\phi^0 \rightarrow b\bar{b})$ to determine the total width of the ϕ^0 .

Let us now consider what gains can be achieved by combining NLC information with LHC/Tev/Tev* measurements. As summarized in an earlier section, we can presume that we have determinations of

- (a) $\sigma(gg \rightarrow \phi^0)BR(\phi^0 \rightarrow \gamma\gamma)$,
- (b) $\sigma(W\phi^0)BR(\phi^0 \rightarrow \gamma\gamma)$,
- (c) $\sigma(t\bar{t}\phi^0)BR(\phi^0 \rightarrow \gamma\gamma)$, and either
- (d) $\sigma(gg \rightarrow \phi^0)BR(\phi^0 \rightarrow ZZ^*)$ (for $m_{\phi^0} \gtrsim 120$ GeV) or
- (e) $\sigma(t\bar{t}\phi^0)BR(\phi^0 \rightarrow b\bar{b})$ and
- (f) $\sigma(W\phi^0)BR(\phi^0 \rightarrow b\bar{b})$ (for, very optimistically, $m_{\phi^0} \lesssim 120$ GeV).

Tevatron measurements that contribute are assumed to be extrapolated to the LHC energy. Consider first $m_{\phi^0} \lesssim 120$ GeV. From the NLC we have a reasonable determination of $BR(\phi^0 \rightarrow b\bar{b})$; (e) and (f) then allow us to determine $\sigma(t\bar{t}\phi^0)$ and $\sigma(W\phi^0)$. The former (latter) provides us with a cross check on the NLC determination of the $\phi^0 t\bar{t}$ ($\phi^0 WW$) coupling. The value of $\sigma(W\phi^0)$ [$\sigma(t\bar{t}\phi^0)$] combined with (b) [(c)] each allows an independent determination of $BR(\phi^0 \rightarrow \gamma\gamma)$, which can then be combined with (a) to determine the $\phi^0 gg$ coupling. This latter can then be checked against the assumption of t -loop dominance given the previous determinations of the $\phi^0 t\bar{t}$ coupling. As noted previously, the presence of extra (heavy) colored particle loop contributions to the $\phi^0 gg$ coupling would be easily apparent as a large discrepancy. Deviations of $BR(\phi^0 \rightarrow \gamma\gamma)$ from expectations would be symptomatic of heavy charged particle loop contributions to the $\phi^0 \gamma\gamma$ coupling and/or deviations of the total width from expectations. For $m_{\phi^0} \gtrsim 120$ GeV, the value of $BR(\phi^0 \rightarrow ZZ^{(*)})$ computed and/or measured at the NLC combined with (d) yields $\sigma(gg \rightarrow \phi^0)$ (which determines the $\phi^0 t\bar{t}$ coupling if no extra loops are present). The determination of $\sigma(gg \rightarrow \phi^0)$ combined with (a) yields a determination of $BR(\phi^0 \rightarrow \gamma\gamma)$. An independent determination of the $\gamma\gamma$ branching ratio is possible using (b) and the value of the $\phi^0 WW$ coupling as computed from the NLC determination of the $\phi^0 ZZ$ coupling and as measured directly in WW fusion production.

Thus, for both $m_{\phi^0} \lesssim 120 \text{ GeV}$ and $m_{\phi^0} \gtrsim 120 \text{ GeV}$, combining NLC with hadron collider data will provide a series of cross checks and a determination of $BR(\phi^0 \rightarrow \gamma\gamma)$. An accurate determination of the $\phi^0 \rightarrow b\bar{b}$ partial width and coupling remains elusive for all m_{ϕ^0} values, and a determination of the total ϕ^0 width is not possible until far enough into the $m_{\phi^0} \gtrsim 120 \text{ GeV}$ region that $\sigma(Z\phi^0)BR(\phi^0 \rightarrow WW^*)$ can be measured with reasonable accuracy at the NLC. This is unfortunate. For example, for $m_{\phi^0} \lesssim 120 \text{ GeV}$ an enhanced $b\bar{b}$ coupling for the Higgs would enhance both the $b\bar{b}$ partial width and the Higgs total width without changing $BR(\phi^0 \rightarrow b\bar{b})$ very much (see Eq. 21), and thus could easily escape notice. And, as noted earlier, unexpected contributions to the total width could be present and would lead to deviations in $BR(\phi^0 \rightarrow b\bar{b})$. However, there is an ace in the hole. As we shall describe in a later section, the $\gamma\gamma$ collider mode of operation would allow ϕ^0 discovery and determination of the partial width $\Gamma(\phi^0 \rightarrow \gamma\gamma)$. This, combined with the hadron collider determination of $BR(\phi^0 \rightarrow \gamma\gamma)$ then yields the total ϕ^0 width! If $BR(\phi^0 \rightarrow b\bar{b})$ is measured with reasonable accuracy (requiring $m_{\phi^0} \lesssim 145 \text{ GeV}$) then by combining with the total width determination we obtain $\Gamma(\phi^0 \rightarrow b\bar{b})$ and a determination of the $\phi^0 b\bar{b}$ coupling. In short, for $m_{\phi^0} \lesssim 2m_W$ *all three machines — LHC, NLC and $\gamma\gamma$ collider — are needed to complete a model-independent study of the ϕ^0 .*

Let us now quantify the expected errors in the relevant measurements. The most optimistic expectations in the ‘intermediate’ $m_{\phi^0} < 2m_W$ mass region are reviewed in Ref. [132]. There it is assumed that the machine will be run at the optimal energy for the $Z\phi^0$ cross section, $\sqrt{s} \sim m_Z + m_{\phi^0} + 20/30 \text{ GeV}$, that luminosity of $L = 30 \text{ fb}^{-1}$ is accumulated, *and* that the detector has the characteristics of the proposed “super” performance JLC detector [128], especially the super momentum resolutions and the high b -tagging efficiency. With these assumptions, m_{ϕ^0} can be measured to $\sim 0.1\%$ using direct m_{ϕ^0} reconstruction in the $Z\phi^0 \rightarrow \nu\bar{\nu}jj, \ell^+\ell^-jj, jjjj$ channels. This estimate is based on the roughly 4 GeV uncertainty per event for reconstructing the mass from the detector information, divided by \sqrt{N} , where N is the total number of events. Further, the mass resolution for the recoil mass peak in $Z\phi^0$ events is of order 0.3 GeV per event for $Z \rightarrow \ell^+\ell^-$ decays, leading to a measurement of m_{ϕ^0} to $\pm 20 \text{ MeV}$ for $m_{\phi^0} \lesssim 140 \text{ GeV}$ and $L = 50 \text{ fb}^{-1}$. The total width, $\Gamma_{\phi^0}^{\text{tot}}$ can be measured down to $\sim 0.2 \text{ GeV}$ using $Z\phi^0$ events with $Z \rightarrow \ell^+\ell^-$ and examining the recoil mass. Unfortunately, this latter sensitivity is not adequate for a direct observation of the SM Higgs boson width until m_{ϕ^0} approaches the WW decay threshold. For example, the width is predicted to be in the range $\Gamma_{\phi^0} \lesssim 10 \text{ MeV}$ for $m_{\phi^0} \lesssim 140 \text{ GeV}$; see Fig. 6. (However, in this mass range the width can be much larger than this for some of the Higgs bosons in models such as the MSSM.) Perhaps most critical is the determination of the $e^+e^- \rightarrow Z\phi^0$ total cross section, which (as noted above) is the best means for directly determining the $\phi^0 ZZ$ coupling. This determination is best made by employing the $Z\phi^0 \rightarrow \ell^+\ell^-X$ mode. Greatest sensitivity to a Higgs boson

is obtained by specifically excluding events in which X is a single γ (a channel to which Higgs decay does not contribute) because of the large radiative contribution to this channel. The Higgs boson is then observed as a bump in the recoiling X mass. Ref. [132] finds that $\sigma(e^+e^- \rightarrow Z\phi^0)$ can be measured with a relative error of $\sim 7\%$, thereby allowing a $\sim 3.5\%$ determination of the $\phi^0 ZZ$ coupling. Note that this technique automatically sums over all possible decay modes of the ϕ^0 , including invisible channels — knowledge of the Higgs decays is not required to extract the $\phi^0 ZZ$ coupling from the inclusive recoil mass spectrum.

Turning to the relative (and absolute) branching ratios of the ϕ^0 , for the “super”-JLC detector and a Higgs mass in the vicinity of ~ 110 GeV, Ref. [132] states that $\sigma(e^+e^- \rightarrow Z\phi^0)BR(\phi^0 \rightarrow b\bar{b})$ can be measured with a precision of $\sim 2\%$ for $L = 80 \text{ fb}^{-1}$ (or $\sim 2.5\%$ for $L = 50 \text{ fb}^{-1}$), which yields a roughly 8% determination of $BR(\phi^0 \rightarrow b\bar{b})$ itself, given the 7% error in $\sigma(Z\phi^0)$. Further, $BR(\phi^0 \rightarrow \tau^-\tau^+)/BR(\phi^0 \rightarrow b\bar{b})$ can be determined within $\sim 6\%$, whereas $BR(\phi^0 \rightarrow c\bar{c})/BR(\phi^0 \rightarrow b\bar{b})$ could only be determined within a roughly 100% error. However, even this rough a measurement might be adequate to determine that the Higgs boson has enhanced $b\bar{b}$ and suppressed $c\bar{c}$ couplings as is possible in extended Higgs sector models.

The accuracy of some of these measurements would not be this good if a detector of the generic SLC/LEP variety is employed. The expectations for this case have been examined with particular care in Ref. [133] (see also the review of Ref. [134]), again for a relatively light Higgs boson. We shall quote results for $m_{\phi^0} \sim 120$ GeV and $m_{\phi^0} \sim 140$ GeV. The simulations have assumed that the Higgs mass is known with an accuracy of ~ 5 GeV (as would be easily achieved using the various discovery modes), that the machine energy is set to the optimal value for the $Z\phi^0$ mode — $\sqrt{s} \sim m_Z + m_{\phi^0} + 20/30$ GeV, and that luminosity of $L = 50 \text{ fb}^{-1}$ is accumulated.

To measure $\sigma(Z\phi^0)BR(\phi^0 \rightarrow X)$ for all the relevant channels X , Ref. [133] uses high-impact-parameter track counting (in the precision microvertex detector) to help distinguish between the $b\bar{b}$, $\tau\tau$, WW , and $c\bar{c} + gg$ decay modes. The $b\bar{b}$ decay mode is singled out after b -tagging in the available decay topologies, and $\sigma(Z\phi^0)BR(\phi^0 \rightarrow b\bar{b})$ can be measured with a precision of about 7% (12%) for $m_{\phi^0} = 120$ GeV (140 GeV). The $c\bar{c} + gg$ modes are dominant if anti- b -tagging is implemented, and the corresponding $\sigma(Z\phi^0)BR$ can be measured with a combined statistical precision of 39% (116%), with much larger errors associated with extracting $c\bar{c}$ alone. The $\tau\tau$ mode can be rather cleanly separated from the others in the $\tau\tau q\bar{q}$ topology and $\sigma(Z\phi^0)BR(\phi^0 \rightarrow \tau\tau)$ can be measured to within $\pm 14\%$ ($\pm 22\%$). Finally, measurement of $\sigma(Z\phi^0)BR(\phi^0 \rightarrow WW^*)$ requires an analysis which selects the ZWW^* final state. This state can be reconstructed in either of the two modes $WW^* \rightarrow q\bar{q}q\bar{q}$ or $WW^* \rightarrow q\bar{q}\ell\nu$ using the W , Z , and Higgs boson mass constraints and energy-momentum conservation. Anti- b -tagging removes six-jet events from $e^+e^- \rightarrow t\bar{t}$, leaving a relatively clean signal from $\phi^0 \rightarrow WW^*$.

The product $\sigma(Z\phi^0)BR(\phi^0 \rightarrow WW^*)$ can then be determined with a precision, which is limited by the relatively small branching fraction of $\phi^0 \rightarrow WW^*$, of $\pm 48\%$ ($\pm 24\%$) at Higgs masses of 120 GeV (140 GeV). The same analysis can also be applied to measure the smaller $\sigma(Z\phi^0)BR(\phi^0 \rightarrow ZZ^*)$, although with rather limited accuracy.

Explicit studies have not been performed by the experimentalists of the corresponding errors for the various $\sigma(WW \rightarrow \phi^0)BR(\phi^0 \rightarrow X)$. ($\sigma(WW \rightarrow \phi^0)$ itself is not directly measurable.) Nonetheless, for $100 \lesssim \phi^0 \lesssim 150$ GeV, the rates for $WW \rightarrow \phi^0$ fusion are larger than those for $Z\phi^0$ associated production, and backgrounds are well under control after appropriate cuts and b -tagging. For example Fig. 13b, for $m_{\phi^0} = 115$ GeV, appearing on p. 60 of Ref. [126], shows very little background in the $WW \rightarrow \phi^0 \rightarrow b\bar{b}$ mode. The total event rate after cuts would be roughly of order $S \sim 100$ in the background-free invariant mass region, implying a $1/\sqrt{S} = 10\%$ measurement of $\sigma(WW \rightarrow \phi^0)BR(\phi^0 \rightarrow b\bar{b})$. In general, it seems reasonable to suppose that errors for $\sigma(WW \rightarrow \phi^0)BR(\phi^0 \rightarrow X)$ will be comparable to those found for $\sigma(Z\phi^0)BR(\phi^0 \rightarrow X)$ for any given channel, X .

Even if the Higgs is too light for direct decays into $t\bar{t}$, we have noted that it can be produced at an observable rate in $e^+e^- \rightarrow t\bar{t}\phi^0$ for $m_{\phi^0} \lesssim 120$ GeV. By focusing on the $t\bar{t}b\bar{b}$ final state (for example) we obtain $\sigma(t\bar{t}\phi^0)BR(\phi^0 \rightarrow b\bar{b})$. The number of events is a sharply declining function of m_{ϕ^0} [131], ranging from ~ 150 for $m_{\phi^0} \sim 80$ GeV to ~ 20 for $m_{\phi^0} \sim 120$ GeV (assuming $L = 50 \text{ fb}^{-1}$, and without cuts *etc.*). Including a factor of 2 reduction for efficiencies and cuts, and assuming negligible background, we find errors in the determination of $\sigma(t\bar{t}\phi^0)BR(\phi^0 \rightarrow b\bar{b})$ ranging from $\sim 10\%$ at $m_{\phi^0} = 80$ GeV to $\gtrsim 30\%$ at $m_{\phi^0} = 120$ GeV. Since $BR(\phi^0 \rightarrow b\bar{b})$ is well determined from the $Z\phi^0$ procedures, we can then obtain $\sigma(e^+e^- \rightarrow t\bar{t}\phi^0)$ with roughly the same errors; the cross section is a direct measure of the $\phi^0 t\bar{t}$ coupling squared. For Higgs masses above $2m_t \sim 350$ GeV, the strategy would be to measure $\sigma(Z\phi^0)BR(\phi^0 \rightarrow t\bar{t})$; a $\sqrt{s} > 500$ GeV machine would be required. But if available, $BR(\phi^0 \rightarrow t\bar{t})$ (predicted to be above 10% for $m_{\phi^0} \gtrsim 400$ GeV) could be obtained and the $\phi^0 t\bar{t}$ coupling determined using knowledge of the total width. An estimate of the errors involved is not easily obtained and requires further study. For m_{ϕ^0} values between ~ 120 GeV and $\sim 2m_t$, a determination of the $\phi^0 t\bar{t}$ coupling would require greatly enhanced machine luminosity and/or energy.

Finally, the rate for $\gamma\gamma \rightarrow \phi^0 \rightarrow X$ is proportional to the product $\Gamma(\phi^0 \rightarrow \gamma\gamma)BR(\phi^0 \rightarrow X)$. The accuracy with which this product can be measured is estimated in Ref. [135] to be $\pm 5\%$ for $m_{\phi^0} \lesssim 150$ GeV in the channel $X = b\bar{b}$ and $\pm 10\%$ for $180 \text{ GeV} \lesssim m_{\phi^0} \lesssim 300$ GeV in the $X = ZZ$ channel. For m_{ϕ^0} in the 160 – 170 GeV range the $\phi^0 \rightarrow WW$ decay is dominant (but has an enormous background) and the combined $X = b\bar{b} + ZZ$ error rises to nearly 25%. We have already noted that for $m_{\phi^0} \lesssim 120$ GeV the error in $BR(\phi^0 \rightarrow b\bar{b})$ will be $\gtrsim 7\%$, implying (using quadrature) an error for $\Gamma(\phi^0 \rightarrow \gamma\gamma)$ of $\gtrsim 9\%$. By $m_{\phi^0} \sim 140$ GeV this rises to $\gtrsim 15\%$ (much worse in the $m_{\phi^0} = 160 - 170$ GeV range).

Errors for the LHC measurements have not been quoted by the experimentalists. We have made some crude estimates using the event rate information provided in the Technical Proposals, Refs. [92, 93]. In all cases we have used $\sqrt{S+B}/S$ as our fractional 1σ error estimate; here, S and B are the signal and background rates, respectively. For the $gg \rightarrow \phi^0 \rightarrow \gamma\gamma$ mode we have employed the CMS results appearing in their Figs. 12.3 and 12.5; for the $W\phi^0, t\bar{t}\phi^0$ with $\phi^0 \rightarrow \gamma\gamma$ modes we employ CMS Table 12.3; for $gg \rightarrow \phi^0 \rightarrow 4\mu$ we employ CMS Table 12.4b; for the $t\bar{t}\phi^0$ with $\phi^0 \rightarrow b\bar{b}$ mode we employ ATLAS Table 11.8. We focus only on high luminosity, assuming that $L = 300 \text{ fb}^{-1}$ is accumulated by each of the two detectors. Our errors are obtained by combining the statistics of the two detectors, corresponding to a total luminosity of $L = 600 \text{ fb}^{-1}$. The results of the figures and tables mentioned above have been extrapolated to this luminosity. Note that we have not quoted any error for the $W\phi^0$ with $\phi^0 \rightarrow b\bar{b}$ channel, since it is not certain that this channel can be isolated at high luminosity. However, Tevatron or Tev* data should ultimately provide errors on this channel that are comparable to the $t\bar{t}\phi^0$ with $\phi^0 \rightarrow b\bar{b}$ errors quoted for the LHC if $m_{\phi^0} \lesssim 120 \text{ GeV}$.

The estimated errors for directly measured quantities are summarized in Table 6. The particular m_{ϕ^0} masses for which we have tabulated results are those for which a significant number of NLC estimates by experimentalists have appeared, see above. In the table, question marks (?) indicate that we have had to extrapolate or make educated guesses. In $Z\phi^0$ production, errors on ratios of branching ratios are approximately given by adding in quadrature the errors on particular channel rates; and the error on a particular $BR(\phi^0 \rightarrow X)$ is given by adding in quadrature the error on the $\sigma(Z\phi^0)$ itself and the error on $\sigma(Z\phi^0)BR(\phi^0 \rightarrow X)$. In Table 6 we have also included some results for a possible $\mu^+\mu^-$ collider operating at $\sqrt{s} = 500 \text{ GeV}$ (the FMC) with a super energy resolution of 0.01% for the energy of each of the colliding beams. These results will be discussed in a later section. Most notable is the great precision with which m_{ϕ^0} and $\Gamma_{\phi^0}^{\text{tot}}$ can be measured (if $m_{\phi^0} \lesssim 2m_W$). It will be important for experimentalists to refine all these results and obtain errors for a given detector over the full range of possible Higgs masses.

8.3.2 Determination of the Higgs quantum numbers

A direct verification that the SM Higgs is CP-even would be highly desirable. Of course, if the $Z\phi^0$ cross section is such that the $\phi^0 ZZ$ coupling is maximal (in agreement with the SM prediction), then the ϕ^0 must be CP-even. However, a direct test can be difficult. Several approaches have been explored. These are reviewed in Refs. [130, 136, 137]. They rely on the fact that a CP-even Higgs boson will lead to very different angular production and decay distributions and/or correlations as compared to a *purely* CP-odd Higgs boson. The difficulty with these approaches is that any distribution or correlation that derives from the coupling to WW or ZZ will only be sensitive to the CP-even part of the CP-mixed state,

Table 6: NLC ($L = 50 \text{ fb}^{-1}$), LHC ($L = 300 \text{ fb}^{-1}$ per detector) and FMC ($L = 50 \text{ fb}^{-1}$) Measurement Errors. Question marks indicate extrapolations of existing studies or crude estimates.

NLC ($L = 50 \text{ fb}^{-1}$) Detector ($m_{\phi^0} \text{ (GeV)}$)	Super-JLC (110)	SLD (120)	SLD (140)
m_{ϕ^0} (final state)	$\sim 0.1\%$	$\sim 0.1\%$	$\sim 0.1\%$
m_{ϕ^0} (recoil mass)	$\sim 0.02\%$	$> 0.1\%$	$> 0.1\%$
$\Gamma_{\phi^0}^{\text{tot}}$	0.2 GeV	0.2 GeV	0.2 GeV
$\sigma(Z\phi^0)$	7%	7%	7%
$\sigma(Z\phi^0)BR(\phi^0 \rightarrow b\bar{b})$	2.5%	7%	12%
$\sigma(Z\phi^0)BR(\phi^0 \rightarrow \tau^+\tau^-)$	6%	14%	22%
$\sigma(Z\phi^0)BR(\phi^0 \rightarrow c\bar{c} + gg)$	100%	39%	116%
$\sigma(Z\phi^0)BR(\phi^0 \rightarrow WW^*)$	$\sim 100\%$?	48%	24%
$\sigma(WW \rightarrow \phi^0)BR(\phi^0 \rightarrow X)$	similar to above	for any given	final state X ?
$\Gamma(\phi^0 \rightarrow \gamma\gamma)BR(\phi^0 \rightarrow b\bar{b})$	$< 5\%$?	5%	5%
$\sigma(t\bar{t}\phi^0)BR(\phi^0 \rightarrow b\bar{b})$	$\gtrsim 25\%$?	$\gtrsim 30\%$?	unmeasurable?
LHC ($L = 600 \text{ fb}^{-1}$)	(110)	(120)	(140)
$\sigma(gg \rightarrow \phi^0)BR(\phi^0 \rightarrow \gamma\gamma)$	$\sim 4\%$?	$\sim 4\%$?	$\sim 4\%$?
$\sigma(W\phi^0)BR(\phi^0 \rightarrow \gamma\gamma)$	$\sim 13\%$?	$\sim 13\%$?	unmeasurable?
$\sigma(t\bar{t}\phi^0)BR(\phi^0 \rightarrow \gamma\gamma)$	$\sim 13\%$?	$\sim 13\%$?	unmeasurable?
$\sigma(gg \rightarrow \phi^0)BR(\phi^0 \rightarrow ZZ^*)$	unmeasurable?	large?	$\sim 10\%$?
$\sigma(W\phi^0)BR(\phi^0 \rightarrow b\bar{b})$	unmeasurable?	unmeasurable?	unmeasurable?
$\sigma(t\bar{t}\phi^0)BR(\phi^0 \rightarrow b\bar{b})$	$\sim 20\%$?	$\sim 28\%$?	unmeasurable?
FMC ($L = 50 \text{ fb}^{-1}$)	(110)	(120)	(140)
m_{ϕ^0}	$\lesssim 0.00015\%$,	$\lesssim 0.00015\%$	$\lesssim 0.0003\%$
$\Gamma_{\phi^0}^{\text{tot}}$	$\sim 10\%$	$\sim 10\%$	$\sim 10\%$
$\Gamma(\phi^0 \rightarrow \mu^+\mu^-)BR(\phi^0 \rightarrow b\bar{b})$	$\sim 0.3\%$	$\sim 0.3\%$	$\sim 0.5\%$

unless this CP-even part happens to be as small relative to the CP-odd part as the CP-odd coupling to ZZ, WW (arising only at one-loop) is relative to the CP-even coupling to ZZ, WW . However, in this limit, or in the case of a purely CP-odd Higgs boson, the production rate will be so suppressed in production channels relying on the ZZ, WW coupling that the angular analysis could not be performed with even marginal statistics anyway.

A few examples will illustrate the potential, but also the difficulties. In the discussion to follow we generically denote a neutral Higgs boson by h , where $h = \phi^0$ is presumed to be only one of many possibilities. In $e^+e^- \rightarrow Z^* \rightarrow Zh$ production, consider the distribution $d\sigma/d\cos\theta$, where θ is the angle of the produced Z in the center of mass with respect to the direction of collision of the initial e^+ and e^- . The distribution takes the form $\frac{d\sigma}{d\cos\theta} \propto \frac{8m_Z^2}{s} + \beta^2 \sin^2\theta$ in the CP-even case, as compared to $1 + \cos^2\theta$ for a CP-odd h , where β is the center-of-mass velocity of the final Z . Thus, in principle one can measure this distribution and determine the quantum numbers of the h being produced. The difficulty with this conclusion is best illustrated by considering an h which is a mixture of CP-even and CP-odd components, as described above. The crucial point is that only the CP-even portion of the h couples at tree-level to ZZ , whereas the CP-odd component of the h couples weakly to ZZ via one-loop diagrams (barring anomalous sources for this dimension-5 coupling). Consequently, the $d\sigma/d\cos\theta$ distribution will reflect only the CP-even component of the h , even if the h has a fairly large CP-odd component. The h would have to be almost entirely CP-odd in order for the $\cos\theta$ distribution to deviate significantly towards the CP-odd prediction. However, in this case, the $e^+e^- \rightarrow Z^* \rightarrow Zh$ production rate would be very small, and the h would probably not be detectable in the Zh associated production mode in any case. In summary, any h which is not difficult to detect in the Zh mode will automatically have a $\cos\theta$ distribution that matches the CP-even prediction, even if there is a significant CP-odd component in the h . Unfortunately, the Zh production rate itself cannot be used as a measure of the CP-even vs. CP-odd component of the h ; in a general 2HDM, even a purely CP-even h can have a ZZ coupling that is suppressed relative to SM strength.

Turning to decay distributions, one encounters a similar problem. In $h \rightarrow WW \rightarrow 4$ fermions, one can determine the angle ϕ between the decay planes of the two W 's. One finds: $\frac{d\sigma}{d\phi} \propto 1 + \alpha \cos\phi + \beta \cos 2\phi$ [$\propto 1 - (1/4) \cos 2\phi$] for a CP-even [CP-odd] h , where α and β depend upon the types of fermions observed and the kinematics of the final state. In general these two distributions are distinguishable. However, in analogy to the previous case, it is almost entirely the CP-even component of the h which will be responsible for its decays to WW , and the ϕ distribution will thus closely match the CP-even prediction, even if the h has a substantial CP-odd component. This is explicitly verified in the calculations of Ref. [138]. (See also Refs. [139]-[142].) In order for the ϕ distribution to deviate significantly towards the CP-odd prediction, the CP-even component(s) of the h

must be small. Consequently, decays of the h to WW channels will be substantially suppressed, and either the $b\bar{b}$ or $t\bar{t}$ channel will dominate. In the $b\bar{b}$ channel, the CP-even and CP-odd components of the h cannot be separated. The distribution $d\sigma/d\cos\theta^*$ (where θ^* is the b angle relative to the boost direction in the h rest frame) is predicted to be flat, independent of the CP nature of the h .

Much more promising are $\tau^-\tau^+$ and $t\bar{t}$ decay modes. The basic ideas and techniques for a pure-CP eigenstate are nicely reviewed in Ref. [137]. These techniques are optimized and extended to the case of a mixed-CP eigenstate in Ref. [143]. There, a fairly realistic evaluation of their potential on a statistics basis is given. The techniques rely on measuring the azimuthal angle (ϕ) correlation between certain ‘effective-spin’ directions associated with the fermion and anti-fermion in the final state. These effective spins can only be defined by reference to the final states of the τ and t decays. Roughly, after integrating over all but the angle ϕ , one obtains $\frac{1}{N}\frac{dN}{d\phi} = \frac{1}{2\pi}(1 + \alpha\cos\phi + \beta\sin\phi)$. For a pure CP state, $\beta = 0$ and α has a predicted magnitude but its sign is $-$ or $+$ depending upon whether the state is pure CP-even or pure CP-odd, respectively. In the case of a mixed-CP state (such as can arise in a general 2HDM), α is much smaller in magnitude than for a CP-pure state (perhaps nearly zero), while β is quite substantial. (There is a sum rule of the form $\alpha^2 + \beta^2 = C^2$, where C is a kinematically determined constant.) The statistical analysis of Ref. [143] shows that for the ϕ^0 a statistically reliable determination that $\alpha = -C$ and that $\beta = 0$ would be possible at the 10-20% level in the $\tau^-\tau^+$ final state for $m_{\phi^0} \lesssim 2m_W$. For m_{ϕ^0} between $2m_W$ and $2m_t$, the WW and ZZ decays would be dominant and one would ‘automatically’ (as described above) observe correlations between the WW, ZZ decay planes and the like that are typical of a CP-even state, but that do not guarantee that the state is purely CP-even. For $m_{\phi^0} > 2m_t$, the $t\bar{t}$ distributions of the appropriately-defined ϕ would again be available. However, statistics are predicted to be such (at $L = 85 \text{ fb}^{-1}$) that one could at best measure α and β at the 50% level relative to the maximum possible values of C (*i.e.* $\delta\alpha \sim \delta\beta > 0.5C$). Substantially higher luminosity would be called for.

8.3.3 Summary for the ϕ^0

Overall, we find that many of the properties of the ϕ^0 can be determined at a linear e^+e^- collider with enough energy to produce the ϕ^0 with a significant rate in the first place. This reflects the clean environment and kinematics of e^+e^- collisions. With regard to couplings and widths, the most important exceptions are the *total* width and $b\bar{b}$ partial width (equivalently, coupling). In particular, the total width cannot be determined in a model-independent fashion for $m_{\phi^0} \lesssim 140 \text{ GeV}$, while the $b\bar{b}$ partial width is difficult for almost all values of m_{ϕ^0} . However, for $m_{\phi^0} \lesssim 140 \text{ GeV}$ we have noted that the total width and $b\bar{b}$ partial width, as well as $\Gamma(\phi^0 \rightarrow \gamma\gamma)$, can be determined by combining the NLC data with data from the

LHC and from $\gamma\gamma$ collisions. We have also seen that a *direct* verification that the ϕ^0 is purely CP even is predicted to be very difficult for $m_{\phi^0} \gtrsim 2m_W$.

8.4 The General 2HDM

As noted earlier, in the general 2HDM the neutral Higgs bosons need not be CP eigenstates. We have already discussed the probes of the CP quantum number of a Higgs boson that might be experimentally viable. Let us for the moment assume that CP is conserved in the 2HDM, and recall the two important angles that enter into the phenomenology of the five physical Higgs bosons of the 2HDM: $\tan\beta = v_2/v_1$ and α , the mixing angle in the CP-even neutral Higgs sector. In the CP-conserving case the $Z^* \rightarrow Zh^0$ [ZH^0] cross section is proportional to $\sin^2(\beta - \alpha)$ [$\cos^2(\beta - \alpha)$], whereas the $Z^* \rightarrow h^0A^0$ [H^0A^0] cross section is proportional to $\cos^2(\beta - \alpha)$ [$\sin^2(\beta - \alpha)$]. In the limit of a small value for $\cos(\beta - \alpha)$, or $\sin(\beta - \alpha)$, either the Zh^0 and H^0A^0 , or the ZH^0 and h^0A^0 , respectively, cross sections will be large. That is there is a strong complementarity among these four cross sections such that, given sufficient machine energy, it will always be possible to detect all three neutral Higgs bosons. However, there are certainly scenarios in which no Higgs boson would be seen at the NLC. For example, it is possible that $Z^* \rightarrow Zh^0$ could be kinematically allowed but coupling suppressed, while $Z^* \rightarrow h^0A^0$ and $Z^* \rightarrow ZH^0$ could be kinematically forbidden. No Higgs boson would be seen without raising the machine energy. This is not the case in the MSSM, as we shall shortly discuss.

8.5 MSSM Higgs bosons

In the MSSM, the important production mechanisms are mainly determined by the parameters m_{A^0} and $\tan\beta$. In general, we shall try to phrase our survey in terms of the parameter space defined by $(m_{A^0}, \tan\beta)$, keeping fixed the other MSSM parameters. The most important general point is the previously noted complementarity of the $e^+e^- \rightarrow Zh^0$ and $e^+e^- \rightarrow A^0H^0$ cross sections, which are proportional to $\sin^2(\beta - \alpha)$, and the $e^+e^- \rightarrow ZH^0$ and $e^+e^- \rightarrow A^0h^0$ cross sections, proportional to $\cos^2(\beta - \alpha)$. Since $\cos^2(\beta - \alpha)$ and $\sin^2(\beta - \alpha)$ cannot simultaneously be small, if there is sufficient energy then there is a large production cross section for all three of the neutral Higgs bosons. In the more likely case that m_{A^0} is large, $\sin^2(\beta - \alpha)$ will be large and the h^0 will be most easily seen in the Zh^0 channel, while the A^0 and H^0 will have a large production rate in the A^0H^0 channel if \sqrt{s} is adequate. If $\cos^2(\beta - \alpha)$ is large, then m_{A^0} must be small and A^0h^0 and ZH^0 will have large rates.

Finally, we note that the Higgs sector of the MSSM is automatically CP-conserving [16]. Thus, if a neutral Higgs boson is found to have a mixed CP-nature (by employing the techniques discussed earlier, or those to be reviewed in

the $\gamma\gamma$ collision section) then supersymmetry requires a more complicated Higgs sector than the simple two-doublet structure of the MSSM. Such models will be discussed later.

8.5.1 Detection of the h^0

In the MSSM, the lightest Higgs boson is accessible in the Zh^0 and WW -fusion modes for all *but* the $m_{A^0} \lesssim m_Z$, $\tan\beta \gtrsim 7-10$ corner of parameter space. Outside this region the h^0 rapidly becomes SM-like. This is illustrated in the first and third windows of Fig. 23, where we give the contours in $(m_{A^0}, \tan\beta)$ parameter space for 50, 150 and 1500 events at $\sqrt{s} = 500$ GeV and $L = 50$ fb $^{-1}$, where $m_t = 175$ GeV and $m_{\tilde{t}} = 1$ TeV is assumed. (This type of figure has appeared in Refs. [145, 130]. More detailed experimental discussions can be found in Refs. [75, 127].) After efficiencies, somewhere between 50 and 150 events will be sufficient for detection; 150 events would be sufficient in the Zh^0 mode even if the h^0 decays mostly invisibly to a $\tilde{\chi}_1^0\tilde{\chi}_1^0$ pair. (For the relatively light h^0 other SUSY decay modes are unlikely to be present. For a review of some supergravity/superstring scenarios in which $h^0 \rightarrow \tilde{\chi}_1^0\tilde{\chi}_1^0$ decays are dominant, see Ref. [146].) If such SUSY decays are not important for the h^0 , then to a very good approximation, the entire SM $Z\phi^0$ discussion can be taken over for Zh^0 for large m_{A^0} . The interesting question, to which we shall return below, is for what portion of moderate- m_{A^0} parameter space can the cross sections, branching ratios and/or couplings be measured with sufficient precision to distinguish an approximately SM-like h^0 from the ϕ^0 at the NLC. (The results we obtain should be compared to those summarized earlier in the case of the LHC.) Presumably, large numbers of events would be required. We see from the Zh^0 window of Fig. 23 that at least 1500 events are predicted for all *but* the $m_{A^0} \lesssim 100$, $\tan\beta \gtrsim 2-5$ corner of parameter space.

Although strongly disfavored by model building, there is still a possibility that $m_{A^0} \lesssim m_Z$. The important production process will then be $e^+e^- \rightarrow Z^* \rightarrow h^0 A^0$, the $h^0 ZZ$ and $h^0 WW$ couplings being suppressed for such m_{A^0} values. As discussed earlier, if LEP2 runs at $\sqrt{s} = 200$ GeV $h^0 A^0$ associated production will be kinematically allowed and detectable for all *but very* large $m_{\tilde{t}}$ values. The NLC could be run at a \sqrt{s} value optimized for detailed studies of the $h^0 A^0$ final state. At $\sqrt{s} = 500$ GeV, at least 1500 events are predicted for precisely the $m_{A^0} \lesssim 100$ GeV, $\tan\beta \gtrsim 2-5$ section of parameter space for which fewer events than this would be found in the Zh^0 mode. Thus, $e^+e^- \rightarrow h^0 A^0$ will give us a large number of h^0 's if Zh^0 does not. We will confine ourselves primarily to general remarks regarding the small- m_{A^0} scenario in this report; our focus will be on large m_{A^0} .

8.5.2 Detection of the H^0 , A^0 and H^\pm

For $m_{A^0} \lesssim m_Z$, the A^0 , along with the h^0 , can be easily detected in the $h^0 A^0$ mode, as discussed above. If 50 events are adequate, detection of both the h^0

NLC-500 Event Number Contours ($L=50 \text{ fb}^{-1}$)

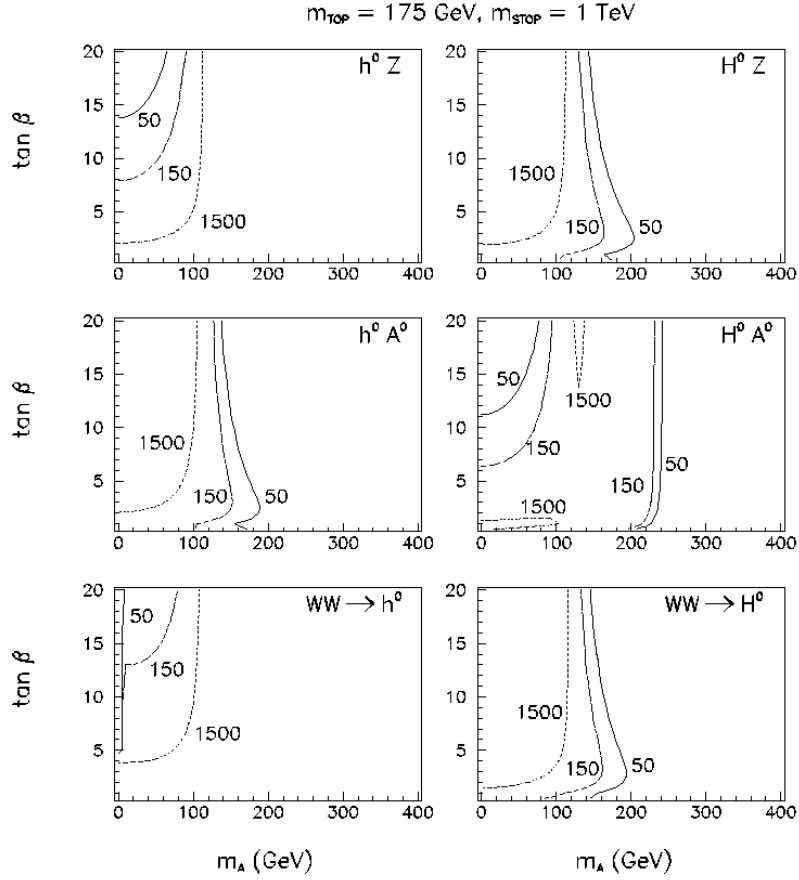


Figure 23: Event number contours at the NLC for the MSSM Higgs bosons in $(m_{A^0}, \tan \beta)$ parameter space. Two-loop/RGE-improved radiative corrections to the MSSM Higgs sector have been included, taking $m_{\tilde{t}} = 1 \text{ TeV}$ and neglecting squark mixing.

and A^0 in this mode will even be possible for m_{A^0} up to ~ 120 GeV. As seen in the fourth and sixth windows of Fig. 23, in this same region the H^0 will be found via ZH^0 and WW -fusion production [145, 127, 130]. In addition, H^+H^- pair production will be kinematically allowed and easily observable [145, 127, 130]. In this low to moderate m_{A^0} region, the only SUSY decay mode that has a real possibility of being present is the invisible $\tilde{\chi}_1^0\tilde{\chi}_1^0$ mode for the neutral Higgs bosons. If this mode were to dominate the decays of all three neutral Higgs bosons, then only the H^0 could be detected, using the recoil mass technique in the ZH^0 channel. However, in the H^+H^- channel the final states would probably not include SUSY modes and H^+ discovery would be straightforward. If a light H^\pm is detected, then one would know that the Higgs detected in association with the Z was most likely the H^0 and not the h^0 . A dedicated search for the light A^0 and h^0 through (rare) non-invisible decays would then be appropriate.

For $m_{A^0} \gtrsim 120$ GeV, $e^+e^- \rightarrow H^0A^0$ and $e^+e^- \rightarrow H^+H^-$ must be employed for detection of the three heavy Higgs bosons. Assuming that SUSY decays are not dominant, and using the 50 event criterion, the mode H^0A^0 is observable up to $m_{H^0} \sim m_{A^0} \sim 240$ GeV, and H^+H^- can be detected up to $m_{H^\pm} = 230$ GeV [145, 127, 130]. The $\gamma\gamma$ collider mode could potentially extend the reach for the H^0, A^0 bosons up to 400 GeV if $\tan\beta$ is not large. This is reviewed in Ref. [45], and will be discussed in more detail later.

The upper limits in the H^0A^0 and H^+H^- modes are almost entirely a function of the machine energy (assuming an appropriately higher integrated luminosity is available at a higher \sqrt{s}). At $\sqrt{s} = 1$ TeV with an integrated luminosity of 200 fb^{-1} , H^0A^0 and H^+H^- detection would be extended to $m_{H^0} \sim m_{A^0} \sim m_{H^\pm} \sim 450$ GeV [145, 45, 127, 130]. As frequently noted, models in which the MSSM is implemented in the coupling-constant-unification, radiative-electroweak-symmetry-breaking context often predict masses above 200 GeV, suggesting that this extension in mass reach over that for $\sqrt{s} = 500$ GeV might be crucial. For some review and references, see Refs. [46, 146].

8.5.3 Distinguishing the MSSM h^0 from the SM ϕ^0 at the NLC

We will discuss this issue in the most interesting case where a direct discovery of the other MSSM Higgs bosons is not possible, that is in the limit where $m_{A^0} \gtrsim 230 - 240$ GeV. Although there are many potentially useful techniques for distinguishing the ϕ^0 from the h^0 , only a few could have the required accuracy for such high m_{A^0} values. In discussing expected experimental errors below we extrapolate the NLC/SLC $m_{\phi^0} = 120$ GeV results and NLC/JLC $m_{\phi^0} = 110$ GeV results (see Table 6) to $m_{\phi^0} = 113$ GeV, the maximum m_{h^0} value for our canonical choices of $m_t = 175$ GeV, $m_{\tilde{t}} = 1$ TeV and no squark mixing. Most uncertain is the error on the WW^* channel which worsens very rapidly as m_{ϕ^0} decreases below 120 GeV. At $m_{\phi^0} = 113$ GeV we estimate that the $\pm 48\%$ that applies at $m_{\phi^0} = 120$ GeV will

worsen to $\sim \pm 70\%$ because of the factor of two decrease in the event rate.

First, there is the simple magnitude of the $Z\phi^0$ cross section. Deviations as large as the best possible error (of order 7%, as summarized earlier) are only possible if $\sin^2(\beta - \alpha)$ deviates from unity by this amount. Unfortunately, we shall see below that deviations of this size are only predicted for $m_{A^0} \lesssim 160$ GeV.

Next there are measurements of $\sigma(Zh^0)BR(h^0 \rightarrow X)$ for various channels $X = b\bar{b}, WW^*, (c\bar{c} + gg)$. As noted earlier, excellent measurement accuracy ($\pm 2.5\%$ for the super-JLC detector and $\pm 7\%$ for SLC/LEP type detectors) is possible for $\sigma(Zh^0)BR(h^0 \rightarrow b\bar{b})$ with $L = 50 \text{ fb}^{-1}$ of integrated luminosity. As detailed below (see also Figs. 17 and 18 of Ref. [127], but keep in mind that that these figures do not include the full two-loop/RGE-improved radiative corrections whereas those presented below do) an excess in this quantity for the MSSM relative to the SM is predicted to be larger than $\sim 2.5\%$ for relatively large m_{A^0} values; *e.g.* 5% deviations are predicted for $m_{A^0} \sim 300$ GeV at larger $\tan \beta$ values. However, the absolute value of $BR(h^0, \phi^0 \rightarrow b\bar{b})$ is quite sensitive to radiative corrections, the ‘current’ b -quark mass (appearing in the $\phi^0 \rightarrow b\bar{b}$ coupling), and ‘extra’ contributions to the total width. While the radiative corrections can eventually be calculated with the required precision, the value of the running mass (\overline{MS}) $m_b(m_b)$ is likely to remain somewhat uncertain due to uncertainty in $m_b(m_b)$. This could be critical. For example, a 5% uncertainty in $m_b(m_b)$ leads to an uncertainty in $BR(h \rightarrow b\bar{b})$ ($h = h^0$ or ϕ^0) of order 3%; see Eq. 21. The value of $\sigma(Zh^0)BR(h \rightarrow WW^*)$ [$\sigma(Zh)BR(h \rightarrow c\bar{c} + gg)$] can be measured to $\pm 48\%$ [$\pm 39\%$] at $m_h = 120$ GeV; somewhat larger errors will apply to $m_h = 113$ GeV in the WW^* case — as noted above, we estimate $\pm 70\%$. The graph presented below will show that such accuracies are adequate for distinguishing the h^0 from the ϕ^0 only for $m_{A^0} \lesssim 200$ GeV.

The relative branching ratios to different channels provide additional information. The modes with branching ratios most sensitive to the small differences between the h^0 and ϕ^0 couplings are the WW^* and $c\bar{c} + gg$. The h^0 branching ratios to these modes can be much smaller at large $\tan \beta$ as compared to the ϕ^0 , so long as m_{A^0} is not too large. Some discussion of such differences as computed at the one-loop level appears in Refs. [133, 134]. Below we shall present some results obtained after including two-loop/RGE-improved corrections to the h^0 , taking $m_t = 175$, $m_{\tilde{t}} = 1$ TeV and neglecting squark mixing. The error in the determination of a ratio $r = x/y$ is computed as

$$\delta r = r \sqrt{(\delta x/x)^2 + (\delta y/y)^2} \quad (24)$$

For $m_{\phi^0} = 113$ GeV, we find:

$$r_{WW^*} \equiv \frac{BR(\phi^0 \rightarrow WW^*)}{BR(\phi^0 \rightarrow b\bar{b})} \sim 0.05, \quad r_{c\bar{c}+gg} \equiv \frac{BR(\phi^0 \rightarrow c\bar{c} + gg)}{BR(\phi^0 \rightarrow b\bar{b})} \sim 0.125, \quad (25)$$

Using the above-quoted errors for the individual channels and the r values given in Eq. 25, we find from Eq. 24 the results $\delta r_{WW^*}/r_{WW^*} \sim 0.7$ and $\delta r_{c\bar{c}+gg}/r_{c\bar{c}+gg} \sim 0.4$

(all at the 1σ level). We shall see below that the former error renders r_{WW^*} rather ineffective, while $r_{c\bar{c}+gg}$ is only capable of probing the difference between the h^0 and the ϕ^0 (for the $m_t = 175$ GeV, $m_{\tilde{t}} = 1$ TeV, no-squark-mixing case being considered) for m_{A^0} values below about 300 GeV.

The quantitative predictions [116] for the deviations of h^0 predictions from ϕ^0 predictions for the above quantities are plotted in Fig. 24. There we display contours in $(m_{A^0}, \tan\beta)$ parameter space corresponding to fixed ratios of MSSM h^0 to SM ϕ^0 predictions taking $m_{\phi^0} = m_{h^0}$. A stop squark mass of 1 TeV and $m_t = 175$ GeV are employed in this figure. For $\sigma(Zh^0)$, 95%, 90% and 85% contours are shown. For $\sigma(Zh^0)BR(b\bar{b}, \tau\tau)$, 98%, 101%, 102%, 105%, and 110% contours are shown. In all other cases, 80%, 50%, and 30% contours are shown. (Our $\sigma(Zh^0)BR(h^0 \rightarrow b\bar{b})$ results differ somewhat from those of Ref. [127]; we have included two-loop/RGE-improved corrections.) As can be seen, to distinguish the h^0 from the ϕ^0 for m_{A^0} values beyond ~ 200 GeV, a much better than 5% measurement of $\sigma(Zh^0)$ must be performed, while $\sigma(Zh^0)BR(h^0 \rightarrow b\bar{b}$ or $\tau\tau)$ must be measured (and reliably computed) to better than 10%, and $\sigma(Zh^0)BR(h^0 \rightarrow gg + c\bar{c})$ or $\sigma(Zh^0)BR(h^0 \rightarrow WW^*)$ to better than 50%. As discussed above, such errors are at the limit of what can be achieved experimentally. The ratio of branching ratios, $r_{c\bar{c}+gg}$ provides some sensitivity to h^0 vs. ϕ^0 differences for m_{A^0} values up to about $m_{A^0} \sim 300$ GeV so long as $\tan\beta \gtrsim 2-3$. (Values of $\tan\beta$ near 1 do not lead to the enhanced $b\bar{b}$ and $\tau^+\tau^-$ partial widths that cause significant deviations.)

Predicted deviations are smaller at any given $(m_{A^0}, \tan\beta)$ location if $m_{\tilde{t}}$ is significantly below 1 TeV. For example, if $m_{\tilde{t}} \sim 500$ GeV the 1.01 contour in $\sigma(Zh^0)BR(h^0 \rightarrow b\bar{b}, \tau\tau)$ falls in about the same location as the 1.02 contour in the $m_{\tilde{t}} = 1$ TeV case illustrated in Fig. 24, and the 0.8 contours for the $c\bar{c} + gg$ (WW^*) deviations move about 50 GeV (10 GeV) lower in m_{A^0} at larger $\tan\beta$. Experimental errors on the WW^* channel will also increase as the large- m_{A^0} value of m_{h^0} decreases with decreasing $m_{\tilde{t}}$.

8.5.4 The influence of supersymmetric decays

For some MSSM parameter choices, the h^0 can decay primarily to invisible modes, including a pair of the lightest supersymmetric neutralinos or a pair of invisibly decaying sneutrinos [146]. The h^0 would still be easily discovered at e^+e^- colliders in the Zh^0 mode using recoil-mass techniques [127, 130]. Of course, if the h^0 decays invisibly to $\tilde{\chi}_1^0\tilde{\chi}_1^0$, this implies that the overall mass scale is quite light and that direct continuum production of $\tilde{\chi}\tilde{\chi}$ pairs with visible decays would also be easily detected at the NLC. These additional experimental signals would make it clear that a supersymmetric model is nature's choice.

The H^0 , A^0 , and H^\pm decays can be dominated by chargino and neutralino pair final states and/or slepton pair final states [16, 45, 147, 146]. Such modes

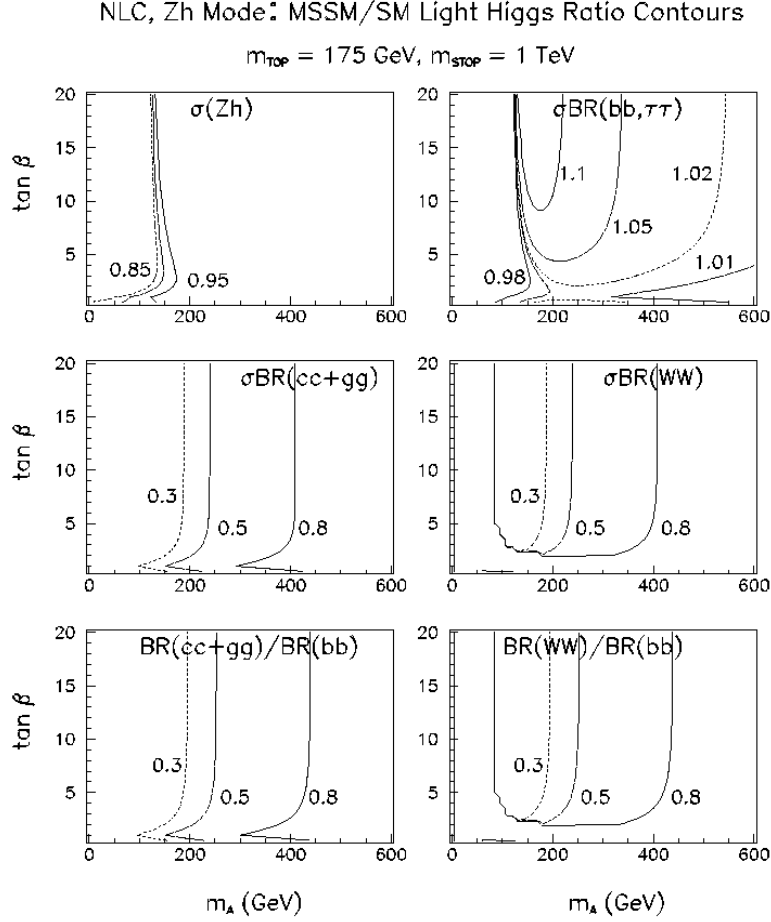


Figure 24: Contours for ratios of MSSM h^0 results to SM ϕ^0 results for $m_{h^0} = m_{\phi^0}$, in $(m_{A^0}, \tan \beta)$ parameter space. Two-loop/RGE-improved radiative corrections are included, taking $m_{\tilde{t}} = 1 \text{ TeV}$ and neglecting squark mixing.

can decrease the chances of detecting these heavier MSSM Higgs bosons at a e^+e^- collider; H^0 , A^0 and H^\pm detection up to the earlier quoted (largely kinematical) limits depends upon the complexity of their decays. There are MSSM parameter choices such that the decay modes of these heavier Higgs are extremely diverse and/or even invisible, in which case their detection in the normal A^0H^0 , H^+H^- associated production modes could be challenging. A survey of the possibilities is in progress [148].

8.6 Extensions of the MSSM

As previously discussed, the supersymmetric Higgs sector must contain at least two-doublets in order to give masses to both the up and down type quarks. We have also noted that gauge unification requires that there be no more than two Higgs doublets. Further, Higgs triplet representations create even more problems than they do in extending the minimal SM Higgs sector. Thus, the most attractive extensions of the MSSM Higgs sector are those in which one or more singlet Higgs fields are added. Indeed, it should be noted that many string-motivated models contain one or more extra singlet fields.

The minimal such extension is that of a single additional singlet Higgs field. This extension was first considered in Ref. [149]. The extremely attractive feature of this model is that it provides a natural source for the μ term required to give the A^0 a non-zero mass. Recall that in the MSSM, it is necessary to introduce the superpotential term $W = \mu \hat{H}_1 \hat{H}_2$, where $\hat{H}_{1,2}$ are the two doublet Higgs superfields. The parameter μ appears in association with the soft-supersymmetry breaking parameter, B , in the soft mass term $B\mu H_1 H_2$ which mixes the two Higgs scalar doublets, thereby giving mass to the m_{A^0} . In many models of supersymmetry breaking, it is most natural that μ should have a magnitude of order the unification scale M_X . There would be no reason for $B\mu$ (and hence m_{A^0}) to be of order the electroweak scale (*i.e.* below a TeV) if μ is of order M_X . Many solutions to this so-called ‘ μ -problem’ have been proposed (see Ref. [46]), but the most natural is the presence of an extra Higgs singlet superfield, which we denote by \hat{N} . There would then be a superpotential term of the form $W = \lambda \hat{H}_1 \hat{H}_2 \hat{N}$, and an associated soft-supersymmetry breaking term of the form $V_{soft} = \lambda A_\lambda H_1 H_2 N$, where A_λ is the soft-supersymmetry-breaking parameter associated with λ at the superpotential level. If $\langle N \rangle \lesssim 1$ TeV and λ is in the perturbative domain, then at least one of the pseudoscalar Higgs bosons (there are two in this model) would generally have mass below a TeV. Values of $\langle N \rangle \lesssim 1$ TeV emerge naturally in perturbative RGE/unification treatments of the model and are technically natural in the sense that they are protected against large quadratic loop corrections.

In the CP-conserving case, this minimal non-minimal extension of the MSSM (often denoted MNMSSM) would contain three neutral scalar Higgs bosons, two neutral pseudoscalar Higgs bosons, and a single charged Higgs pair. In the CP-

violating case, where some of the soft-supersymmetry-breaking parameters related to the Higgs sector are allowed to be complex (spontaneous CP violation in the MNMSSM Higgs sector is also possible, but only if the soft-supersymmetry-breaking potential has a full complement of terms, and not just the minimal $\lambda A_\lambda H_1 H_2 N$ and $k A_k N^3$ forms) there would be five neutral Higgs bosons of mixed-CP character. Clearly, either version of the MNMSSM would present many new phenomenological opportunities and issues.

Consider the CP-conserving model, and label the three CP-even Higgs bosons as $S_{1,2,3}$ in order of increasing mass. The first question is whether or not a $\sqrt{s} = 500$ GeV e^+e^- collider would still be guaranteed to discover at least one of the MNMSSM Higgs bosons. In the MSSM, there is such a guarantee because the h^0 has an upper mass bound, *and* because it has near maximal $h^0 ZZ$ coupling when m_{h^0} approaches its upper limit. In the MNMSSM model, it is in principle possible to choose parameters such that $S_{1,2}$ have such suppressed ZZ coupling strength that their $ZS_{1,2}$ and $WW \rightarrow S_{1,2}$ production rates are too low for observation, while the heavier S_3 Higgs is too heavy to be produced in the ZS_3 or $WW \rightarrow S_3$ modes. This issue has been studied recently in Refs. [150, 151, 152, 153]. The result of Ref. [151] is that if the model is placed within the normal unification context, with simple boundary conditions at M_X , *and if all couplings are required to remain perturbative in evolving up to scale M_X* (as is conventional), then at least one of the three neutral scalars will have $\sigma(e^+e^- \rightarrow ZS) \gtrsim 0.04$ pb for any e^+e^- collider with $\sqrt{s} \gtrsim 300$ GeV. For $L = 10 \text{ fb}^{-1}$, this corresponds to roughly 30 events in the incontrovertible ZS with $Z \rightarrow \ell^+\ell^-$ recoil-mass discovery mode. To what extent this result generalizes to models with still more singlets is not known. However, the proof of the above statement relies on the observation that the more the lighter Higgs bosons decouple from ZZ , the lower the upper bound is on the next heaviest Higgs boson. This could easily generalize. This result has been confirmed by the recent work of Refs. [152, 153]. However, Refs. [150, 151, 152, 153] all make it clear that there is no guarantee that LEP2 will detect a Higgs boson of the MNMSSM. This is because the Higgs boson with significant ZZ -Higgs coupling can easily have mass beyond the kinematical reach of LEP2.

Once a neutral Higgs boson is discovered, it will be crucial to measure all its couplings and to determine its CP character, not only to try to rule out the possibility that it is the SM ϕ^0 , but also to try to determine whether or not the supersymmetric model is the MSSM or the MNMSSM (or still further extension). Measurement of the CP-nature of the Higgs boson would be especially important. As previously mentioned, in the MSSM CP violation cannot arise in the Higgs sector [16], whereas we have noted that Higgs sector CP violation is possible in the MNMSSM (although spontaneous (explicit) CP violation is not (is) possible in the version of the MNMSSM with the most minimal superpotential). In the CP-violating version of the MNMSSM, the previously discussed techniques for exploring the CP-nature of any Higgs boson that is detected in Zh production

would generally be expected to be very useful. In particular, in the unification context many of the neutral Higgs bosons are most naturally below $2m_W$ in mass, and the $h \rightarrow \tau^+\tau^-$ mode could well allow a determination of whether or not any such Higgs boson is a mixed-CP state.

8.7 The role of a back-scattered laser beam facility

It is now widely anticipated (see, *e.g.*, Ref. [154, 135]) that the NLC can be operated in a mode in which laser beams are back-scattered off of one or both of the incoming e^+, e^- in such a way as to allow $e\gamma$ or $\gamma\gamma$ collisions at high luminosity and high energy. (Operation of the NLC as an e^-e^- collider would be even more suitable for the $\gamma\gamma$ collider mode of operation, and polarization of both the e^- beams would be possible.) The luminosity for $\gamma\gamma$ collisions can even be substantially larger than that for e^+e^- collisions in the normal mode of operation. The energy spectrum of the collisions depends upon the choice of electron and laser beam polarizations, but can be either broad or peaked. For instance, in $\gamma\gamma$ collisions a spectrum peaked narrowly in the vicinity of $E_{\gamma\gamma} \sim 0.8\sqrt{s}$ is possible. We will focus first on the $\gamma\gamma$ collision option, with some remarks on the $e\gamma$ collision possibility.

8.7.1 The SM ϕ^0 at a $\gamma\gamma$ collider

In the last few years the possibility of employing collisions of back-scattered laser beams to discover the SM Higgs boson at a linear e^+e^- collider has been explored [155, 156, 157]. The event rate is directly proportional to $\Gamma(\phi^0 \rightarrow \gamma\gamma)$. The interest in this mode derives primarily from two facts. First, observation of the ϕ^0 in this production mode provides probably the only access to the $\phi^0\gamma\gamma$ coupling at an e^+e^- linear collider. The $\phi^0 \rightarrow \gamma\gamma$ decay channel has (at best) a branching ratio of order 2×10^{-3} ; too few events will be available in direct e^+e^- collisions to allow detection of such decays. Second, in principle it might be possible to detect the ϕ^0 for m_{ϕ^0} somewhat nearer to \sqrt{s} than the $0.7\sqrt{s}$ that appears to be feasible via direct e^+e^- collisions. Indeed, the full $\gamma\gamma$ center-of-mass energy, $W_{\gamma\gamma}$, goes into creating the ϕ^0 , and (as noted above) the back-scattered laser beam facility can be configured so that the $W_{\gamma\gamma}$ spectrum peaks slightly above $0.8\sqrt{s}$. The general prospects for ϕ^0 discovery in $\gamma\gamma$ collisions are delineated in Refs. [155, 156, 157]. The result is that by employing appropriate laser and electron polarizations, a viable signal in either the $b\bar{b}$ or ZZ final state decay mode of the ϕ^0 can be extracted for m_{ϕ^0} up to ~ 350 GeV; unfortunately, as detailed below, beyond this point the 1-loop ZZ background overwhelms the signal [158, 159, 160].

The importance of determining the $\phi^0\gamma\gamma$ coupling derives from the fact that it is determined by the sum over all 1-loop diagrams containing any charged particle whose mass arises from the Higgs field vacuum expectation value. In particular, the 1-loop contribution of a charged particle with mass $\gtrsim m_{\phi^0}/2$, approaches a

constant value that depends upon whether it is spin-0, spin-1/2, or spin-1. (The contributions are in the ratio $-1/3 : -4/3 : 7$, respectively.) For a light Higgs boson, in the SM the dominant contribution is the W -loop diagram. The next most important contribution is that from the top quark loop, which tends to cancel part of the W -loop contribution. A fourth fermion generation with both a heavy lepton, L , and a heavy (U, D) quark doublet would lead to still further cancellation. For $m_{\phi^0} \gtrsim 2m_W$, the W -loop contribution decreases, and the heavy family ultimately dominates. Illustrations are given in Refs. [99] and [155]. For example, the ratio of $\Gamma(\phi^0 \rightarrow \gamma\gamma)$ as computed in the presence of an extra generation with $m_L = 300 \text{ GeV}$ and $m_U = m_D = 500 \text{ GeV}$ to the value computed in the SM rises from below 0.2 at $m_{\phi^0} \sim 60 \text{ GeV}$ to above 10 for $m_{\phi^0} \gtrsim 500 \text{ GeV}$. Except for m_{ϕ^0} in the vicinity of 300 GeV, where the full set (mainly the heavy generation) of contributions accidentally matches the SM result, even a rough measurement (or bound) on the $\phi^0\gamma\gamma$ coupling would reveal the presence of the otherwise unobservable heavy generation. Note in particular that a heavy generation would greatly enhance the event rate (and hence prospects) for detecting a Higgs boson with mass up near 500 GeV (the probable kinematic limit for a first generation NLC) in $\gamma\gamma$ collisions. Conversely, for $m_{\phi^0} \lesssim 2m_W$ such an extra generation could make it difficult to detect the ϕ^0 in $\gamma\gamma$ collisions.

Because of the dominance of the W loop contribution in the three family case, the $\phi^0\gamma\gamma$ coupling is also very sensitive to any deviations of the $WW\gamma$ and $WW\phi^0$ couplings from SM values, such as those considered in Refs. [161, 162]. The sensitivity to anomalies in these couplings can be substantially greater than that provided by LEP I data, and comparable to that provided by LEP2 data.

In general, although the $\gamma\gamma$ mode may not extend the discovery reach of an e^+e^- collider, it *will* allow a first measurement of the $\phi^0\gamma\gamma$ coupling of any Higgs boson that is found in direct e^+e^- collisions. The accuracy that can be expected has been studied in Refs. [157, 135]. Two final states were considered: the $\phi^0 \rightarrow b\bar{b}$ channel with b -tagging, and the $\phi^0 \rightarrow ZZ$ channel with one Z required to decay to $\ell^+\ell^-$. In the former case, it is important, as noted in Ref. [155], to polarize the laser beams so that the colliding photons have $\langle\lambda_1\lambda_2\rangle$ near 1. This suppresses the $\gamma\gamma \rightarrow b\bar{b}$ background which is proportional to $1 - \langle\lambda_1\lambda_2\rangle$. It was found that if $35 \lesssim m_{\phi^0} \lesssim 150 \text{ GeV}$, then the $b\bar{b}$ mode will allow a 5-10% determination of $\Gamma(\phi^0 \rightarrow \gamma\gamma)$, while for $185 \lesssim m_{\phi^0} \lesssim 300 \text{ GeV}$ the ZZ mode will provide a 8-11% determination. In the 150–185 GeV window, the WW and $b\bar{b}$ decays are in competition, and the accuracy of the measurement might not be better than 20-25%.

Let us discuss in more detail how high in mass the ϕ^0 can be detected in $\gamma\gamma$ collisions in the case of the SM Higgs. For $\sqrt{s} = 500 \text{ GeV}$, the range of greatest interest is that which cannot be accessed by direct e^+e^- collisions, *i.e.* $m_{\phi^0} \gtrsim 350 \text{ GeV}$. In this mass region, $\phi^0 \rightarrow ZZ$ decays provide the best signal. Certainly, the tree-level $\gamma\gamma \rightarrow W^+W^-$ continuum background completely overwhelms the

$\phi^0 \rightarrow W^+W^-$ mode [155, 163]. As summarized in [155], if there were no continuum ZZ background, and if one of the Z 's is required to decay to $\ell^+\ell^-$, the event rate would be adequate for ϕ^0 detection up to $m_{\phi^0} \sim 400$ GeV, *i.e.* $m_{\phi^0} \sim 0.8\sqrt{s}$. Unfortunately, even though there is no tree-level ZZ continuum background, such a background does arise at one-loop. A full calculation of this background was performed in Refs. [158, 159]. The W^\pm loop is dominant, and leads to a large rate for ZZ pairs with large mass, when one or both of the Z 's is transversely polarized. This background is such that ϕ^0 observation in the ZZ mode is probably not possible for $m_{\phi^0} \gtrsim 350$ GeV, *i.e.* no better than what can be achieved in direct e^+e^- collisions.

If the machine energy is significantly increased, then a new possibility opens up for finding a heavy ϕ^0 in $\gamma\gamma$ collisions. The ϕ^0 can be produced in the reaction where each incoming γ turns into a virtual WW pair, followed by one W from each such pair fusing to form the ϕ^0 ; *i.e.* a $\gamma\gamma$ collision version of WW -fusion. This possibility has been evaluated quantitatively in Refs. [164]-[167]. The result is that a SM Higgs boson with m_{ϕ^0} up to 700 GeV (1 TeV) could be found in this mode at a collider with $\sqrt{s} = 1.5$ TeV (2 TeV), assuming integrated luminosity of $L = 200$ fb $^{-1}$ (300 fb $^{-1}$).

A number of authors have explored further backgrounds to detecting the ϕ^0 in the $\gamma\gamma$ collision mode. In general, these additional backgrounds can be kept small, with the exception of the $\gamma\gamma \rightarrow ZZ$ continuum background from the W -loop graphs just discussed. First, there is the issue of whether or not the $b\bar{b}g$ gluon radiation background (which a priori is comparable to the $b\bar{b}$ background) can be effectively suppressed by the same helicity choices that were used to suppress the basic $b\bar{b}$ background. The speculation [155] that this could be accomplished by vetoing the gluon was quantitatively confirmed in Ref. [168].

The processes $\gamma\gamma \rightarrow Z\ell^+\ell^-$ and $Zq\bar{q}$ yield a reducible background to the ZZ mode to the extent that the $q\bar{q}$ or $\ell^+\ell^-$ have mass near m_Z [169]. The magnitude of this background depends upon the detector resolution and photon polarizations. If $\langle\lambda_1\lambda_2\rangle$ is not near 1, then this background can be significant (though not as large as the ZZ continuum background). However, like the $b\bar{b}$ and basic ZZ continuum background, these processes are proportional to $1 - \langle\lambda_1\lambda_2\rangle$ and can be suppressed substantially by appropriate polarization choices for the incoming back-scattered laser beams.

The $b\bar{b}$ channel receives a background contribution from “resolved” photon processes [170]. The most important example is that where one incoming γ fragments to a spectator jet and a gluon. The subprocess $\gamma g \rightarrow b\bar{b}$ then yields a large $b\bar{b}$ rate. However, this background will not be a problem in practice for two reasons. First, it will be possible to veto against the spectator jet that accompanies the g . This probably already reduces the background to a level below the true $\gamma\gamma \rightarrow b\bar{b}$ continuum. Second, for the range of m_{ϕ^0} such that the $b\bar{b}$ mode is appropriate ($m_{\phi^0} \lesssim 150$ GeV), the ϕ^0 will already have been discovered in direct e^+e^- colli-

sions, *i.e.* m_{ϕ^0} will be known. To study the ϕ^0 in $\gamma\gamma$ collisions it will be easy to adjust the machine energy and laser beam polarizations so that the $\gamma\gamma$ spectrum is peaked at $W_{\gamma\gamma} \sim m_{\phi^0} \sim 0.8\sqrt{s}$. (See, for instance, Ref. [157].) In this case, the secondary gluon in the “resolved”-photon process is quite unlikely to have sufficient energy to create a $b\bar{b}$ pair with mass as large as m_{ϕ^0} .

Finally, we note that a variety of other final states containing the ϕ^0 can be produced in $\gamma\gamma$ collisions. For instance, the $\gamma\gamma \rightarrow t\bar{t}\phi^0$ analogue of $e^+e^- \rightarrow t\bar{t}\phi^0$ could provide another measure of the $t\bar{t}\phi^0$ coupling [171, 172]. However, because of phase space suppression, the rate for this reaction is quite small for $\sqrt{s} = 500$ GeV, and only becomes competitive with $e^+e^- \rightarrow t\bar{t}\phi^0$ when $\sqrt{s} \gtrsim 1$ TeV. As an aside, radiative corrections to $\gamma\gamma \rightarrow t\bar{t}$ and ZZ due to 1-loop Higgs exchange graphs are also sensitive to the $t\bar{t}\phi^0$ coupling. Sufficiently precise measurements of these processes at high luminosity and energy might allow a determination of the coupling over a significant range of m_t and m_{ϕ^0} values, *assuming no other new physics in the 1-loop graphs* [171].

Turning now to $e\gamma$ collisions, we merely note here that $e\gamma \rightarrow W\phi^0\nu \rightarrow jjb\bar{b}\nu$ may be viable for ϕ^0 searches for $\sqrt{s} \gtrsim 1$ TeV [173]-[175]. (The last reference includes some background studies.) This process is interesting in that it probes the $\gamma W \rightarrow \phi^0 W$ subprocess which is determined by a combination of graphs with different basic SM couplings. Should the couplings deviate from SM predictions, the large cancellations among the graphs might be reduced and the event rate significantly enhanced. Another mode of interest is $e\gamma \rightarrow e\gamma\gamma \rightarrow e\phi^0$, in which a secondary γ collides with the primary γ to create the ϕ^0 [176]. The cross section for this process is bigger than that for $e\gamma \rightarrow W\phi^0\nu$ and might allow detection of the ϕ^0 at $\sqrt{s} = 500$ GeV in the $b\bar{b}$ mode. (Resolved photon backgrounds would have to be suppressed by spectator jet vetoing.)

8.7.2 The MSSM Higgs bosons at a $\gamma\gamma$ collider

The most important limitation of a e^+e^- collider in detecting the MSSM Higgs bosons is the fact that the parameter range for which the production process, $Z^* \rightarrow H^0 A^0$ has adequate event rate is limited by the machine energy to $m_{A^0} \sim m_{H^0} \lesssim \sqrt{s}/2 - 20$ GeV (recall that $m_{H^0} \sim m_{A^0}$ at large m_{A^0}). At $\sqrt{s} = 500$ GeV, this means $m_{A^0} \lesssim 230$ GeV. Meanwhile, $e^+e^- \rightarrow H^+H^-$ is also limited to $m_{H^\pm} \sim m_{A^0} \lesssim 220 - 230$ GeV, as we have noted. Thus, it could happen that only a rather SM-like h^0 is detected in e^+e^- collisions at the linear collider, and none of the other Higgs bosons are observed.

However, $\gamma\gamma$ collisions using back-scattered laser beams might allow discovery of the H^0 and/or A^0 up to higher masses [155]. Furthermore, detection of the h^0 in $\gamma\gamma$ collisions is relatively certain to be possible. Observation of any of the three neutral Higgs bosons would constitute a measurement of a $\gamma\gamma$ Higgs coupling, which in principle is sensitive to loops involving other charged supersymmetric

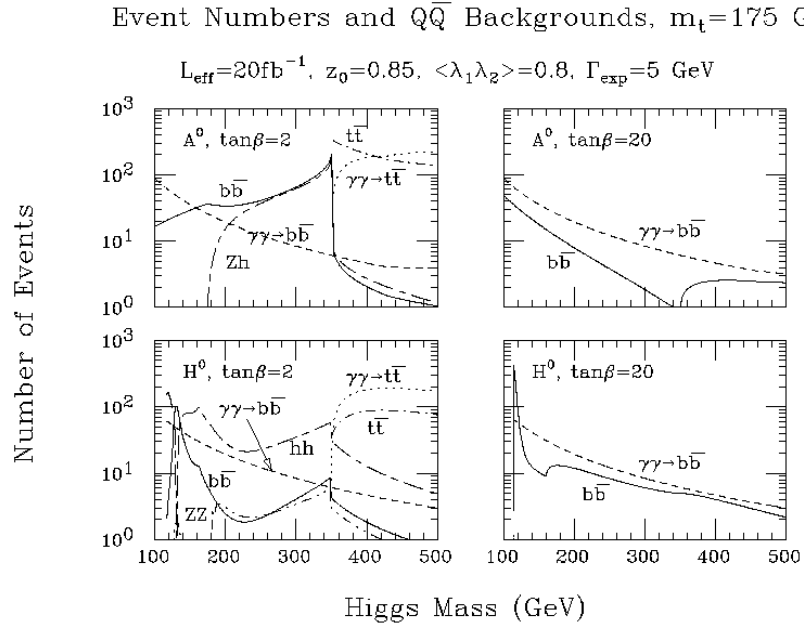


Figure 25: Number of events as a function of Higgs mass in various channels for $\gamma\gamma \rightarrow H^0$ and $\gamma\gamma \rightarrow A^0$ at $m_t = 175$ GeV. Two-loop/RGE-improved radiative corrections are included, taking $m_{\tilde{t}} = 1$ TeV and neglecting squark mixing. Results for $\tan\beta = 2$ and $\tan\beta = 20$ are shown.

particles such as squarks and charginos. Fig. 25 illustrates the discovery potential for the H^0 and A^0 at $m_t = 175$ GeV in various final state channels. [Superpartner masses have been taken to be large and machine energy is assumed to be about 20% higher than the Higgs mass. For the $b\bar{b}$ and $t\bar{t}$ channels, the continuum $\gamma\gamma \rightarrow b\bar{b}$ and $t\bar{t}$ background rates are shown for $\Delta m_{\phi^0} = \max(\Gamma_h, 5 \text{ GeV})$, where 5 GeV is the most optimistic possible experimental resolution.] Particularly interesting channels at moderate $\tan\beta$ and below $t\bar{t}$ threshold are $H^0 \rightarrow h^0 h^0$ (leading to a final state containing 4 b quarks) and $A^0 \rightarrow Zh^0$. These channels are virtually background free unless $m_{h^0} \sim m_W$, in which case the large $\gamma\gamma \rightarrow W^+W^-$ continuum background would have to be eliminated by b -tagging. Above $t\bar{t}$ threshold, $H^0, A^0 \rightarrow t\bar{t}$ decays dominate (at moderate $\tan\beta$). We see that the event rate is high and that the $\gamma\gamma \rightarrow t\bar{t}$ continuum background is of the same general size as the signal rate. Discovery of the A^0 and H^0 up to roughly $0.8\sqrt{s}$ would be possible.

For large $\tan\beta$, it is necessary to look for the A^0 and H^0 in the $b\bar{b}$ final state. For the effective integrated luminosity chosen, $L = 20 \text{ fb}^{-1}$, Fig. 25 shows that detection will be difficult except at such low masses that it would also be possible to observe $Z^* \rightarrow H^0 A^0$ in e^+e^- collisions. However, it is technically feasible (although quite power intensive) to run the $\gamma\gamma$ collider at very high instantaneous luminosity [177, 154] such that accumulated effective luminosities as high as 200 fb^{-1} can be considered. In this case, detection of the A^0 and H^0 in the $b\bar{b}$ channel should be possible for masses $\lesssim 0.8\sqrt{s}$.

Of course, the above results require re-assessment if the A^0 and H^0 have supersymmetric decays. A variety of scenarios of this type have been examined in Ref. [179]. The focus there is on MSSM parameter choices motivated by minimal supergravity/superstring boundary conditions. As already noted, the decays of the Higgs bosons can be very complex, being spread out over many different modes, with the SUSY modes dominating unless $\tan\beta$ is large. In fact, for a $\gamma\gamma$ luminosity of 10 fb^{-1} it is found that for most such scenarios the A^0 and H^0 could not be found for m_{A^0}, m_{H^0} in the critical mass region above ~ 200 GeV unless $\tan\beta$ is large enough that the $b\bar{b}$ mode dominates over the many supersymmetric-pair channels. At moderate $\tan\beta$, an integrated luminosity of $L \gtrsim 50 \text{ fb}^{-1}$ would be required before statistically significant signals would be present on a general basis in background-free modes such as $H^0 \rightarrow h^0 h^0 \rightarrow b\bar{b}b\bar{b}$ or $A^0 \rightarrow Zh^0 \rightarrow Zb\bar{b}$, and still higher luminosity would be needed to see the supersymmetric decay mode background-free channels, such as $jj + jj + \cancel{E}_T$, $\ell\ell + jj + \cancel{E}_T$, or $\ell\ell + \ell\ell + \cancel{E}_T$, coming from $\tilde{\chi}_2^0 \tilde{\chi}_2^0$ decays of the H^0 and A^0 . Fortunately, such high integrated luminosities may well lie within the reach of a properly designed back-scattered-laser-beam facility.

Assuming that one or more of the MSSM Higgs bosons can be seen in $\gamma\gamma$ collisions, a particularly interesting question is the extent to which the $\gamma\gamma$ widths (or simply the production rates in a specific channel) depend upon the the SUSY context and/or superpartner masses. Some exploration of this issue has appeared in

Refs. [155, 178]. Potentially, these widths are sensitive to loops containing heavy charged particles. However, it must be recalled that supersymmetry decouples when the SUSY scale is large. (In particular, superpartner masses come primarily from soft SUSY-breaking terms in the Lagrangian and not from the Higgs field vacuum expectation value(s).) We discuss several scenarios. First, suppose the lightest CP-even Higgs boson has been discovered, but that no experimental evidence for either the heavier Higgs bosons or any supersymmetric particles has been found. Could a measurement of the $h^0\gamma\gamma$ coupling provide indirect evidence for physics beyond the SM? Figure 26 [116] illustrates the fact that for our standard scenario ($m_t = 175$ GeV, $m_{\tilde{t}} = 1$ TeV with all other SUSY particles also heavy — labelled ‘heavy inos’ in the figure) the deviations in the width $\Gamma(h^0 \rightarrow \gamma\gamma)$ [$b\bar{b}$ event rate proportional to $\Gamma(h^0 \rightarrow \gamma\gamma)BR(h^0 \rightarrow b\bar{b})$] relative to the corresponding results for the SM ϕ^0 are not easily observed. If $m_{A^0} \gtrsim 250$ GeV, then the deviations are less than 1% [8%]. This is because of decoupling; as the SUSY breaking scale and the scale of the heavier Higgs bosons become large, all couplings of the h^0 approach their SM values and the squark and chargino loops become negligible. Ref. [135] (see also Ref. [157]) claims measurement accuracies for $\Gamma(\gamma\gamma)BR(b\bar{b})$ that are at best of order 5% (see Table 6 and associated discussion), making h^0 *vs.* ϕ^0 discrimination very difficult. Extraction of $\Gamma(\gamma\gamma)$ would introduce additional errors from the experimental uncertainties in the measured value of $BR(b\bar{b})$ as obtained, for example, from associated Z plus Higgs production (see Table 6).

Lowering the mass scales of the SUSY particles does not necessarily help. Also illustrated in Fig. 26 are cases where the MSSM parameters are chosen such that the neutralinos and charginos lie only just beyond the kinematic reach of a $\sqrt{s} = 500$ GeV e^+e^- collider (MSSM soft-SUSY-breaking parameter choices are $M = -\mu = 300$ GeV, all $m_{\tilde{q}} = 1$ TeV, $A = 0$ — labelled in the figure by ‘light inos’) and where *all* SUSY particles lie only just above the kinematic reach (MSSM soft-SUSY-breaking parameter choices are $M = -\mu = 300$ GeV, all $m_{\tilde{q}} = 400$ GeV, $A = 0$ — labelled in the figure by ‘light SUSY’). Deviations larger than 8% do not occur for $m_{A^0} \gtrsim 250$ GeV, again implying that it will not be easy to distinguish the h^0 from the ϕ^0 using either the $\gamma\gamma$ decay width or the $b\bar{b}$ final state event rate. Of course, lowering the SUSY scale still further, so that some SUSY particles are observable at the NLC can lead to observable deviations.

On the other hand, suppose that the H^0 or A^0 is light enough to be seen in $\gamma\gamma$ collisions ($\lesssim 400$ GeV). In this case, a measurement of its $\gamma\gamma$ width or of the rate in $\gamma\gamma$ collisions for the $b\bar{b}$ final state can provide useful information on the spectrum of charged supersymmetric particles even if the latter are too heavy to be directly produced. Figure 27 provides some examples. There we display the ratios of $\Gamma(\gamma\gamma)$ and $\Gamma(\gamma\gamma)BR(b\bar{b})$ in the previously described ‘light inos’ and ‘light SUSY’ scenarios to the results obtained in the ‘heavy inos’ scenario. (Results for the ‘light SUSY’ scenario in the case of the A^0 are not plotted; they are very close to those for the ‘light inos’ scenario since squark loop contribution to the $A^0\gamma\gamma$ coupling are absent

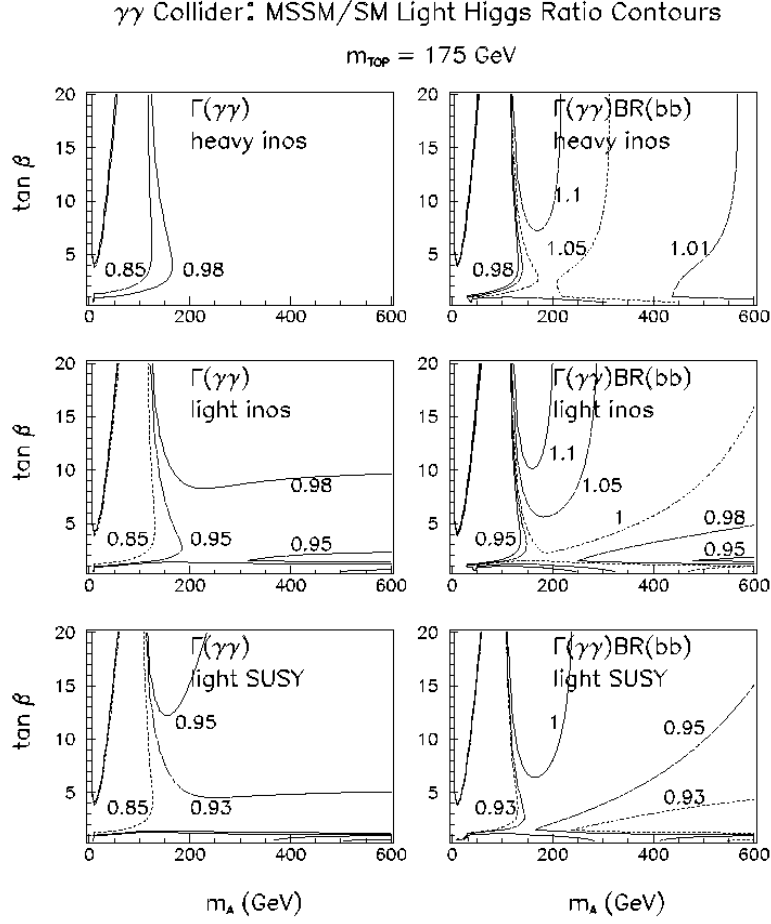


Figure 26: Ratios of $\Gamma(\gamma\gamma)$ and $\Gamma(\gamma\gamma)BR(b\bar{b})$ for the h^0 relative to the SM ϕ^0 (at $m_{\phi^0} = m_{h^0}$) in the three different cases described in the text: ‘heavy inos’, where all SUSY particles are heavy; ‘light inos’, where the neutralinos and charginos are only just beyond kinematic reach of the $\sqrt{s} = 500 \text{ GeV}$ NLC but squarks and sleptons are all heavy; and ‘light SUSY’, where the inos, sleptons and squarks are all only just beyond reach. Two-loop/RGE-improved radiative corrections are included, neglecting squark mixing.

in the limit of degenerate \tilde{q}_L and \tilde{q}_R 's.) Scenario ratios that differ by more than 10% from unity are the rule, with factor of 2 or larger differences common. Thus, observation of the H^0 and A^0 in the $b\bar{b}$ final state of $\gamma\gamma$ collisions could provide insight as to the mass scale of the SUSY particles in the case that they cannot be directly produced.

Finally, we note that since charged Higgs bosons can only be pair produced in $\gamma\gamma$ collisions, e^+e^- collisions will yield the greatest kinematical reach in m_{H^\pm} . For a study of the $\gamma\gamma \rightarrow H^+H^-$ process see Ref. [180].

8.7.3 Probing a general 2HDM in $\gamma\gamma$ collisions

In general, $\gamma\gamma$ collisions could play a very vital role in sorting out a general 2HDM model. The basic reason is simply that the $\gamma\gamma$ coupling receives contributions of similar strength from both the CP-even and CP-odd components of a typical neutral h . Further, any neutral Higgs boson can be produced singly in $\gamma\gamma$ collisions, including a pure CP-odd A^0 , whose $\gamma\gamma$ coupling is determined by fermion loops (with large mass asymptotic limit of 2, compared to the $-4/3$ quoted earlier for the CP-even ϕ^0). The cross section for any given Higgs boson depends upon the precise weighting of the different loop diagrams, as determined by the appropriate β - and α -dependent coupling constant factors [16]. Generally speaking the $\gamma\gamma$ width of all the neutral Higgs bosons of the general two-doublet model can be substantial, and their detection in $\gamma\gamma$ collisions would be possible over a large range of parameter space. Thus, simply a determination of the cross section(s) for the different Higgs in $\gamma\gamma$ collisions would be very useful.

8.7.4 Determining a Higgs boson's CP properties in $\gamma\gamma$ collisions

In the presence of CP violation in the Higgs sector, as could be present in the general 2HDM, $\gamma\gamma$ collisions could play an even more important role. Consider a general neutral Higgs, h , of mixed CP character. The CP-even component of the h will couple to $\gamma\gamma$ in the fashion of the ϕ^0 , although the relative weights of W and fermion loops can easily be different. In terms of the polarization vectors $\vec{e}_{1,2}$ of the two photons in the photon-photon center of mass, the coupling is proportional to $\vec{e}_1 \cdot \vec{e}_2$. The CP-odd component of the h will also develop a $\gamma\gamma$ coupling at one-loop. As noted earlier, only fermion loops contribute. The coupling is proportional to $(\vec{e}_1 \times \vec{e}_2)_z$ (assuming the photons collide along the z axis). Writing the net coupling as $\vec{e}_1 \cdot \vec{e}_2 \mathcal{E} + (\vec{e}_1 \times \vec{e}_2)_z \mathcal{O}$, one finds that \mathcal{E} and \mathcal{O} are naturally of similar size if the CP-odd and CP-even components of the h are comparable.

The most direct probe of a CP-mixed state is provided by comparing the Higgs boson production rate in collisions of two back-scattered-laser-beam photons of various different polarizations [181]. The difference in rates for photons colliding with $++$ vs. $--$ helicities is non-zero only if CP violation is present. A term in the cross section changes sign when both λ_1 and λ_2 are simultaneously flipped,

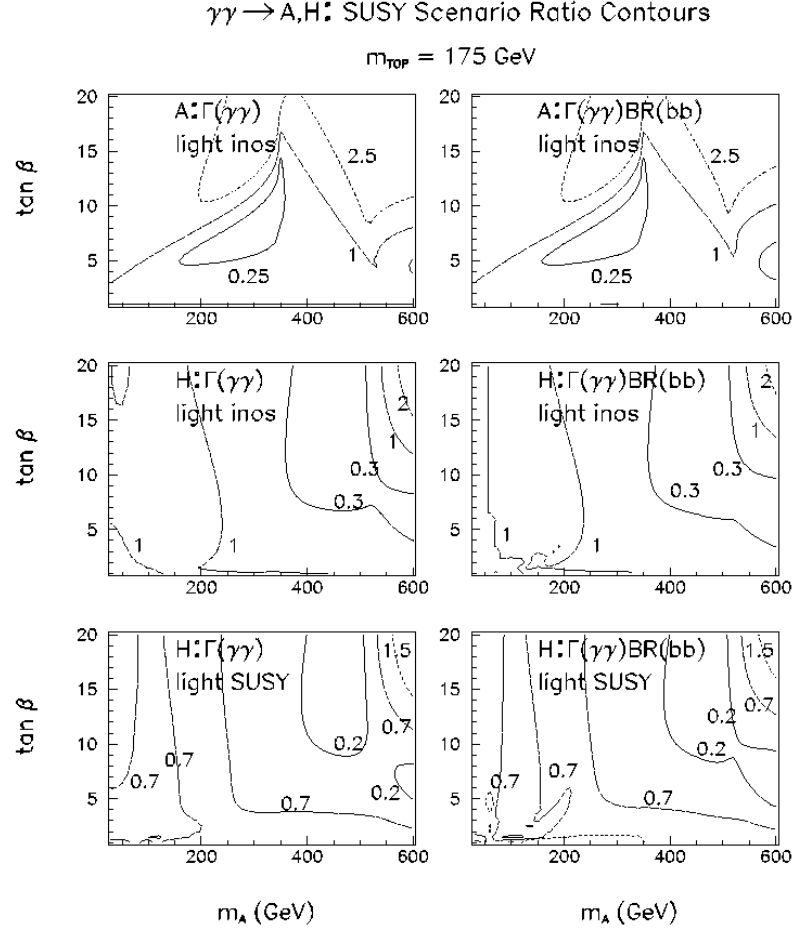


Figure 27: Ratios of $\Gamma(\gamma\gamma)$ and $\Gamma(\gamma\gamma)BR(b\bar{b})$ for the H^0 and A^0 : the labelling ‘light inos’ (‘light SUSY’) refers to the ratio of the results for the ‘light inos’ (‘light SUSY’) scenario to the ‘heavy inos’ scenario — see text. Two-loop/RGE-improved radiative corrections are included, neglecting squark mixing.

and is thus best measured by taking $\langle\lambda_1\lambda_2\rangle$ as near 1 as possible (which suppresses backgrounds anyway), and then comparing the event rate for $\langle\lambda_1\rangle$ and $\langle\lambda_2\rangle$ both positive, to that obtained when both are flipped to negative values. Experimentally this is achieved by simultaneously flipping the helicities of both of the initiating back-scattered laser beams. One finds [181] that the asymmetry is typically larger than 10% and is observable for a large range of two-doublet parameter space if CP violation is present in the Higgs potential.

In the case of a CP-conserving Higgs sector, the earlier outline makes clear that there is strong dependence of the $\gamma\gamma \rightarrow h$ cross section on the relative orientation of the transverse polarizations of the two colliding photons. Clearly then, to extract parallel vs. perpendicular cross section asymmetry experimentally requires that the colliding photons have substantial transverse polarization. This is achieved by transversely polarizing the incoming back-scattered laser beams (while maintaining the ability to rotate these polarizations relative to one another) and optimizing the laser beam energy. This optimization has been discussed in Refs. [182, 137], and it is found that $\gamma\gamma$ collisions may well allow a determination of whether a given h is CP-even or CP-odd.

8.8 Final NLC remarks

Extension of the energy of the e^+e^- collider beyond $\sqrt{s} = 1$ TeV is not required for detecting and studying a weakly-coupled SM Higgs boson, but could be very important for a strongly-coupled electroweak-symmetry-breaking scenario. Detection of H^0A^0 and H^+H^- production in the MSSM model would be extended to higher masses, as could easily be required if the MSSM parameters are typical of those predicted by minimal supergravity/superstring boundary conditions.

9 A $\mu^+\mu^-$ collider

Although design and development are at a very early stage compared to the NLC, and feasibility is far from proven, there is now considerable interest in the possibility of constructing a $\mu^+\mu^-$ collider [183, 184]. Two specific muon collider schemes are under consideration. A high energy machine with 4 TeV center-of-mass energy (\sqrt{s}) and luminosity of order $10^{35} \text{ cm}^{-2} \text{ s}^{-1}$ [186] would have an energy reach appropriate for pair production of A^0H^0 up to very large masses and the study of a strongly interacting WW sector. A lower energy machine, hereafter called the First Muon Collider (FMC), could have c.m. energy around 0.5 TeV with a luminosity of order $2 \times 10^{33} \text{ cm}^{-2} \text{ s}^{-1}$ [186] for unpolarized beams. Not only would the FMC be able to accomplish everything that the NLC could (for the same integrated luminosity), but also the FMC would be extremely valuable for discovery and precision studies of Higgs bosons produced directly in the s -channel.

The most costly component of a muon collider is the muon source (decays of pions produced by proton collisions) and the muon storage rings would comprise a modest fraction of the overall cost [187]. Consequently, full luminosity can be maintained at all c.m. energies where Higgs bosons are either observed or expected by constructing multiple storage rings optimized for c.m. energies centered on the observed masses or spanning the desired range. We summarize below the results of Ref. [185] regarding s -channel Higgs discovery and precision measurements.

For s -channel studies of narrow resonances, the energy resolution is an important consideration. A Gaussian shape for the energy spectrum of each beam is expected to be a good approximation (beamstrahlung being negligible) with an rms deviation most naturally in the range $R = 0.04\%$ to 0.08% [188]. By additional cooling this can be decreased to $R = 0.01\%$. The corresponding rms error σ in \sqrt{s} is given by

$$\sigma = (0.04 \text{ GeV}) \left(\frac{R}{0.06\%} \right) \left(\frac{\sqrt{s}}{100 \text{ GeV}} \right). \quad (26)$$

A critical issue is how this resolution compares to the calculated total widths of Higgs bosons. Widths for the Standard Model Higgs ϕ^0 and the three neutral Higgs bosons h^0 , H^0 , A^0 of the Minimal Supersymmetric Standard Model (MSSM) were illustrated in Fig. 6. An s -channel Higgs resonance would be found by scanning in \sqrt{s} using steps of size $\sim \sigma$; its mass would be simultaneously determined with roughly this same accuracy in the initial scan. For sufficiently small σ , the Breit-Wigner resonance line-shape would be revealed and the Higgs width could be deduced. For $R \lesssim 0.06\%$, the energy resolution in Eq. 26 can be smaller than the Higgs widths in many cases; and for $R \lesssim 0.01\%$ the energy resolution becomes comparable to even the very narrow width of an intermediate-mass SM ϕ^0 .

In the simplest approximation, the effective cross section for Higgs production in the s -channel followed by decay to channel X , $\bar{\sigma}_h$, is obtained by convoluting the standard s -channel pole form with a Gaussian distribution in \sqrt{s} of rms width σ . For $\Gamma_h \gg \sigma$, $\Gamma_h \ll \sigma$, $\bar{\sigma}_h$ at $\sqrt{s} = m_h$ is given by:

$$\bar{\sigma}_h = \begin{cases} \frac{4\pi BR(h \rightarrow \mu^+ \mu^-) BR(h \rightarrow X)}{m_h^2}, & \Gamma_h \gg \sigma; \\ \frac{\pi \Gamma_h}{2\sqrt{2}\pi\sigma} \frac{4\pi BR(h \rightarrow \mu^+ \mu^-) BR(h \rightarrow X)}{m_h^2}, & \Gamma_h \ll \sigma. \end{cases} \quad (27)$$

Since the backgrounds vary slowly over the expected energy resolution interval $\bar{\sigma}_B = \sigma_B$. In terms of the integrated luminosity L , total event rates are given by $L\bar{\sigma}$; roughly $L = 20 \text{ fb}^{-1}/\text{yr}$ is expected for the FMC.

The above results do not include the spreading out of the Gaussian luminosity peak due to photon bremsstrahlung. Although this is much reduced as compared to an e^+e^- collider, it is still important for Higgs bosons that are narrow compared to the beam resolution. For such a Higgs boson, the s -channel production rate for $\sqrt{s} = m_h$ decreases proportionally to the decrease in the peak luminosity. The

amount by which the latter decreases depends upon the resolution R and \sqrt{s} . For $\sqrt{s} = m_h = 100$ GeV, L_{peak} decreases by a factor of 0.61 (0.68) for $R = 0.01\%$ ($R = 0.06\%$) when photon bremsstrahlung is included. By $\sqrt{s} = 500$ GeV these factors have decreased to 0.53 (0.61), respectively. Meanwhile, the background will decrease by a smaller factor due to the fact that it varies smoothly with \sqrt{s} and one must integrate over a final state mass interval of order the final state mass resolution (~ 5 GeV). As a result S/\sqrt{B} typically decreases by about 30% for $m_{\phi^0} \sim 100$ GeV. The result is that for any Higgs boson with width much smaller than the energy resolution σ , a factor of $\lesssim 3 - 5$ larger luminosity is required than would be computed were bremsstrahlung smearing not included. For a Higgs boson with width much larger than σ , the increase in luminosity required for a given measurement is much less. The results that follow include the bremsstrahlung smearing.

9.1 The SM ϕ^0

Predictions for $\bar{\sigma}_{\phi^0}$ for inclusive SM Higgs production are given in Fig. 28 versus $\sqrt{s} = m_{\phi^0}$ for resolutions of $R = 0.01\%$, 0.06% , 0.1% and 0.6% . For comparison, the $\mu^+\mu^- \rightarrow Z^* \rightarrow Z\phi^0$ cross section is also shown, evaluated at the energy $\sqrt{s} = m_Z + \sqrt{2}m_{\phi^0}$ for which it is a maximum. The s -channel $\mu^+\mu^- \rightarrow \phi^0$ cross sections for small R and $m_{\phi^0} \lesssim 2m_W$ are much larger than the corresponding $Z\phi^0$ cross section. The increase in the $\mu^+\mu^- \rightarrow \phi^0$ cross section that results if bremsstrahlung smearing is removed is illustrated in the most sensitive case ($R = 0.01\%$).

The optimal strategy for SM Higgs *discovery* at a lepton collider is to use the $\mu^+\mu^- \rightarrow Zh$ mode (or $e^+e^- \rightarrow Zh$) because no energy scan is needed. Studies of e^+e^- collider capabilities indicate that the SM Higgs can be discovered if $m_{\phi^0} < 0.7\sqrt{s}$. If $m_{\phi^0} \lesssim 140$ GeV, its mass will be determined to a precision given by the event-by-event mass resolution of about 4 GeV in the $h + Z \rightarrow \tau^+\tau^- + q\bar{q}$ and $X + \ell^+\ell^-$ channels divided by the square root of the number of events in these channels, after including efficiencies [189, 127]. A convenient formula is $\Delta m_{\phi^0} \lesssim 0.4 \text{ GeV} \left(\frac{10 \text{ fb}^{-1}}{L} \right)^{\frac{1}{2}}$, yielding, for example, ± 180 MeV for $L = 50 \text{ fb}^{-1}$ [127]. As noted earlier, the super-JLC detector could do even better, achieving a $\sim \pm 20$ MeV measurement of m_{ϕ^0} via the recoil mass spectrum in the $Z\phi^0$ mode. At the LHC the $\phi^0 \rightarrow \gamma\gamma$ mode is deemed viable for $80 \lesssim m_{\phi^0} \lesssim 150$ GeV, with a better than 1% mass resolution [92, 93]. Once the ϕ^0 signal is found, precision determination of its mass and measurement of its width become the paramount issues, and s -channel resonance production at a $\mu^+\mu^-$ collider is uniquely suited for this purpose.

For $m_{\phi^0} < 2m_W$ the dominant ϕ^0 -decay channels are $b\bar{b}$, WW^* , and ZZ^* , where the star denotes a virtual weak boson. The light quark backgrounds to the $b\bar{b}$ signal can be rejected by b -tagging. For the WW^* and ZZ^* channels we employ only the

Standard Model Higgs Cross Sections

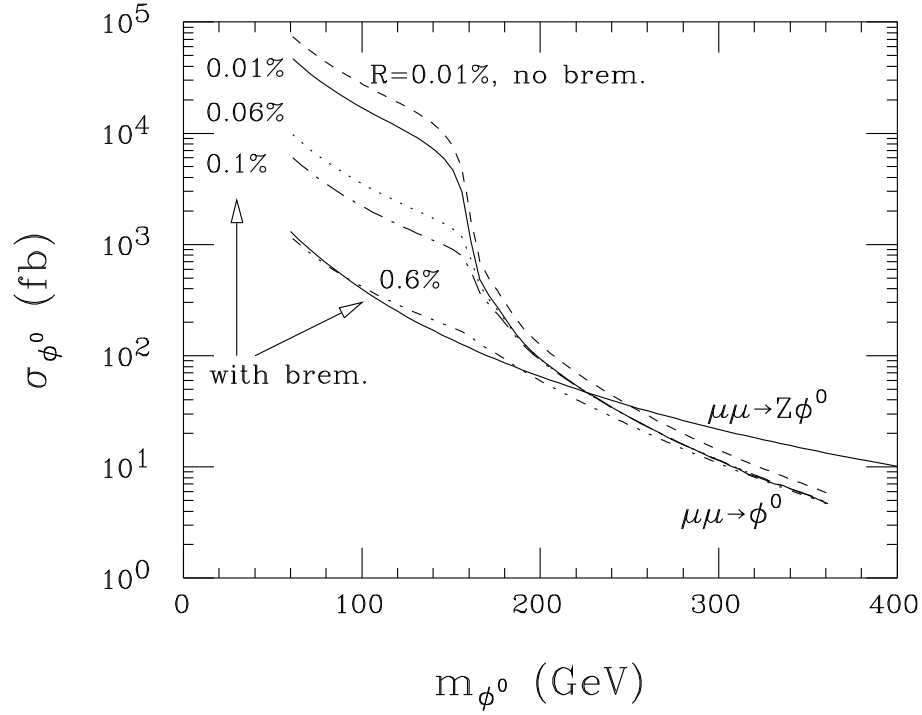


Figure 28: Cross sections versus m_{ϕ^0} for inclusive SM Higgs production: (i) the s -channel $\bar{\sigma}_h$ for $\mu^+\mu^- \rightarrow \phi^0$ with $R = 0.01\%$, 0.06% , 0.1% and 0.6% , and (ii) $\sigma(\mu^+\mu^- \rightarrow Z\phi^0)$ at $\sqrt{s} = m_Z + \sqrt{2}m_{\phi^0}$.

mixed leptonic/hadronic modes ($\ell\nu 2j$ for WW^* and $2\ell 2j$, $2\nu 2j$ for ZZ^* , where $\ell = e$ or μ and j denotes a quark jet), and the visible purely-leptonic ZZ^* modes (4ℓ and $2\ell 2\nu$), taking into account the major electroweak QCD backgrounds. For all channels we assume a general signal and background identification efficiency of $\epsilon = 50\%$, after selected acceptance cuts. In the case of the $b\bar{b}$ channel, this is to include the efficiency for tagging at least one b . The signal and background channel cross sections $\epsilon\bar{\sigma}BR(X)$ at $\sqrt{s} = m_{\phi^0}$ for $X = b\bar{b}$, WW^* and ZZ^* are presented in Fig. 29 versus m_{ϕ^0} for a resolution $R = 0.01\%$; $BR(X)$ includes the Higgs decay branching ratios for the signal, and the branching ratios for the W, W^* and Z, Z^* decays in the WW^* and ZZ^* final states for both the signal and the background. The background level is essentially independent of R , while the signal rate depends strongly on R as illustrated in Fig. 28.

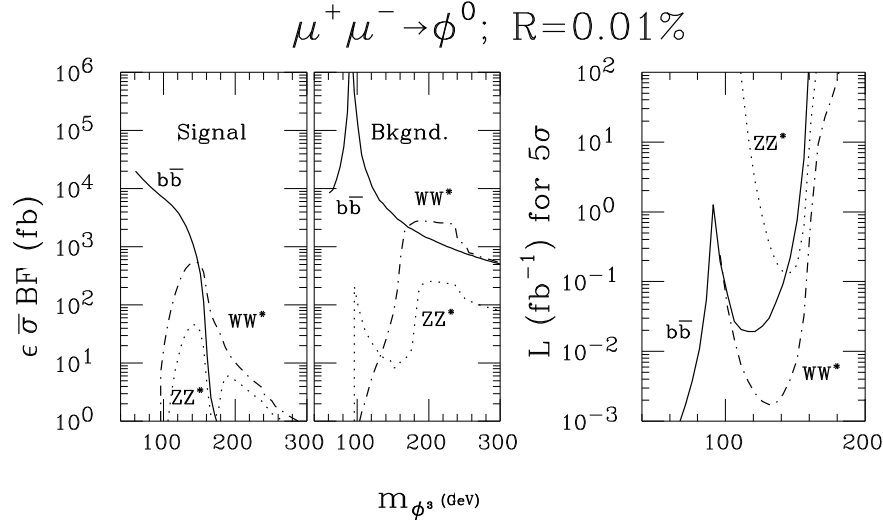


Figure 29: The (a) ϕ^0 signal and (b) background cross sections, $\epsilon\bar{\sigma}BR(X)$, for $X = b\bar{b}$, and useful WW^* and ZZ^* final states (including a channel-isolation efficiency of $\epsilon = 0.5$) versus m_{ϕ^0} for SM Higgs s -channel production with resolution $R = 0.01\%$. Also shown: (c) the luminosity required for $S/\sqrt{B} = 5$ in the three channels as a function of m_{ϕ^0} for $R = 0.01\%$. Bremsstrahlung effects are included.

The luminosity required to achieve $n_\sigma = S/\sqrt{B} = 5$ (where S and B are the signal and background rates) in the $b\bar{b}$, WW^* and ZZ^* channels is also shown in Fig. 29 — results for $R = 0.01\%$ as a function of m_{ϕ^0} are illustrated. For $R = 0.01\%$, $L = .1 \text{ fb}^{-1}$ would yield a detectable s -channel Higgs signal for all m_{ϕ^0} values between the current LEP I limit and $2m_W$ except in the region of the Z peak; a luminosity $L \sim 1 \text{ fb}^{-1}$ at $\sqrt{s} = m_{\phi^0}$ is needed for $m_{\phi^0} \sim m_Z$. For

$R = 0.06\%$, $n_\sigma = 5$ signals typically require about 20 times the luminosity needed for $R = 0.01\%$! Note that a search for the ϕ^0 (or any Higgs with width smaller than the achievable resolution) by scanning would be most efficient for the smallest possible R due to the fact that the L required at each scan point decreases as (roughly) $R^{1.7}$, whereas the number of scan points would only grow like $1/R$. If the Higgs resonance is broad, using small R is not harmful since the data from a fine scan can be re-binned to test for its presence.

Once the Higgs is observed, the highest priority will be to determine its precise mass and width. This can be accomplished by scanning across the Higgs peak. The luminosity required for this is strongly dependent upon R (*i.e.* σ) and the width itself. Precision determinations of the Higgs mass and, particularly, its width are most challenging when the width is smaller than the \sqrt{s} resolution, σ . This is typically the case for a light SM Higgs boson in the intermediate mass range; *e.g.* for $m_{\phi^0} = 120$ GeV, $\Gamma_{\phi^0} \sim 0.003$ GeV is significantly smaller than the best possible ($R = 0.01\%$) value of $\sigma \sim .008$ GeV. Nonetheless, unless the beam energy resolution is poor, the mass is relatively easily determined by simply measuring the rates at a few values of \sqrt{s} near m_h . A model-independent determination of the Higgs width (*i.e.* one that does not rely on knowing normalization of the peak, as fixed by $BR(h \rightarrow \mu^+\mu^-)BR(h \rightarrow X)$) is more difficult; it requires determining accurately the ratio of the rate at a central $\sqrt{s} \sim m_h$ position to the rate at a position on the tail of the peak (as spread out by the Gaussian smearing).

The minimal number of measurements needed to simultaneously determine the Higgs mass and width is three. Sensitivity is roughly optimized if these three measurements are separated in \sqrt{s} by 2σ ; the first would be taken at \sqrt{s} equal to the current best central value of the mass (from the initial detection scan). The second and third would be at \sqrt{s} values 2σ below and 2σ above the first, with about 2.5 times the integrated luminosity expended on the first measurement being employed for each of these latter two measurements. In Fig. 30 we plot the total combined luminosity required for a $\delta\Gamma/\Gamma = 1/3$ measurement of the width in the $b\bar{b}$ channel as a function of m_{ϕ^0} . For given R , luminosity requirements vary by up to 25%, depending upon luck in placement of the first scan point, as quantified by the ratio $|\sqrt{s} - m_{\phi^0}|/\sigma$. The figure also shows that luminosity requirements increase rapidly as R worsens. For the best possible resolution of $R = 0.01\%$, total luminosities of at least $L = 3.2, 2.4$, and 3.1 fb^{-1} are needed for a $\delta\Gamma/\Gamma = 1/3$ width measurement at $m_{\phi^0} = 110, 120$, and 140 GeV, respectively; and for $m_{\phi^0} \sim m_Z$, nearly $L = 200 \text{ fb}^{-1}$ is needed. Clearly, the excellent $R = 0.01\%$ resolution is mandatory if one is to have a good chance of being able to measure the total width regardless of what m_{ϕ^0} turns out to be. In the narrow width region ($m_{\phi^0} \lesssim 150$ GeV) the Higgs mass is simultaneously determined using this procedure to the accuracy of $\delta m_h \sim 0.5\delta\Gamma$. To a first approximation, $\delta\Gamma$ scales statistically, *i.e.* as $1/\sqrt{L}$. Thus, $L \gtrsim 30 - 35 \text{ fb}^{-1}$ would be required for a 10% measurement of the Higgs width for $110 \lesssim m_{\phi^0} \lesssim 140$ GeV. Allowing for the fact

that our ‘central’ position measurement might be slightly off center, we claim in Table 6 that $L = 50 \text{ fb}^{-1}$ is fairly certain to allow a 10% determination of the SM Higgs width. The corresponding errors on the Higgs mass are also given in the Table.

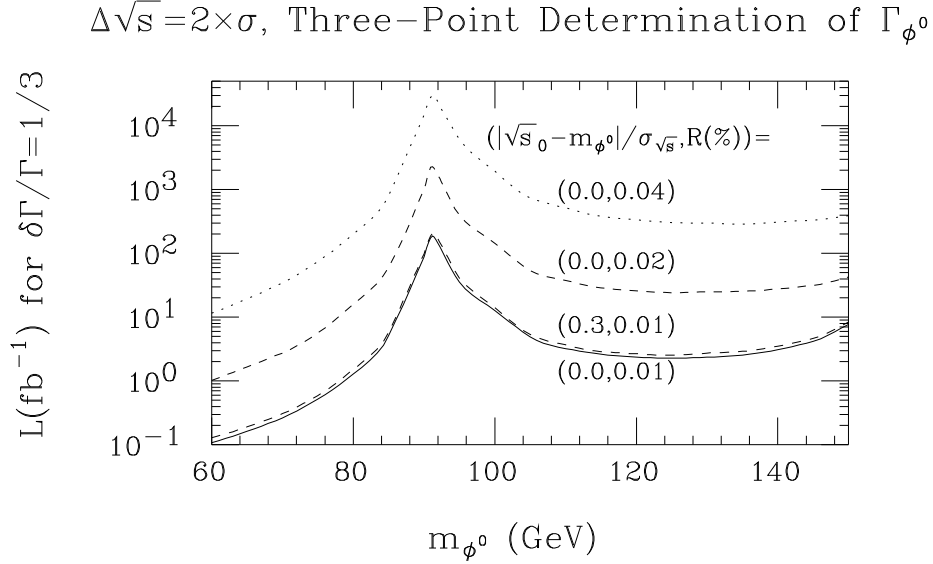


Figure 30: The luminosity required for a $\delta\Gamma/\Gamma = 1/3$ measurement of the ϕ^0 width as a function of m_{ϕ^0} for various choices of $(|\sqrt{s} - m_{\phi^0}|/\sigma, R)$. Bremsstrahlung effects are included.

In addition, the event rate in a given channel measures $\Gamma(\phi^0 \rightarrow \mu^+\mu^-) \times BR(\phi^0 \rightarrow X)$. Then, using the branching fractions (most probably already measured in $Z\phi^0$ associated production), the $\phi^0 \rightarrow \mu\mu$ partial width can be determined, providing an important test of the Higgs coupling. The accuracy with which the $X = b\bar{b}, WW^*, ZZ^*$ rates can be measured is plotted in Fig. 31 as a function of m_{ϕ^0} for $L = 50 \text{ fb}^{-1}$ and resolution choices of $R = 0.01\%$ and 0.06% . For $R = 0.01\%$, a better than $\pm 1.5\%$ measurement of the $X = b\bar{b}$ channel rate can be performed for all $m_{\phi^0} \lesssim 150 \text{ GeV}$. Thus, in obtaining a direct determination of $\Gamma(\phi^0 \rightarrow \mu^+\mu^-)$ we will be limited by the $\sim \pm 7\% - \pm 10\%$ measurement of $BR(\phi^0 \rightarrow b\bar{b})$ obtained at the NLC by combining the $e^+e^- \rightarrow Z\phi^0$ inclusive rate with the $e^+e^- \rightarrow Z\phi^0 \rightarrow Zb\bar{b}$ partial rate (the uncertainty in the inclusive $Z\phi^0$ measurement dominates the error).

9.2 The MSSM Higgs bosons

A $\mu^+\mu^-$ collider provides two particularly unique probes of the MSSM Higgs sector. First, the couplings of the h^0 deviate sufficiently from exact SM Higgs couplings

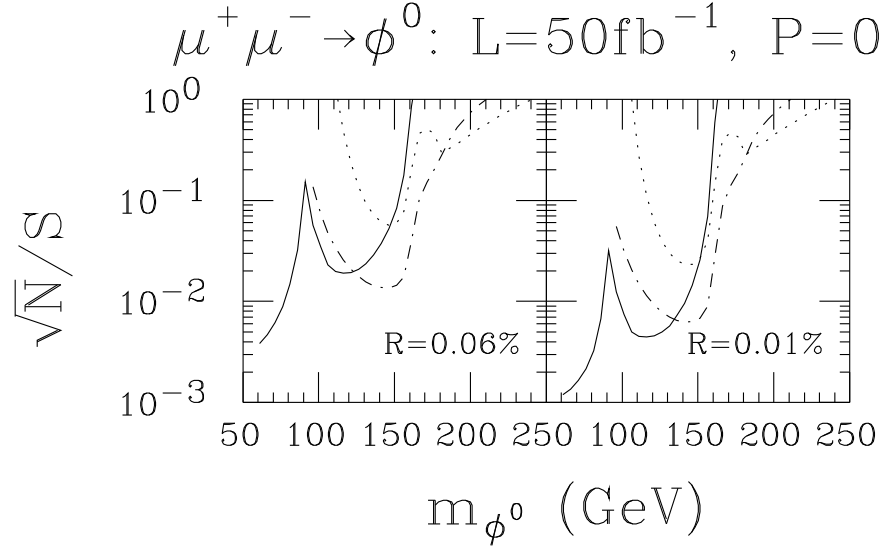


Figure 31: The error \sqrt{N}/S in the measurement of $\Gamma(\phi^0 \rightarrow \mu^+\mu^-) \times BR(\phi^0 \rightarrow X)$ for $X = b\bar{b}$ (solid), and useful WW^* (dotdash) and ZZ^* (dots) final states (including a channel-isolation efficiency of $\epsilon = 0.5$) versus m_{ϕ^0} for SM Higgs s -channel production with resolutions $R = 0.06\%, 0.01\%$, for an integrated luminosity of $L = 50 \text{ fb}^{-1}$. Bremsstrahlung effects are included.

that it may well be distinguishable from the ϕ^0 by measurements of Γ_h and $\Gamma(h \rightarrow \mu^+\mu^-)$ at a $\mu^+\mu^-$ collider, using the s -channel resonance process (here we use the notation h for a generic Higgs boson). For instance, in the $b\bar{b}$ channel Γ_h and $\Gamma(h \rightarrow \mu^+\mu^-) \times BR(h \rightarrow b\bar{b})$ can both be measured with good accuracy. The expected size of the relevant deviations is illustrated in Fig. 32 [116]. Unless $m_h \sim m_Z$, $L = 50 \text{ fb}^{-1}$ of luminosity will yield a better than $\pm 10\%$ determination of Γ_h (as noted earlier) and a better than $\pm 1\%$ determination of $\Gamma(h \rightarrow \mu^+\mu^-) \times BR(h \rightarrow b\bar{b})$ (see Fig. 31). However, one must also account for systematic uncertainties. As discussed in the NLC section, our ability to predict $BR(h \rightarrow b\bar{b})$ is limited by uncertainty in m_b , an uncertainty of order $\pm 5\%$ in m_b leading to a $\pm 3\%$ uncertainty in the branching ratio. Uncertainty in m_b also implies uncertainty in the total width prediction of order $\frac{\delta\Gamma_h}{\Gamma_h} \sim 2 \frac{\delta m_b}{m_b} BR(h \rightarrow b\bar{b})$ which is of order $8\% - 10\%$ for $\frac{\delta m_b}{m_b} \sim \pm 5\%$. We see from Fig. 32 that so long as we can keep systematic and statistical errors below the 10% level, one can reasonably expect that these quantities will probe the h^0 *vs.* ϕ^0 differences for m_{A^0} values as large as $400 - 500 \text{ GeV}$.

FMC: MSSM/SM Light Higgs Ratio Contours

$m_{\text{TOP}} = 175 \text{ GeV}, m_{\text{STOP}} = 1 \text{ TeV}$

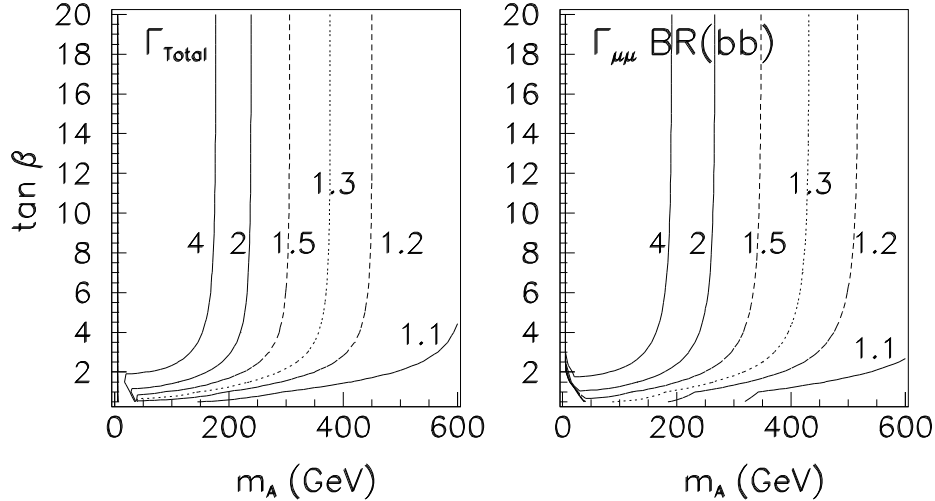


Figure 32: Ratio of h^0 to ϕ^0 predictions at $m_{\phi^0} = m_{h^0}$ for the total width Γ_h and $\Gamma(h \rightarrow \mu^+\mu^-)BR(h \rightarrow b\bar{b})$. We have taken $m_t = 175 \text{ GeV}$. Two-loop/RGE-improved radiative corrections are included, taking $m_{\tilde{t}} = 1 \text{ TeV}$ and neglecting squark mixing.

The second dramatic advantage of a $\mu^+\mu^-$ collider in MSSM Higgs physics is the ability to study the non-SM-like Higgs bosons, *e.g.* for $m_{A^0} \gtrsim 2m_Z$ the

H^0, A^0 . An e^+e^- collider can only study these states via $Z^* \rightarrow A^0 H^0$ production, which could easily be kinematically disallowed since GUT scenarios typically have $m_{A^0} \sim m_{H^0} \gtrsim 200\text{--}250$ GeV. In s -channel production the H^0, A^0 can be even more easily observable than a SM-like Higgs if $\tan\beta$ is not near 1. This is because the partial widths $\Gamma(H^0, A^0 \rightarrow \mu^+\mu^-)$ grow rapidly with increasing $\tan\beta$, implying (see Eq. 27) that $\bar{\sigma}_{H^0, A^0}$ will become strongly enhanced relative to SM-like values. $BR(H^0, A^0 \rightarrow b\bar{b})$ is also enhanced at large $\tan\beta$, implying an increasingly large rate in the $b\bar{b}$ final state. Thus, we concentrate here on the $b\bar{b}$ final states of H^0, A^0 although the modes $H^0, A^0 \rightarrow t\bar{t}$, $H^0 \rightarrow h^0 h^0, A^0 A^0$ and $A^0 \rightarrow Z h^0$ can also be useful.

Despite the enhanced $b\bar{b}$ partial widths, the suppressed (absent) coupling of the H^0 (A^0) to WW and ZZ means that, unlike the SM Higgs boson, the H^0 and A^0 remain relatively narrow at high mass, with widths $\Gamma_{H^0}, \Gamma_{A^0} \sim 0.1$ to 6 GeV for $\tan\beta \lesssim 20$ (see Fig. 6). Since these widths are generally comparable to or broader than the expected \sqrt{s} resolution for $R = 0.06\%$ and $\sqrt{s} \gtrsim 200$ GeV, measurements of these Higgs widths could be straightforward with a scan over several \sqrt{s} settings, provided that the signal rates are sufficiently high. The results of a fine scan can be combined to get a coarse scan appropriate for broader widths. One subtlety is the fact that the H^0 and A^0 are sufficiently degenerate in mass at large $m_{A^0} \sim m_{H^0}$ that their resonance peaks can overlap substantially. In this case, the event rate at say $\sqrt{s} = m_{A^0}$ would include automatically some H^0 events, and vice versa. A detailed scan with small R might be required to separate the two overlapping peaks and determine the A^0 and H^0 widths using a fit employing two Breit-Wigner forms.

The cross section for $\mu^+\mu^- \rightarrow A^0 \rightarrow b\bar{b}$ production with $\tan\beta = 2, 5$ and 20 (including an approximate cut and b -tagging efficiency of 50%) is shown versus m_{A^0} in Fig. 33 for beam resolution $R = 0.01\%$. Overlapping events from the tail of the H^0 resonance are automatically included. Also shown is the significance of the $b\bar{b}$ signal for delivered luminosity $L = 0.1 \text{ fb}^{-1}$ at $\sqrt{s} = m_{A^0}$. Discovery of the A^0 and H^0 will require an energy scan if $Z^* \rightarrow H^0 + A^0$ is kinematically forbidden; a luminosity of 20 fb^{-1} would allow a scan over 200 GeV at intervals of 1 GeV with $L = 0.1 \text{ fb}^{-1}$ per point. The $b\bar{b}$ mode would yield at least a 10σ signal at $\sqrt{s} = m_{A^0}$ for $\tan\beta \gtrsim 2$ for $m_{A^0} \lesssim 2m_t$ and at least a 5σ signal for $\tan\beta \gtrsim 5$ for all $m_{A^0} \lesssim 500$ GeV. Results for $R = 0.06\%$ are displayed in the corresponding figure in Ref. [185]. The resulting statistical significance is only noticeably affected in the $\tan\beta = 2$ case, for which it declines by about a factor of 2. For $\tan\beta \gtrsim 5$, the A^0 is sufficiently broad that very narrow resolution is not helpful. For $m_{A^0} \gtrsim m_Z$ ($m_{A^0} \lesssim m_Z$), the H^0 (h^0) has very similar couplings to those of the A^0 and would also be observable in the $b\bar{b}$ mode for $\tan\beta \gtrsim 5$. For $\tan\beta \sim 2$, $BR(H^0 \rightarrow b\bar{b})$ is smaller than in the case of the A^0 due to the presence of the $H^0 \rightarrow h^0 h^0$ decay mode. For such $\tan\beta$ values, detection would be easier in the $h^0 h^0$ final state. Overall, discovery of *both* the H^0 and A^0 MSSM Higgs bosons (either separately or

as overlapping resonances) would be possible over a large part of the $m_{A^0} \gtrsim m_Z$ MSSM parameter space.

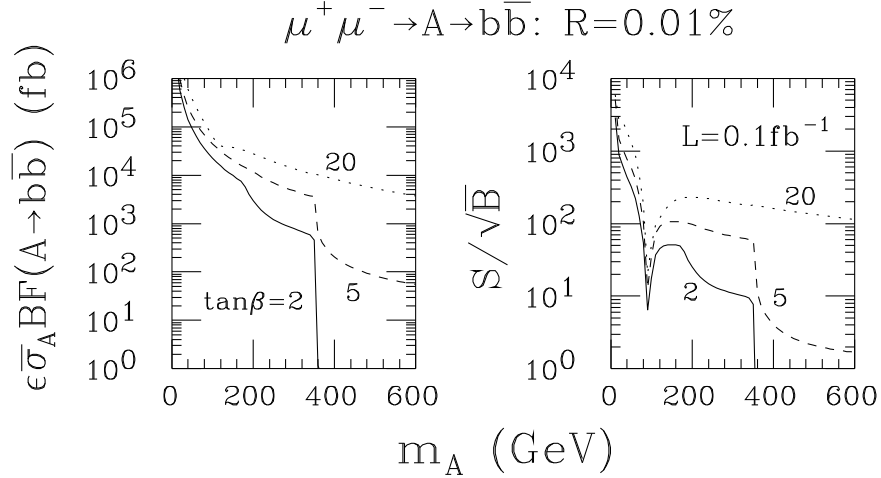


Figure 33: (a) The effective $b\bar{b}$ -channel cross section, $\epsilon\sigma_{A^0}BR(A^0 \rightarrow b\bar{b})$, for s -channel production of the MSSM Higgs boson A^0 versus $\sqrt{s} = m_{A^0}$, for $\tan\beta = 2, 5$ and 20 , beam resolution $R = 0.01\%$ and channel isolation efficiency $\epsilon = 0.5$; and (b) corresponding statistical significance of the $A^0 \rightarrow b\bar{b}$ signal for $L = 0.1 \text{ fb}^{-1}$ delivered at $\sqrt{s} = m_{A^0}$. Plots are for $m_t = 175 \text{ GeV}$. Two-loop/RGE-improved radiative corrections are included, taking $m_{\tilde{t}} = 1 \text{ TeV}$ and neglecting squark mixing.

9.3 The advantages of polarized beams

Polarized beams would allow a reduction in backgrounds relative to signals in the discovery and study of any Higgs boson. If longitudinal polarization P is possible for *both* beams, then, relative to the unpolarized case, the signal is enhanced by the factor $(1 + P^2)$ while the background is suppressed by $(1 - P^2)$. The luminosity required for a signal of given statistical significance is then proportional to $(1 - P^2)/(1 + P^2)^2$. For example, if 85% polarization could be achieved with less than a factor of 10 decrease in luminosity, Higgs studies would benefit.

9.4 Determining a Higgs boson's CP properties in $\mu^+\mu^-$ Collisions

A $\mu^+\mu^-$ collider might well prove to be the best machine for directly probing the CP properties of a Higgs boson that can be produced and detected in the s -channel

mode. This issue has been explored in Refs. [143, 190] in the case of a general two-Higgs-doublet model.

The first possibility is to measure correlations in the $\tau^+\tau^-$ or $t\bar{t}$ final states, using the same techniques as discussed earlier with regard to Zh production at an e^+e^- collider. (Note that as in Zh production the rest frame of the h is precisely known for $\mu^+\mu^-$ collisions.) The results of the above references imply that a $\mu^+\mu^-$ collider is likely to have greater sensitivity to the Higgs boson CP properties for $L = 20 \text{ fb}^{-1}$ than will the e^+e^- collider for $L = 85 \text{ fb}^{-1}$ if $\tan\beta \gtrsim 10$ or $2m_W \lesssim m_h \lesssim 2m_t$. Indeed, there is a tendency for the $\mu^+\mu^-$ CP-sensitivity to be best precisely for parameter choices such that CP-sensitivity in the $e^+e^- \rightarrow Zh$ mode is worst. Somewhat higher total luminosity ($L \sim 50 \text{ fb}^{-1}$) is generally needed in order to use these correlations to distinguish a pure CP-odd state from a pure CP-even state.

The second possibility arises if it is possible to transversely polarize the muon beams. The basic idea is as simple as that discussed with regard to CP determination using collisions of two polarized photon beams. Assume that we can have 100% transverse polarization and that the μ^+ transverse polarization is rotated with respect to the μ^- transverse polarization by an angle ϕ . The production cross section for a h with coupling $a + ib\gamma_5$ then behaves as

$$\sigma(\phi) \propto 1 - \frac{a^2 - b^2}{a^2 + b^2} \cos \phi + \frac{2ab}{a^2 + b^2} \sin \phi. \quad (28)$$

To prove that the h is a CP admixture, use the asymmetry

$$A_1 \equiv \frac{\sigma(\pi/2) - \sigma(-\pi/2)}{\sigma(\pi/2) + \sigma(-\pi/2)} = \frac{2ab}{a^2 + b^2}. \quad (29)$$

For a pure CP eigenstate the asymmetry

$$A_2 \equiv \frac{\sigma(\pi) - \sigma(-\pi)}{\sigma(\pi) + \sigma(-\pi)} = \frac{a^2 - b^2}{a^2 + b^2} \quad (30)$$

is +1 or -1 for a CP-even or CP-odd h , respectively. Of course, background processes in the final states where a Higgs boson can be most easily observed (*e.g.* $b\bar{b}$ for the MSSM Higgs bosons) will typically dilute these asymmetries substantially. Whether or not they will prove useful depends even more upon our very uncertain ability to transversely polarize the muon beams, especially while maintaining high luminosity.

Note that longitudinally polarized beams are not useful for studying the CP properties of a Higgs produced in the s -channel. Regardless of the values of a and b in the h coupling, the cross section is simply proportional to $1 - \lambda_{\mu^+}\lambda_{\mu^-}$ (the λ 's being the helicities), and is only non-zero for $L - R$ or $R - L$ transitions, up to corrections of order m_μ^2/m_h^2 .

9.5 $\mu^+\mu^-$ final remarks and summary

In summary, $\mu^+\mu^-$ colliders offer significant new opportunities for probing the Higgs sector. The s -channel resonance production process is especially valuable for precision Higgs mass measurements, Higgs width measurements, and the search for Higgs bosons with negligible hZZ couplings, such as the H^0, A^0 Higgs bosons of the MSSM. It could also prove valuable for determining the CP properties of a Higgs boson that is produced at a high rate. For an extremely narrow Higgs boson, such as a light SM Higgs, excellent energy resolution is mandatory for precision measurements of the width and individual channel rates, and could allow us to distinguish between the SM Higgs and the SM-like Higgs of the MSSM. The techniques discussed here in the SM and MSSM theories are generally applicable to searches for any Higgs boson or other scalar particle that couples to $\mu^+\mu^-$. If any narrow-width Higgs or scalar particle is observed at either the LHC or NLC, a $\mu^+\mu^-$ collider of appropriate energy would become a priority simply on the basis of its promise as a Higgs/scalar factory.

10 Conclusions

We now present a brief overall summary of the capabilities of present and proposed future colliders to search for the SM Higgs boson and the MSSM Higgs bosons. The SM Higgs discovery limits for the most useful discovery modes are summarized in Table 7. The corresponding MSSM Higgs discovery limits are summarized in Table 8, where we employ the convenient MSSM Higgs sector parameterization in terms of m_{A^0} and $\tan\beta$. All values of $m_{A^0} \leq 1000$ GeV and $1 \leq \tan\beta \leq 60$ (as preferred in the MSSM) have been surveyed. Results employ two-loop/RGE-improved radiative corrections as computed for $m_t = 175$ GeV and $m_{\tilde{t}} = 1$ TeV, neglecting squark mixing.² Details regarding the claims made in this summary are to be found in the main body of this review and the references quoted therein.

A few examples should help clarify the meaning of the discovery regions presented in Table 8. At LEP2 with $\sqrt{s} = 175$ GeV and 600 pb^{-1} integrated luminosity (summing over all four detectors), either h^0 or A^0 (or both) can be discovered via $e^+e^- \rightarrow Zh^0, h^0A^0$ if $m_{A^0} \lesssim 75$ GeV and $\tan\beta \gtrsim 1$. A second discovery region also exists, beginning at $\tan\beta \lesssim 4$ (at $m_{A^0} = 75$ GeV) and ending at $m_{A^0} \lesssim 1000$ GeV (at $\tan\beta \sim 2$). If \sqrt{s} is increased to 192 GeV, both discovery regions become larger; in particular, the latter region now begins at $\tan\beta \lesssim 5$ (at $m_{A^0} = 80$ GeV) and ends at $\tan\beta \lesssim 3$ for the maximal value of m_{A^0} considered — see the LEP-192 curves in Fig. 18, for example. At the NLC-500, h^0 can be detected via $e^+e^- \rightarrow Zh^0$ unless $\tan\beta \gtrsim 8$ and $m_{A^0} \lesssim 90$ GeV. A similar discovery region exception appears for $WW \rightarrow h^0$. The reason such restrictions arise is

²The results of Ref. [62] differ slightly since these did not include two-loop/RGE-improved corrections.

Table 7: Standard Model Higgs boson discovery modes. All masses are specified in GeV; LEP2 and LHC luminosities are detector-summed requirements.

Machine (\sqrt{s} , $\int \mathcal{L} dt$)	Mode	Discovery Region
LEP	$e^+e^- \rightarrow Z^*\phi^0$	$m_{\phi^0} \lesssim 65$
LEP2, (175 GeV, 600 pb $^{-1}$)	$e^+e^- \rightarrow Z\phi^0$	$m_{\phi^0} \lesssim 82$
LEP2, (192 GeV, 600 pb $^{-1}$)	$e^+e^- \rightarrow Z\phi^0$	$m_{\phi^0} \lesssim 95$
LEP2, (205 GeV, 600 pb $^{-1}$)	$e^+e^- \rightarrow Z\phi^0$	$m_{\phi^0} \lesssim 103$
Tevatron, (2 TeV, 5 fb $^{-1}$)	$p\bar{p} \rightarrow W\phi^0; \phi^0 \rightarrow b\bar{b}$	$m_{\phi^0} \lesssim 60 - 80$
Tev*, (2 TeV, 30 fb $^{-1}$)	$p\bar{p} \rightarrow W\phi^0; \phi^0 \rightarrow b\bar{b}$	$m_{\phi^0} \lesssim 95$
	$p\bar{p} \rightarrow W\phi^0; \phi^0 \rightarrow \tau^+\tau^-$	$110 \lesssim m_{\phi^0} \lesssim 120$
DiTeV, (4 TeV, 30 fb $^{-1}$)	$p\bar{p} \rightarrow W\phi^0; \phi^0 \rightarrow b\bar{b}$	$m_{\phi^0} \lesssim 95$
	$p\bar{p} \rightarrow ZZ \rightarrow 4\ell$	$m_{\phi^0} \sim 200$
LHC, (14 TeV, 600 fb $^{-1}$)	$pp \rightarrow \phi^0 \rightarrow ZZ^{(*)} \rightarrow 4\ell$	$120 \lesssim m_{\phi^0} \lesssim 800$
	$pp \rightarrow \phi^0 \rightarrow \gamma\gamma$	$80 \lesssim m_{\phi^0} \lesssim 150$
	$pp \rightarrow t\bar{t}\phi^0, W\phi^0; \phi^0 \rightarrow \gamma\gamma$	$80 \lesssim m_{\phi^0} \lesssim 120 - 130$
	$pp \rightarrow t\bar{t}\phi^0; \phi^0 \rightarrow b\bar{b}$	$m_{\phi^0} \lesssim 120$
NLC, (500 GeV, 50 fb $^{-1}$)	$e^+e^- \rightarrow Z\phi^0$	$m_{\phi^0} \lesssim 350$
	$WW \rightarrow \phi^0$	$m_{\phi^0} \lesssim 300$
	$e^+e^- \rightarrow t\bar{t}\phi^0$	$m_{\phi^0} \lesssim 120$
NLC, (1 TeV, 200 fb $^{-1}$)	$e^+e^- \rightarrow Z\phi^0$	$m_{\phi^0} \lesssim 800$
	$WW \rightarrow \phi^0$	$m_{\phi^0} \lesssim 700$
FMC, ($\sqrt{s} = m_{\phi^0}$, 50 fb $^{-1}$)	$\mu^+\mu^- \rightarrow \phi^0$	$m_{\phi^0} \lesssim 2m_W$

Table 8: MSSM Higgs boson discovery modes. All masses are specified in GeV. The ordered pair $(m_{A^0}, \tan \beta)$ fixes the MSSM Higgs sector masses and couplings. The parameter regime $m_{A^0} \leq 1000$ GeV and $1 \leq \tan \beta \leq 60$ is surveyed. If a range of $\tan \beta$ values is specified below, then the first (second) number in the range corresponds to the appropriate minimal (maximal) value of m_{A^0} . Luminosities are those obtained after summing over all detectors (4 detectors at LEP2 and ATLAS+CMS at the LHC). In the case of the LHC we include the Wh with $h \rightarrow b\bar{b}$ mode which may not, however, prove viable when running at high luminosity. See text for further clarifications.

Machine(\sqrt{s} , $\int \mathcal{L} dt$)	Mode	$(m_{A^0}, \tan \beta)$ Discovery Region
LEP I	$e^+e^- \rightarrow Z^*h^0, h^0A^0$	$(\lesssim 45, \gtrsim 1)$
LEP2 (175 GeV, 600 pb $^{-1}$)	$e^+e^- \rightarrow Zh^0, h^0A^0$	$(\lesssim 75, \gtrsim 1)$ or $(\gtrsim 75, \lesssim 4-2)$
LEP2 (192 GeV, 600 pb $^{-1}$)	$e^+e^- \rightarrow Zh^0, h^0A^0$	$(\lesssim 80, \gtrsim 1)$ or $(\gtrsim 80, \lesssim 5-3)$
LEP2 (205 GeV, 600 pb $^{-1}$)	$e^+e^- \rightarrow Zh^0, h^0A^0$	$(\lesssim 90, \gtrsim 1)$ or $(\gtrsim 90, \lesssim 10-8)$
Tev* (2 TeV, 30 fb $^{-1}$)	$p\bar{p} \rightarrow Wh^0; h^0 \rightarrow b\bar{b}; 2b\text{-tag}$	$(\gtrsim 130-150, \geq 1)$
DiTeV (4 TeV, 30 fb $^{-1}$)	$p\bar{p} \rightarrow Wh^0; h^0 \rightarrow b\bar{b}; 2b\text{-tag}$	$(\gtrsim 130-150, \geq 1)$
LHC (14 TeV, 600 fb $^{-1}$)	$pp \rightarrow Wh^0, t\bar{t}h^0; h^0 \rightarrow b\bar{b}; 2, 3b\text{-tag}$ $pp \rightarrow t\bar{t}; t \rightarrow H^+b; 1b\text{-tag}$ $pp \rightarrow H^0; H^0 \rightarrow ZZ^{(*)} \rightarrow 4\ell$ $pp \rightarrow h^0, Wh^0, t\bar{t}h^0; h^0 \rightarrow \gamma\gamma$ $pp \rightarrow b\bar{b}A^0, H^0; A^0, H^0 \rightarrow \tau^+\tau^-$ $pp \rightarrow b\bar{b}A^0, H^0; A^0, H^0 \rightarrow \mu^+\mu^-$ $pp \rightarrow b\bar{b}h^0; h^0 \rightarrow b\bar{b}; 3b\text{-tag}$ $pp \rightarrow b\bar{b}H^0; H^0 \rightarrow b\bar{b}; 3b\text{-tag}$ $pp \rightarrow b\bar{b}A^0; A^0 \rightarrow b\bar{b}; 3b\text{-tag}$ $pp \rightarrow A^0; A^0 \rightarrow Zh^0; Zh^0 \rightarrow \ell\ell b\bar{b}; 2b\text{-tag}$ $pp \rightarrow H^0, A^0; H^0, A^0 \rightarrow t\bar{t}; 2b\text{-tag}$ $pp \rightarrow H^0; H^0 \rightarrow h^0h^0; h^0h^0 \rightarrow b\bar{b}\gamma\gamma; 2b\text{-tag}$ $pp \rightarrow H^0; H^0 \rightarrow h^0h^0; h^0h^0 \rightarrow b\bar{b}b\bar{b}; 3b\text{-tag}$	$(\gtrsim 130-150, \geq 1)$ $(\lesssim 130, \geq 1)$ $(\lesssim 2m_t, \lesssim 3)$ $(\gtrsim 170, \geq 1)$ $(\gtrsim 70, \gtrsim 1-40)$ $(\gtrsim 100, \gtrsim 10-40)$ $(\lesssim 140, \gtrsim 4-6)$ $(\gtrsim 90, \gtrsim 5-20)$ $(\gtrsim 45, \gtrsim 4-20)$ $(200 - 2m_t, \lesssim 3)$ $(\gtrsim 2m_t, \lesssim 3-1.5)$ $(175 - 2m_t, \lesssim 4-5)$ $(175 - 2(m_t + 50), \lesssim 5-3)$
NLC (500 GeV, 50 fb $^{-1}$)	$e^+e^- \rightarrow Zh^0$ $WW \rightarrow h^0$ $e^+e^- \rightarrow h^0A^0$ $e^+e^- \rightarrow ZH^0, WW \rightarrow H^0$ $e^+e^- \rightarrow H^0A^0$ $e^+e^- \rightarrow H^+H^-$	visible unless $(\lesssim 90, \gtrsim 8)$ visible unless $(\lesssim 80, \gtrsim 13)$ $(\lesssim 120, \geq 1)$ $(\lesssim 140, \geq 1)$ $(\lesssim 230, \geq 1)$, unless $(\lesssim 90, \gtrsim 7)$ $(\lesssim 230, \geq 1)$
NLC (1 TeV, 200 fb $^{-1}$)	$e^+e^- \rightarrow H^0A^0$ $e^+e^- \rightarrow H^+H^-$	$(\lesssim 450, \geq 1)$, unless $(\lesssim 90, \gtrsim 7)$ $(\lesssim 450, \geq 1)$
FMC ($\sqrt{s} = m_h$, 50 fb $^{-1}$)	$\mu^+\mu^- \rightarrow h^0$ $\mu^+\mu^- \rightarrow H^0, A^0$	$(\text{all}, \geq 1)$ $(\lesssim \sqrt{s}_{\text{max}}, \geq 5)$ or $(\lesssim 2m_t, \gtrsim 2)$

that in the indicated region of parameter space, H^0 is roughly SM-like in its couplings, while the h^0ZZ and $h^0W^+W^-$ couplings are very suppressed. The ZH^0A^0 coupling is likewise suppressed in the same parameter regime, which explains the other two discovery region exceptions listed in Table 8. Nonetheless, it should be re-stressed that at least one of the MSSM Higgs bosons is visible throughout all of parameter space. For example, in the $\tan\beta \gtrsim 8$ and $m_{A^0} \lesssim 90$ GeV region where the Zh^0 and $WW \rightarrow h^0$ modes lose viability, h^0A^0 production occurs with full strength and would allow discovery of both the h^0 and A^0 . For a more direct pictorial representation of these e^+e^- regions see the earlier Fig. 23.

10.1 A Tour of Higgs Search Techniques at Future Colliders

The goal of the Higgs search at present and future colliders is to examine the full mass range of the SM Higgs boson, and the full parameter space of the MSSM Higgs sector. The LHC can cover the entire range of SM Higgs boson masses from the upper limit of LEP2 ($m_{\phi^0} = 80\text{--}95$ GeV, depending on machine energy) to a Higgs mass of 700 GeV (and beyond). The most difficult region for high luminosity hadron colliders is the ‘low’ intermediate-mass range $m_{\phi^0} = 80\text{--}130$ GeV. The LHC detectors are being designed with the capability of fully covering the intermediate Higgs mass region. The Tev* and DiTevatron may also have some discovery potential in this mass region. In contrast, the intermediate mass Higgs search at the NLC (which makes use of the same search techniques employed at LEP II) is straightforward. At design luminosity, the NLC discovery reach is limited only by the center-of-mass energy of the machine.

In the search for the Higgs bosons of the MSSM, two objectives are: (i) the discovery of h^0 and (ii) the discovery of the non-minimal Higgs states (H^0 , A^0 , and H^\pm). Two theoretical results play a key role in the MSSM Higgs search. First, the mass of the h^0 is bounded. For a top-quark pole mass $m_t = 175$ GeV, $m_{\tilde{t}} \sim M_{SUSY} \lesssim 1$ TeV, and no squark mixing, $m_{h^0}^{\max} \simeq 113$ GeV. For $m_t = 175$ GeV, $M_{SUSY} \sim 1$ TeV, and maximal squark mixing, $m_{h^0}^{\max} \simeq 125$ GeV. Second, if the properties of h^0 deviate significantly from the SM Higgs boson, then $m_{A^0} \lesssim \mathcal{O}(m_Z)$ and the H^0 and H^\pm masses must lie in the intermediate Higgs mass region. As a result, experiments that are sensitive to the intermediate Higgs mass region have the potential for detecting at least one of the MSSM Higgs bosons over the entire MSSM Higgs parameter space (parameterized by $\tan\beta$ and m_{A^0}). LEP2 does not have sufficient energy to cover the entire MSSM Higgs parameter space if $M_{SUSY} \sim m_{\tilde{t}} \sim 1$ TeV and/or squark mixing is large, since then $m_{h^0}^{\max}$ lies above the LEP2 Higgs mass reach. The Tev*, DiTevatron and LHC all possess the capability of detecting Higgs bosons in the intermediate mass range, and consequently can probe regions of the MSSM Higgs parameter space not accessible to LEP2. The most recent results suggest that the LHC, when operating at full energy and luminosity,

will guarantee the discovery (or exclusion) of at least one MSSM Higgs boson for *all* values of m_{A^0} and $\tan\beta$ not excluded by the LEP2 search. A number of specialized modes have been developed to close the gap in the MSSM parameter space that arose when only the most basic $\gamma\gamma$ and ZZ^* final decays of a neutral Higgs were considered. However, these modes do demand efficient and pure b quark and/or τ identification in hadron collider events. Because of the relative simplicity of the NLC Higgs search in the intermediate mass region, the NLC is certain to discover at least one MSSM Higgs boson (either h^0 or H^0) if the supersymmetric approach is correct. If h^0 is discovered and proves to be SM-like in its properties, then one must be in the region of MSSM Higgs parameter space where the non-minimal Higgs states are rather heavy and approximately degenerate in mass. In this case, the LHC may not be capable of discovering any Higgs bosons beyond the h^0 , and detection of the H^0 , A^0 and H^\pm at the NLC would only be possible for center-of-mass energy $\sqrt{s} \gtrsim 2m_{A^0}$.

Below is an outline of the Higgs potential of present and future colliders. A Higgs boson is deemed observable if a 5σ -excess of events can be detected in a given search channel. We assume $m_t = 175$ GeV. For the MSSM Higgs results we employ $m_{\tilde{t}} = 1$ TeV and neglect squark mixing in the radiative mass corrections; further, SUSY decays are assumed to be absent.

- LEP — The current lower bound on the SM Higgs mass is 64.5 GeV, and will increase by at most a few GeV. The lower bounds on the MSSM Higgs masses (scanning over *all* parameters of the model) are $m_{h^0} > 45$ GeV, $m_{A^0} > 45$ GeV (for $\tan\beta > 1$), and $m_{H^\pm} > 45$ GeV.
- LEP2 — For $\sqrt{s} = 175$ GeV, the SM Higgs is accessible via $Z\phi^0$ production up to 82 GeV for an integrated luminosity of 600 pb^{-1} summed over all experiments. For $\sqrt{s} = 192$ GeV, m_{ϕ^0} values as high as 95 GeV can be probed with 600 pb^{-1} of data, using b -tagging in the region $m_{\phi^0} \sim m_Z$. The reach for $\sqrt{s} = 205$ GeV is about 103 GeV for $L = 600 \text{ pb}^{-1}$. In the MSSM, the same mass reaches apply to h^0 if $m_{A^0} \gtrsim m_Z$, since in this case Zh^0 is produced at about the same rate as $Z\phi^0$. If $m_{A^0} \lesssim m_Z$, then the h^0ZZ coupling (which controls the Zh^0 cross section) becomes suppressed while the ZA^0h^0 coupling becomes maximal. In the latter parameter region, $e^+e^- \rightarrow A^0h^0$ can be detected for all values of $m_{A^0} \lesssim \sqrt{s}/2 - 10$ GeV, assuming that $\tan\beta > 1$. Since $m_{h^0} \lesssim 113$ GeV if $m_{\tilde{t}} \leq 1$ TeV and squark mixing is negligible, increasing the LEP2 energy to roughly $\sqrt{s} = 220$ GeV while maintaining the luminosity would be sufficient to guarantee the detection of at least one Higgs boson (via Zh^0 and/or A^0h^0 final states) over the entire MSSM Higgs parameter space. Large squark mixing with $m_{\tilde{t}} \sim 1$ TeV would, however, necessitate still larger \sqrt{s} .
- Tevatron ($\sqrt{s} = 2$ TeV, $\mathcal{L} = 10^{32} \text{ cm}^{-2} \text{ s}^{-1}$ with the Main Injector) — The most promising mode for the SM Higgs is $W\phi^0$ production, followed by $\phi^0 \rightarrow b\bar{b}$. With 5 fb^{-1} of integrated luminosity, this mode could potentially explore a Higgs mass region of 60–80 GeV, a region which will already have been covered by LEP2 via

the $Z\phi^0$ process.

- Tev* ($\sqrt{s} = 2$ TeV, $\mathcal{L} \geq 10^{33} \text{ cm}^{-2} \text{ s}^{-1}$) — The Higgs mass reach in the $W\phi^0$ mode, with $\phi^0 \rightarrow b\bar{b}$, is extended over that of the Tevatron. With 30 fb^{-1} of integrated luminosity, a Higgs of mass 95 GeV is potentially accessible, but the peak will not be separable from the WZ , $Z \rightarrow b\bar{b}$ background. The mode $(W, Z)\phi^0$, followed by $\phi^0 \rightarrow \tau^+\tau^-$ and $W, Z \rightarrow jj$ (where j stands for a hadronic jet), is potentially viable for Higgs masses sufficiently far above the Z mass. With 30 fb^{-1} of integrated luminosity, a Higgs in the mass range 110–120 GeV may be detectable. However, the Higgs peak will be difficult to recognize on the slope of the much larger Zjj , $Z \rightarrow \tau^+\tau^-$ background. Both of these modes are of particular significance for h^0 . For $\tan\beta > 1$ and $m_{A^0} \lesssim 1.5m_Z$, the enhanced coupling of the h^0 to b 's and τ 's makes it unobservable at the LHC via $h^0 \rightarrow \gamma\gamma$ or $h^0 \rightarrow ZZ^* \rightarrow 4\ell$.
- DiTevatron ($\sqrt{s} = 4$ TeV, $\mathcal{L} \geq 10^{33} \text{ cm}^{-2} \text{ s}^{-1}$) — For the SM Higgs, the “gold-plated” mode, $\phi^0 \rightarrow ZZ \rightarrow 4\ell$, requires about 30 fb^{-1} for the optimal Higgs mass in this mode, $m_{\phi^0} = 200$ GeV. If 100 fb^{-1} can be collected, this mode covers the mass region $m_{\phi^0} = 200 - 300$ GeV and $m_{\phi^0} \sim 150$ GeV. The 4ℓ mode is not useful for any of the MSSM Higgs bosons. The Higgs mass reach in the $W\phi^0$, $\phi^0 \rightarrow b\bar{b}$ mode is only marginally better than at the Tev*, due to the increase in the top-quark backgrounds relative to the signal. The mode $(W, Z)\phi^0$, with $\phi^0 \rightarrow \tau^+\tau^-$ and $W, Z \rightarrow jj$, has less promise than at the Tev* due to the relative increase in the background.
- LHC ($\sqrt{s} = 14$ TeV, $\mathcal{L} = 10^{33}\text{--}10^{34} \text{ cm}^{-2} \text{ s}^{-1}$) — For the SM Higgs boson, the “gold-plated” mode, $\phi^0 \rightarrow ZZ^{(*)} \rightarrow 4\ell$, including the case where one Z boson is virtual, covers the range of Higgs masses 130–700 GeV and beyond with 100 fb^{-1} . For $m_{\phi^0} > 700$ GeV, the Higgs is no longer “weakly coupled”, and search strategies become more complex.

The CMS detector is planning an exceptional (PbWO_4 crystal) electromagnetic calorimeter which will enable the decay mode $\phi^0 \rightarrow \gamma\gamma$ to cover the Higgs mass range 85–150 GeV with 100 fb^{-1} of integrated luminosity. This range overlaps the reach of LEP2 (with $\sqrt{s} = 192$ GeV) and the lower end of the range covered by the gold-plated mode. The ATLAS detector covers the range 110–140 GeV with this mode. Both CMS and ATLAS find that the modes $t\bar{t}\phi^0$ and $W\phi^0$, with $\phi^0 \rightarrow \gamma\gamma$, are viable in the mass range 80–120 GeV with 100 fb^{-1} of integrated luminosity. Since backgrounds are smaller, these modes do not require such excellent photon resolutions and jet-photon discrimination as does the inclusive $\gamma\gamma$ mode. CMS has also studied the production of the Higgs in association with two jets, followed by $\phi^0 \rightarrow \gamma\gamma$, and concludes that this mode covers the Higgs mass range 70–130 GeV.

The modes $t\bar{t}\phi^0$ and $W\phi^0$, with $\phi^0 \rightarrow b\bar{b}$, are useful in the intermediate-mass region. The reach with 100 fb^{-1} of integrated luminosity is 100 GeV, reduced to 80 GeV with 30 fb^{-1} , and extended to 120 GeV for $L = 600 \text{ fb}^{-1}$ (summed over experiments). Overall, ATLAS will cover the Higgs mass region 80–140 GeV with 100 fb^{-1} using a combination of $\phi^0 \rightarrow \gamma\gamma$; $t\bar{t}\phi^0$, $W\phi^0$ with $\phi^0 \rightarrow \gamma\gamma$; and $t\bar{t}\phi^0$ with

$\phi^0 \rightarrow b\bar{b}$; CMS has not yet completed their studies of the b -tagged modes.

The main search mode for the lightest MSSM Higgs boson is $h^0 \rightarrow \gamma\gamma$, which is viable when m_{h^0} is near $m_{h^0}^{\max}$. The processes $t\bar{t}h^0$ and Wh^0 , with $h^0 \rightarrow b\bar{b}$, can potentially extend h^0 detection to the somewhat lower m_{h^0} values (corresponding to somewhat lower m_{A^0}) that would be one way to assure that at least one MSSM Higgs boson can be detected over all of the MSSM parameter space. Adapting the ATLAS study for the SM Higgs to h^0 suggests that the required sensitivity could be achieved in the $t\bar{t}h^0$ mode. Due to the large top-quark background, the Wh^0 with $h^0 \rightarrow b\bar{b}$ mode at the LHC has little advantage over this mode at the Tev^{*} or the DiTevatron for the same integrated luminosity. Other modes whose inclusion will guarantee discovery of at least one MSSM Higgs boson appear below.

The other MSSM Higgs bosons are generally more elusive. There are small regions of parameter space in which H^0 can be observed decaying to $\gamma\gamma$ or $ZZ^{(*)}$. The possibility exists that the charged Higgs can be discovered in top decays. For $m_{A^0} > 2m_Z$ and moderate to large $\tan\beta$, H^0 and A^0 can have sufficiently enhanced b quark couplings that they would be observed when produced in association with $b\bar{b}$ and decaying via $H^0, A^0 \rightarrow \tau^+\tau^-$. In the most recent studies the region of viability for the $\tau^+\tau^-$ modes at $L = 600 \text{ fb}^{-1}$ (combined luminosity of ATLAS and CMS) is bounded from below by $\tan\beta \gtrsim 1$ at $m_{A^0} \sim 70 \text{ GeV}$ rising to $\tan\beta \gtrsim 20$ at $m_{A^0} \sim 500 \text{ GeV}$. CMS has demonstrated that the H^0 and A^0 can be observed in their $\mu^+\mu^-$ decay channel, using enhanced production in association with $b\bar{b}$, in a slightly more limited region.

For enhanced couplings of the Higgs bosons to b quarks (which occurs for large $\tan\beta$), the modes $b\bar{b}(h^0, H^0, A^0)$, with $h^0, H^0, A^0 \rightarrow b\bar{b}$, and $\bar{t}bH^+$, with $H^+ \rightarrow t\bar{b}$, are potentially viable. Parton-level Monte Carlo studies suggest that the combined discovery region for the former processes covers a region that begins at $\tan\beta \gtrsim 3-4$ at low m_{A^0} rising to $\tan\beta \gtrsim 14$ at $m_{A^0} = 500 \text{ GeV}$.

CMS and ATLAS have considered the process $gg \rightarrow A^0 \rightarrow Zh^0 \rightarrow \ell^+\ell^-b\bar{b}$. They each claim an observable signal with single and double b tagging in the region $175 \lesssim m_{A^0} \lesssim 2m_t$ and $\tan\beta \lesssim 2-3$ for $L = 100 \text{ fb}^{-1}$ (in a given detector). This region expands somewhat if the data from the two detectors is combined and a combined $L = 600 \text{ fb}^{-1}$ is achieved. Recent results for the modes $H^0 \rightarrow h^0h^0$ and $H^0, A^0 \rightarrow t\bar{t}$ are also available. ATLAS and CMS claim that for $2m_t \lesssim m_{A^0} \lesssim 500 \text{ GeV}$ one can detect $A^0, H^0 \rightarrow t\bar{t}$ for $\tan\beta \lesssim 2$ with $30-100 \text{ fb}^{-1}$ of integrated luminosity; good knowledge of the magnitude of the $t\bar{t}$ background is required. This region expands to $\tan\beta \lesssim 3$ for combined ATLAS+CMS $L = 600 \text{ fb}^{-1}$. The $H^0 \rightarrow h^0h^0$ mode can potentially be employed in the channels $h^0h^0 \rightarrow b\bar{b}b\bar{b}$ and $h^0h^0 \rightarrow b\bar{b}\gamma\gamma$. A parton-level Monte-Carlo study using 3 b -tagging and requiring that there be two $b\bar{b}$ pairs of mass $\sim m_{h^0}$ yields a viable signal for $2(m_t + 50) \gtrsim m_{A^0} \gtrsim 175$ and $\tan\beta \lesssim 5-3$, assuming $L = 600 \text{ fb}^{-1}$ [112]. Because of uncertainty on the ability to trigger on the $4b$ final state, ATLAS and CMS have examined the $H^0 \rightarrow h^0h^0 \rightarrow b\bar{b}\gamma\gamma$ final state. This is a very clean

channel (with b tagging), but is rate limited. For $L = 600 \text{ fb}^{-1}$ of luminosity the discovery region $175 \text{ GeV} \lesssim m_{A^0} \lesssim 2m_t$, $\tan \beta \lesssim 5$ is claimed.

Putting together all these modes, we can summarize by saying that for moderate $m_{A^0} \lesssim 2m_t$ there is an excellent chance of detecting more than one of the MSSM Higgs bosons. However, for large $m_{A^0} \gtrsim 400 \text{ GeV}$ (as often preferred in the GUT scenarios) only the three $h^0 \rightarrow \gamma\gamma$ production/decay modes ($gg \rightarrow h^0$, $t\bar{t}h^0$, and Wh^0 , all with $h^0 \rightarrow \gamma\gamma$) are guaranteed to be observable if $\tan \beta$ is neither near 1 nor large.

- e^+e^- linear collider ($\sqrt{s} = 500 \text{ GeV}$ to 1 TeV , $\mathcal{L} \geq 5 \times 10^{33} \text{ cm}^{-2} \text{ s}^{-1}$) — At $\sqrt{s} = 500 \text{ GeV}$ with an integrated luminosity of 50 fb^{-1} , the SM Higgs boson is observable via the $Z\phi^0$ process up to $m_{\phi^0} = 350 \text{ GeV}$. Employing the same process, a Higgs boson with $m_{\phi^0} = 130 \text{ GeV}$ (200 GeV) would be discovered with 1 fb^{-1} (10 fb^{-1}) of data. Other Higgs production mechanisms are also useful. With 50 fb^{-1} of data, the WW -fusion process is observable up to $m_{\phi^0} = 300 \text{ GeV}$. The $t\bar{t}\phi^0$ process is accessible for $m_{\phi^0} \lesssim 120 \text{ GeV}$, thereby allowing a direct determination of the $t\bar{t}\phi^0$ Yukawa coupling. The $\gamma\gamma$ collider mode of operation does not extend the reach of the machine for the SM Higgs, but does allow a measurement of the $\phi^0 \rightarrow \gamma\gamma$ partial width up to $m_{\phi^0} = 300 - 350 \text{ GeV}$.

In the MSSM, for $m_{A^0} \lesssim m_Z$, the h^0 and A^0 will be detected in the $h^0 A^0$ mode, the H^0 will be found via ZH^0 and WW -fusion production, and H^+H^- pair production will be kinematically allowed and easily observable. At higher values of the parameter m_{A^0} , the lightest Higgs boson is accessible in both the Zh^0 and WW -fusion modes. However, the search for the heavier Higgs boson states is limited by machine energy. The mode $H^0 A^0$ is observable up to $m_{H^0} \sim m_{A^0} \sim 230 - 240 \text{ GeV}$, and H^+H^- can be detected up to $m_{H^\pm} = 230 \text{ GeV}$. The $\gamma\gamma$ collider mode could potentially extend the reach for H^0 and A^0 up to 400 GeV if $\tan \beta$ is not large.

At $\sqrt{s} = 1 \text{ TeV}$ with an integrated luminosity of 200 fb^{-1} , the SM Higgs boson can be detected via the WW -fusion process up to $m_{\phi^0} = 700 \text{ GeV}$. In the MSSM, $H^0 A^0$ and H^+H^- detection would be extended to $m_{H^0} \sim m_{A^0} \sim m_{H^\pm} \sim 450 \text{ GeV}$.

- Influence of MSSM Higgs decays into supersymmetric particle final states — For some MSSM parameter choices, the h^0 can decay primarily to invisible modes, including a pair of the lightest supersymmetric neutralinos or a pair of invisibly decaying sneutrinos. The h^0 would still be easily discovered at e^+e^- colliders in the Zh^0 mode using missing-mass techniques. At hadron colliders, the Wh^0 and $t\bar{t}h^0$ modes may be detectable via large missing energy and lepton plus invisible energy signals, but determination of m_{h^0} would be difficult. The H^0 , A^0 , and H^\pm decays can be dominated by chargino and neutralino pair final states and/or slepton pair final states. Such modes can either decrease or increase the chances of detecting these heavier MSSM Higgs bosons at a hadron collider, depending upon detailed MSSM parameter choices. At e^+e^- colliders H^0 , A^0 and H^\pm detection up to the earlier quoted (largely kinematical) limits should in general remain possible.

- Hadron collider beyond the LHC — It could provide increased event rates and more overlap of discovery modes for the SM Higgs boson. However, its primary impact would be to extend sensitivity to high mass signals associated with strongly-coupled electroweak symmetry breaking scenarios. In the case of the MSSM Higgs bosons, the increased event rates would significantly extend the overlap of the various discovery modes, expanding the parameter regions where several and perhaps all of the MSSM Higgs bosons could be observed.
- e^+e^- collider beyond $\sqrt{s} = 1$ TeV — Such an extension in energy is not required for detecting and studying a weakly-coupled SM Higgs boson, but could be very important for a strongly-coupled electroweak-symmetry-breaking scenario. Detection of $H^0 A^0$ and $H^+ H^-$ production in the MSSM model would be extended to higher masses.
- $\mu^+\mu^-$ collider with $\sqrt{s} = 500$ GeV and $\mathcal{L} \geq 2 - 5 \times 10^{33} \text{ cm}^{-2} \text{ s}^{-1}$ — Such a collider would accomplish many of the same tasks as the corresponding e^+e^- collider, except that the $\gamma\gamma$ collider option would not be possible.
- $\mu^+\mu^-$ collider with $\sqrt{s} = m_h$ — Such a collider (dubbed the first muon collider or FMC) can be used to discover a SM Higgs boson with $m_{\phi^0} \lesssim 2m_W$ or the h^0 of the MSSM by scanning. The enhanced $b\bar{b}$ and $\mu^+\mu^-$ couplings of the H^0 and A^0 imply that they can be discovered by scanning for $\tan\beta \gtrsim 2$ if their masses are below $2m_t$, and for $\tan\beta \gtrsim 5$ regardless of mass.

10.2 Precision Measurements of Higgs Properties

Once discovered, the next priority will be to carry out detailed studies of the properties of the Higgs bosons. In the outline below, h denotes the lightest CP-even neutral Higgs. It may be ϕ^0 or h^0 (of the MSSM), or perhaps a scalar arising from a completely different model. Once discovered, determining the identity of h is the crucial issue.

The largest number of precision measurements can be performed at an e^+e^- collider (or $\mu^+\mu^-$ collider with the same energy and luminosity). The LHC and FMC (run in the s -channel Higgs production mode) provide more limited information. At an e^+e^- collider measurements of cross sections, branching ratios, and angular distributions of Higgs events will determine most model parameters and test much of the underlying theory of the scalar sector. In particular, the hZZ coupling-squared can be measured using inclusive Zh production with $Z \rightarrow \ell^+\ell^-$ to an accuracy of better than 10%. The hWW coupling can then be computed assuming custodial symmetry and compared with the value measured via the $WW \rightarrow h$ fusion production process. If $m_h \lesssim 120$ GeV or $m_h \gtrsim 2m_t$, there is a good chance that the $ht\bar{t}$ coupling can be measured with reasonable accuracy. Further, for a SM-like Higgs with $m_h \sim 120$ GeV, statistical precisions of 7%, 14%, 39%, and 48% can be achieved for $\sigma(Zh) \times BR(h \rightarrow b\bar{b})$, $\sigma(Zh) \times BR(h \rightarrow \tau^+\tau^-)$, $\sigma(Zh) \times BR(h \rightarrow c\bar{c} + gg)$, and $\sigma(Zh) \times BR(h \rightarrow WW^*)$, respectively.

However, in the case of a SM-like Higgs boson, the total Higgs width and coupling to $b\bar{b}$ and $\tau^+\tau^-$ would remain poorly determined. Measurement of the $h \rightarrow \gamma\gamma$ coupling would require the $\gamma\gamma$ -collider mode of operation. LHC measurements of $\sigma(t\bar{t}h) \times BR(h \rightarrow \gamma\gamma)$ and $\sigma(Wh) \times BR(h \rightarrow \gamma\gamma)$ can be combined with the NLC determinations of the hWW and (if $m_h \lesssim 120$ GeV, $ht\bar{t}$) coupling to determine $BR(h \rightarrow \gamma\gamma)$. This can be combined with the $\gamma\gamma$ -collider measurement of the $h\gamma\gamma$ coupling itself to obtain a value for the total h width. This would then allow determination of the partial $h \rightarrow b\bar{b}$ width from $BR(h \rightarrow b\bar{b})$ as measured at the NLC, for example. (An accurate determination of $BR(h \rightarrow b\bar{b})$ requires $m_h \lesssim 145$ GeV.) However, the accumulation of errors in reaching the total h width or partial $h \rightarrow b\bar{b}$ width will limit the accuracy with which they can be determined. For $m_h \lesssim 2m_W$, s -channel Higgs production at a $\mu^+\mu^-$ collider with sufficiently good energy resolution can provide a very accurate direct scan determination of Γ_h with error of order $\pm 10\%$ and a determination of the $h\mu^+\mu^-$ coupling. The precision of the latter is limited only by the errors on determinations of $BR(h \rightarrow b\bar{b})$ (and/or $BR(h \rightarrow WW^*)$) from other sources.

At an e^+e^- collider with $L = 50 \text{ fb}^{-1}$, the central value of the Higgs mass can be determined with a statistical accuracy of ± 180 MeV for $m_h \lesssim 2m_W$ using direct final state mass reconstruction. A detector with the ultra-excellent resolution of the super-JLC design could measure m_h to ± 20 MeV using the recoil mass spectrum in Zh events where $Z \rightarrow \ell^+\ell^-$. At the LHC, in the intermediate mass region the accuracy will be of order ± 1 GeV using $h \rightarrow \gamma\gamma$ modes. In this same mass region, the FMC with excellent beam energy resolution could determine m_h to within $\lesssim \pm 0.0003\%$. Since most Standard Model parameters only have logarithmic dependence on the Higgs mass, the NLC and FMC accuracies are far greater than what is needed to check the consistency of the Standard Model predictions for precision Z electroweak measurements. The LHC accuracy would be adequate. Of course, one could use the mass determination to make accurate predictions for the Higgs production cross sections and branching fractions.

The expected errors referred to above for all the different measurements are summarized in Table 6 (appearing earlier) for Higgs masses of $m_h = 110, 120$ and 140 GeV. It is a matter of some priority for the experimentalists to refine these estimates and obtain errors for a more complete selection of Higgs masses. As noted below, a complete model-independent study of all the properties of a light Higgs boson can be performed with a useful level of accuracy only if most (if not all) of the measurements can be made with small errors.

For a SM Higgs boson, signals can be selected with small backgrounds and one can easily measure the angular distributions of the Higgs production direction in the process $e^+e^- \rightarrow Zh$ and the directions of the outgoing fermions in the Z^0 rest frame, and verify the expectations for a CP-even Higgs boson. For a more general Higgs eigenstate, since only the CP-even part couples at tree-level to ZZ , these measurements would still agree with the CP-even predictions unless the Higgs is

primarily (or purely) CP-odd, in which case the cross section will be much smaller and the event rate inadequate to easily verify the mixed-CP or CP-odd distribution forms. Analysis of photon polarization asymmetries in $\gamma\gamma \rightarrow h$ production rates, and of angular correlations among secondary decay products arising from primary $h \rightarrow \tau\tau$ or $h \rightarrow t\bar{t}$ final state decays in Zh production, can both provide much better sensitivity to a CP-odd Higgs component in many cases. These latter decay correlations are also very effective in determining the CP character of a Higgs boson produced directly in the s -channel at a $\mu^+\mu^-$ collider. At a $\mu^+\mu^-$ collider if polarization of both beams can be achieved without loss of too much luminosity, one can also probe the CP parity of a Higgs using transverse polarization asymmetries.

An important question is whether or not we can distinguish the SM-like h^0 from the simple standard model ϕ^0 in the large m_{A^0} portion of MSSM parameter space, $m_{A^0} \gtrsim 400$ GeV, where it is more than likely that only the h^0 will be seen directly at the NLC or LHC. The most promising possibilities are: (i) the NLC measurement of the rare branching fraction ratio $r_{c\bar{c}+gg} \equiv BR(h \rightarrow c\bar{c} + gg)/BR(h \rightarrow b\bar{b})$; and (ii) the FMC measurements of the total width (as measured by a careful scan) and $\Gamma(h \rightarrow \mu^+\mu^-)BR(h \rightarrow b\bar{b})$ (which is directly determined from event rate). The total width can be combined with a direct determination of $BR(h \rightarrow b\bar{b})$ (using Zh associated production, for example) to determine in a model-independent way the $h \rightarrow b\bar{b}$ partial width and coupling; similarly $\Gamma(h \rightarrow \mu^+\mu^-)BR(h \rightarrow b\bar{b})$ can be combined with $BR(h \rightarrow b\bar{b})$ to obtain a model-independent determination of $\Gamma(h \rightarrow \mu^+\mu^-)$. Deviations in the quantities $r_{c\bar{c}+gg}$, Γ_h^{tot} , and $\Gamma(h \rightarrow \mu^+\mu^-)$ can potentially distinguish between $h = \phi^0$ and $h = h^0$ for m_{A^0} values above 400 GeV.

Reasonably precise measurements of certain $\sigma \times BR$ combinations will also be possible at hadron colliders. For example, at the LHC a good determination of $\sigma(gg \rightarrow h) \times BR(h \rightarrow \gamma\gamma)$ should be possible for a SM-like Higgs in the 80 to 150 GeV mass range, and of $\sigma(gg \rightarrow h) \times BR(h \rightarrow ZZ)$ for $m_h > 130$ GeV; $\sigma(t\bar{t}h) \times BR(h \rightarrow b\bar{b})$ would be roughly determined for $m_h \lesssim 100 - 120$ GeV. However, it would appear that these cannot probe as far out in m_{A^0} as can the NLC and FMC precision measurements. In addition, deviations from SM predictions can arise from other types of new physics.

In the absence of a $\mu^+\mu^-$ collider, model-independent determinations of Γ_h^{tot} and $\Gamma(h \rightarrow b\bar{b})$ require combining data from the LHC with data from *both* e^+e^- and $\gamma\gamma$ collisions at the NLC. Let us repeat in detail the shortest and probably most accurate procedure outlined earlier.

- (a) Determine $BR(b\bar{b})$ from Zh events at the NLC.
- (b) Combine $BR(b\bar{b})$ with $\sigma(WW \rightarrow h)BR(b\bar{b})$ at the NLC to obtain the WWh coupling.
- (c) Use the WWh coupling and a measurement of $\sigma(Wh)BR(\gamma\gamma)$ at the LHC to determine $BR(\gamma\gamma)$.

- (d) Combine $BR(b\bar{b})$ with the $\gamma\gamma$ -Collider measurement of $\sigma(\gamma\gamma \rightarrow h)BR(b\bar{b})$ to obtain $\Gamma(h \rightarrow \gamma\gamma)$.
- (e) Compute $\Gamma_h^{\text{tot}} = \Gamma(h \rightarrow \gamma\gamma)/BR(\gamma\gamma)$.
- (f) Compute $\Gamma(h \rightarrow b\bar{b}) = BR(b\bar{b})\Gamma_h^{\text{tot}}$.

The accumulation of errors will be significant. However, it is worth re-emphasizing the basic point that *data from all three colliders will be required in order to complete a **model-independent** determination of all the properties of a light Higgs boson.*

Overall, if either the minimal standard model or the minimal supersymmetric standard model, or something like them, is correct, one or more Higgs bosons will be discovered at all three types of machines discussed here: a hadron collider — perhaps the Tev or Tev*, but certainly the LHC; an e^+e^- collider — perhaps LEP2, but certainly the NLC; and, assuming target luminosity goals can be met, a $\mu^+\mu^-$ collider. These machines are remarkably complementary, each revealing new windows on the Higgs boson(s); only the combination of data from all three types of machines can over constrain the Higgs sector and provide a fully definitive test of, for example, the minimal standard model Higgs predictions, including all ($f\bar{f}$, VV , $\gamma\gamma$, and gg) couplings and the total width. Higgs physics should provide a rich source of vital experimental results far into the future.

11 Acknowledgements

We are grateful for advice and assistance from T. Barklow, D. Burke, A. Caner, M. Carena, J.-L. Contreras, A. Djouadi, D. Froidevaux, F. Gianotti, H. Haber, T. Han, P. Janot, S. Keller, T. Liss, E. Richter-Was, A. Sopczak, M. Spira, and C. Wagner. J. G. was supported in part by Department of Energy grant DE-FG03-91ER40674 and the Davis Institute for High Energy Physics. S. W. was supported in part by Department of Energy grant DE-FG02-91ER40677.

References

- [1] L. Susskind, Phys. Rev. **D20**, 2619 (1979).
- [2] S. Weinberg, Phys. Rev. **D13**, 974 (1976); **D19**, 1277 (1979).
- [3] P. Sikivie, L. Susskind, M. Voloshin, and V. Zakharov, Nucl. Phys. **B173**, 189 (1980).
- [4] M. Veltman, Acta. Phys. Pol. **B8**, 475 (1977).

- [5] M. Peskin and T. Takeuchi, Phys. Rev. Lett. **65**, 964 (1990); B. Holdom and J. Terning, Phys. Lett. **B247**, 88 (1990); M. Golden and L. Randall, Nucl. Phys. **B361**, 3 (1991).
- [6] S. Glashow and S. Weinberg, Phys. Rev. **D15**, 1958 (1977).
- [7] S. Weinberg, Phys. Rev. Lett. **19**, 1264 (1967); A. Salam, in *Elementary Particle Theory: Relativistic Groups and Analyticity*, edited by N. Svartholm, proceedings of the Nobel Symposium No. 8 (Almqvist and Wiksell, Stockholm, 1968).
- [8] L. Maiani, G. Parisi, and R. Petronzio, Nucl. Phys. **B136**, 115 (1978); N. Cabibbo, L. Maiani, G. Parisi, and R. Petronzio, Nucl. Phys. **B158**, 295 (1979).
- [9] R. Dashen and H. Neuberger, Phys. Rev. Lett. **50**, 1897 (1983).
- [10] U. Heller, M. Klomfass, H. Neuberger, and P. Vranas, Nucl. Phys. **405**, 555 (1993).
- [11] G. Altarelli and G. Isidori, Phys. Lett. **B337**, 141 (1994).
- [12] CDF Collaboration, F. Abe *et al.*, Phys. Rev. **D50**, 2966 (1994); Phys. Rev. Lett. **73**, 225 (1994); Phys. Rev. Lett. **74**, 2626 (1995).
- [13] D0 Collaboration, S. Abachi *et al.*, Phys. Rev. Lett. **74**, 2632 (1995).
- [14] G. Montagna, O. Nicrosini, G. Passarino, and F. Piccinini, Phys. Lett. **B335**, 484 (1994).
- [15] J.A. Casas, J.R. Espinosa and M. Quiros, Phys. Lett. **B342**, 171 (1995).
- [16] See J.F. Gunion, H.E. Haber, G.L. Kane and S. Dawson, *The Higgs Hunters Guide*, Addison-Wesley Publishing.
- [17] H.E. Haber, G.L. Kane, T. Sterling Nucl. Phys. **161**, 493 (1979).
- [18] For recent summaries, see, for example, J. Hewett, SLAC-PUB-6521 and C.-H. Chang and C. Lu, AS-ITP-95-23.
- [19] See, for example, H.E. Haber, SCIPP-94-39, Workshop on Electro-Weak Symmetry Breaking, Budapest, Hungary, July 11-15, 1994 and the Joint U.S.-Polish Workshop on Physics from Planck Scale to Electro-Weak Scale (SUSY 94), Warsaw, Poland, 21-24 September, 1994.
- [20] J.A. Grifols and A. Mendez, Phys. Rev. **D22**, 1725 (1980).
- [21] H. Georgi and M. Machacek, Nucl. Phys. **B262**, 463 (1985).

- [22] M. Chanowitz and M. Golden, Phys. Lett. **B165**, 105 (1985).
- [23] J.F. Gunion, R. Vega, and J. Wudka, Phys. Rev. **D42**, 1673 (1990); Phys. Rev. **D43**, 2322 (1991).
- [24] J.C. Pati and A. Salam, Phys. Rev. **D10**, 275 (1974); R.N. Mohapatra and J.C. Pati, Phys. Rev. **D11**, 566 (1975); R.N. Mohapatra and G. Senjanovic, Phys. Rev. **D12**, 1502 (1975); Phys. Rev. Lett. **44**, 912 (1980); Phys. Rev. **D23**, 165 (1981).
- [25] F. Olness and M.E. Ebel, Phys. Rev. **D32**, 1769 (1985); R.N. Mohapatra and P.B. Pal, Phys. Lett. **179B**, 105 (1986); J.F. Gunion, B. Kayser, R.N. Mohapatra, N.G. Deshpande, J.A. Grifols, A. Mendez, F. Olness, P.B. Pal, Snowmass Summer Study 1986, p. 197; J.A. Grifols, J.F. Gunion, and A. Mendez, Phys. Lett. **197B**, 266 (1987); J.F. Gunion, A. Mendez, and F. Olness, Int. J. Mod. Phys. **A2**, 1085 (1987); J.A. Grifols, A. Mendez, and G.A. Schuler, Mod. Phys. Lett. **A4**, 1485 (1989); J.F. Gunion, J. Grifols, A. Mendez, B. Kayser and F. Olness, Phys. Rev. **D40**, 1546 (1989); L. Roszkowski, Phys. Rev. **D41**, 2266 (1990); N. G. Deshpande, J.F. Gunion, B. Kayser and F. Olness, Phys. Rev. **D44**, 837 (1991); K. Huitu and J. Maalampi, Phys. Lett. **B344**, 217 (1995).
- [26] A sampling of references is: N.T. Shaban and W.J. Stirling, Phys. Lett. **B291**, 281 (1992); N.G. Deshpande, E. Keith and T.G. Rizzo, Phys. Rev. Lett. **70**, 3189 (1993); M. Bando, T. Sato and T. Takahashi, Phys. Rev. **D52**, 3076 (1995); B. Brahmachari, Phys. Rev. **D52**, 1 (1995); B. Brahmachari and R.N. Mohapatra, Phys. Lett. **B357**, 566 (1995); E. Ma, Phys. Rev. **D51**, 236 (1995); D.-G. Lee and R.N. Mohapatra, Phys. Rev. **D52**, 4125 (1995).
- [27] J.F. Gunion *Proceedings of the 2nd International Workshop on "Physics and Experiments with Linear e^+e^- Colliders"*, eds. F. Harris, S. Olsen, S. Pakvasa and X. Tata, Waikoloa, HI (1993), World Scientific Publishing, p. 903.
- [28] J.F. Gunion, UCD-95-36, Proceedings of the Santa Cruz Workshop on e^-e^- Colliders, September 4-5, 1995.
- [29] J.A. Coarasa, A. Mendez and J. Sola, UAB-FT-378.
- [30] H. Georgi and S. Glashow, Phys. Rev. Lett. **32**, 438 (1974).
- [31] M. Veltman, Acta Phys. Polon. B **12**, 437 (1981); L. Maiani, *Proceedings of the Summer School on Particle Physics*, Gif-Sur-Yvette, 1979, (Paris, 1980), p. 1; E. Witten, Nucl. Phys. **B188**, 513 (1981).
- [32] S. Dimopoulos, S. Raby, and F. Wilczek, Phys. Rev. **D24**, 1681 (1981).

- [33] S. Dimopoulos and H. Georgi, Nucl. Phys. **B193**, 150 (1981); N. Sakai, Z. Phys. **C11**, 153 (1981); L. Ibáñez and G. Ross, Phys. Lett. **B105**, 439 (1981); M. Einhorn and D. R. T. Jones, Nucl. Phys. **B196**, 475 (1982); W. Marciano and G. Senjanovic, Phys. Rev. **D25**, 3092 (1982).
- [34] J. Ellis, S. Kelley, and D. Nanopoulos, Phys. Lett. **B260**, 131 (1991); U. Amaldi, W. de Boer, and H. Fürstenau, Phys. Lett. **B260**, 447 (1991); P. Langacker and M. Luo, Phys. Rev. **D44**, 817 (1991).
- [35] J. Lykken and S. Willenbrock, Phys. Rev. **D49**, 4902 (1994).
- [36] L. Ibáñez and G. Ross, Phys. Lett. **B110**, 215 (1982); K. Inoue, A. Kakuto, H. Komatsu, and S. Takeshita, Prog. Theor. Phys. **68**, 927 (1982); L. Alvarez-Gaumé, J. Polchinski, and M. Wise, Nucl. Phys. **B221**, 495 (1983); J. Ellis, D. Nanopoulos, and K. Tamvakis, Phys. Lett. **B125**, 275 (1983).
- [37] H.E. Haber and R. Hempfling, Phys. Rev. Lett. **66**, 1815 (1991); Y. Okada, M. Yamaguchi and T. Yanagida, Prog. Theor. Phys. **85** (1991); J. Ellis, G. Ridolfi and F. Zwirner, Phys. Lett. **B257**, 83 (1991). For a review and references, see H. Haber, in *Perspectives on Higgs Physics*, ed. G. Kane, World Scientific Publishing, p. 79. See also, V. Barger, K. Cheung, R. Phillips, and A. Stange, Phys. Rev. **46**, 4914 (1992).
- [38] H. Haber, R. Hempfling and A. Hoang, CERN-TH/95-216.
- [39] J. Ellis, G. Ridolfi and F. Zwirner, Ref. [37].
- [40] M. Carena, J.R. Espinosa, M. Quiros and C.E.M. Wagner, Phys. Lett. **B355**, 209 (1995); J.A. Casas, J.R. Espinosa, M. Quiros and A. Riotto, Nucl. Phys. **B436**, 3 (1995).
- [41] P. Chankowski, S. Pokorski and J. Rosiek, Phys. Lett. **B274**, 191 (1992); Nucl. Phys. **B423**, 437 (1994); A. Dabelstein, Z. Phys. **C67**, 495 (1995).
- [42] H.E. Haber and R. Hempfling, Phys. Rev. **D48**, 4280 (1993).
- [43] R. Hempfling and A.H. Hoang, Phys. Lett. **B331**, 99 (1994).
- [44] J.F. Gunion, in *Perspectives on Higgs Physics*, ed. G. Kane, World Scientific Publishing, p. 179.
- [45] J. Gunion, in *Properties of SUSY Particles*, Proceedings of the 23rd Workshop of the INFN Eloisatron Project, Erice, Italy, Sept. 28 - Oct. 4 1992, eds. L. Cifarelli and V. Khoze, p. 279; and references therein.
- [46] The general structure and predictions of unified versions of the MSSM are reviewed in the companion reports by H. Baer *et. al.* and by M. Drees *et. al.*.

- [47] For a ‘typical’ scenario see J.F. Gunion and H. Pois, Phys. Lett. **B329**, 136 (1994). Further references are given in [46].
- [48] V. Barger *et al.*, *Proceedings of the 2nd International Workshop on “Physics and Experiments with Linear e^+e^- Colliders”*, eds. F. Harris, S. Olsen, S. Pakvasa and X. Tata, Waikoloa, HI (1993), World Scientific Publishing, p. 840.
- [49] For a convenient mini-review focusing on these two models, see H. Baer, J.F. Gunion, C. Kao and H. Pois, Phys. Rev. **D51**, 2159 (1995), and references therein. See also Ref. [46].
- [50] B. W. Lee, C. Quigg, and H. Thacker, Phys. Rev. **D16**, 1519 (1977).
- [51] T. Rizzo, Phys. Rev. **D22**, 722 (1980); W.-Y. Keung and W. Marciano, Phys. Rev. **D30**, 248 (1984).
- [52] M. Spira, A. Djouadi, D. Graudenz and P.M. Zerwas, Nucl. Phys. **B453**, 17 (1995).
- [53] J. P. Leveille, Phys. Lett. **B83**, 123 (1979); A. Vainshtein, M. Voloshin, V. Zakharov, and M. Shifman, Yad. Fiz. **30**, 1368 (1979) [Sov. J. Nucl. Phys. **30**, 711 (1979)].
- [54] R. Cahn, M. Chanowitz, and N. Fleishon, Phys. Lett. **B82**, 113 (1979).
- [55] W. Hollik, presented at the European Physical Society International Europhysics Conference on High Energy Physics, Brussels, Belgium, July 27 - August 2, 1995.
- [56] H. Haber, presented at the European Physical Society International Europhysics Conference on High Energy Physics, Brussels, Belgium, July 27 - August 2, 1995.
- [57] P. Chankowski, presented at the European Physical Society International Europhysics Conference on High Energy Physics, Brussels, Belgium, July 27 - August 2, 1995.
- [58] J. Ellis, G.L. Fogli and E. Lisi, CERN-TH/95-202.
- [59] P. Langacker, private communication.
- [60] The LEP Electroweak Working Group, CERN Report No. LEPEWWG/95-01.
- [61] P.H. Chankowski and S. Pokorski, MPI-Ph/95-39.
- [62] J.F. Gunion, A. Stange, and S. Willenbrock, included in *Electroweak Symmetry Breaking and Beyond the Standard Model*, T. Barklow *et al.*, SLAC-PUB-95-6893.

- [63] J. Bjorken, in *Weak Interactions at High Energy and the Production of New Particles*, proceedings of the SLAC Summer Institute on Particle Physics, 1976, edited by M. Zipf (SLAC Report No. 198, 1977).
- [64] ALEPH Collaboration, Phys. Rep. **216**, 253 (1992); Phys. Lett. **B313**, 299 (1993);
 DELPHI Collaboration, P. Abreu *et al.*, Nucl. Phys. **B421**, 3 (1994);
 L3 Collaboration, O. Adriani *et al.*, Phys. Lett. **B303**, 391 (1993);
 OPAL Collaboration, R. Akers *et al.*, Phys. Lett. **B327**, 397 (1994).
- [65] F. Richard, presented at the 27th International Conference on High Energy Physics, Glasgow, July 20-27, 1994, LAL 94-50 (1994).
- [66] J.F. Grivaz, presented at the European Physical Society International Europhysics Conference on High Energy Physics, Brussels, Belgium, July 27 - August 2, 1995.
- [67] ALEPH Collaboration, D. Buskulic *et al.*, Phys. Lett. **B313**, 312 (1993);
 DELPHI Collaboration, P. Abreu *et al.*, Nucl. Phys. **B373**, 3 (1992);
 Z. Phys. **C67**, 213 (1995);
 L3 Collaboration, O. Adriani *et al.*, Z. Phys. **C57**, 355 (1993);
 OPAL Collaboration, R. Akers *et al.*, Z. Phys. **C64**, 1 (1994).
- [68] G. Altarelli *et al.*, “Interim Report on the Physics Motivations for an Energy Upgrade of LEP2”, CERN-TH/95-151 and CERN-PPE/95-78 (1995).
- [69] J. Rosiek and A. Sopczak, Phys. Lett. **B341**, 419 (1995).
- [70] M. Frank, ALEPH Collaboration, presented at the European Physical Society International Europhysics Conference on High Energy Physics, Brussels, Belgium, July 27 - August 2, 1995.
- [71] P. Janot, in preparation.
- [72] A. Sopczak, Int. J. Mod. Phys. **A9**, 1747 (1994).
- [73] D. R. T. Jones and S. Petcov, Phys. Lett. **B84**, 440 (1979).
- [74] S. L. Wu *et al.*, in *Proceedings of the ECFA Workshop on LEP 200*, Aachen, 1986, eds. A. Böhm and W. Hoogland, CERN 87-08, Vol. II, p. 312.
- [75] P. Janot, in ‘92 *Electroweak Interactions and Unified Theories, Proceedings of the XXVII Rencontre de Moriond*, edited by J. Trân Thanh Vân (Éditions Frontières, Gif-sur-Yvette, 1992), p. 317.
- [76] H. Georgi, S. Glashow, M. Machacek, and D. Nanopoulos, Phys. Rev. Lett. **40**, 692 (1978).

- [77] R. Cahn and S. Dawson, Phys. Lett. **B136**, 196 (1984); G. Kane, W. Repko, and W. Rolnick, Phys. Lett. **B148**, 367 (1984).
- [78] S. Glashow, D. Nanopoulos, and A. Yildiz, Phys. Rev. **18**, 1724 (1978).
- [79] Z. Kunszt, Nucl. Phys. **B247**, 339 (1984).
- [80] D. Dicus and S. Willenbrock, Phys. Rev. **D39**, 751 (1989).
- [81] D. Graudenz, M. Spira, and P. Zerwas, Phys. Rev. Lett. **70**, 1372 (1993); A. Djouadi and M. Spira, private communication.
- [82] T. Han, G. Valencia, and S. Willenbrock, Phys. Rev. Lett. **69**, 3274 (1992).
- [83] T. Han and S. Willenbrock, Phys. Lett. **B273**, 167 (1990).
- [84] H. Lai *et al.*, MSU-HEP-41024, CTEQ-404 (1994).
- [85] J. Gunion, G. Kane, and J. Wudka, Nucl. Phys. **B299**, 231 (1988).
- [86] J. Gunion, Phys. Lett. **B261**, 510 (1991); W. Marciano and F. Paige, Phys. Rev. Lett. **66**, 2433 (1991).
- [87] A. Stange, W. Marciano, and S. Willenbrock, Phys. Rev. **D50**, 4491 (1994).
- [88] D. Froidevaux and E. Richter-Was, Z. Phys. **C67**, 213 (1995).
- [89] S. Mrenna and G. Kane, CALT-68-1938 (1994).
- [90] P. Agrawal, D. Bowser-Chao, and K. Cheung, Phys. Rev. **D51**, 6114 (1995).
- [91] J. Dai, J. Gunion, and R. Vega, Phys. Rev. Lett. **71**, 2699 (1993).
- [92] ATLAS Technical Proposal, CERN/LHCC/94-43, LHCC/P2 (1994).
- [93] CMS Technical Proposal, CERN/LHCC 94-38, LHCC/P1 (1994).
- [94] D. Froidevaux, F. Gianotti, and E. Richter-Was, ATLAS Internal Note PHYS-No-64 (1995).
- [95] T. Liss, private communication.
- [96] F. Gianotti, to appear in the Proceedings of the European Physical Society International Europhysics Conference on High Energy Physics, Brussels, Belgium, July 27 - August 2, 1995.
- [97] D. Froidevaux, F. Gianotti, L. Poggioli, E. Richter-Was, D. Cavalli, and S. Resconi, ATLAS Internal Note, PHYS-No-74 (1995).

- [98] T. Garavaglia, W. Kwong, and D.-D. Wu, Phys. Rev. **D48**, 1899 (1993).
- [99] These effects were first explored in J.F. Gunion and S. Geer, *Proceedings of the “Workshop on Physics at Current Accelerators and the Supercollider”*, eds. J. Hewett, A. White, and D. Zeppenfeld, Argonne National Laboratory, 2-5 June (1993), ANL-HEP-CP-93-92, p. 335.
- [100] E. W. N. Glover, J. Ohnemus, and S. Willenbrock, Phys. Rev. **D37**, 3193 (1988); V. Barger, G. Bhattacharya, T. Han, and B. Kniehl, Phys. Rev. **D43**, 779 (1991).
- [101] T. Han, M. Golden, and G. Valencia, this volume.
- [102] D. Dicus, A. Stange, and S. Willenbrock, Phys. Lett. **B333**, 126 (1994).
- [103] Z. Kunszt and F. Zwirner, Nucl. Phys. **B385**, 3 (1992).
- [104] H. Baer, M. Bisset, C. Kao, and X. Tata, Phys. Rev. **D46**, 1067 (1992); H. Baer, M. Bisset, D. Dicus, C. Kao, and X. Tata, Phys. Rev. **D47**, 1062 (1993).
- [105] J. Gunion and L. Orr, Phys. Rev. **D46**, 2052 (1992).
- [106] V. Barger, K. Cheung, R. Phillips, and A. Stange, Phys. Rev. **D46**, 4914 (1992).
- [107] R. K. Ellis, I. Hinchliffe, M. Soldate, and J. van der Bij, Nucl. Phys. **B297**, 221 (1988).
- [108] J. Dai, J. Gunion, and R. Vega, Phys. Lett. **B315**, 355 (1993).
- [109] J. Dai, J. Gunion, and R. Vega, Phys. Lett. **B345**, 29 (1995).
- [110] J. Dai, J. Gunion, and R. Vega, presented by J. Dai at *Tahoe CMS Week*, Granlibakken, Tahoe City, CA, September 25-27, 1995, and UCD-95-46 (1995).
- [111] J. Gunion, Phys. Lett. **B322**, 125 (1994); V. Barger, R. Phillips, and D. Roy, Phys. Lett. **B324**, 236 (1994).
- [112] J. Dai, J. Gunion, and R. Vega, preprint UCD-95-25 (1995).
- [113] J. Gunion, Phys. Rev. Lett. **72**, 199 (1994).
- [114] S.G. Frederiksen, N. Johnson, G. Kane, Phys. Rev. **D50**, 4244 (1994).
- [115] D. Choudhury, D.P. Roy, Phys. Lett. **B322**, 368 (1994).

- [116] J.F. Gunion, H.E. Haber, and M. Hildreth, in preparation.
- [117] C. Davies, K. Hornbostel, A. Langnau, G. Lepage, A. Lidsey, C. Morningstar, J. Shigemitsu, and J. Sloan, Phys. Rev. Lett. **73**, 2654 (1994).
- [118] *Report of the Tev2000 Study Group on Future Electroweak Physics at the Tevatron*, eds. D. Amidei and R. Brock, D0 Note 2589/CDF Note 3177 (1995).
- [119] A. Stange, W. Marciano, and S. Willenbrock, Phys. Rev. **D49**, 1354 (1994).
- [120] J. Gunion and T. Han, Phys. Rev. **D51**, 1051 (1995).
- [121] A. Belyaev, E. Boos, and L. Dudko, Mod. Phys. Lett. **A10**, 25 (1995).
- [122] S. Kuhlmann, in Ref. [118].
- [123] U. Heintz, in Ref. [118].
- [124] T. Barklow, P. Chen, and W. Kozanecki, in *e^+e^- Collisions at 500 GeV: the Physics Potential*, DESY 92-123 (1992), ed. P.M. Zerwas, Feb. 4 - Sept. 3 (1991) — Munich, Annecy, Hamburg, p. 845.
- [125] A. Miyamoto, *Proceedings of the 2nd International Workshop on “Physics and Experiments with Linear e^+e^- Colliders”*, eds. F. Harris, S. Olsen, S. Pakvasa and X. Tata, Waikoloa, HI (1993), World Scientific Publishing, p. 141.
- [126] For recent studies, see P. Grosse-Wiesemann, D. Haidt, and H.J. Schreiber, in *e^+e^- Collisions at 500 GeV: the Physics Potential*, DESY 92-123A (1992), ed. P.M. Zerwas, Feb. 4 - Sept. 3 (1991) — Munich, Annecy, Hamburg, p. 37; P. Janot, *ibid.*, p. 107; A. Djouadi, D. Haidt, B.A. Kniehl, B. Mele, and P.M. Zerwas, *ibid.*, p. 11; and references therein.
- [127] P. Janot, *Proceedings of the 2nd International Workshop on “Physics and Experiments with Linear e^+e^- Colliders”*, eds. F. Harris, S. Olsen, S. Pakvasa and X. Tata, Waikoloa, HI (1993), World Scientific Publishing, p. 192; and references therein.
- [128] See “JLC-I”, KEK-92-16, December 1992.
- [129] P. Burchat, D. Burke, and A. Petersen, Phys. Rev. **D38**, 2735 (1988).
- [130] For an overview, see J.F. Gunion, *Proceedings of the 2nd International Workshop on “Physics and Experiments with Linear e^+e^- Colliders”*, eds. F. Harris, S. Olsen, S. Pakvasa and X. Tata, Waikoloa, HI (1993), World Scientific Publishing, p. 166.
- [131] A. Djouadi, J. Kalinowski, and P.M. Zerwas, Z. Phys. **C54**, 255 (1992).

- [132] K. Kawagoe, *Proceedings of the 2nd International Workshop on “Physics and Experiments with Linear e^+e^- Colliders”*, eds. F. Harris, S. Olsen, S. Pakvasa and X. Tata, Waikoloa, HI (1993), World Scientific Publishing, p. 660.
- [133] M. Hildreth, T. Barklow, and D. Burke, *Phys. Rev.* **D49**, 3441 (1994).
- [134] M. Hildreth, *Proceedings of the 2nd International Workshop on “Physics and Experiments with Linear e^+e^- Colliders”*, eds. F. Harris, S. Olsen, S. Pakvasa and X. Tata, Waikoloa, HI (1993), World Scientific Publishing, p. 635.
- [135] D. Borden, *Proceedings of the 2nd International Workshop on “Physics and Experiments with Linear e^+e^- Colliders”*, eds. F. Harris, S. Olsen, S. Pakvasa and X. Tata, Waikoloa, HI (1993), World Scientific Publishing, p. 323.
- [136] M.L. Stong and K. Hagiwara, *Proceedings of the 2nd International Workshop on “Physics and Experiments with Linear e^+e^- Colliders”*, eds. F. Harris, S. Olsen, S. Pakvasa and X. Tata, Waikoloa, HI (1993), World Scientific Publishing, p. 631.
- [137] M. Kramer, J. Kuhn, M. Stong, and P. Zerwas, *Z. Phys.* **C64**, 21 (1994).
- [138] A. Soni and R.M. Xu, preprint *Phys. Rev.* **D48**, 5259 (1993).
- [139] D. Chang and W.-Y. Keung, *Phys. Lett.* **B305**, 261 (1993).
- [140] D. Chang, W.-Y. Keung, and I. Phillips, *Phys. Rev.* **D48**, 3225 (1993).
- [141] V. Barger, K. Cheung, A. Djouadi, B.A. Kniehl and P.M. Zerwas, *Phys. Rev.* **D49**, 79 (1994).
- [142] A. Skjold, *Phys. Lett.* **B311**, 261 (1993); *Phys. Lett.* **B329**, 305 (1994).
- [143] B. Grzadkowski and J.F. Gunion, *Phys. Lett.* **B350**, 218 (1995).
- [144] F. Zwirner, in *Properties of SUSY Particles*, Proceedings of the 23rd Workshop of the INFN Eloisatron Project, Erice, Italy, Sept. 28 - Oct. 4 1992, eds. L. Cifarelli and V. Khoze, p. 509; and references therein.
- [145] A. Brignole, J. Ellis, J.F. Gunion, M. Guzzo, F. Olness, G. Ridolfi, L. Roszkowski and F. Zwirner, in *e^+e^- Collisions at 500 GeV: The Physics Potential*, Munich, Annecy, Hamburg Workshop, DESY 92-123A, DESY 92-123B, DESY 93-123C, ed. P. Zerwas, p. 613; A. Djouadi, J. Kalinowski, P.M. Zerwas, *ibid.* p. 83 and *Z. Phys.* **C57**, 569 (1993); and references therein.
- [146] For a review and references, see J. Gunion, in *Proceedings of the Zeuthen Workshop on Elementary Particle Theory — “LEP 200 and Beyond”*, Teupitz/Brandenburg, Germany, 10-15 April (1994), eds. T. Riemann and J. Blumlein, p. 253.

- [147] H. Baer and X. Tata, in *Properties of SUSY Particles*, Proceedings of the 23rd Workshop of the INFN Eloisatron Project, Erice, Italy, Sept. 28 - Oct. 4 1992, eds. L. Cifarelli and V. Khoze, p. 244; and references therein.
- [148] J.F. Gunion, J. Kelly, J. Ohnemus, work in progress.
- [149] J. Ellis, J.F. Gunion, H.E. Haber, L. Roszkowski and F. Zwirner, Phys. Rev. **D39**, 844 (1989).
- [150] B.R. Kim, S.K. Oh and A. Stephan, *Proceedings of the 2nd International Workshop on "Physics and Experiments with Linear e^+e^- Colliders"*, eds. F. Harris, S. Olsen, S. Pakvasa and X. Tata, Waikoloa, HI (1993), World Scientific Publishing, p. 860.
- [151] J. Kamoshita, Y. Okada and M. Tanaka, Phys. Lett. **B328**, 67 (1994).
- [152] S.F. King and P.L. White, preprint SHEP-95-27 (1995).
- [153] U. Ellwanger, M.R. de Trautenberg and C.A. Savoy, Z. Phys. **C67**, 665 (1995).
- [154] V. Telnov, *Proceedings of the 2nd International Workshop on "Physics and Experiments with Linear e^+e^- Colliders"*, eds. F. Harris, S. Olsen, S. Pakvasa and X. Tata, Waikoloa, HI (1993), World Scientific Publishing, p. 551.
- [155] J.F. Gunion and H.E. Haber, *Proceedings of the 1990 DPF Summer Study on High Energy Physics: "Research Directions for the Decade"*, editor E. Berger, Snowmass (1990), p. 206; Phys. Rev. **D48**, 5109 (1993).
- [156] T. Barklow, *Proceedings of the 1990 DPF Summer Study on High Energy Physics: "Research Directions for the Decade"*, editor E. Berger, Snowmass (1990), p. 440.
- [157] D. Borden, D. Bauer, and D. Caldwell, Phys. Rev. **D48**, 4018 (1993).
- [158] G.V. Jikia, Phys. Lett. **B298**, 224 (1993); *Proceedings of the 2nd International Workshop on "Physics and Experiments with Linear e^+e^- Colliders"*, eds. F. Harris, S. Olsen, S. Pakvasa and X. Tata, Waikoloa, HI (1993), World Scientific Publishing, p. 558.
- [159] M.S. Berger, Phys. Rev. **D48**, 5121 (1993).
- [160] D. Dicus and C. Kao, Phys. Rev. **D49**, 1265 (1994).
- [161] A. de Rujula *et al.*, Nucl. Phys. **B384**, 3 (1992).
- [162] M.A. Perez and J.J. Toscano, Phys. Lett. **B289**, 381 (1992).

- [163] D. Morris, T. Truong, and D. Zappala, Phys. Lett. **B323**, 421 (1994).
- [164] S.J. Brodsky, *Proceedings of the 2nd International Workshop on “Physics and Experiments with Linear e^+e^- Colliders”*, eds. F. Harris, S. Olsen, S. Pakvasa and X. Tata, Waikoloa, HI (1993), World Scientific Publishing, p. 295.
- [165] M. Baillargeon, G. Belanger, and F. Boudjema, ENSLAPP-A-473-94 (1994).
- [166] K. Cheung, Phys. Lett. **B323**, 85 (1994); Phys. Rev. **D50**, 4290 (1994).
- [167] G. Jikia, preprints hep-ph/9406395; Nucl. Phys. **B347**, 520 (1995).
- [168] D.L. Borden, V.A. Khoze, W.J. Stirling, and J. Ohnemus, Phys. Rev. **D50**, 4499 (1994).
- [169] D. Bowser-Chao and K. Cheung, Phys. Rev. **D48**, 89 (1993).
- [170] O.J.P. Eboli, M.C. Gonzalez-Garcia, F. Halzen and D. Zeppenfeld, Phys. Rev. **D48**, 1430 (1993).
- [171] E. Boos *et al.*, Z. Phys. **C56**, 487 (1992).
- [172] K. Cheung, Phys. Rev. **D47**, 3750 (1993).
- [173] K. Hagiwara, I. Watanabe, P.M. Zerwas, Phys. Lett. **B278**, 187 (1992).
- [174] E. Boos, M. Dubinin, V. Ilyin, A. Pukhov, G. Jikia, S. Sultanov, Phys. Lett. **B273**, 173 (1991).
- [175] K. Cheung, Phys. Rev. **D48**, 1035 (1993).
- [176] O.J.P. Eboli, M.C. Gonzalez-Garcia, S.F. Novaes, Phys. Rev. **D49**, 91 (1994).
- [177] D. Borden, private communication.
- [178] B. Kileng, Z. Phys. **C63**, 87 (1994).
- [179] J.F. Gunion, J. Kelly, J. Ohnemus, Phys. Rev. **D51**, 2101 (1995).
- [180] D. Bowser-Chao, K. Cheung, and S. Thomas, Phys. Lett. **B315**, 399 (1993).
- [181] B. Grzadkowski and J.F. Gunion, Phys. Lett. **B294**, 361 (1992).
- [182] J.F. Gunion and J. Kelley, Phys. Lett. **B333**, 110 (1994).
- [183] *Proceedings of the First Workshop on the Physics Potential and Development of $\mu^+\mu^-$ Colliders*, Napa, California (1992), Nucl. Instru. and Meth. **A350**, 24 (1994).

- [184] *Proceedings of the Second Workshop on the Physics Potential and Development of $\mu^+\mu^-$ Colliders*, Sausalito, California (1994), ed. by D. Cline, p. 55.
- [185] V. Barger, M. Berger, J. Gunion and T. Han, Phys. Rev. Lett. **75**, 1462 (1995); UCD-96-1, in preparation.
- [186] R.B. Palmer and A. Tollestrup, unpublished report.
- [187] R.B. Palmer, private communication.
- [188] G.P. Jackson and D. Neuffer, private communications.
- [189] T. Barklow and D. Burke, private communication.
- [190] D. Atwood and A. Soni, Phys. Rev. **D52**, 6271 (1995).